B cell development, activation, and autoimmunity in mice with altered B cell receptor signalling

ASHLEY RICHARD HUDSON

A thesis submitted to the University of Birmingham for the degree of

DOCTOR OF PHILOSOPHY

Institute of Immunology and Immunotherapy

College of Medical and Dental Science

University of Birmingham

December 2022

Abstract

B cell receptor (BCR) signalling plays an important role at multiple stages of B cell development, differentiation, and activation. Naïve B cells co-express BCRs of IgM and IgD isotype, but when activated, B cells often class-switch to another isotype such as IgG1. IgG1 transduces stronger BCR signalling, thought to be largely due to inherent signalling capabilities in the cytoplasmic tail. To investigate the effect of altered BCR signalling on B cell development, B cell activation and development of autoimmunity, we have used a mouse model where B cells express chimeric BCRs that have the IgM extracellular region and the IgG1 cytoplasmic tail (IgMg1 mouse), as well as a second mouse model where B cells express fully IgG1 BCRs (IgG1M mouse).

In IgMg1 mice, B cells had evidence of increased negative selection during B cell development, reduced BCR expression and a dampened response to BCR stimulation *in vitro*, supporting the previous observation that B cells in these mice display an anergic phenotype. Gene expression was analysed in IgMg1 B cells and genes that may play a role in regulating B cell anergy were identified. IgMg1 mice were able to make germinal centre (GC) responses following immunisation with T cell-dependent (TD) antigen. However, there was a higher affinity threshold for B cell participation in the GC, and reduced survival and positive selection. The B cells had greater ability to present antigen and activate T follicular helper cells. Aged IgMg1 mice were more prone to developing spontaneous tissue-specific autoantibodies than aged wildtype mice.

In IgG1M mice, IgG1-only expressing B cells also underwent increased negative selection and BCR downregulation. However, unlike the IgMg1 B cells, this did not

result in an anergic phenotype; instead, B cells were hyper-responsive to BCR stimulation *in vitro*. Despite the hyperactive BCR signalling, T cell-independent and TD responses were unexpectedly impaired.

This work provides insight into how stronger BCR signalling can inhibit or increase B cell activation in different contexts. It also establishes how different BCRs can affect interactions with Tfh cells within the GC. Additionally, the importance of the BCR extracellular region relative to the cytoplasmic region for signalling at different stages of development was explored. These mouse models should be useful to further investigate how regulation of enhanced BCR signalling can prevent inappropriate activation of B cells and the development of autoimmunity.

Acknowledgments

First, I would like to thank Professor Kai-Michael Toellner for the opportunity to do a PhD, supervising me and this project, teaching me so much about B cells and germinal centres, and for helping me develop as a scientist.

Dr Yang Zhang and Dr Juan Carlos Yam-Puc, thank you very much for all the help and advice you have given me in the lab. A special thanks is due for all the help with mouse experiments while COVID restrictions did not allow me to enter the BMSU. Additionally, thank you to Dr Lingling Zhang for several helpful discussions about the IgMg1 mice.

I would also like to acknowledge: Dr David Bending for providing the Nr4a3-Tocky mouse and for valuable advice and discussions; Dr Abid Karim for help with analysis of autoimmune tissue slides; to the Francis Crick Institute bioinformatics service for help with bulk RNA sequencing data processing; Professor Adam Croft and members of his group (Charlotte Smith and Samuel Kemble) for help with collagen-induced arthritis experiments; Anetta Ptasinska for help with 10x single cell sequencing library preparation and sequencing; BMSU staff, flow cytometry facility staff and imaging facility staff for support with experiments and assistance with pieces of equipment.

Thank you to MIBTP and BBSRC for my funding, and training in programming and bulk RNA-seq analysis.

To all the other PhD students on the 4th floor, and especially Cameron, Fernanda and Khaled who have been with me in the Toellner lab all the way through my PhD: thank you for your emotional support and company in the lab. I wish you all the best of luck with your future careers.

To my parents and family, thank you for being there for me throughout my entire life and for giving me the encouragement and confidence to do this. I'm grateful that you have always provided a relaxing and fun environment to escape from the stresses of PhD life.

Finally, to Maria. Your continuous emotional support over the last 4 years has made this possible. Thank you for keeping me sane! I am looking forward to enjoying our post-PhD lives together.

Contents

List of figures

List of tables

Abbreviations

ACK	Ammonium-Chloride-Potassium
AGPCA	Anti-gastric parietal cell antibodies
AID	Activation-induced cytidine deaminase
Alum	Aluminium potassium sulphate
ANA	Anti-nuclear antibodies
ANOVA	Analysis of variance
AP	Alkaline phosphatase
APC	Allophycocyanin
APRIL	A proliferation-inducing ligand
Ars	p-azophenylarsonate
ASMA	Anti-smooth muscle antibodies
ATR	ataxia telangiectasia and Rad3-related protein
BAFFR	B cell activating factor receptor
Bcl	B cell lymphoma
BCA	bicinchoninic acid
BCR	B cell receptor
Blimp-1	B lymphocyte-induced maturation protein-1
BLNK	B cell linker
BMP	Bone morphogenetic protein
BSA	Bovine serum albumin
BTK	Bruton's tyrosine kinase
CD	Cluster of differentiation
CDR	Complementarity-determining region
CFA	Complete Freund's adjuvant
CGG	chicken gamma globulin
CIA	Collagen-induced arthritis
CLP	Common lymphoid progenitor
CTLA-4	cytotoxic T-lymphocyte-associated protein 4
CXCL	C-X-C motif chemokine ligand
CXCR	C-X-C motif chemokine receptor
D	diversity
D-PBS	Dulbecco's phosphate buffered saline
DAPI	4′,6-diamidino-2-phenylindole
DC	Dendritic cell
DEL	Duck egg lysozyme
DMSO	Dimethyl sulfoxide
DNA	Deoxyribonucleic acid
DNP-LPS	2,4-Dinitrophenyl Lipopolysaccharide
DOK1	Docking protein 1
DSB	Double strand DNA breaks
DZ	Dark zone
ELISA	Enzyme-linked immunosorbent assay
ELISpot	Enzyme-linked immune absorbent spot
ERK	Extracellular signal-regulated kinase
FACS	Fluorescence activated cell sorting
FBS	Fetal bovine serum
FcR	Fc receptor
FDC	Follicular dendritic cell
FDR	False discovery rate
FITC	Fluorescein isothiocyanate
Fo	Follicular
FoxO	Forkhead box protein O
Fr	Fraction

FRC	Follicular reticular cell
GC	Germinal centre
GM-CSF	Granulocyte macrophage-colony-stimulating factor
GO	Gene ontology
GPCR	G-protein coupled receptor
Grb2	Growth factor receptor-bound 2
GSEA	Gene set enrichment analysis
GTIRC	fibroblastic reticular cells at the interface between the GC and T cell zone
H_2O	Water
HBSS	Hank's buffered salt solution
HEL	Hen egg lysozyme
i.p.	intraperitoneal
IFA	Incomplete Freund's adjuvant
Ig	Immunoglobulin
IGHV	Immunoglobulin heavy variable
IGKV	Immunoglobulin kappa variable
IGLV	Immunoglobulin lambda variable
IL	Interleukin
IP_3	Inositol 1,4,5-trisphosphate
IRF4	Interferon regulatory factor 4
ITAM	Immunoreceptor tyrosine-based activation motif
ITT	Immunoglobulin tail tyrosine
J	Joining
KLH	keyhole limpet hemocyanin
KLM	Kidney liver microsomal antibody
LMP2A	Latent membrane protein 2a
LPS	Lipopolysaccharide
LZ	Light zone
MAdCAM-1	Mucosal adressin cell adhesion molecule 1
MAPK	Mitogen-activated protein kinase
MHC	Major histocompatibility complex
MZ	Marginal zone
NF-AT	Nuclear factor of activated T cells
NF-κB	Nuclear factor kappa-light-chain-enhancer of activated B cells
NK	Natural killer
NOD	Non-obese diabetic
NP	(4-hydroxy-3-nitrophenyl)-acetyl
NP-OSu	4-Hydroxy-3-nitrophenylacetic acid Succinimide Ester
Nr4a1	Nuclear receptor 4a1
Nr4a3	Nuclear receptor 4a3
OCT	Optimal cutting temperature
PAMP	Pathogen-associated molecular patterns
PC	Plasma cell
PCA	Principal components analysis
PE	Phycoerythrin
PIP_2	Phosphatidylinositol 4,5-biphosphate
PLCγ2	Phospholipase Cγ2
PMA	Phorbyl myristate acetate
PNA	Peanut allergen
Pol η	DNA polymerase eta
PtC	Phosphatidylcholine
PTEN	Phosphatase and tensin homolog
PTK	Protein tyrosine kinase
QM	Quasimonoclonal
RA	Rheumatoid arthritis

RAG	Recombination activating gene
RNA	Ribonucleic acid
s.c.	Sub-cutaneous
SAP97	Synapse-associated protein 97
SARS-CoV-2	Severe acute respiratory syndrome coronavirus 2
SHIP-1	Src homology 2 domain containing inositol polyphosphate 5-phosphatase 1
SHP-1	Src homology region 2 domain-containing phosphatase-1
SLE	Systemic lupus erythematosus
Sm	Smith antigen
STZ	Streptozocin
T	Transitional
T1D	Type 1 diabetes
TCR	T cell receptor
TD	T cell-dependent
Tfh	Follicular helper T cells
Th	T helper
TI	T cell-independent
TI-I	T cell-independent type I
TI-II	T cell-independent type II
TLR	Toll-like receptor
tSNE	t-distributed stochastic neighbour embedding
V	Variable
UMI	Unique molecular identifier
VH	Variable heavy
WAS	Wiskott-Aldrich syndrome
WT	wildtype
Xid	X-linked immunodeficient
κ	Kappa
λ	Lambda

Chapter 1. Introduction

1.1 The immune system

The immune system is the body's defence against foreign invaders such as bacteria, viruses, and toxins. It acts to recognise and remove pathogens, and restrict the damage caused by them. It can be broadly divided into the innate and adaptive immune system (Murphy et al., 2008; Chaplin, 2010). The cells of the innate immune system recognise and respond to pathogen-associated molecular patterns (PAMPs) expressed by broad classes of pathogens. These are well conserved as they are structures essential for survival of the pathogen (Medzhitov and Janeway, 1997). The innate immune system cells include neutrophils, dendritic cells (DCs), macrophages, eosinophils, mast cells, and natural killer (NK) cells. Neutrophils and macrophages are primarily involved in engulfing microorganisms (phagocytosis), whereas eosinophils are involved in killing of parasites. Mast cells release granules causing inflammation, and finally, NK cells recognise and kill abnormal cells such as virus-infected cells and some tumour cells (Murphy et al., 2008).

The adaptive immune system consists of B and T lymphocytes (also known as B and T cells). Both of them have large random repertoires of antigen receptors with different specificities, generated from somatic rearrangement of relatively few germline gene segments (Chaplin, 2010). B and T cells express antigen receptors that have specificity for different types of target antigens. T cell receptors (TCRs) recognise processed antigen peptide fragments in complex with major histocompatibility (MHC) molecules, whereas B cell receptors (BCRs) recognise conformational epitopes on antigens. After

development in the bone marrow or thymus, lymphocytes circulate lymphoid tissues in search for antigens that may bind and activate their antigen receptors. T cells differentiate into two different types of effector cells: T helper cells (Th cells) and cytotoxic T cells. B cells can differentiate into plasma cells which specialise in secreting antibodies, the secreted form of the BCR (Murphy et al., 2008). Another crucial aspect of adaptive immunity is the generation of long-lived “memory” effector cells, which allow a more rapid response in a subsequent infection with the same pathogen.

1.2 Antibodies

B cells are a specialised set of lymphocytes responsible for humoral immunity. They recognise antigens through their BCRs and once activated may differentiate into plasma cells to secrete antibodies. Antibodies are made up of two identical heavy chains and two identical light chains (Figure 1.1). The light chain may be either kappa (κ) or lambda (λ) class. The specificity of the antibody depends on the variable region (Figure 1.1), especially the complementarity-determining regions (CDRs), which are hypervariable. These form the antigen binding sites (Murphy et al., 2008). During an immune response these regions can undergo extensive mutation to increase affinity to the antigen.

The diversity of the antibody repertoire in humans is estimated to be at least 10^{11} (Murphy et al., 2008). This high diversity results from a process of somatic recombination to join gene segments together in random combinations during B cell development in the bone marrow. This process is mediated by enzymes called recombination activating genes (RAG) 1 and 2, which are expressed during

lymphocyte development (Kuo and Schlissel, 2009). In humans the kappa light chain locus has 40 variable (V) and 5 joining (J) segments that can be recombined randomly, and the lambda light chain locus has 30 V and 4 J segments. The heavy chain locus has 40 V, 25 diversity (D) and 6 J segments. The combinatorial diversity from random recombination of these segments is known as VDJ recombination, and the random pairing of heavy and light chain can produce approximately $1.9x10^6$ possible combinations. Extra diversity arises from the random addition and deletion of nucleotides at the junctions between the segments. This in particular causes a high degree of diversity in CDR3 (Tonegawa, 1983; Murphy et al., 2008).

Antibodies raised against a pathogen contribute to protection in several ways, for example neutralisation of pathogens or toxins (Brenneman et al., 2011; Boyer et al., 2011; Dumas et al., 2020; Dispinseri et al., 2021; Khoury et al., 2021; Tea et al., 2021; Pang et al., 2021), or recruitment of other components of the immune system such as complement or innate cell subsets (Murphy et al., 2008; Merle et al., 2015a, 2015b). As a result of class-switch recombination, the isotype of the antibody, as determined by the heavy chain constant region, can switch during an immune response. The isotype that results from class-switching is influenced by the type of antigen, and by cytokines released by other cells of the immune system (Snapper and Mond, 1993). The different isotypes (IgM, IgD, IgG, IgA and IgE) have diverse functions due to having distinct structures (Schroeder and Cavacini, 2010), and differences in ability to engage Fc receptors (FcRs) (Nimmerjahn and Ravetch, 2005) and activate complement (Neuberger and Rajewsky, 1981). IgM is the first isotype expressed in response to a pathogen. Secreted IgM forms pentamers, which improves avidity to antigen even if the BCR is low affinity. Pentameric IgM has high capacity for forming immune complex

with complement C1q and activating the complement pathway (Gong and Ruprecht, 2020). IgG is the most abundant antibody class in the circulation and has a monomeric structure. Several IgG sub-classes exist, each with differences in abundance and ability to induce effector functions. In humans the subclasses are IgG1, IgG2, IgG3 and IgG4. IgG1 is involved in response to soluble protein and membrane-expressed protein antigens and has high affinity for most of the FcRs. IgG2 responds to bacterial capsular polysaccharide antigens. IgG3 is efficient at induction of effector functions and activation of complement. IgG4 is often induced by allergens or by long-term exposure to antigen (Vidarsson et al., 2014). Mice also have 4 IgG subclasses (IgG1, IgG2a, IgG2b and IgG3), although the functions of the human and mouse subclasses are not comparable (Collins, 2016). Mouse IgG1 is inefficient at activating complement (Neuberger and Rajewsky, 1981) and has high affinity for the inhibitory FcR FcγRIIb and relatively low affinity for the activating FcRs such as FcγRIII. Mouse IgG2a has relatively high affinity for FcγRIV, making it effective at clearing pathogens through opsonisation (Nimmerjahn et al., 2005). Mouse IgG3 has greater bactericidal and phago-opsonisation ability (Michaelsen et al., 2004) but less ability to induce cytotoxicity through binding to FcRs on neutrophils and eosinophils (Lopez et al., 1983). IgA forms dimers and is the main antibody class in secretions, for example in the intestinal and respiratory tracts, and is an important part of the immune response at these sites (Woof and Ken, 2006). IgE is thought to have originally evolved to provide immunity to parasites and venom toxins, but is commonly associated with allergy (Sutton et al., 2019). In summary, the protective role of antibodies is crucial in the immune response to many different pathogens, by a range of different mechanisms, dependent on the isotype of the antibody.

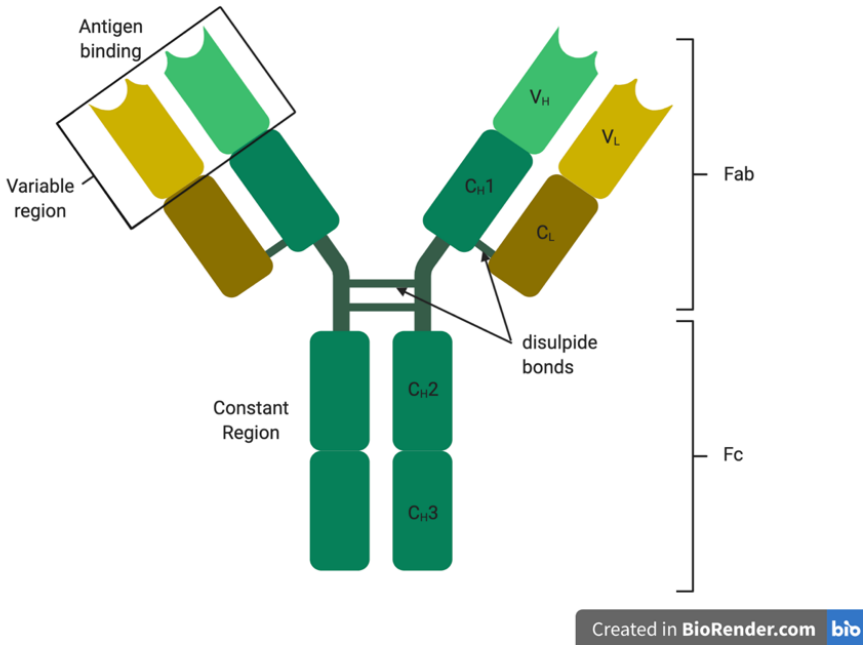

Figure 1.1. Structure of an antibody molecule.

Schematic representation of an IgG molecule showing the heavy chains (green) and light chains (yellow). The variable regions are made up of the V_H and V_L domains (lighter colours), while the constant regions are made up of the C_L and C_H domains (darker colours). The heavy chains are linked by disulphide bonds at the hinge region, as are the C_L and C_H1 domains. The antigen binding fragment (Fab) binds to antigens. The Fc fragment can bind to Fc receptors (FcRs) on other cell surfaces. Adapted from Murphy et al., (2008). Created in BioRender.

1.3 B cell development

1.3.1 B cell development in the bone marrow

B cell development (Figure 1.2) in adult mice begins in the bone marrow. They are derived from common lymphoid progenitors (CLPs), from which T cells and NK cells also originate (Akashi et al., 1999). The earliest stage of the B cell lineage is the pro-B cell. Heavy chain immunoglobulin gene rearrangement occurs in pro-B cells. Once they have a functioning heavy chain following successful VDJ recombination, they reach the pre-B cell stage. Pre-B cells express a pre-BCR in which the newly rearranged heavy chain is paired with a surrogate light chain, made up of VpreB and λ5 peptides. At this point the light chain genes undergo rearrangement. Once the heavy

and light chain genes have been rearranged, pre-B cells become immature B cells and express IgM on the cell surface as the BCR (Hardy, 2012).

B cell development in the bone marrow has been extensively characterised by Richard Hardy based on expression of surface markers, with the different stages being designated as Hardy fractions (Fr) A to F. B lineage cells specifically express B220, an isoform of CD45Ra. The $B220^{+}$ cells can be split into an early $CD43^{+}$ fraction and a later $CD43^{-}$ fraction. The $CD43^{+}$ fraction can be further split into early fractions A (pre-pro-B cells), B and C (pro-B cells), and C' (large pre-B cells) based on expression of CD24 and BP-1. The $CD43^{-}$ fraction can be separated into fractions D (small pre-B cells), E (immature B cells), and F (mature B cells) based on IgM and IgD surface expression (Hardy et al., 1991).

The bone marrow microenvironment provides the niche required for B cell development from CLPs, for example factors secreted by bone marrow stromal cells such as interleukin (IL)-7 and the chemokine CXCL12. IL-7 is important for B cell development as it promotes the survival and proliferation of pro-B and pre-B cells. CXCL12 helps localise the developing B cells to the bone marrow, through expression of CXCL12 receptor CXCR4 by the B cell progenitors and precursors (Carsetti, 2000; Nagasawa, 2006; Hardy, 2012; Zehentmeier and Pereira, 2019).

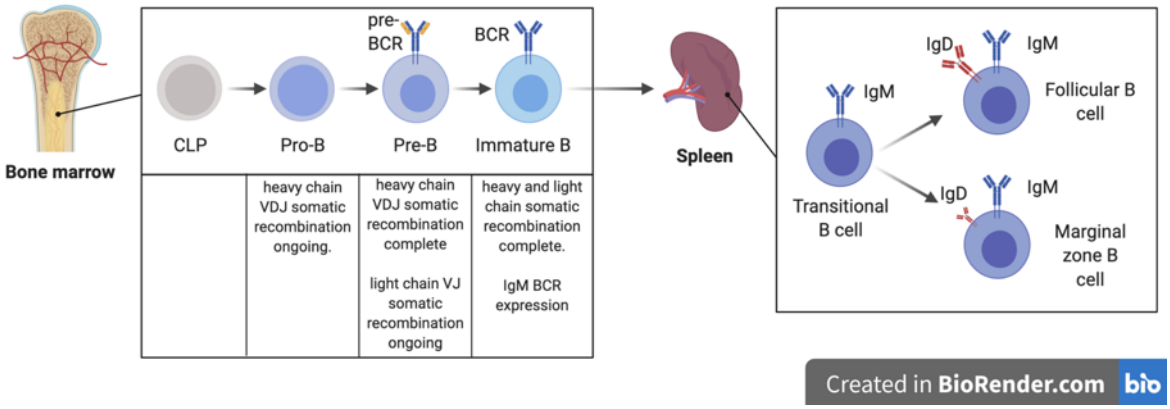

Figure 1.2. B cell development.

B cell development starts in the bone marrow. B cells develop from common lymphoid progenitor (CLP) cells. The earliest stage of the B cell lineage is the pro-B cell which undergoes heavy chain VDJ recombination. Once a functional heavy chain is expressed, they become a pre-B cell. Pre-B cells undergo light chain VJ rearrangement. Once the cell has functional heavy and light chain genes, the immature B cells migrate to the spleen, to complete their maturation as transitional B cells. They mature into either follicular B cells or marginal zone B cells. Adapted from Murphy et al. (2008) and Yam-Puc et al (2018). Created in BioRender.

1.3.2 B cell maturation in the spleen

Immature B cells migrate from the bone marrow to the spleen as transitional B cells, where they complete their maturation into either follicular B cells or marginal zone B cells (Loder et al., 1999; Pillai and Cariappa, 2009), and co-express IgD along with IgM through an alternative splicing mechanism (Maki et al., 1981; Gutzeit et al., 2018). The spleen is a highly organised tissue with most lymphocytes residing in areas of white pulp, separated by areas of red pulp. The white pulp itself is further segregated into B cell follicles (with follicular B cells) and T cell zones, surrounded by a marginal zone made up of marginal zone B cells and macrophages (Lewis et al., 2019). B cells express chemokine receptor CXCR5 and are attracted to follicles by the chemokine CXCL13, expressed by follicular dendritic cells (FDCs) (Ansel et al., 2000).

The fate decision to become either a follicular or marginal zone B cell depends on signals received through the BCR, as well as signals received through Notch2 and B cell activating factor receptor (BAFFR) (Pillai and Cariappa, 2009). However, the role of BCR signalling in the fate decision is controversial. Various mouse models with altered BCR signalling have reported differences to frequencies of follicular and marginal zone B cells. In some mouse models it has been reported that weak BCR signalling favours development into a marginal zone B cell, whereas relatively strong BCR signalling favours development into a follicular B cell (Cariappa et al., 2001, 2009; Samardzic et al., 2002; Setz et al., 2018; Härzschel et al., 2021). However other studies have reported that in other mouse models with stronger BCR signalling, there is an increase in marginal zone B cells (Wen et al., 2005; Kanayama et al., 2005; Horikawa et al., 2007; Waisman et al., 2007; Tsiantoulas et al., 2017; Geier et al., 2018; Ottens and Satterthwaite, 2021). These studies are summarised in Table 1.1.

Table 1.1 Mouse models with altered B cell receptor signalling showing differential effects on B cell maturation

	Mouse model	Effect on BCR signalling	Effect on marginal zone B cells	Reference
Evidence for increased BCR signalling favouring follicular B cell development	CD22-deficient	Increased	Decreased	(Samardzic et al., 2002)
	Aiolos-deficient	Increased	Decreased	(Cariappa et al., 2001)
	$Siae^{\Delta 2/\Delta 2}$ (truncated)	Increased	Decreased	(Cariappa et al., 2009)
	Pten-deficient B cells	Decreased	Increased	(Setz et al., 2018)
	B cell-specific Kindlin3-knock-out	Increased	Decreased	(Härzschel et al., 2021)
Evidence for increased BCR signalling favouring marginal zone B cell development	Soluble IgM knock-out	Increased	Increased	(Tsiantoulas et al., 2017)
	Anti-hen egg lysozyme (HEL) transgenic chimeric IgM/IgG1 B cell receptor	Increased	Increased	(Horikawa et al., 2007)
	$IgH^{\gamma 1\mu}$	Increased	Increased	(Waisman et al., 2007)
	Interferon regulatory factor 4 (IRF4)-deficient mice	Increased	Increased	(Ottens and Satterthwaite, 2021)
	Monoclonal BCR specific to self Thy-1/CD90	Increased (due to self-reactivity)	Increased	(Wen et al., 2005)
	Quasimonoclonal (QM) mouse ($VH_T/\lambda 1$ and $VH_T/\lambda 2$ B cells)	Increased BCR signalling in λ2 B cells due to increased polyreactivity	Increased MZ, enriched for the polyreactive λ2 B cells	(Kanayama et al., 2005)
	Hypomorphic mutations in B cell linker (BLNK) and Bruton's tyrosine kinase (BTK)	Decreased	Decreased	(Geier et al., 2018)

Follicular B cells make up 80-90% of the mature B cells in the spleen (Vale et al., 2015). In addition to being located in the follicles of the spleen, they recirculate through the blood and lymphatic system and to the follicles in other secondary lymphoid organs such as lymph nodes, to maximise the chance of encountering antigen. Follicles are positioned next to T cell zones so that follicular B cells are able to receive costimulatory signals from follicular helper T cells (Tfh cells) and participate in a T cell-dependent (TD) response when activated (Victora and Nussenzweig, 2022).

In mice, marginal zone B cells are confined to the spleen, where they make up 5-10% of the mature B cells (Vale et al., 2015). They take part in T cell-independent (TI) responses against blood-borne TI antigens such as lipopolysaccharides (LPS). This type of response does not require help from cognate helper T cells, and results in low-affinity plasma cells (Oliver et al., 1997; Guinamard et al., 2000; Martin et al., 2001). Additionally, they function to capture blood-borne protein antigen and shuttle it to the follicles (Cinamon et al., 2008; Arnon et al., 2013). They may also activate Tfh cells in the T cell zone (Attanavanich and Kearney, 2004). Recently it has been shown that they can acquire antigen-MHC class II complex from conventional dendritic cells by trogocytosis, and this may provide an additional means for activation of T cells (Schriek et al., 2022).

1.3.3 B-1 cells

In addition to conventional B cells (also known as B-2 cells), there is another subset of B cells in mice: B-1 cells. B-1 cells are considered part of the innate immune system. Unlike B-2 cells, they are not the product of B cell development in the bone marrow.

Instead, they develop in the fetal liver, and the population in adults is maintained by self-renewal. B-1 cells make up a large proportion of the B cells in the peritoneal and pleural cavities and are also found at a lower frequency in the spleen (Baumgarth, 2011). The splenic B-1 cells are thought to be derived from the peritoneal cavity B-1 cells (Kawahara et al., 2003), but are phenotypically and functionally distinct (Tumang et al., 2004).

They can be split into B-1a cells, which express CD5, and B-1b cells, which do not express CD5. B-1a and B-1b cells have functional differences. B-1b cells may have broader BCR repertoire and are important in the response to some bacterial infections, for example *Salmonella,* and may be able to generate long-lived memory response (Marshall et al., 2012; Cunningham et al., 2014). B-1a cells secrete “natural antibodies”, a polyreactive repertoire of IgM antibodies that bind to common bacterial and viral epitopes such as constituents of bacterial cell walls. These antibodies act as an important first line of defence against many pathogens (Baumgarth, 2011).

Unlike B-2 cells, B-1a cells are not activated by antigen binding to their BCR (Baumgarth, 2011). They do not enter cell cycle in response to BCR crosslinking, and Nuclear factor kappa-light-chain-enhancer of activated B cells (NF-κB) is not induced in response to BCR crosslinking (although it is induced in response to mitogens such as LPS and phorbyl myristate acetate (PMA)) (Morris and Rothstein, 1993). They also do not mobilise calcium in response to BCR stimulation (Chumley et al., 2002). Signalling through TLRs is required for activation and secretion of antibodies (Kreuk et al., 2019). In response to some infections, for example influenza, they may be recruited to the lymph node and be activated in an antigen-independent manner (Choi and

Baumgarth, 2008). B-1a cells have also been linked to a role in immune tolerance. Mice with B cell-specific deletion of cytotoxic T-lymphocyte-associated protein 4 (CTLA-4) develop spontaneous germinal centres and autoimmunity, and this was linked to dysfunctional CTLA-4-deficient B-1a cells (Yang et al., 2021). B-1 cells appear to be susceptible to disruptions to BCR signalling with several mouse models with impaired BCR signalling having reduced B-1 cells, while models with deleted negative regulators of BCR signalling have increased B-1 cells (Berland and Wortis, 2002).

Although B-1 cells are a distinct and well-studied subset in mice, it is unclear if they are present in humans. A population of cells ($CD20^+$ $CD27^+$ $CD43^+$ $CD70^-$) has been identified as human B-1 cells based on their phenotype: spontaneous secretion of IgM, ability to stimulate T cells, tonic intracellular signalling, and a skewed variable heavy (VH) repertoire (Griffin et al., 2011). However, the identification of this population as B-1 cells is controversial (Griffin and Rothstein, 2012; Tangye, 2013) and the population has been alternatively identified as a pre-plasmablast population based on gene expression profiling (Covens et al., 2013). Another potential human equivalent of B-1 cells is $CD21^{low}$ cells which have similar gene expression profile, phenotype, function and tissue location as mouse B-1 cells (Rakhmanov et al., 2009).

1.4 B cell activation

1.4.1 Antigen capture and presentation to T cells

Conventional B cells encounter antigen in either soluble or membrane bound form (Batista and Harwood, 2009). It is usually captured from cells that present intact antigen, for example FDCs (Suzuki et al., 2009; Tew et al., 1997), subcapsular sinus

macrophages in lymph nodes (Junt et al., 2007; Phan et al., 2007; Carrasco and Batista, 2007), or migratory dendritic cells (Bergtold et al., 2005; Wykes et al., 1998; Colino et al., 2002; Qi et al., 2006; Heath et al., 2019). It has also been reported that B cells can capture small-molecular weight soluble antigens directly (Pape et al., 2007). In a TD response, once the antigen has been captured by the B cell it is internalised, degraded and presented on the surface as a MHC class II-peptide complex to Th cells (Yuseff et al., 2013; Lankar et al., 2002). B cells migrate to the border of the T cell zone and B cell follicle, and interact with cognate Th cells (Toellner et al., 1996; Garside et al., 1998; Okada et al., 2005), forming an immunological synapse (Duchez et al., 2011). Recognition of MHC class II-peptide complex by the cognate Th cell triggers expression of molecules that activate the B cell and induce proliferation. For example, Tfh cells express CD40L on their surface, and secrete IL-4. This provides pro-mitotic and pro-survival signals to B cells (Crotty, 2011; Murphy et al., 2008; Biram et al., 2019). The importance of these signals has been shown in *in vitro* experiments, where human B cells can be activated with an anti-CD40 monoclonal antibody and IL-4 (Vallé et al., 1989).

1.4.2 Extrafollicular response

Some of the activated B cells move out of the follicles and differentiate into short-lived plasmablasts that secrete relatively low-affinity antibodies that form the early protective antibody response. This is known as the extrafollicular response. The affinity of the antibodies for the antigen is not high because they are not affinity matured, but they may be immunoglobulin class-switched (MacLennan et al., 2003). The decision for activated B cells to take part in the extrafollicular response may be driven by affinity of

the BCR for the antigen, with the highest-affinity clones becoming short-lived plasmablasts, and the lower-affinity clones entering the germinal centre reaction where they will undergo affinity maturation (Paus et al., 2006; O'Connor et al., 2006). It has also been reported that memory B cells may develop early in the immune response outside of germinal centres as part of the extrafollicular response (Taylor et al., 2012).

1.4.3 Germinal centres

Germinal centres (GCs) (Figure 1.3) are transient structures within the follicles consisting of several cell types, including activated B cells, Tfh cells, and FDCs. They develop 4-5 days after B cell activation by a TD antigen (De Silva and Klein, 2015). GCs have primarily been studied *in vivo* in mice immunised with model antigens, as it is not yet possible to completely recapitulate the complexity of a GC *in vitro*. GCs support affinity maturation and selection of B cells with high-affinity BCR to become memory B cells and long-lived plasma cells that secrete high-affinity antibody (MacLennan, 1994a; Victora and Nussenzweig, 2022). Until recently it was thought that GCs were also the site of class-switch recombination, however it is now thought that this occurs prior to formation of GCs, and that class-switching within the GCs is uncommon (Toellner et al., 1996, 1998; Marshall et al., 2011; Roco et al., 2019).

The GC is split into a dark zone (DZ), with a high density of proliferating B cells, and a light zone (LZ), with a lower density of B cells and a network of FDCs and Tfh cells. The DZ B cells, known as centroblasts, and the LZ B cells, known as centrocytes, are spatially separated as well as phenotypically distinct, with DZ B cells being $CXCR4^{hi}$ $CD83^{lo}$ $CD86^{lo}$ and LZ B cells being $CXCR4^{lo}$ $CD83^{hi}$ $CD86^{hi}$ (Victora et al., 2010). The

organisation into the zones is mediated by chemokine gradients with $CXCR4^+$ B cells directed to the $CXCL12^+$ DZ, and $CXCR5^+$ B cells being directed to the $CXCL13^+$ LZ (Allen et al., 2004). B cells migrate between the two zones (Schwickert et al., 2007; Allen et al., 2007; Victora et al., 2010).

In the DZ, B cells undergo clonal expansion and somatic hypermutation to mutate the variable region of the BCR (MacLennan, 1994b; Mesin et al., 2016; Victora and Nussenzweig, 2022). Somatic hypermutation requires activation-induced cytidine deaminase (AID) (Muramatsu et al., 2000), which is expressed in DZ B cells (Victora et al., 2012). AID catalyses cytidine deamination on single stranded DNA exposed during transcription (Chaudhuri et al., 2003; Dickerson et al., 2003; Ramiro et al., 2003). This results in double-strand DNA breaks (DSBs) that are repaired by error-prone repair mechanisms (Di Noia and Neuberger, 2007), such as by DNA polymerase eta (Pol η) which is highly expressed in DZ B cells (Victora et al., 2010).

B cells that have damaging BCR mutations undergo apoptosis in the DZ, whereas B cells with functional BCR migrate to the LZ to test the newly mutated BCRs (Mayer et al., 2017; Stewart et al., 2018). Here, B cells compete for antigen and T cell help. Higher-affinity B cells are selected based on the amount of antigen they capture via the BCR and present to cognate T cells, and the amount of T cell help they subsequently receive (Victora et al., 2010). Early antigen-specific antibodies may also re-enter the GC and compete for antigen, thus driving the selection of B cells with increasingly higher affinity BCR (Zhang et al., 2013; Toellner et al., 2018). Myc-expression is upregulated following selection, which drives cell cycle in the selected cells (Calado et al., 2012; Dominguez-Sola et al., 2012). Selected cells return to the

DZ, and undergo further clonal expansion and somatic hypermutation, in proportion to the amount of antigen captured and displayed to Tfh cells in the LZ (Gitlin et al., 2014, 2015). The B cells that have not been selected undergo apoptosis due to lack of survival signals (Liu et al., 1989, 1991; Mayer et al., 2017). As the GC reaction proceeds, and GC B cells go through multiple cycles of proliferation, somatic hypermutation and selection, the affinity of the B cells for the target antigen increases (Kuraoka et al., 2016; Tas et al., 2016). Gene expression profiling comparing LZ and DZ B cells showed that LZ B cells upregulate genes associated with BCR and CD40 signalling, whereas DZ B cells upregulate genes associated with mitosis (Victora et al., 2010).

The commitment to GC phenotype begins after B cells encounter antigen and begin expression of B cell lymphoma (Bcl)-6 (Kerfoot et al., 2011; Kitano et al., 2011). Bcl-6 has been described as “the master regulator of the GC reaction” (Basso and Dalla-Favera, 2010), and Bcl-6-deficient mice are unable to form GCs (Ye et al., 1997). It is a transcriptional repressor which acts to maintain the functional phenotype of GC B cells. Bcl-6 targets include: genes involved in the response to DNA damage, such as the genes encoding p53 (Phan and Dalla-Favera, 2004) and ataxia telangiectasia and Rad3-related protein (ATR) (Ranuncolo et al., 2007), which allows DNA breaks induced during somatic hypermutation to be tolerated; anti-apoptotic gene Bcl-2 (Saito et al., 2009), which allows apoptosis of B cells that are not selected (Smith et al., 2000); inhibition of plasma cell transcriptional regulator B lymphocyte-induced maturation protein-1 (Blimp-1) (Shaffer et al., 2000), which helps to maintain GC B cell phenotype until output or apoptosis; and cell cycle control genes including p27kip1 (Shaffer et al., 2000) and p21 (Phan et al., 2005), which allows rapid cell cycle progression. There

may be additional, indirect effects of Bcl-6 mediated gene repression that contribute to GC function. For example, suppression of Blimp-1, leads to increased AID expression (Shaffer et al., 2002; Minnich et al., 2016). A computation analysis has identified over 1200 genes with a predicted Bcl-6 binding site in GC B cells (Basso et al., 2010).

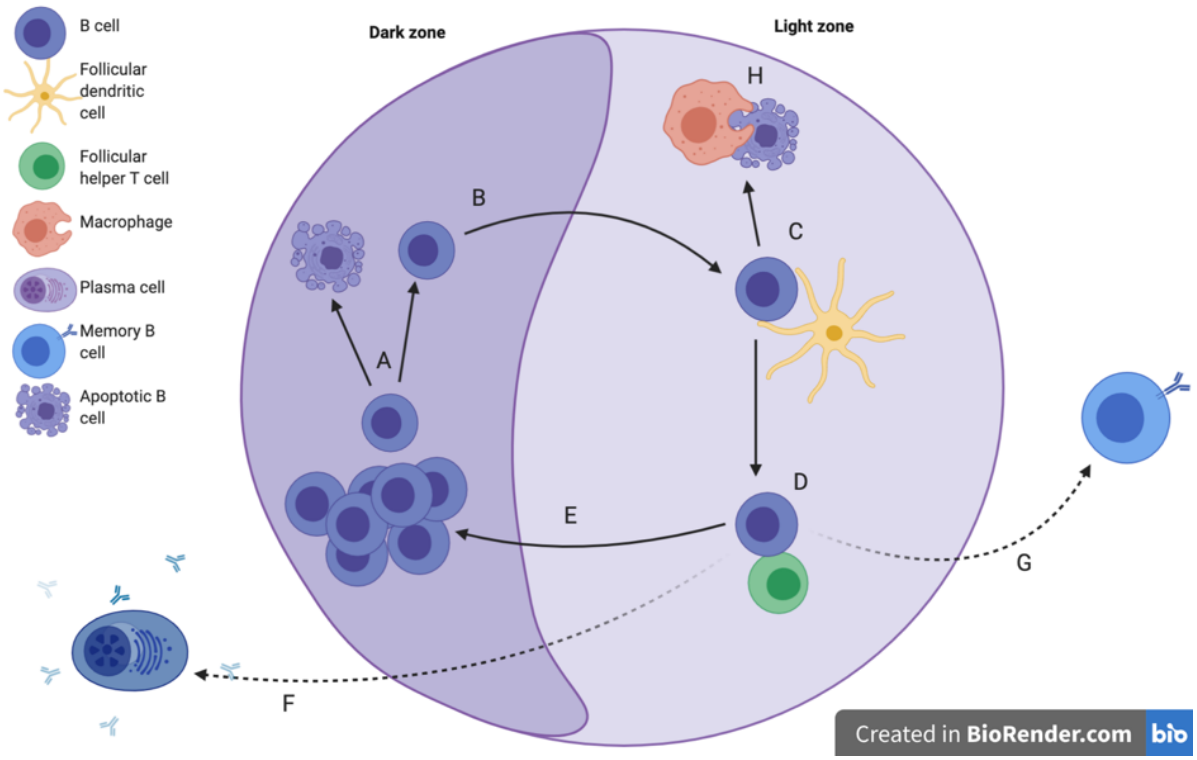

Figure 1.3. Germinal centre reaction.

Activated B cells undergo affinity maturation in a germinal centre. (A) In the dark zone B cells proliferate and undergo somatic hypermutation to introduce mutations into the variable region genes. B cells that introduce damaging mutations undergo apoptosis. (B) B cells with functional BCR migrate to the light zone, where (C) they test their newly mutated BCR by competing with other B cells to capture antigen presented by follicular dendritic cells. (D) Higher affinity B cells are selected based on the amount of antigen they can present to cognate follicular helper T cells, and the amount of T cell help they subsequently receive and upregulate Myc expression. (E) Selected B cells cycle back into the dark zone where they proliferate in proportion to the amount of T cell help they receive and undergo further cycles of somatic hypermutation and selection. (F) Selected cells may also differentiate into antibody secreting plasma cells, or (G) memory B cells. (H) B cells that are not selected in the light zone undergo apoptosis. Adapted from (MacLennan, 1994a; Zhang et al., 2016; Victora and Nussenzweig, 2022). Created in BioRender.

1.4.4 Tfh cells

Tfh cells play an important role in the selection of GC B cells. Evidence for their importance in GC reactions comes from studies where CD40:CD40L interactions were inhibited in immunised mice with anti-CD40L antibody. This resulted in inhibition of the GC response, and reduced affinity of plasma cells (Han et al., 1995a; Takahashi et al., 1998). Gene expression analysis has shown that human Tfh cells are a distinct subset from other T helper cells specialised for providing help to GC B cells (Chtanova et al., 2004). Expression of CXCR5 allows them to home to the follicles where they are positioned for interaction with B cells (Breitfeld et al., 2000; Schaerli et al., 2000). Expression of IL-21 stimulates B cells to express Bcl-6, required for the GC program (Zotos et al., 2010; Linterman et al., 2010). Tfh cells also express Bcl-6, where it is required for efficient interaction with B cells and CD40L signalling (Liu et al., 2021).

The differentiation and activation of Tfh cells is a multistep process. Antigen presentation from dendritic cells is enough to initiate the differentiation into pre-Tfh cells that upregulate CXCR5 and move in to the follicles (Goenka et al., 2011). However, further antigen-presentation from B cells is required to complete the differentiation (Barnett et al., 2014). Consequently, there is a reciprocal relationship between GC B cells and Tfh cells, where each is required for activation of the other. Antigen presentation and expression of ICOSL by B cells induces calcium signalling in Tfh cells, resulting in expression of IL-21 and IL-4 by Tfh cells and increased CD40 signalling in B cells. This causes B cells to upregulate ICOSL in a positive feedback loop (Shulman et al., 2014; Liu et al., 2015). Recently Tfh cells have been shown to undergo clonal selection within a GC reaction, with proliferation driven by the affinity of the TCR for MHC-antigen peptide complex presented by GC B cells and increased

TCR signalling (Merkenschlager et al., 2021). Therefore, the interactions between GC B cells and Tfh cells are bidirectional and complex.

1.4.5 Differentiation of GC B cells into plasma cells or memory B cells

Some of the B cells selected in the GC differentiate into either long-lived plasma cells, which secrete high-affinity antibody (Nutt et al., 2015), or memory B cells, which upon antigen re-encounter can either differentiate directly into plasma cells, or re-enter GCs (Inoue et al., 2018). Plasma cells are responsible for secretion of antibodies. The plasma cell phenotype is driven by the transcription factor Blimp-1, that upregulates genes associated with secretion of antibodies (Angelin-Duclos et al., 2000; Shaffer et al., 2002; Minnich et al., 2016; Tellier et al., 2016). Plasma cell precursors expressing Blimp-1 can be seen early in the GC reaction (Angelin-Duclos et al., 2000). The decision to differentiate to a plasma cell over a memory cell is thought to be driven by affinity with the highest affinity GC B cells becoming plasma cells (Smith et al., 1997; Phan et al., 2006; Viant et al., 2020). Signals from Tfh cells also regulate plasma cell differentiation. CD40 signalling results in the upregulation of IRF4, which acts to repress Bcl-6 (Saito et al., 2007; Ding et al., 2013), and IL-21 signalling results in expression of Blimp-1 (Ding et al., 2013; Zhang et al., 2018), however it can also induce expression of Bcl-6 (Ozaki et al., 2004). There is also a role for stromal cells in the GC; fibroblastic reticular cells at the interface between the GC and T cell zone (GTIRCs) express A Proliferation-Inducing Ligand (APRIL), which also supports plasmablast differentiation (Zhang et al., 2018).

The decision to become a memory B cell is less-well understood. It is not known what causes a B cell that is selected in the GC to become a memory B cell rather than re-cycling in the GC reaction. However, GC B cells with low affinity for antigen are more prone to becoming memory B cells (Viant et al., 2020). The lower affinity GC B cells that become memory B cells express high levels of Bach2, which is required for development of memory B cells. Bach-2 expression inversely correlated with the level of T cell help (Shinnakasu et al., 2016). Memory B cell precursors (defined by CCR6 expression) have been reported to be generally lower affinity, although some are of high affinity (Suan et al., 2017). Myc, which is expressed in positively selected GC B cells, forms a complex with a co-repressor Miz1 which acts to suppress memory B cell differentiation (Toboso-Navasa et al., 2020). However, it is likely that some T cell help is required, as GC B cells *in vitro* will not survive unless they are rescued from apoptosis by co-culturing them with GC T cells, in a CD40L-dependent manner. After receiving T cell help these cells differentiate to a memory-like phenotype (Casamayor-Palleja et al., 1996). In support of this, memory B cell precursors have been identified within a subset of Myc^{+} positively-selected GC B cells (Nakagawa et al., 2021).

One proposed model for GC B cell fate decision is that the cells that receive strong cognate T cell help will become plasma cells and those that receive weak T cell help will become memory B cells, while those that receive a moderate level of T cell help will recirculate in the GC (Inoue et al., 2018). Alternatively, the T cell signalling required for both plasma cell differentiation and recirculation may be the same, but additional signals from the environment, such as APRIL on GTIRCs, promote plasma cell differentiation (Zhang et al., 2018).

1.4.6 TI antigens

TI antigens do not require T cell help to activate the B cell. They can be split into TI-I and TI-II antigens based on whether they are capable of eliciting an immune response in X-linked immunodeficient (Xid) mice (Fairfax et al., 2008). TI-I antigens are mitogenic and activate B cells by co-stimulation of toll-like receptors (TLRs) by PAMPs, and BCRs by another epitope on the antigen. TI-II antigens are not intrinsically mitogenic. They are usually bacterial polysaccharides that most likely activate B cells by extensive cross-linking of BCRs, and are not capable of eliciting an immune response in Xid mice (Murphy et al., 2008; Fairfax et al., 2008). Extrafollicular plasma cells form in response to TI antigens, and have been reported to persist for at least 90 days (Vinuesa et al., 1999; Hsu et al., 2006). GCs may form, but they are short-lived and until recently were thought to be non-productive (Vinuesa et al., 2000; Lentz and Manser, 2001). However, it has now been shown that TI antigen-induced GCs may be productive: a recent study showed that GCs induced by a model TI-II antigen are short-lived but produce plasma cells and memory B cells which survive for at least 19 days (Liu et al., 2022), which explains why TI antigens such as pneumococcal capsular polysaccharides can be used effectively as human vaccines (Watson et al., 2002). This also provides evidence that T cells may not be required for production of plasma cells and memory B cells from GCs, and suggests that alternative signals such as BCR signalling may be important (Zhang and Toellner, 2022).

1.5 B cell receptors and signalling

Signalling through the BCR has an impact on fate decisions and differentiation of B cells at several stages of development, and during the immune response (Yam-Puc et

al., 2018). Mature naïve B cells co-express IgM and IgD BCRs by an alternative splicing mechanism, although the role of IgD is not well understood (Gutzeit et al., 2018). Following BCR ligation, B cell signalling is initiated, mediated by immunoreceptor tyrosine-based activation motif (ITAM) domains on the BCR co-receptor – a heterodimer of Igα and Igβ. Protein tyrosine kinases (PTKs) are activated, leading to recruitment and activation of adaptor proteins, and downstream signalling molecules. The signalling cascade results in release of intracellular calcium, activation of the mitogen activated protein kinase (MAPK) pathway, and transcriptional activation or regulation of NF-κB, Nuclear factor of activated T-cells (NF-AT), Forkhead Box Protein O (FoxO), ultimately leading to B cell proliferation and differentiation (Xu et al., 2014) (Figure 1.4).

Activated B cells may undergo class-switching of the BCRs to IgG, IgA or IgE isotype. Class switched B cells are able to rapidly transmit signals for efficient reactivation in a secondary immune response (Chen et al., 2015; Kurosaki et al., 2015; Palm and Henry, 2019) and they also have a selective advantage over unswitched IgM+ cells in the GC (Sundling et al., 2021). It is thought that the stronger signalling of the IgG BCR is conferred by the cytoplasmic tail (Chen et al., 2015) (Figure 1.4). The IgG BCR has a large cytoplasmic tail of 28 amino acids, compared with the 3 amino acid cytoplasmic tail of the IgM BCR (Figure 1.5) (Unanue et al., 1973). Studies have shown that IgG with a truncated cytoplasmic tail is unable to transmit signals as efficiently, resulting in an impaired antibody response (Kaisho et al., 1997). B cells that have chimeric IgM BCRs with the IgG cytoplasmic tail have enhanced calcium signalling, longer half-life, and rapidly expand and differentiate to plasma cells (Martin and Goodnow, 2002; Horikawa et al., 2007). It has also been reported that the IgG cytoplasmic tail has

intrinsic signalling ability independent of Igα/β, as B cells with the IgG cytoplasmic tail could partially rescue B cell development defects in mice with truncated Igα (Waisman et al., 2007). The increased signalling capability may be due to a conserved immunoglobulin tail tyrosine (ITT) motif. When the ITT is phosphorylated, there is increased recruitment of the adaptor protein, growth factor receptor-bound 2 (Grb2), leading to sustained protein kinase activation and B cell expansion (Engels et al., 2009). Recruitment of synapse-associated protein 97 (SAP97) has also been shown to be important for the heightened signalling capabilities of the IgG cytoplasmic tail, resulting in enhanced oligomerisation of BCRs into microclusters, and more robust calcium responses. Recruitment of SAP97 was independent of the ITT (Liu et al., 2010, 2012). Recent work has however shown a potential role for the IgG1 extracellular region in enhanced BCR signalling. Using a series of BCR mutants, Sundling et al. (2021) showed that the ability of IgG1+ B cells to outcompete IgM+ B cells in the GC was not dependent on the presence of the IgG1+ cytoplasmic tail. It was postulated that the increased flexibility of the IgG1 hinge region may allow increased contact with antigen.

In summary, the IgG cytoplasmic tail is thought to confer enhanced BCR signalling capabilities, which allows a rapid secondary immune response. However, there may also be a role for the IgG extracellular region in the increased activity.

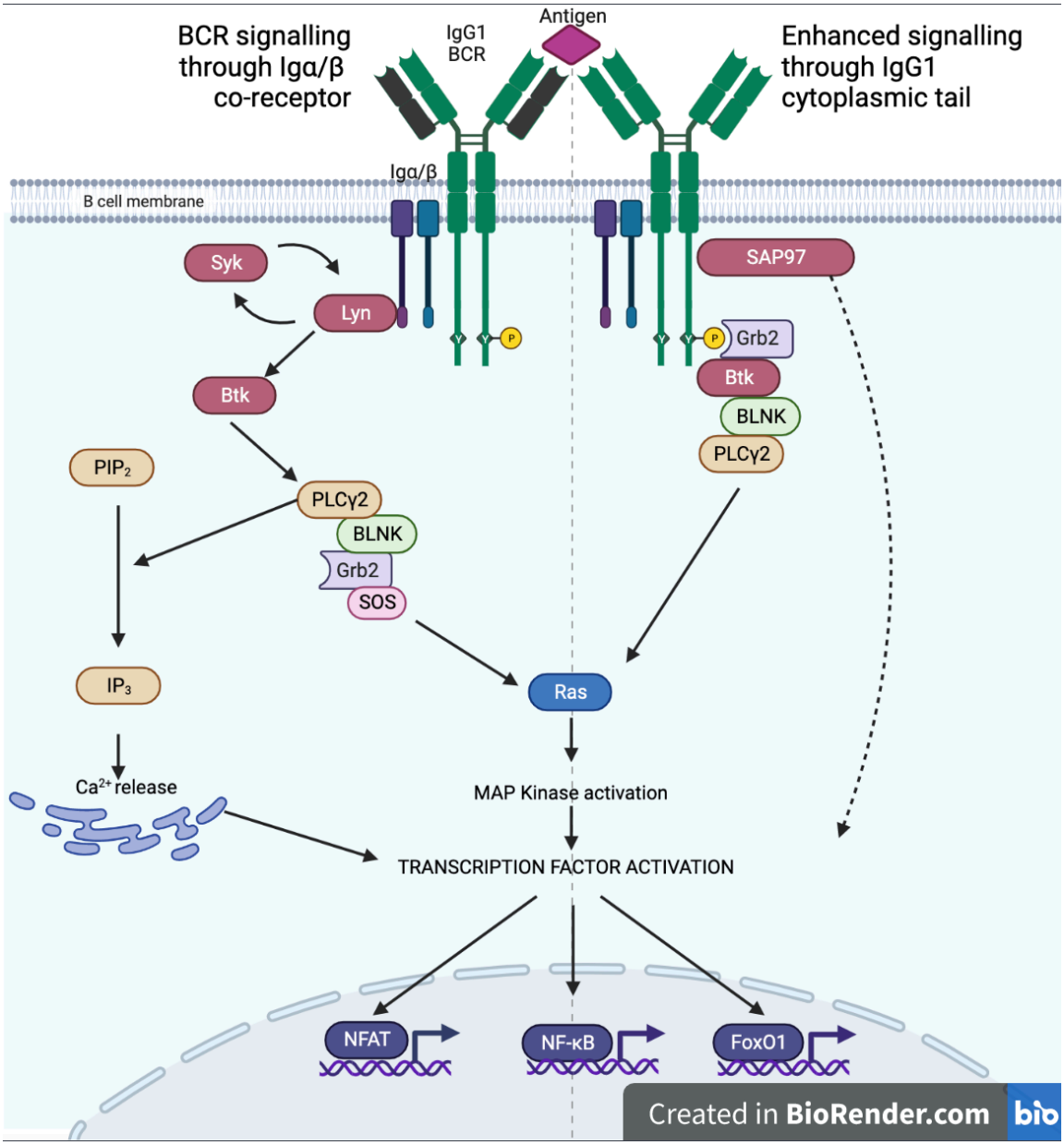

Figure 1.4 BCR signalling pathways downstream of the BCR and enhanced signalling mediated by the IgG1 cytoplasmic tail.

Left – a simplified schematic showing signalling pathway directly downstream of the BCR, mediated by the Igα/β co-receptor. Protein tyrosine kinases (PTKs) Syk, Lyn and Bruton's tyrosine kinase (Btk) are activated and phosphorylate adaptor proteins including Grb2 and Blnk, forming the membrane-proximal signalosome. Phospholipase Cγ2 (PLCγ2) is recruited and hydrolyses phosphatidylinositol 4,5-biphosphate (PIP_2) to inositol 1,4,5-trisphosphate (IP_3), which results in release on intracellular calcium. The signalosome activates Ras, which activates the Mitogen activated protein kinase (MAPK) cascade. The signalling results in activation of transcription factors Nuclear factor of activated T-cells (NFAT), Nuclear factor kappa-light-chain-enhancer of activated B cells (NF-κB) and Forkhead Box Protein O (FoxO1). Right – schematic showing enhanced signalling mediated by the IgG1 cytoplasmic tail. Adapter protein Grb2 can be recruited directly to the phosphorylated immunoglobulin tail tyrosine (ITT) residue. Synapse associated protein 97 (SAP97) can be recruited in a mechanism independent of the ITT, and also contributes to enhanced signalling via an unknown mechanism. Adapted from Xu et al., 2014 and Chen et al., 2015. Created in Biorender.

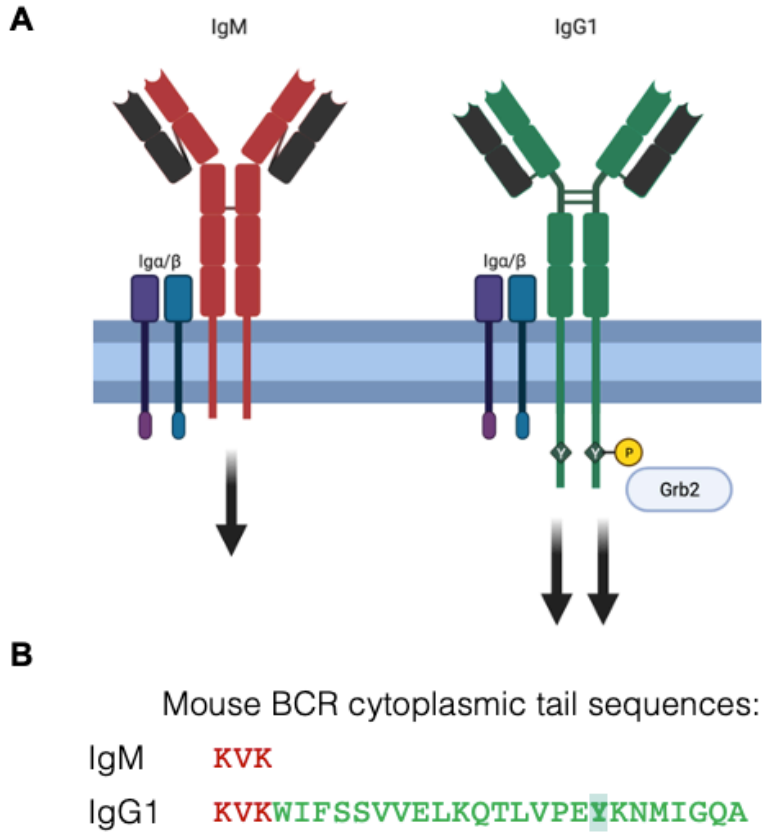

Figure 1.5. IgM and IgG1 B cell receptors.

(A) Schematic of IgM and IgG1 B cell receptors (BCRs). IgM B cell has a short cytoplasmic tail and mediates BCR signalling through the Igα/β co-receptor. IgG1 has a longer cytoplasmic tail, which has additional signalling capabilities independent of Igα/β, for example immunoglobulin tail tyrosine (ITT) motif, allowing induction of a stronger BCR signal. Adapted from Chen et al. (2015). Created in BioRender. (B) Comparison of IgM and IgG1 cytoplasmic tail amino acid sequences, with ITT residue on IgG1 highlighted in green box.

1.6 Tolerance and autoimmunity

A crucial aspect of immunity is the ability to differentiate between foreign and self. Immune cells should not respond to normal tissues. B cells are made self-tolerant by shaping the BCR repertoire to ensure that self-reactive B cells are eliminated or controlled. This mainly occurs at three stages: (i) central tolerance in the bone marrow during B cell development; (ii) peripheral tolerance of B cells that have left the bone marrow as immature B cells; (iii) negative selection of B cells that acquire mutations

that make them self-reactive in the GC (Murphy et al., 2008). These tolerance mechanisms are in place to prevent development of autoantibodies specific to self-antigens.

During B cell development in the bone marrow, immature B cells test their newly generated BCR for binding to self-antigens. B cells that encounter signal through their BCR will be controlled by either receptor editing, clonal anergy, or clonal deletion. Clonal deletion is where the autoreactive B cells are developmentally arrested, and then undergo cell death by apoptosis (Nemazee and Bürki, 1989; Hartley et al., 1993). Receptor editing involves activation of RAG enzymes and induction of further rearrangements of the light chain gene segments, to try and remove the autoreactivity (Gay et al., 1993; Tiegs et al., 1993; Halverson et al., 2004; Nemazee, 2006). If receptor editing fails to remove autoreactivity, cells default to clonal deletion (Halverson et al., 2004). Clonal anergy is where the autoreactive B cells survive but are left in an inactive state. They downregulate surface IgM BCR, and respond less efficiently to antigen stimulation (Goodnow et al., 1988; Merrell et al., 2006; Quách et al., 2011; Zikherman et al., 2012; Cambier et al., 2007).

Once they have migrated from the bone marrow, immature B cells can still be tested for autoreactivity in the periphery. This is important for tissue-specific antigens which are not present in the bone marrow. B cells autoreactive to tissue-specific antigens undergo clonal deletion (Russell et al., 1991; Ota et al., 2011; Shukla et al., 2019). Induction of clonal anergy in mature autoreactive B cells in the periphery, after encounter with self-antigen, has also been reported (Goodnow et al., 1989; Hartley et

al., 1991). The fate of an autoreactive B cell to undergo clonal deletion or clonal anergy may depend on the type of antigen, and BCR occupancy (Hartley et al., 1991).

The process of somatic hypermutation in the GC gives a potential risk of producing autoreactive B cells. Negative selection within the GC has been demonstrated, in which GC B cells which acquire mutations that increase self-reactivity are deleted depending on expression of the self-antigen within, or proximal to, the GC (Chan et al., 2012). Experiments where soluble antigen was injected at the peak of the GC response, to model acquisition of self-reactivity in the GC, resulted in apoptosis of specific GC B cells (Shokat and Goodnow, 1995; Pulendran et al., 1995). Further evidence for a mechanism of selection against autoreactive B cells in GCs comes from experiments in a mouse model of B cell anergy which showed that self-reactive B cells may be recruited into GCs but acquire mutations that reduce their affinity to self-antigen (Burnett et al., 2018). It is possible that this is driven by an inability of self-reactive B cells to receive T cell help from cognate T cells because self-peptide-specific T cells are negatively selected during T cell development (Daley et al., 2017). Apoptotic clearance of GC B cells by tingible body macrophages may play a role in removal of GC B cells that acquire self-reactivity, as mice with impaired apoptosis by tingible body macrophages produce increased antibody secreting cells and develop autoimmune disease (Rahman et al., 2010), and a subgroup of patients with the autoimmune disease systemic lupus erythematosus (SLE) have reduced tingible body macrophages and reduced clearance of apoptotic GC B cells (Baumann et al., 2002). Self-reactive B cells that do emerge from the GC may also later undergo negative selection: apoptosis in post-GC memory B cells and plasma cells has been shown to have a role in prevention of autoantibodies (Mayer et al., 2020).

Self-reactive B cells that evade these tolerance checkpoints may differentiate into plasma cells that secrete self-reactive autoantibodies that contribute to autoimmune diseases. There are over 100 autoimmune diseases where the immune system has made an inappropriate response to the body's own cells and tissues, because of a failure of B and T cell tolerance (Wang et al., 2015). Autoantibodies are a feature of many autoimmune diseases, including SLE, rheumatoid arthritis (RA) and type I diabetes (T1D). They may arise due to pathogens using molecular mimicry. For example, infection by *Yersinia enterocolitica* may drive the expansion and affinity-maturation of anti-thyrotropin receptor antibodies in Grave's disease (Hargreaves et al., 2013). Alternatively, affinity maturation of autoantibodies may be driven by the self-antigen itself. For example, a study showed that a panel of anti-granulocyte macrophage-colony-stimulating factor (GM-CSF) antibodies isolated from idiopathic pulmonary alveolar proteinosis patients bound to 4 distinct, non-overlapping epitopes so were likely driven by affinity maturation to GM-CSF, rather than a pathogen using molecular mimicry (Wang et al., 2013). Neo-antigens or neo-epitopes can drive autoantibody production. For example, antibodies to abnormally post-translationally modified proteins are common in RA (Sebbag et al., 2009); and it is thought that accumulation of apoptotic cells and cell debris in the GC may reveal DNA and associated nuclear-proteins, and drive production of the anti-nuclear antibodies that are characteristic of SLE (Brink, 2014). Autoantibodies may contribute to the pathogenesis of autoimmune diseases by directly binding to self-antigens, or alternatively may form immune complexes which engage complement or FcRs, and induce inflammation (Martin and Chan, 2004).

Interestingly, although self-reactive B-2 cells undergo negative selection during B cell development, there is evidence that B-1a cells undergo positive selection for self-reactivity during their development. The B-1a cell BCR repertoire is enriched for "evolutionary useful specificities" (Baumgarth, 2011) against common bacterial antigens, but is also skewed towards self-reactivity, for example to self-antigens such as phosphatidylcholine (PtC). In one study mice were generated that were transgenic for a self-reactive anti-Thy-1 BCR and crossed with either Thy-1-deficient mice or wildtype (Thy-1$^+$) mice. The Thy-1$^+$ mice had a large population of Thy-1-specific peritoneal cavity B cells that were absent in the Thy-1 deficient mice (Hayakawa et al., 1999). Another study used a model of weak or strong constitutive BCR signalling. The mice with weak constitutive signalling mainly generated B-2 cells but the mice with strong constitutive signalling mainly generated B-1 cells (Casola et al., 2004). The differences in B-1 cell BCR-mediated selection may be related to differences in their development. B-1 cell development appears to bypass expression of the surrogate light chain and the pre-BCR stage through promotion of kappa gene recombination at the early pro-B cell stage (Wong et al., 2019). Due to the high degree of self-reactivity in the B-1a cell repertoire, they are often implicated in autoimmunity (Duan and Morel, 2006).

1.7 B cell anergy

Anergic B cells are self-reactive B cells that are not eliminated by apoptosis but are maintained in an inactive state and do not respond to antigenic stimulation. It may be the main mechanism of B cell tolerance, with as many as 50% of the newly produced B cells becoming anergic (Merrell et al., 2006). It is thought that anergy is induced by

chronic BCR stimulation due to constant occupancy of the BCR by self-antigen. This may result in altered BCR signalling. For example, a negative regulator of BCR signalling, Lyn, may be activated, resulting in increased phosphorylation of Lyn targets, Src homology 2 domain containing inositol polyphosphate 5-phosphatase 1 (SHIP-1) and Docking protein 1 (DOK1). Other negative regulators of BCR signalling such as Src homology region 2 domain-containing phosphatase-1 (SHP-1) and Phosphatase and tensin homolog (PTEN) may also be involved (Yarkoni et al., 2010).

Inappropriate activation of self-reactive anergic B cells may contribute to autoimmune disease. For example, SLE is associated with N-acetyllactosamine-specific 9G4 autoantibodies. B cells bearing this BCR are present in healthy humans, but they are in an anergic state and are excluded from GCs. However in SLE patients, 9G4 B cells are not anergic and are expanded within GCs as well as within the plasma cell and memory B cell compartments (Cappione et al., 2005).

Until recently, it was not clear why the immune system has evolved to keep self-reactive B cells around with the risk of inappropriate inactivation leading to autoimmunity. However, it has now been shown that anergic B cells can be recruited into GCs and reactivated if they receive BCR signalling above a certain activation threshold. Once in the GC they acquire mutations that reduce affinity to self-antigen, and increase affinity to foreign antigen (Sabouri et al., 2014; Reed et al., 2016; Burnett et al., 2018). This has been termed ‘clonal redemption’. Therefore, the purpose of maintaining self-reactive B cells in a state of anergy may be so that they are able to respond more rapidly to pathogens that mimic self-proteins (Burnett et al., 2018, 2019). The identification of rare broadly neutralising antibodies in HIV patients that are cross-

reactive with the phospholipid cardiolipin is an example of the evolutionary benefit of having B cells with self-reactive BCRs (Haynes et al., 2005).

1.8 Models of B cell anergy

B cell anergy has been predominantly studied using transgenic models in which B cells are transgenic for a BCR specific for a self-antigen (Cambier et al., 2007). One of the first described anergy models was a double transgenic mouse that expresses soluble hen egg lysozyme (HEL) as a self-antigen and an anti-HEL BCR (MD4 x ML5 mouse) (Goodnow et al., 1988) and has since become one of the most commonly used models for investigating B cell anergy. B cells in these mice have reduced levels of surface IgM (but normal levels of IgD) and are unable to secrete anti-HEL antibody. Anti-DNA BCR transgenic mice are also commonly used to study anergy. For example, Erikson et al. (1991) found that B cells from mice transgenic for anti-DNA BCR could bind to DNA but were developmentally arrested and failed to secrete anti-DNA antibody. A p-azophenylarsonate (Ars)-specific BCR mouse model (Ars/A1) has anergic B cells due to cross-reactivity with DNA. These mice make a reduced primary response to Ars, and the B cells have impaired calcium flux following BCR stimulation (Benschop et al., 2001). Other transgenic BCR models of anergy include the low affinity anti-Smith antigen (Sm) BCR model, in which the anti-Sm B cells are long-lived B-2 cells but fail to respond to LPS stimulation in vitro (Borrero and Clarke, 2002), and the anti-insulin BCR model, in which the anti-insulin B cells fail to take part in a TD response or secrete anti-insulin antibody following immunisation (Rojas et al., 2001). The commonly recognised characteristics of anergic B cells have been elucidated from a combination of these anergy models. They tend to downregulate surface IgM expression, are

developmentally arrested, are excluded from B cell follicles, are often described as having a decreased lifespan, and have defects in antigen-stimulated activation, for example calcium flux and protein phosphorylation (Cambier et al., 2007).

However, transgenic BCR models are limited by the fact that the anergic B cells have monoclonal specificity, and may not reflect the biology of natural, anergic B cells in a polyclonal environment. Self-reactive B cells have been estimated to make up 10-20% of the mature B cell repertoire of healthy humans (Wardemann et al., 2003; Watanabe et al., 2019), indicating that self-reactive anergic B cells may make up a surprisingly large proportion of mature B cells. In mice, a natural population of anergic B cells has been described, which have low expression of IgM, do not respond to BCR stimulation, and are enriched for self-reactivity (Merrell et al., 2006). These cells phenotypically resemble transitional 3 (T3) B cells, which have been suggested to be the natural anergic B cell population. An additional natural anergic B cell subset, $CD93^{-}$ IgD^{hi} $IgM^{-/lo}$, has been identified which also has low IgM expression, has reduced calcium response to BCR stimulation and is enriched for autoreactivity. This subset is longer lived than the $CD93^{+}$ T3 cells (Nojima et al., 2020).

Recently our lab has generated a mouse model that has altered BCR signalling due to replacement of the IgM cytoplasmic tail with the IgG1 cytoplasmic tail, resulting in a chimeric IgMg1 BCR with hyperactive BCR signalling. Experiments with the IgMg1 mice indicated that the B cells were functionally anergic due to increased negative selection during B cell development. Evidence for this included reduced IgM expression, reduced calcium flux and reduced phosphorylation of proteins downstream of BCR in response to BCR stimulation in vitro, and impaired ability to take part in TI

responses. However, they were able to take part in TD responses, supporting the role of T cell help in the activation of anergic B cells (Zhang, 2019). This model potentially provides a new system for investigating the activation of anergic B cells within a polyclonal repertoire. Additionally, early experiments indicated that the IgMg1 mice developed autoantibodies as they aged, suggesting the model may be suitable for investigation of how anergic, self-reactive B cells can be activated and cause autoimmunity.

1.9 Thesis aims

BCR signalling plays an important role of almost all stages of B cell development and activation. Alterations to the strength of BCR signalling therefore have an impact on different B cell populations, their ability to take part in immune responses and the fate of cells that become activated. Our lab has previously described a mouse model which has the IgM cytoplasmic tail replaced with the IgG1 cytoplasmic tail resulting in a chimeric IgMg1 BCR. It was expected that the IgG1 cytoplasmic tail would confer hyperactive signalling due to the inherent signalling motifs, and that this would allow the mice to induce a more sensitive B cell response. However, surprisingly, the IgMg1 B cells had a phenotype reminiscent of B cell anergy. IgMg1 mice had a significant reduction in marginal zone B cells, and there was increased usage of the lambda light chain in mature B cells, which is evidence of increased receptor editing during B cell development. Despite the anergic B cell phenotype, IgMg1 mice appeared to develop autoantibodies with ageing (Zhang, 2019).

The IgH$^{\gamma 1 \mu}$ (IgG1M) mouse model is another mouse model with altered BCR signalling. IgG1 is the sole BCR expressed by B cells in this model at all stages of development (Waisman et al., 2007). As the mice express BCR with the IgG1 extracellular region and transmembrane region in addition to the cytoplasmic tail, comparing B cell development and activation in these mice with the IgMg1 mice will reveal the relative importance of the different regions of the BCR for BCR signalling in different contexts.

The general aims of this thesis are to:

1. Investigate B cell populations in IgMg1 and IgG1M mice to assess roles of IgM cytoplasmic or extracellular regions in BCR signalling and function at different phases of B cell development, and in development of B cell anergy.
2. Investigate T cell independent and GC responses in IgMg1 and IgG1M mice to gain insights into anergic B cell participation in GCs, and the roles of BCR signalling during B cell activation.
3. Investigate the development of autoantibodies and autoimmunity in IgMg1 mice to determine the role of BCR signalling in breaking tolerance.

Chapter 2. Materials and Methods

2.1 Mice

Mice were bred and maintained under specific pathogen-free conditions at the Biomedical Services Unit, University of Birmingham. All animal experiments were approved by the institutional ethics committee and the Home Office UK (project license: PP8702596). IgMg1 C57BL/6N mice were generated by Medimmune (construction detailed in Zhang (2019)) and were homozygous for IgMg1 allele. $IgH^{\gamma 1\mu}$ mice (referred to as IgG1M in this thesis) have been previously described (Waisman et al., 2007) and were homozygous for the $IgH^{\gamma 1\mu}$ allele. C57BL/6N mice were used as wildtype (WT) controls. Nr4a3-Tocky mice were obtained from Professor David Bending (University of Birmingham) (Bending et al., 2018) and were bred with IgMg1 mice or WT mice to generate mice homozygous for the IgMg1 or WT IgM allele and either heterozygous or homozygous for Nr4a3-Tocky allele. Genotyping was performed by Transnetyx (Cordova, TN), and zygosity for Nr4a3-Tocky was determined from the PCR raw data signal.

For aged mice experiments, mice were aged until 12-18 months old. For other experiments, 8-16 week-old mice were used. For all experiments, groups of mice were age-matched and sex-matched as much as allowed by availability of mice. At the end of experiments, mice were culled by schedule 1 method. If sera were required for analysis, mice were bled to exsanguination by cardiac puncture under anaesthetic prior to schedule 1. To isolate peritoneal cavity cells, Dulbecco's phosphate buffered saline pH 7.1-7.5 (D-PBS) (Sigma D8537-500ML) was injected into the peritoneal cavity, and

the peritoneum was massaged to dislodge cells, and then the peritoneal cavity fluid was removed. Other tissues (spleen, popliteal lymph nodes, bone marrow, kidneys, pancreas, liver, intestines) were dissected from the mice for analysis as required.

2.2 Immunisations

2.2.1 T cell-independent type II response

For immunisations to induce a T cell-independent type II (TI-II) response, mice were immunised with 30 µg soluble (4-hydroxy-3-nitrophenyl)-acetyl (NP)-Ficoll intraperitoneally (i.p.) (total volume 200 µL).

2.2.2 T cell-dependent response

For immunisations to induce a T cell-dependent response localised to the popliteal lymph node, mice were immunised subcutaneously (s.c.) on the plantar surface of one foot with 10 µg alum precipitated antigen (described in section 2.4) and $5x10^6$ heat inactivated *Bordetella pertussis* (total volume of 20 µL). For boost immunisations, mice were injected s.c. into the plantar surface of the same foot with 10 µg soluble antigen, without adjuvants (total volume of 20 µL).

2.2.3 Collagen-induced arthritis model

Collagen-induced arthritis (CIA) model was performed in collaboration with Professor Adam Croft's group (Institute of Inflammation and Ageing, University of Birmingham), under Home Office project license PP6493771. These immunisations were performed

by Charlotte Smith and Samuel Kemble (Institute of Inflammation and Ageing, University of Birmingham). Mice received an initial inoculation of 100 µg chicken collagen type II/complete Freund's adjuvant (CFA) s.c. at the base of the tail. After 21 days, mice received a booster injection of chicken collagen type II/incomplete Freund's adjuvant (IFA) s.c. at the base of the tail. Mice were bled via saphenous vein bleed at days 15, 21, and 23. Mice were culled by schedule 1 method at day 26 with blood collected via cardiac puncture or saphenous vein bleed.

Table 2.1 Antigens used for immunisations

Antigen	Source	Catalogue Number
Chicken collagen type II	Chrondex (used for TD response immunisations)	20012
Chicken collagen type II	Sigma (used for CIA-model)	C9301-25MG
NP_{18}-chicken gamma globulin (CGG)	In-house	N/A
NP_{24}-keyhole limpet hemocyanin (KLH) or NP_{32}-KLH	Biosearch	N-5060-5
NP_{27}-KLH	In-house	N/A
NP-Ficoll	Biosearch	F-1420-100MG

2.3 NP-conjugation

For preparation of NP-KLH and NP-bovine serum albumin (BSA), KLH powder (Merck Millipore 374805-250MG) or BSA powder (Sigma A7906-100G) were dissolved in freshly made 0.2 M $NaHCO_3$ (Sigma 55761-1KG) at 2 mg/mL. 4-Hydroxy-3-nitrophenylacetic acid Succinimide Ester (NP-OSu) (Biosearch N-1010) dissolved in dimethyl sulfoxide (DMSO) (Sigma D4818-50ML) was added dropwise to the protein while stirring constantly. This mixture was then incubated on a rotator for 2 hours at

room temperature, protected from light. The protein was then dialysed (with 3 buffer changes in $NaHCO_3$ and 2 changes in phosphate buffered saline pH 7.45 (PBS) (Gibco 18912-014)) using a 10K molecular weight cut-off Slide-A-Lyzer dialysis cassette (Thermo Scientific) at 4 °C, protected from light. Following dialysis, the recovered protein was quantified using Pierce bicinchoninic acid (BCA) Protein Assay kit. The absorbance was measured at 430 nm using a Nanodrop 1000 (Thermo Scientific), and from this the concentration of NP was calculated using Beer's law.

$$\text{Concentration (M)} = \frac{\text{absorbance at 430 nm}}{\varepsilon \times L} = \frac{\text{absorbance at 430 nm}}{4230\ \text{M}^{-1}\ \text{cm}^{-1} \times 1\ \text{cm}}$$

The conjugation ratio was then determined from the ratio of the molar concentration of NP to the molar concentration of the protein.

2.4 Alum precipitation

For primary immunisations the protein was precipitated in aluminium potassium sulphate (alum) (Fisher Chemical A/2400/53). The protein was mixed 1:1 with 9% alum and the pH was adjusted to 6.5-7 using 10 M sodium hydroxide (Sigma S5881-1KG). The protein was then incubated for 1 hour at room temperature (protected from light) on a rotator. The protein was centrifuged for 5 min at 5000 rpm and the pellet was washed with PBS. The protein was then centrifuged for 5 min at 5000 rpm and the pellet was resuspended in PBS at 10 µg per 20µL for s.c. injections, or at 50 µg per 200 µL for i.p. injections.

2.5 Flow cytometry

2.5.1 Single cell preparation

For flow cytometry analysis, tissues were first processed into a single cell suspension in RPMI 1640 medium (Gibco 21875-034). Spleens were mashed up through a 70 µm strainer (BD Biosciences) with the end of a plunger from a syringe; lymph nodes and Peyer's patches were lacerated using 25-gauge needles (Terumo); and bone marrow was flushed from femurs using a syringe with 25-gauge needle. Cells were then filtered through 70 µm cell strainers to ensure single cell suspensions. The cells were then centrifuged at 1400 rpm for 5 min at 4 °C. Lymph node or Peyer's patches cells were resuspended in flow cytometry buffer (Table 2.4); spleen, bone marrow or peritoneal cavity cells were resuspended in 1-2 mL Ammonium-Chloride-Potassium (ACK) buffer (Sigma A10492-01) for red blood cell lysis for 3 min, before adding the same volume of PBS to neutralise the reaction. Cells were then centrifuged and resuspended in flow cytometry buffer.

2.5.2 Surface staining

For surface staining, cells were transferred to a 96-well V-bottom plate (Thermo 277143). Cells were first incubated for 20 min with 50 µL purified rat anti-CD16/32 antibody (Thermo Fisher Scientific 14-0161-82) (diluted 1/200 in flow cytometry buffer) to block non-specific Fc binding. If required, they were then incubated with 50 µL biotinylated antibody for 20 min. The cells were then incubated with 50 µL of fluorescence-conjugated surface antibody cocktail, including streptavidin conjugate, for 20 min. Cells were then stained with 50 µL LIVE/DEAD fixable near-IR dead cell stain (Thermo Fisher Scientific L10119) (diluted 1/1000 in PBS) for 20 min. In some

experiments, cells were fixed by incubating with 50 µL BD Cytofix Fixation Buffer (BD Biosciences 554655) to allow acquisition the following day. After staining, cells were suspended in 200 µl flow cytometry buffer and filtered through 70 µm cell strainer into flow cytometry tubes. Antibodies used for staining are detailed in Table 2.2. All incubations were performed on ice and protected from light. Between incubations, cells were washed by suspending in 100 µl flow cytometry buffer, centrifuging (1400 rpm, 5 min, 4 °C) and discarding supernatant.

For staining of Tfh cells, cells were first incubated with purified anti-rat CXCR5 antibody (diluted 1/125 in flow cytometry buffer) for 60 min. Cells were then incubated with a donkey anti-rat AF647 secondary antibody (diluted 1/400 in flow cytometry buffer) for 30 min, and then 10% normal rat serum (Sigma R9759-5ML) (diluted in flow cytometry buffer) for 20 min. Staining then proceeded as above with the fluorescence-conjugated antibody cocktail incubation steps.

2.5.3 Intracellular staining

In some experiments, cells were stained for intracellular markers using Foxp3 transcription factor staining kit (eBioscience 00-5523-00). Following staining with surface markers and near-IR viability stain as described above, cells were washed and resuspended in Foxp3 fixation/permeabilization working solution. Cells were incubated for 30 min at 4 °C and then washed twice with 1x Foxp3 permeabilization buffer. Cells were incubated with 100 µL purified rat anti-CD16/32 antibody (diluted 1/200 in permeabilization buffer) for 15 min at room temperature protected from light. Without washing, the required amount of intracellular antibody was added to the cells and

incubated for 1 hour at room temperature. After incubation cells were again washed twice in permeabilization buffer. If required, cells were incubated with 100 µL streptavidin conjugate (diluted in permeabilization buffer) at room temperature for 30 min and washed twice in permeabilization buffer. Cells were resuspended in 200 µL flow cytometry buffer and then filtered through 70 µm cell strainers into flow cytometry tubes.

2.5.4 Acquisition and data analysis

Stained cells were acquired on Fortessa X20 (BD Biosciences) using FACS Diva software. Single colour controls were acquired for compensation. Data was analysed using FlowJo (BD Biosciences; version 10.8.1).

To perform tSNE analysis (Van Der Maaten and Hinton, 2008) on the peritoneal cavity flow cytometry data, B cells from each sample were downsampled and concatenated so that 15,000 B cells from each genotype were in one single FCS file. FlowJo was used to perform t-distributed stochastic neighbour embedding (tSNE) analysis with default parameters. Genotypes were re-separated within the concatenated file by sample number.

2.5.5 Antibodies used for flow cytometry

Antibodies used for flow cytometry experiments are detailed in Table 2.2.

Table 2.2 Antibodies used for flow cytometry

Antibody specificity	Conjugate	Isotype	Clone	Supplier	Catalogue Number	Dilution
Active Caspase-3 (intracellular)	FITC	Rabbit	Polyclonal	BD Biosciences	550480	20 µL per sample
B220	biotin	Rat IgG2a, κ	RA3-6B2	eBioscience	13-0452-85	1/300
B220	BUV395	Rat IgG2a, κ	RA3-6B2	BD Biosciences	563793	1/800
B220	BUV510	Rat IgG2a, κ	RA3-6B2	Biolegend	103247	1/200
B220	PE-CF594	Rat IgG2a, κ	RA3-6B2	BD Biosciences	562313	1/500
B220	PerCP-Cy5.5	Rat IgG2a, κ	RA3-6B2	BD Biosciences	552771	1/200
BP-1 (CD249)	PE	Mouse IgG2a, κ	BP-1	BD Biosciences	553735	1/100
CD3	BUV395	Rat IgG2b, κ	17A2	BD Biosciences	740268	1/300
CD3	BV510	Rat IgG2b, κ	17A2	Biolegend	100233	1/100
CD3	FITC	Armenian Hamster IgG1, κ	145-2C11	eBioscience	11-0031-82	1/100-1/200
CD3	PE	Armenian Hamster IgG1, κ	145-2C11	BD Biosciences	553064	1/50
CD3	PE-Cy5	Armenian Hamster IgG1, κ	145-2C11	eBioscience	15-0031-83	1/200
CD3	PerCP-Cy5.5	Armenian Hamster IgG1, κ	145-2C11	BD Biosciences	551163	1/200
CD4	BV421	Rat IgG2b, κ	GK1.5	Biolegend	100438	1/400
CD4	FITC	Rat IgG2b, κ	GK1.5	eBioscience	11-0041-85	1/100
CD5	AF700	Rat IgG2a, κ	53-7.3	Biolegend	100636	1/400
CD5	APC	Rat IgG2a, κ	53-7.3	eBioscience	45-0051-82	1/800-1/1000

Antibody specificity	Conjugate	Isotype	Clone	Supplier	Catalogue Number	Dilution
CD5	PE-Cy5	Rat IgG2a, κ	53-7.3	BD Biosciences	553024	1/400
CD5	PerCP-Cy5.5	Rat IgG2a, κ	53-7.3	eBioscience	45-0051-82	1/400
CD8	FITC	Rat IgG2a, κ	53-6.7	eBioscience	11-0081-85	1/100
CD8	PE	Rat IgG2a, κ	53-6.7	eBioscience	12-0081-83	1/200
CD8	PerCP-Cy5.5	Rat IgG2a, κ	53-6.7	eBioscience	45-0081-82	1/200
CD11b	BV510	Rat IgG2b, κ	M1/70	Biolegend	101245	1/500
CD11c	PE-Cy7	Armenian Hamster IgG1, λ2	HL3	BD Biosciences	558079	1/300
CD19	AF700	Rat IgG2a, κ	6D5	Biolegend	115527	1/100
CD19	BUV737	Rat IgG2a, κ	1D3	BD Biosciences	612781	1/800
CD19	eF450	Rat IgG2a, κ	1D3	eBioscience	48-0193-82	1/200
CD21/35	BV605	Rat IgG2b, κ	7G6	BD Biosciences	563176	1/400
CD23	PE-Cy7	Rat IgG2a, κ	B3B4	eBioscience	25-0232-82	1/1000
CD24	BV510	Rat IgG2c, κ	M1/69	Biolegend	101831	1/200
CD25	PE-Cy7	Rat IgG1	PC61.5	eBioscience	25-0251-82	1/100
CD38	AF700	Rat IgG2a, κ	90	eBioscience	56-0381-82	1/600
CD38	BUV737	Rat IgG2a, κ	90	BD Bioscience	741748	1/400
CD38	PerCP-Cy5.5	Rat IgG2a, κ	90	Biolegend	102772	1/300
CD43	Biotin	Rat IgG2a, κ	S7	BD Bioscience	553269	1/200
CD44	PerCP-Cy5.5	Rat IgG2b, κ	IM7	eBioscience	45-0041-82	1/300
CD62L	AF700	Rat IgG2a, κ	MEL-14	Biolegend	104426	1/400
CD62L	BV510	Rat IgG2a, κ	MEL-14	Biolegend	104441	1/200

Antibody specificity	Conjugate	Isotype	Clone	Supplier	Catalogue Number	Dilution
CD86	PE	Rat IgG2a, κ	GL1	eBioscience	12-0862-81	1/200
CD86	PE-Cy5	Rat IgG2a, κ	GL1	eBioscience	12-0862-82	1/200
CD93	FITC	Rat IgG2b, κ	AA4.1	eBioscience	11-5892-82	1/100
CD93	PerCP-Cy5.5	Rat IgG2b, κ	AA4.1	Biolegend	136512	1/100
CD95 (Fas)	BV605	Armenian Hamster IgG2, λ2	Jo2	BD Biosciences	740367	1/400
CD95 (Fas)	PE-Cy7	Armenian Hamster IgG2, λ2	Jo2	BD Biosciences	557653	1/200
CD138	BV711	Rat IgG2a, κ	281-2	Biolegend	142519	1/300
CXCR4	APC	Rat IgG2b, κ	2B11	eBioscience	17-9991-82	1/100
CXCR4	biotin	Rat IgG2b, κ	2B11	eBioscience	13-9991-82	1/100
CXCR5	purified	Rat IgG2a, κ	2G8	BD Biosciences	551961	1/125
Enolase 1	FITC	Mouse IgG1, κ	A-5	Santa Cruz	sc-271384 FITC	1/50
Foxp3 (intracellular)	biotin	Rat IgG2a, κ	FJK-16s	eBioscience	13-5773-82	1 µL per sample
Gr-1	FITC	Rat IgG2b, κ	RB6-8C5	eBioscience	11-5931-85	1/100
Gr-1	PE	Rat IgG2b, κ	RB6-8C5	eBioscience	12-5931-83	1/300
IgD	BV421	Rat IgG2a, κ	11-26c	Biolegend	405275	1/400
IgD	APC	Rat IgG2a, κ	11-26c	eBioscience	17-5993-82	1/500
IgG1	APC	Rat IgG1, κ	X56	BD Biosciences	550874	1/500
IgG1	PerCP-Cy5.5	Rat IgG	RMG1 1	Biolegend	406612	1/400
IgG3	FITC	Rat IgG2a, κ	R4082	BD Biosciences	553403	1/400
IgM	APC-eFluor780	Rat IgG2a, κ	II/41	eBioscience	47-5790-82	1/400

Antibody specificity	Conjugate	Isotype	Clone	Supplier	Catalogue Number	Dilution
IgM	PE-Cy5	Rat IgG2a, κ	II/41	eBioscience	15-5790	1/1000
IgM	PE-Cy7	Rat IgG2a, κ	RMM-1	BD Biosciences	406514	1/200
IgM	PE-Cy7	Rat IgG2a, κ	II/41	eBioscience	25-5790-82	1/1000
IL5Rα	APC	Human IgG1	REA343	Miltenyi	130-118-689	1/50
Kappa	Biotin	Goat IgG	Polyclonal	Southern Biotech	1050-08	1/250
Kappa	FITC	Rat IgG1, κ	H139.52.1	Southern Biotech	1180-02	1/500-1/1000
Lambda	PE	Rat IgG1, κ	JC5-1	Southern Biotech	1175-09	1/500
NK1.1	PE-Cy7	Rat IgG2a, κ	PK136	BD Biosciences	552878	1/300
NP	APC	N/A	N/A	In-house	N/A	1/800
NP	PE	N/A	N/A	In-house	N/A	1/800
PD-1	biotin	Rat IgG2b, κ	RMP1-30	Biolegend	109105	1/300
PD-1	PE	Rat IgG2b, κ	J43	eBioscience	12-9985-82	1/200
PD-1	PE-Cy7	Rat IgG2a, κ	29F.1A12	Biolegend	135215	1/200
Biotin	BV421	Streptavidin	N/A	Biolegend	405226	1/400
Biotin	BV711	Streptavidin	N/A	Biolegend	405371	1/400
Biotin	FITC	Streptavidin	N/A	BD Biosciences	554060	1/400
Biotin	PE-Cy5	Streptavidin	N/A	BD Biosciences	554062	1/400

2.6 Calcium signalling

Spleen cells were prepared into single cell suspensions as described in section 2.5.1. Cells were suspended at $2x10^6$ cells/mL in R10 medium (Table 2.4) and plated out at

1 mL per well in 24-well plate. The plate was incubated at 37 °C 5% CO_2 for 4 hours to rest the cells.

Indo1-AM (BD Biosciences 565879) was prepared by dissolving a vial in 50 µL DMSO, and then making a working solution diluted to 5 µM in Hank's buffered salt solution (HBSS) (Gibco 14170070). After resting, the cells were centrifuged in 1400 rpm for 5 min at 20 °C) and resuspended in 1 mL Indo1-AM working solution. Cells were incubated for 1 hour at room temperature, protected from the light, with regular agitation. To stop the reaction, 2 mL HBSS with 10% fetal bovine serum (FBS) (Sigma F9665-500ML) was added to the reaction. Cells were then centrifuged and resuspended in 200 µL HBSS with 10% FBS. Cells were incubated at 37 °C, 5% CO_2 for 30 min to allow complete de-esterification. Then cells were transferred to 96-well V-bottom plates. The plates were washed by centrifugation in 1400 rpm for 5 min at 20 °C, and cells were resuspended in 50 µL PE-conjugated anti-CD43 antibody (BD Biosciences 553271) diluted 1/200 in flow cytometry buffer. Cells were incubated at room temp for 30 min, protected from light. After staining, the plate was centrifuged as before, pellets were resuspended in 200 µL flow cytometry buffer and filtered through 70 µm cell strainers into flow cytometry tubes. A further 200 µL flow cytometry buffer was added to make a total volume of 400 µL. Tubes were incubated at 37 °C until analysis.

Fortessa X20 was configured to use measure PE (yellow/green laser, 586/15), Indo-1 Blue (UV laser, 525/50) and Indo-1 Violet (BUV395) (UV laser, 379/28) and to measure the ratio of BUV395 (violet, bound Ca^{2+})/Indo-1 Blue (free Ca^{2+}). For analysis, each sample was acquired on the Fortessa on low flow rate for 1 min. After 1 min, 100 µL of

stimulation was added to the tube, vortexed, and returned to Fortessa sip position for acquisition. Stimulation was either with goat anti-IgM $F(ab)_2$ (Jackson Immunoresearch 115-006-020) (10 µg/mL diluted in flow cytometry buffer), or goat anti-kappa (Southern Biotech 1050-01) and goat anti-lambda (Southern Biotech 1060-01) (10 µg/mL of each diluted in flow cytometry buffer). After stimulation, cells were acquired for a further 8 min. Then, 100 µL ionomycin (Sigma 3909-1ML) (diluted 1/1500 in flow cytometry buffer) was added to the tube, vortexed and returned to the sip position. The tube continued to be acquired for 2 min. In between samples, Fortessa was washed with water (high flow rate) for 5 min to remove stimulus from the fluidics.

Analysis was performed offline with FlowJo software, using ratio of BUV395/Indo-1 Blue as a derived parameter for kinetics analysis.

2.7 Enzyme-linked immunosorbent assay (ELISA)

Nunc Maxisorp ELISA plates (Thermo Fisher 442404) were coated with 5 µg/mL chicken collagen type II (Chrondex, 20012), NP_2-BSA or NP_{14}-BSA, diluted in ELISA coating buffer (Table 2.4), overnight at 4 °C. Plates were washed three times with 200 µL per well of ELISA wash buffer (Table 2.4). Then 200 µL per well of ELISA blocking buffer (Table 2.4) were added and plates were incubated for 1.5 h at room temp. After blocking, plates were washed three times, and 100 µL of sera samples were added per well. Sera samples were serially diluted 1 in 3 in dilution buffer (Table 2.4) from a starting dilution of 1/30-1/300. Where possible, a positive control (a serum sample from another experiment previously shown to bind to the coated antigen) and negative controls (non-immunised mouse serum and blocking buffer only) were included on

plates. Plates were incubated with sera dilutions for 1.5 h at 37 °C (for NP_2-BSA, NP_{14}-BSA or anti-collagen type II IgM ELISAs) or overnight at 4 °C (for anti-collagen type II IgG ELISAs). Following incubation with samples, plates were washed three times, and then 100 µL of alkaline-phosphatase (AP)-conjugated goat anti-mouse IgG (Southern Biotech 1030-04) or AP-conjugated goat anti-mouse IgM (Southern Biotech 1020-04) secondary antibody was added per well (diluted 1/1000 in dilution buffer). Plates were incubated for 1 h at 37 °C. Plates were then washed three times, and 100 µL per well of ELISA substrate was added. Plates were incubated at 37 °C until yellow colour had developed, and then absorbance at 430 nm was read on SpectraMax ABS Plus plate reader (Molecular Devices). Binding for each sample was plotted on Graphpad Prism and fitted with an “asymmetric sigmoidal 5PL, X is concentration” standard curve, and relative serum titre was determined as the dilution where the curve crossed a defined absorbance threshold. In some cases, where the curves did not cross the threshold, the serum titre was estimated by extrapolating the curve.

2.8 Enzyme-linked immune absorbent spot (ELISpot)

ELISpot assay plates (Millipore MSIPS4510) were prepared by adding 15 µL per well 35% ethanol (VWR 20821.330) (diluted in sterile H_2O) for a maximum of 1 min and then tipping out and drying. The plates were then washed 3 times with 200 µL per well sterile H_2O. Plates were then coated with 50 µL NP_2-BSA or NP_{14}-BSA (5 µg/mL in PBS) per well at 4 °C overnight.

The plates were then washed once with 200 µL per well sterile D-PBS and then blocked with 200 µL R10 medium per well for minimum 1 h. While blocking, spleen and

bone marrow cells were prepared into single cell suspensions as described in section 2.5.1, and suspended at $1x10^7$ cells/mL in R10 medium. Plates were washed with 200 µL per well sterile D-PBS, before adding 200 µL per well R10 medium and 50 µL per well cells, giving $5x10^5$ cells per well. The plates were then incubated at 37 °C 5% CO_2 for 6 h. After incubation, plates were washed twice with 200 µL ELISA wash buffer per well. AP-conjugated goat anti-mouse IgG or IgM antibody (diluted 1/1000 in PBS) was added to plates (100 µL per well), and plates were incubated overnight at 4 °C.

Following incubation with the secondary antibody, plates were washed three times with ELISA wash buffer. 100 µL per well Sigma FAST BCIP/NBT solution (Sigma B5655-25TAB) was then added to each well, and plates were incubated for 5-8 min while spots developed. Once the spots were clearly visible, the reaction was quenched with H_2O. Plates were then washed 3 times in H_2O to ensure reaction was completely quenched, and water was then tipped out. The soft plastic was removed from under the plate and then plates were dried at room temperature for 5-24 h. Plates were then read, and spots were counted on AID iSpot Spectrum ELR088IFL ELISpot reader (Autoimmun Diagnostika GmbH, Germany) (software version 7).

2.9 Fluorescent immunohistology

2.9.1 Cryosections

Tissues for histology were snap-frozen on dry ice on pre-labelled pieces of aluminium foil, and stored at -80 °C. Spleens, livers and kidneys were directly frozen, while pancreases, thymuses and lymph nodes were positioned in optimal cutting temperature (OCT) compound (TissueTek 4583) for freezing. Tissue sections of 6-8

μm thickness were taken using a OTF5000 cryostat (Bright Instruments) and placed on slides (Hendley-Essex PH-004 or Epredia J1800AMNZ). Sections were air-dried for a minimum of 20 min before being fixed in acetone (Acros Organics 268310010) at 4 °C for 20 min. Following fixation, the slides were air-dried for a minimum of 10 min before being stored at -20 °C.

2.9.2 Staining

Slides were removed from -20 °C and left to thaw at room temperature before staining. Slides were then rehydrated in fluorescent immunohistology wash buffer (Table 2.4) for 10 min. Tissue sections were incubated with antibodies or blocking solution in humidified chamber at room temperature protected from the light. Washes were performed in between incubations by placing slides in a glass chamber filled with fluorescent immunohistology wash buffer, placed on a magnetic stirrer. Slides were blocked with 50 μL per section PBS with 10% normal horse serum (diluted in dilution buffer (Table 2.4)) for 30 min, and incubations with 50 μL per section primary, secondary and tertiary antibody mixtures (made up in dilution buffer) were for 60 min. In some cases, slides were counterstained with 4′,6-diamidino-2-phenylindole (DAPI) to stain cell nuclei. Slides were submerged in DAPI (Sigma D9542) solution (0.1 μg/mL in PBS) for 30 seconds before being washed again. At the end of the staining, the edges of slides were dried with tissue paper, and cover slips were mounted using Prolong diamond anti-fade mounting medium (Thermo Fisher Scientific P36970). Slides were dried overnight at room temperature in the dark before imaging using Zeiss Axio Scan Z1 imager. Antibodies used for staining are detailed in Table 2.3.

Table 2.3 Antibodies used for fluorescent immunohistology

Specificity	Antibody Species	Conjugate	Supplier	Catalogue Number	Clone	Dilution
Primary and biotin-conjugated primary antibodies:						
B220	Rat	Purified	eBioscience	14-0452-82	RA3-6B2	1/200
B220	Rat	Biotin	eBioscience	13-0452-85	RA3-6B2	1/200
C1q	Rabbit	Purified	Abcam	Ab182451	4.8	1/200
C3	Rabbit	Purified			Polyclonal	1/200
CD3	Hamster	Purified	BD Biosciences	553058	145-2C11	1/400
CD4	Rat	Biotin	eBioscience	13-0042-82	RM4-5	1/800
CD11c	Armenian Hamster	Purified	eBioscience	14-0114	N418	1/50
CD138	Goat	Purified	R&D	MAB2966	Polyclonal	1/600
Gp38 (Podoplanin)	Hamster	Purified	eBioscience	14-5381-82	8.1.1	1/400
IgD	Rat	Biotin	eBioscience	13-5993-85	11-26c	1/200
IgMb	Mouse	Biotin	BD Biosciences	553519	AF6-78	1/100
Insulin	Rabbit	Purified	Abcam	Ab63820	Polyclonal	1/800
Ki67	Rabbit	Purified	Abcam	Ab15580	Polyclonal	1/400
Ly6G	Rat	Biotin	eBioscience	13-5931	RB6-8C5	1/600
NP	Rabbit	Purified	In-house	N/A	N/A	1/500
PNA	N/A	Biotin	Vector	B1075	N/A	1/800
Secondary antibodies:						
Goat IgG (H+L)	Donkey	AF555	Thermo Fisher Scientific	A21432	Polyclonal	1/400
Hamster	Goat	AF647	Jackson	127-605-160	Polyclonal	1/400
Mouse IgG	Rat	APC	eBioscience	17-4010-82	polyclonal	1/400

Specificity	**Antibody Species**	**Conjugate**	**Supplier**	**Catalogue Number**	**Clone**	**Dilution**
Rabbit IgG (H+L)	Donkey	AF488	Jackson	711-545-152	Polyclonal	1/400
Rabbit IgG (H+L)	Donkey	Cy3	Jackson	711-165-152	Polyclonal	1/400
Rat IgG (H+L)	Donkey	AF647	Jackson	712-606-153	Polyclonal	1/400
Biotin	Streptavidin	AF488	Jackson	016-540-084	N/A	1/400
Biotin	Streptavidin	AF555	Thermo Fisher Scientific	S32355	N/A	1/400
Directly conjugated antibodies						
B220	Rat	APC	eBioscience	17-0452-83	RA3-6B2	1/200
CD1d	Rat	PE	eBioscience	12-0011-81	1B1	1/400
CD3	Hamster	FITC	eBioscience	11-0031-82	145-2C11	1/100
CD4	Rat	APC	eBioscience	17-0041-82	GK1.5	1/400
CD8	Rat	PE	eBioscience	12-0081-83	53-6.7	1/200
CD95 (Fas)	Hamster	PE	BD Biosciences	17-0452-83	554258	1/200
CD169	Rat	AF647	Biolegend	142408	3D6.112	1/200
Enolase 1	Rabbit	FITC	Santa Cruz	sc-271384 FITC	A5	1/100
F4/80	Rat	PE	eBioscience	12-4801-80	BM8	1/100
IgD	Rat	BV421	Biolegend	405725	11-26c.2a	1/200
IgG	Rat	APC	BD Biosciences	550874	X56	1/400
IL5Rα	Human	APC	Miltenyi	130-118-689	REA343	1/400
TCRβ	Armenian Hamster	PE	eBioscience	12-5961-82	H57-597	1/200

2.10 Autoantibody tissue array

Nova Lite Rat liver, kidney, and stomach slides (Werfen 704180) were stained by a protocol adapted from the manufacturer. Briefly, 50 µL of each serum sample was added to spots on the slides and incubated overnight at 4 °C in a humidified chamber. All slides included a positive control human serum sample (Werfen) that had either anti-nuclear antibody (ANA), anti-mitochondrial antibody (AMA), or anti-smooth muscle antibody (ASMA) staining pattern, and a negative control of either PBS alone or a negative human serum sample (Werfen). Slides were washed in PBS II (Inova Diagnostics) and then FITC-conjugated goat anti-mouse IgG1 H+L (Southern Biotech, 1070-02) (diluted 1/400 in PBS II) or FITC-conjugated sheep anti-human IgG H+L (Inova Diagnostics) was added. Slides were incubated for 1 h at room temperature, and then washed in PBS II. Slides were counterstained with DAPI (0.1 µg/mL for 30 seconds) and then washed in PBS II. Cover slips were mounted in mounting medium (Inova Diagnostics) and sealed with nail varnish.

In order to identify presence of autoantibodies, slides were analysed blind by Dr Abid Karim (University of Birmingham Clinical Immunology Service). The slides were then imaged using the Axio Scan Z1 imager (Zeiss). For further analysis, images were converted to TIF format and downsampled (x4) using Zeiss converter tool (Zeiss). In Fiji (version 2.3.0/1.53f) (Schindelin et al., 2012), regions of interest for either the whole tissue array or individual tissues (kidney, liver, gut, smooth muscle) were manually drawn. The region of interest was applied to the FITC image (aged mouse sera and anti-mouse IgG H+L) and analyse particles was used to measure fluorescence intensity within the region of interest.

2.11 Anti-islet antibody

Slides with rat pancreas sections were prepared as described in section 2.9.1, and stained with mouse serum similarly to as described in section 2.9.2. Following blocking with 10% normal horse serum (diluted in dilution buffer (Table 2.4)) for 30 min, the sections were incubated with 50 µL mouse serum. After washing, the sections were then incubated with rabbit anti-rat/human insulin antibody (Abcam Ab63820) (diluted 1/800 in dilution buffer), followed by incubation with Cy3-conjugated donkey anti-rabbit (Jackson Immunoresearch 711-165-152) (diluted 1/400 in dilution buffer), and FITC-conjugated goat anti-mouse H+L chain (Southern Biotech, 1070-02) (diluted 1/400 in dilution buffer) antibody. Finally, the slides were counterstained with DAPI (0.1 µg/mL for 30 seconds). At the end of the staining, slides were dried, and cover slips were mounted using Prolong diamond anti-fade mounting medium. Slides were dried overnight at room temperature in the dark before imaging using Zeiss Axio Scan Z1 imager.

2.12 Serum glucose concentration

A Tee2+ blood glucose monitoring system (Spirit Healthcare) was used to measure the glucose concentration in serum samples according to the manufacturer's instructions. Briefly, a Tee2+ blood glucose test strip was inserted into the Tee2+ blood glucose meter with the contact bars facing upwards. 2 µL of serum was absorbed onto the end of the test strip, and the meter gave a reading for the glucose concentration.

2.13 Quantitative Image analysis

Images from Zeiss Axio Scan imager were down sampled (x4) and converted to tiff format using Zeiss converter tool. The converted images were analysed using Fiji (version 2.3.0/1.53f) (Schindelin et al., 2012) as described below.

2.13.1 NP-specific plasma cells

Spleen sections that were stained for NP and CD138 as described in section 2.9 were used to analyse NP-specific plasma cells. Images were cropped to an undamaged area free of blemishes or scratches. NP and CD138 images had background removed (subtract background, rolling = 50) and then images were filtered (3 rounds of median, radius = 2). Images were then thresholded (NP – RenyiEntropy dark; CD138 – Otsu dark) and converted to masks. To analyse the area of total plasma cells, the analyse particles was used on CD138 mask command (size: 100-Infinity). To analyse area of NP-specific plasma cells, the image calculator was used to identify areas that were $CD138^+$ NP^+, and the analyse particles command was used with the calculated image (size: 100-Infinity).

2.13.2 Plasma cells (aged spleens)

Spleen sections that were stained for B220 and CD138 as described in section 2.9 were used to analyse plasma cells. Images were cropped to an undamaged area free of blemishes or scratches. The CD138 image was used for plasma cell analysis. The background was removed (subtract background, rolling = 50) and then the image was filtered (3 rounds of median, radius = 2) to blur the image. The image was thresholded

(default dark) and converted to a mask. The analyse particles command (size: 100-Infinity) was then used to measure the plasma cell area and percentage.

2.13.3 Germinal centres (aged spleens)

Spleen sections that were stained for PNA, Fas, B220 and IgD as described in section 2.9 were used to analyse germinal centres (GCs). Images were cropped to an undamaged area free of blemishes or scratches. Background was removed from PNA, Fas and B220 images (subtract background, rolling = 50) and then images were filtered (3 rounds of median, radius = 8). Images were then thresholded (PNA and Fas – MaxEntropy dark; B220 – IsoData dark) and converted to masks. Image calculator was used to identify areas that were $B220^+$ PNA^+ Fas^+ as GCs. The calculated image was dilated ten times, and holes were filled. The analyse particles command (size: 100-Infinity) was then used to measure germinal centre area and percentage.

2.13.4 Kidney IgM, complement 1q and complement C3 deposits

Kidney sections that were were stained with DAPI and antibodies for podoplanin, IgM and complement C1q or complement C3 as described in section 2.9 were used to analyse kidney IgM and complement deposits. Images were cropped to an undamaged area free of blemishes or scratches. The podoplanin image was used to identify glomeruli as regions of interest (ROIs). The image was filtered (variance, radius = 2; median, radius = 10) and then thresholded (Li Dark) and converted to a mask. Analyse particles (size: 1000 – Infinity, circularity = 0.15 – 1.00) with objects added to ROI manager. ROIs were then applied to the IgM and C1q or C3 images, and measure tool

was used to measure mean pixel brightness within the ROIs. The mean of the mean pixel brightness from all ROIs per image were then calculated for analysis.

2.14 Bulk RNAseq gene expression analysis

Mice were immunised with plantar surface of one foot with 10 µg NP-CGG (precipitated in alum) and $5x10^6$ heat inactivated *B. pertussis*. Popliteal lymph nodes were harvested at day 8. GC B cells ($B220^+$ $CD138^-$ Fas^+ $CD38^-$) were sorted by fluorescence-activated cell sorting (FACS) from the injection-side lymph node, and follicular B cells ($B220^+$ $CD138^-$ Fas^- $CD38^+$ $CD19^+$ $GL7^-$ $CD93^-$ $CD21^+$ $CD23^+$) were sorted from the opposite-side lymph node. Immunisations and FACS sorting were performed by Dr Juan Carlos Yam-Puc in the Kai Toellner group at University of Birmingham. Sequencing and alignment of the raw sequencing data were performed at the bioinformatics facility at the Francis Crick Institute, who provided normalised count data for all samples.

Normalised count data were then analysed using the bioconductor DESeq2 package (Love et al., 2014) on R Studio (version 2022.07.2) to extract differentially expressed genes from all comparisons. All samples were run together on the DESeq2 package, with the contrast argument used to extract differentially expressed genes in individual comparisons between two groups (e.g. IgMg1 follicular B cells vs WT follicular B cells).

Venn diagram tool from Ghent University Bioinformatics & Evolutionary Genomics group (http://bioinformatics.psb.ugent.be/webtools/Venn/) was used to analyse overlap between sets of genes. G:Profiler (version e106_eg53_p16_65fcd97) (https://biit.cs.ut.ee/gprofiler/gost) was used to analyse functional enrichment within lists of differentially expressed genes (Raudvere et al., 2019). Gene set enrichment

analysis (GSEA) was performed using Broad Institute GSEA software (version 4.2.2) (Subramanian et al., 2005). Analysis was performed using gene_set permutation type as recommended for 3 replicates per condition. Mouse gene sets (e.g. hallmark gene sets (Liberzon et al., 2015)) and mouse gene annotations files were downloaded from Molecular Signatures Database (https://www.gsea-msigdb.org/gsea/downloads.jsp) (Liberzon et al., 2011). Cytoscape (version 3.9.1) was used (Shannon et al., 2003; Reimand et al., 2019) to create an enrichment map of significantly enriched gene sets following GSEA.

2.15 10x single cell RNAseq gene expression analysis

Total B cells were purified from spleens using Mojosort Mouse Pan B Cell Isolation Kit II (Biolegend 480088). Purified cells were confirmed to be over 97% B cells ($B220^+$ $CD3^-$) by flow cytometry. Library preparation with Chromium Next GEM single cell kit v2 (10X Genomics), and sequencing using NovaSeq 6000 was performed by Dr Anetta Ptasinska (University of Birmingham genomics service). The library was prepared from 10,000 cells per sample, with 50,000 gene expression reads per cell and 5,000 mouse BCR reads per cell. CellRanger pipeline (10x Genomics) (Zheng et al., 2017) was used to process the raw data to generate counts and VDJ sequences. Loupe Browser and Loupe VDJ Browser (10x Genomics) were used to perform clustering and further analysis of the data. Barcodes were thresholded for 1203-11229 unique molecular identifiers (UMIs) per barcode, 639-2566 genes per barcode and 0.692-3.78% mitochondrial UMIs to remove poor quality cells and multiplets before further analysis.

2.16 Buffers and media

Buffers and media used throughout this thesis are detailed in Table 2.4.

Table 2.4 Details of buffers and media used

Buffer	Components	Concentration	Supplier	Catalogue Number
Flow cytometry buffer	D-PBS		Sigma	D8537-500ML
	FBS	2% (v/v)	Sigma	F9665-500ML
	EDTA	2 mM	Sigma	E7889-100ML
R10 medium	RPMI 1640 (with L-glutamine)		Gibco	21875-034
	FBS	10% (v/v)	Sigma	F9665-500ML
	Pen/Strep	100 U/mL (1X)	Gibco	15140-122
	HEPES buffer	20 mM	Sigma	H0887-100ML
ELISA coating buffer	H_2O			
	Na_2CO_3	0.015 M	Sigma	57795-500G
	$NaHCO_3$	0.035 M	Sigma	55761-1KG
ELISA wash buffer	PBS		Gibco	18912-014
	Tween20	0.05% (v/v)	Sigma	P1379-500ML
ELISA blocking buffer and ELISA/histology dilution buffer	PBS		Gibco	18912-014
	BSA	1% (w/v)	Sigma	A7906-100G
Histology wash buffer	PBS	1X	Gibco	18912-014
	Saponin	0.1% (w/v)	Sigma	84510-100G

2.17 Statistical analysis

All statistical tests were performed in Graphpad Prism (version 9.4.0). The statistical tests used are described in the figure legends. Generally, for comparison of two groups, two-tailed T-test or Mann-Witney test was used; for comparison of three or

more groups, one-way ANOVA with Tukey's multiple comparison test or Kruskall-Wallis test with Dunn’s multiple comparison test was used; for comparison of two or more groups with multiple categories within each group, two-way ANOVA with Tukey's multiple comparison test was used, or mixed-effects analysis with Šídák's multiple comparisons test if data were matched (for example, same mice at multiple timepoints); and for comparison of categorical distributions (i.e. positive or negative for autoantibodies; clustering of cells following single cell gene expression analysis), Chi-squared test or Fisher’s exact test were used. Where data are presented on a log-scale, the statistical tests were performed on log-transformed data.

Chapter 3. B cell development in mouse models with altered B cell receptor signalling

3.1 Introduction

3.1.1 Influence of B cell receptor signalling on B cell development

B cell receptor (BCR) signalling is important at almost all stages of B cell development. The first stage that BCR signalling plays a role is in pre-B cells during bone marrow B cell development. Pre-B cells express a pre-BCR made up of the fully rearranged heavy chain, along with a surrogate light chain made up of VpreB and λ5 (Tsubata and Reth, 1990; Karasuyama et al., 1990). Signalling through the pre-BCR is required for cells to develop from pre-B cells to immature B cells. Mice with targeted disruption of the membrane region of the IgM heavy chain are developmentally arrested at the pre-B cell stage (Kitamura et al., 1991). Mice deficient in surrogate light chain (triple knockouts of VpreB1, VpreB2 and λ5) are also arrested at the pre-B cell stage with reduced numbers of immature and mature bone marrow B cells (Shimizu et al., 2002). Additionally, mutations that target Igα and Igβ, which act as a co-receptor for the BCR and the pre-BCR, result in disrupted early B cell development (Torres et al., 1996; Kraus et al., 2001; Pelanda et al., 2002). Signalling through the pre-BCR complex induces proliferation and differentiation into the late pre-B cell stage where cells undergo light chain VJ gene segment recombination (Hess et al., 2001).

At the bone marrow immature B cell stage, B cells that have successfully rearranged light chain VJ gene segments express the complete BCR on their surface. In these cells, signalling through the BCR mediates central tolerance, to prevent development of B cells with self-reactive BCR. Mechanisms of central tolerance are clonal deletion,

receptor editing or clonal anergy. Clonal deletion is where cells undergo apoptosis as a result of strong BCR signalling (Nemazee and Bürki, 1989; Hartley et al., 1993). Receptor editing is where cells undergo secondary light chain gene rearrangement (Gay et al., 1993; Tiegs et al., 1993; Halverson et al., 2004; Nemazee, 2006). Clonal anergy is the maintenance of the cell in an inactive state, for example, down-regulated BCR expression and reduced response to BCR stimulation (Goodnow et al., 1988; Merrell et al., 2006; Quách et al., 2011; Zikherman et al., 2012; Cambier et al., 2007). Therefore, in the bone marrow BCR signalling is important for positive selection of B cells with functional BCRs, and then negative selection of B cells with self-reactive BCRs.

Immature B cells then migrate to the periphery as transitional B cells where further development is also affected by BCR signalling as they require BCR signalling to mature. In mice deficient in Syk (a kinase required for BCR signal transduction), cells are arrested at an immature stage unable to enter the white pulp (Henderson et al., 2010). As in the bone marrow, transitional B cells in the periphery undergo negative selection to prevent activation of self-reactive B cells. Clonal deletion (Russell et al., 1991; Ota et al., 2011; Shukla et al., 2019) and clonal anergy (Goodnow et al., 1989; Hartley et al., 1991) have been described as peripheral tolerance mechanisms. Transitional cells progress through T1 and T2 stages before maturation into mature B cells. T1 and T2 cells respond differently to BCR stimulation *in vitro*. T2 cells cultured with anti-IgM undergo extensive proliferation, whereas T1 cells die out (Petro et al., 2002). A third transitional B cell subset, T3 cells, has low IgM expression (Allman et al., 2001). T3 cells do not differentiate into mature B cells, but are an alternative development pathway that have reduced response to BCR stimulation (Teague et al.,

2007) and have been suggested to be a natural anergic B cell population (Merrell et al., 2006).

B cells mature into either follicular B cells or marginal zone B cells. As discussed in Section 1.3.2 and Table 1.1, the role of BCR signalling in this fate decision is not clear, as some studies suggest that strong BCR signalling favours follicular B cell development (Cariappa et al., 2001, 2009; Samardzic et al., 2002; Setz et al., 2018; Härzschel et al., 2021), and some studies suggest it favours marginal zone B cell development (Wen et al., 2005; Kanayama et al., 2005; Horikawa et al., 2007; Waisman et al., 2007; Tsiantoulas et al., 2017; Geier et al., 2018; Ottens and Satterthwaite, 2021). However, the fact that several mouse models with altered BCR signalling effect to mature B cell populations shows that BCR signalling is important in this process.

B-1 cell development is also sensitive to BCR signalling. B-1a cells develop in the fetal liver and are enriched for self-reactivity (Baumgarth, 2011). One study showed that B-1a cells are positively selected for self-reactivity. Mice transgenic for anti-Thy-1 BCR were crossed with either Thy-1^+ or Thy-1^- mice. Mice on the Thy-1^+ background developed anti-Thy-1 IgM autoantibodies, predominantly from $CD5^+$ peritoneal cavity B cells (B-1a cells). However, mice on the Thy-1^- background did not make anti-Thy-1 antibodies (Hayakawa et al., 1999). Further evidence of strong BCR signalling favouring B-1 cell development was shown in experiments with mice with constitutively active BCR signalling due to replacement of the BCR with BCR-surrogate, Epstein-Barr virus protein LMP2A. Constitutively active strong BCR signalling from high expression of LMP2A resulted in B-1 cells making up the majority of the B cells (Casola

et al., 2004). Therefore, although conventional B-2 cells undergo BCR-mediated positive and negative selection during development in the bone marrow, B-1a cells that are self-reactive are positively selected.

3.1.2 B cell development in anergy models

Anergic B cells have been mostly characterised from transgenic BCR mouse models. Their distinguishing characteristics are downregulation of surface BCR expression, and reduced response to BCR stimulation (Cambier et al., 2007). One of the best characterised B cell anergy models is the MD4 x ML5 mouse model. These mice are double transgenic for a hen egg lysozyme (HEL)-specific BCR, and soluble HEL as a self-antigen, resulting in B cells that are self-reactive and develop as anergic (Goodnow et al., 1988). Bone marrow B cell development is difficult to assess in these mice, as the development is already altered in the single transgenic MD4 (HEL-specific BCR) mice. In these mice, pre-B cells are severely reduced compared to non-transgenic mice, thought to be because the B cells no not need to undergo heavy or light chain rearrangement. However, bone marrow B cells in MD4 x ML5 mice do not appear substantially different to MD4 mice (Mason et al., 1992). Marginal zone B cells in MD4 x ML5 mice are reduced, whereas follicular B cells appear unaffected (Mason et al., 1992; Phan et al., 2003). The majority of MD4 x ML5 splenic B cells phenotypically resemble transitional T3 cells ($CD93^+$ $CD23^+$ IgM^{lo}), as do splenic B cells in a separate anergy model, the Ars/A1 model (Merrell et al., 2006). Additionally, usage of the lambda light chain gene is increased in splenic B cells in MD4 x ML5 mice (Bai et al., 2007), indicative of increased receptor editing during B cell development (Tiegs et al., 1993; Hertz and Nemazee, 1997; Bai et al., 2007).

3.1.3 Anergic B cell gene expression signature

In the majority of anergic B cell models, anergy is caused by chronic exposure to a self-antigen. However, the anergy is long-lasting, even following removal of exposure to antigen. MD4 x ML5 anergic cells transferred to recipient mice that did not express soluble HEL were able to make an antibody response to HEL immunisation showing that anergy is reversable, but the recovery is only partial as the response was lower than when non-anergic cells were transferred (Goodnow et al., 1991). Ars/A1 anergic B cells removed from exposure to self-antigen made a calcium response to anti-IgM stimulation, but only to 50-70% of the level of the non-anergic control cells (Gauld et al., 2005). This suggested that anergic cells remained in a partially suppressed state after removal from exposure to self-antigen, pointing to additional mechanisms of maintaining anergy.

To examine the gene expression changes explaining B cell anergy, Glynne et al. (2000) used a gene microarray to monitor expression of 6,500 genes in MD4 x ML5 B cells. This study identified 20 genes that were significantly increased and 8 genes that were decreased. Induced genes included negative regulators of signalling and transcription. This was the first published gene signature for anergic B cells (Glynne et al., 2000). A later study by Sabouri et al. (2016) used a larger gene microarray to analyse expression of more than 59,000 genes in mature $CD93^{-}$ $CD23^{+}$ MD4 x ML5 B cells, identifying a more comprehensive anergic gene signature. They identified 97 probes that had a greater than two-fold increased expression in MD4 x ML5 anergic B cells compared with MD4 controls. This included 13 of the genes previously identified by Glynne et al. (2000). An additional 123 genes with evidence of moderate induction

in MD4 x ML5 B cells were identified (Sabouri et al., 2016). Schwickert et al. (2019) performed bulk RNA sequencing to analyse gene expression in follicular B cells from MD4 x ML5 mice. They defined an anergy expression signature of 59 upregulated and 50 downregulated genes, which correlated well with the signature published by Sabouri et al. (2016) (Schwickert et al., 2019).

Therefore, several previously published papers have established a gene expression signature for MD4 x ML5 anergic B cells. However, there are few, if any, published data analysing gene expression in other anergy models, or in naturally occurring anergic B cells.

3.1.4 Chapter aims

In this chapter, IgMg1 and IgG1M mouse models have been used to investigate the effect of altered BCR signalling on B cell development, and to investigate gene expression changes in the IgMg1 polyclonal B cell anergy model. The IgMg1 model (Zhang, 2019) has B cells with a chimeric IgM BCR, made of up the extracellular and transmembrane regions of IgM and the longer cytoplasmic tail of IgG1, but normal IgD. The IgMg1 model has been shown to have defects in splenic B cell development, and an anergic B cell phenotype (such as downregulated surface IgM expression and reduced response to BCR stimulation *in vitro*) (Zhang, 2019). The IgG1M model (also known as $IgH^{G1\mu}$ model) (Waisman et al., 2007) expresses only IgG1 as a BCR from the earliest stages of B cell development, with no expression of IgD. This model also has defective B cell development, although the exact defects differ slightly from the IgMg1 model. In comparison with IgMg1 mice, the BCRs on these mice also have the

IgG1 extracellular and transmembrane regions. The work in this chapter aims to compare B cell development in these models, to assess the importance of the BCR extracellular and cytoplasmic regions for BCR signalling during B cell development.

The aims of this chapter are as follows:

i. Analysis of B cell development in the bone marrow, spleen and peritoneal cavity of IgMg1 mice and IgG1M mice to:
    a. investigate the roles of the BCR extracellular region and cytoplasmic region for efficient B cell development.
    b. Investigate the effect of increased BCR signalling on B cell development.
ii. Comparison of IgG1M and IgMg1 B cells following BCR stimulation *in vitro*.
iii. Identification of genes that are differentially expressed in IgMg1 follicular B cells in comparison with WT follicular B cells to identify genes important in B cell anergy and compare with published data for the classical MD4 x ML5 B cell anergy model.

3.2 Results

3.2.1 Bone marrow B cell development is blocked at pre-B cell stage in IgG1M mice but is normal in IgMg1 mice

B cell receptor signalling affects the ability of B cells to progress through B cell development in the bone marrow. Data from our lab had previously found that IgMg1 mice had no major changes in bone marrow B cell development (Zhang, 2019). However, the earlier stages of development between pre-pro B cells and early pre-B cells had not been sufficiently characterized. As B cells begin rearranging the BCR heavy chain at the pro-B cell stage and express a pre-BCR made up of the heavy chain and a surrogate light chain in the early pre-B cell stage, these were major developmental stages that could potentially be affected by alterations to the BCR.

A flow cytometry strategy was developed to allow assessment of bone marrow B cell development (Figure 3.1), based on the Hardy fractions (Hardy et al., 2000; Hardy, 2012). In this scheme early B cell developmental stages (identified as $B220^+$ $CD43^+$) can be resolved into pre-pro-B cells (fraction A), pro-B cells (fractions B and C) and early pre-B cells (fraction C'), based on expression of CD24 and BP-1 markers. The later stages ($B220^+$ $CD43^-$) can then be resolved into late pre-B cells (fraction D), immature B cells (fraction E), transitional B cells and mature B cells (fraction F), based on expression of IgM and IgD. The IgG1M B cells do not express IgD or IgM, so although immature, transitional, and mature IgG1M B cells cannot be distinguished from each other with this gating scheme, they can be combined into the $IgG1^+$ $CD43^+$ B cells.

As previously described by Zhang (2019), in IgMg1 mice the later stages of B cell development were largely unchanged from wildtype (WT) mice (Figure 3.2A and B).

Additionally, there were no significant differences in the earlier stages of development, fractions A-C'. There were significantly more mature B cells (fraction F) in the IgMg1 bone marrow. However, these cells represent circulating mature B cells rather than a developmental stage within the bone marrow.

In contrast with the IgMg1 mice, bone marrow B cell development in the IgG1M mice was impaired (Figure 3.2A and B). The Hardy fractions representing pre-pro B cells (fraction A) and early pro-B cells (fraction B) had similar frequencies as in WT mice, which was expected as these cells do not express BCR yet. However, there were significantly more cells at the late pro-B cell stage (fraction C), and a significant reduction at all subsequent stages of B cell development (pre-B cell to mature B cells - fractions C', D and E and F). This indicates that there is a block in development at the pre-B cell stage, with cells accumulating at the pro-B cell stage and not efficiently progressing to the pre-B cell stage (Figure 3.2A). Ratios of the frequency of each development stage relative to the frequency of the preceding stage where also calculated, to highlight blocks in development. The ratio of fraction C'/fraction C and fraction D/fraction C' were significantly reduced in IgG1M mice, showing that these were the stages where development was blocked. The ratio of fraction E and F/fraction D was significantly increased suggesting that cells that develop to the pre-B cell stage are able to efficiently continue in their development (Figure 3.2B). This is consistent with published data from Waisman et al. (2007) which show increased pro-B cells and decreased pre-B cells and immature B cells in the development of IgG1M bone marrow B cells.

Furthermore, intracellular active Caspase-3 staining was used to assess apoptosis at the different stages of bone marrow B cell development (Figure 3.3). In all mouse genotypes the frequency of active Caspase-3$^+$ cells was highest in fractions B, C and C' (Figure 3.3A), indicating apoptosis could mainly be detected between pro-B cell and early pre-B cell stages of B cell development as reported in the literature (Lu and Osmond, 2000). There was no significant difference in the frequency of active Caspase-3$^+$ cells in the IgMg1 mice at any of the developmental stages. However, in the IgG1M mice, active Caspase-3$^+$ cells were significantly more frequent than in WT or IgMg1 mice in fraction C' (early pre-B cells) (Figure 3.3A and B), consistent with the block in development at this stage.

Overall, the data from the IgMg1 mice confirm the previous observations that the IgG1 cytoplasmic tail does not have a significant effect on B cell development in the bone marrow. Despite inappropriate signalling of the IgMg1 B cell receptor, and mature IgMg1 B cells having an anergic phenotype (Zhang, 2019) there is no evidence of increased negative selection in the bone marrow resulting in blocked development or increased apoptosis. Surprisingly, IgG1M mice have impaired bone marrow B cell development. The IgG1 extracellular region seems to have a negative impact on development, specifically at the pre-B cell stage, resulting in increased apoptosis and impaired progression to subsequent developmental stages. This is likely due to reduced ability of the IgG1 heavy chain to associate with the surrogate light chain to form the pre-BCR (Waisman et al., 2007). This shows the importance of the IgM extracellular region for efficient B cell development in the bone marrow.

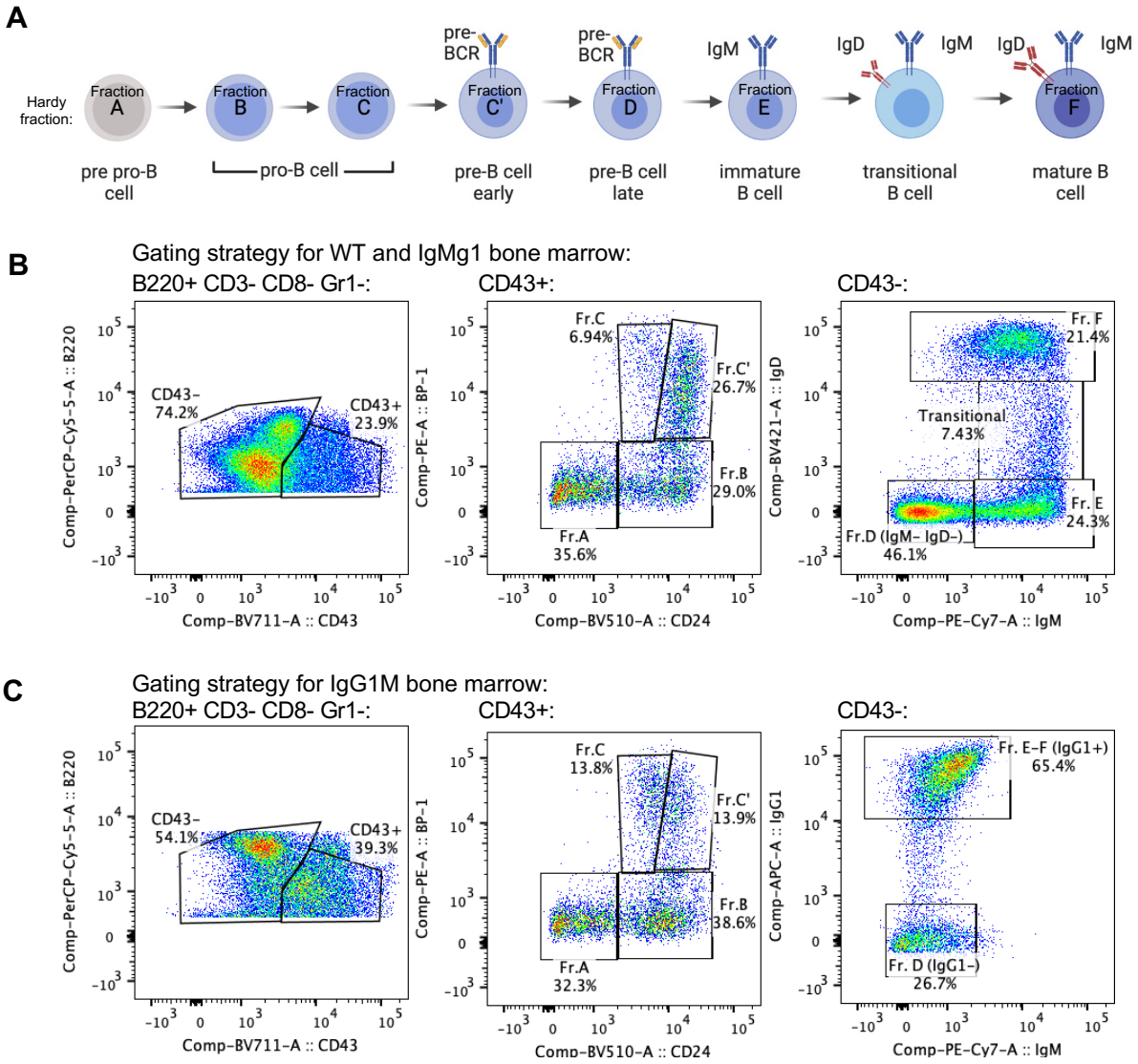

Figure 3.1 Gating strategy for identification of bone marrow fractions.

(A) Schematic showing how Hardy fractions correspond to different stages of bone marrow B cell development; created with Biorender.com. (B) Gating strategy for flow cytometry analysis of WT and IgMg1 bone marrow B cell development from representative WT mouse. From $B220^{+}$ $CD3^{-}$ $CD8^{-}$ $Gr1^{-}$ cells, fractions A to C' can be distinguished as $CD43^{+}$ and fractions D to F can be distinguished as $CD43^{-}$. $CD43^{+}$ cells can be split into fractions A to C' based on CD24 and BP-1 expression. Fractions D to F can be distinguished based on IgM and IgD expression. (C) Alternative flow cytometry gating strategy used for IgG1M bone marrow from representative IgG1M mouse. Fractions A to C' gated as in (B). $CD43^{-}$ cells can be split into fraction D (IgG^{-}) and fractions E to F ($IgG1^{+}$), but fractions E to F are unable to be further separated due to no expression of IgD.

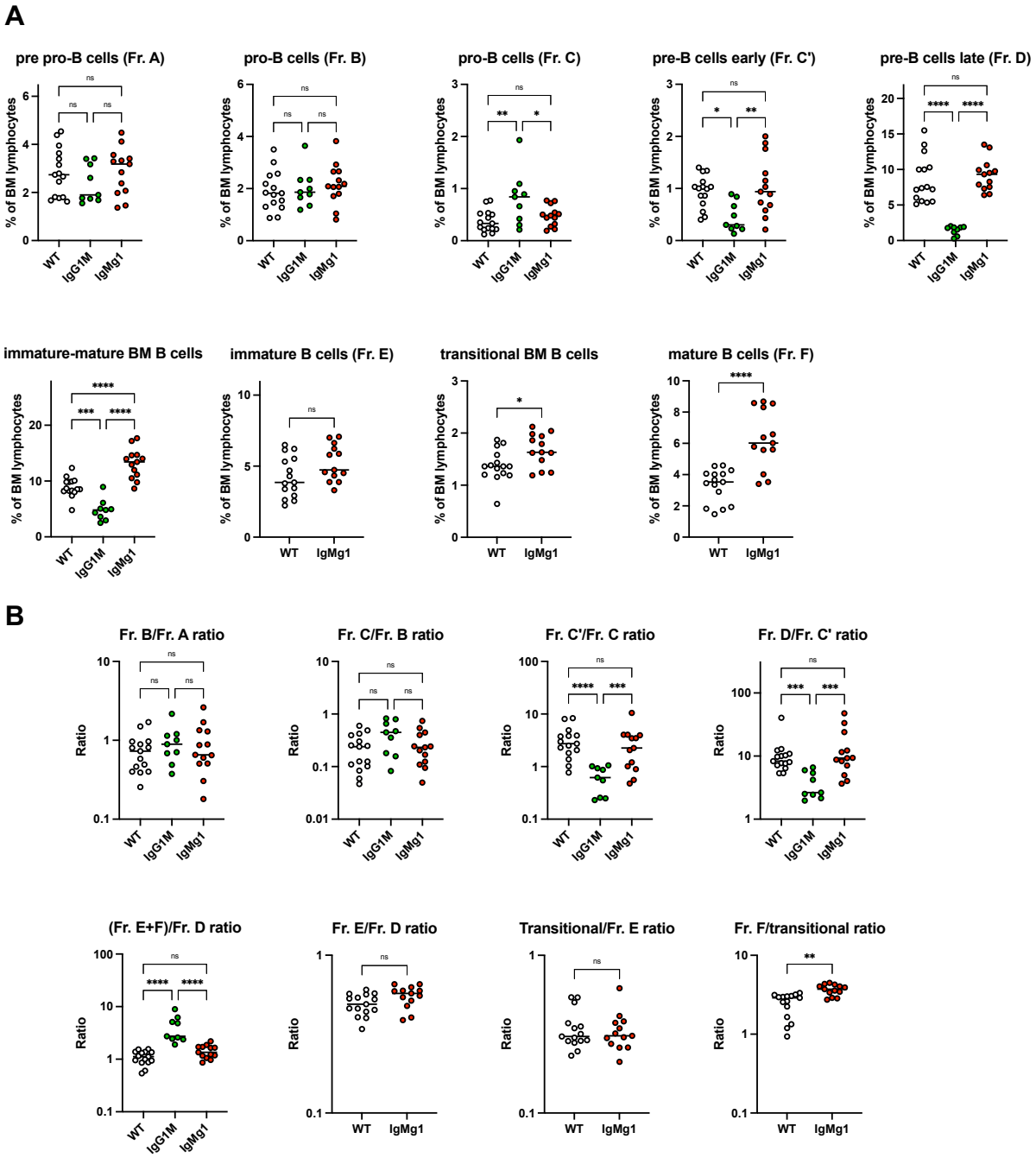

Figure 3.2 Bone marrow B cell development in IgG1M and IgMg1 mice.

Bone marrow from WT, IgG1M and IgMg1 mice was analysed by flow cytometry gating using gating strategy shown in Figure 3.1 (A) Plots showing summaries of B cell fractions in bone marrow assessed by flow cytometry, shown as percentage of bone marrow lymphocytes. (B) Plots showing ratios between frequencies of each bone marrow fraction with the preceding fraction. Data is combined from three experiments. Each symbol represents an individual mouse. Statistical tests were performed by ordinary one-way ANOVA with Tukey's multiple comparison test for comparison of three groups, and two-tailed unpaired T-test for comparison of two groups. (****, $p < 0.0001$; ***, $p < 0.001$; **, $p < 0.01$; *, $p < 0.05$; ns, not significant).

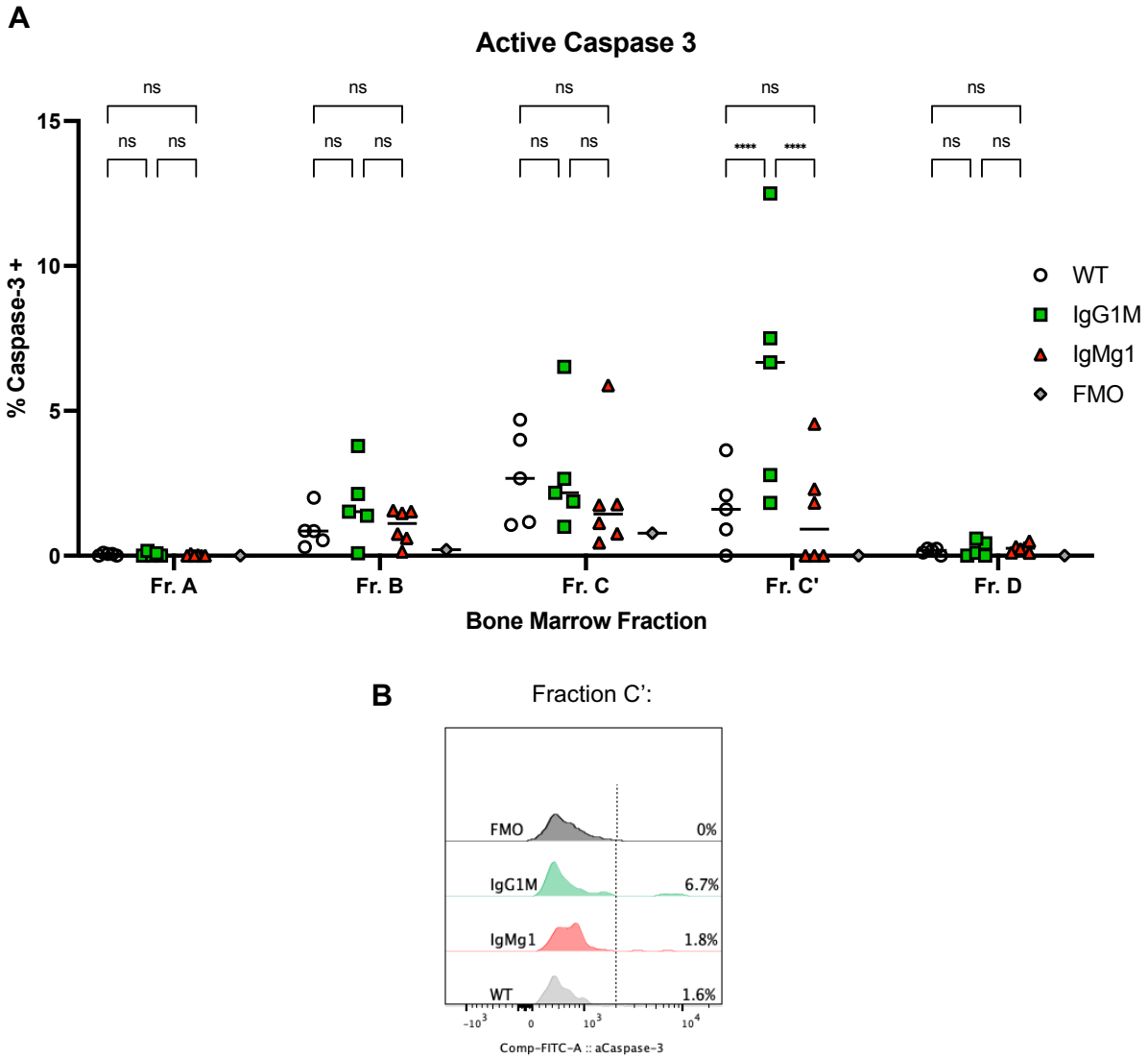

Figure 3.3 Active caspase-3 staining in bone marrow B cell fractions.

Bone marrow fractions were gated as in Figure 3.1 and analysed for percentage stained with anti-active Caspase-3 antibody. Gates for active-Caspase-3$^+$ cells set using fluorescence minus one (FMO) control of cells stained with all antibodies except anti-active Caspase-3. (A) Percentage of active Caspase-3$^+$ cells in bone marrow fractions. Statistical tests performed by 2way ANOVA with Tukey's multiple comparison test. (****, $p < 0.0001$; ns, not significant). Data from one experiment. Each symbol represents an individual mouse. (B) Representative histograms showing active Caspase-3 staining in fraction C' of WT, IgG1M and IgMg1 mice, along with FMO. Histograms normalised to mode.

3.2.2 B cell maturation in the spleen is altered in IgMg1 and IgG1M mice

Previous results analysing B cell development in IgMg1 mice showed that although bone marrow development appeared largely normal, B cell maturation in the spleen was affected. Follicular B cells were found to be slightly increased, whereas marginal zone B cells were severely depleted or absent (Zhang, 2019). Here, splenocytes from IgG1M mice were analysed by flow cytometry and compared with IgMg1 mice (Figure 3.4). As expected, in IgMg1 mice there were decreased numbers of marginal zone B cells and a slight increase in follicular B cells. However, in IgG1M mice, marginal zone B cells were expanded, with a slight non-significant decrease in follicular B cells. The increase in marginal zone B cells in IgG1M spleens was confirmed using fluorescent immunohistology, whereas marginal zone B cells in IgMg1 spleens were virtually absent (Figure 3.5).

B cell subsets were analysed for lambda light chain usage, as an indicator of receptor editing (Figure 3.6A). This confirmed the previous finding from our lab that IgMg1 B cells had increased usage of lambda light chain (Zhang, 2019). Surprisingly, the data showed that lambda light chain usage was even higher in the B cells of IgG1M mice. This was especially pronounced in the marginal zone B cell compartment (Figure 3.6B). To investigate at which point of B cell development receptor editing is increased, lambda expression was analysed in bone marrow B cell subsets. In IgMg1 mice, lambda expression was similar in bone marrow immature B cells (Figure 3.7A and B). However, at the bone marrow transitional B cell stage, lambda$^+$ cells became significantly increased in IgMg1 mice, with a 50% increase relative to WT mice (Figure 3.7C and D). Lambda$^+$ mature B cells were also more frequent in the bone marrow of IgMg1 mice compared to WT mice (Figure 3.7E and F). It is likely that receptor editing

increased in IgG1M mice at a similar developmental stage as the combined post pre-B cell populations had significantly increased frequency of lambda$^+$ cells compared to both WT and IgMg1 mice, although the immature B cells could not be distinguished from the transitional and mature B cells due to absence of IgD (Figure 3.7G and H).

In order to analyse surface BCR expression in mature IgG1M B cells which lack surface IgM expression, anti-kappa and lambda antibodies were used to assess BCR expression in kappa$^+$ and lambda$^+$ B cells respectively (Figure 3.8A).This showed that the BCR density was reduced in IgG1M B cells in both kappa$^+$ and lambda$^+$ cells, with marginal zone B cells showing a stronger reduction in BCR density. Surface BCR expression in IgMg1 B cells was also reduced compared with WT B cells. As previously found (Zhang, 2019), IgMg1 B cells had reduced IgM surface expression in both the follicular B cell and marginal zone B cell compartments (Figure 3.8B and D). However, this was less apparent when using the anti-kappa and lambda antibodies, as they also binding to IgD which was less reduced in IgMg1 follicular B cells and not reduced at all in IgMg1 marginal zone B cells (Figure 3.8C and E). This implies that overall BCR surface expression is more reduced in IgG1M B cells than in IgMg1 B cells. Interestingly, in both WT and IgMg1 mice, lambda$^+$ follicular B cells had higher IgD expression than kappa$^+$ follicular B cells (Figure 3.8C and E), and therefore IgM to IgD ratio was reduced (Figure 3.8F). This may reflect differences in autoreactivity and development of lambda$^+$ follicular B cells, with lambda$^+$ B cells being the fraction that underwent receptor editing due to autoreactivity.

Overall, these data show that B cell maturation is affected by altered BCR signalling in both the IgMg1 as well as IgG1M mice, with opposite effects being seen on follicular

or marginal zone B cell fate choice. Both BCRs induce receptor editing to increase lambda light chain usage, and decrease surface BCR expression suggesting that the presence of the IgG1 cytoplasmic tail during B cell development may induce stronger negative selection.

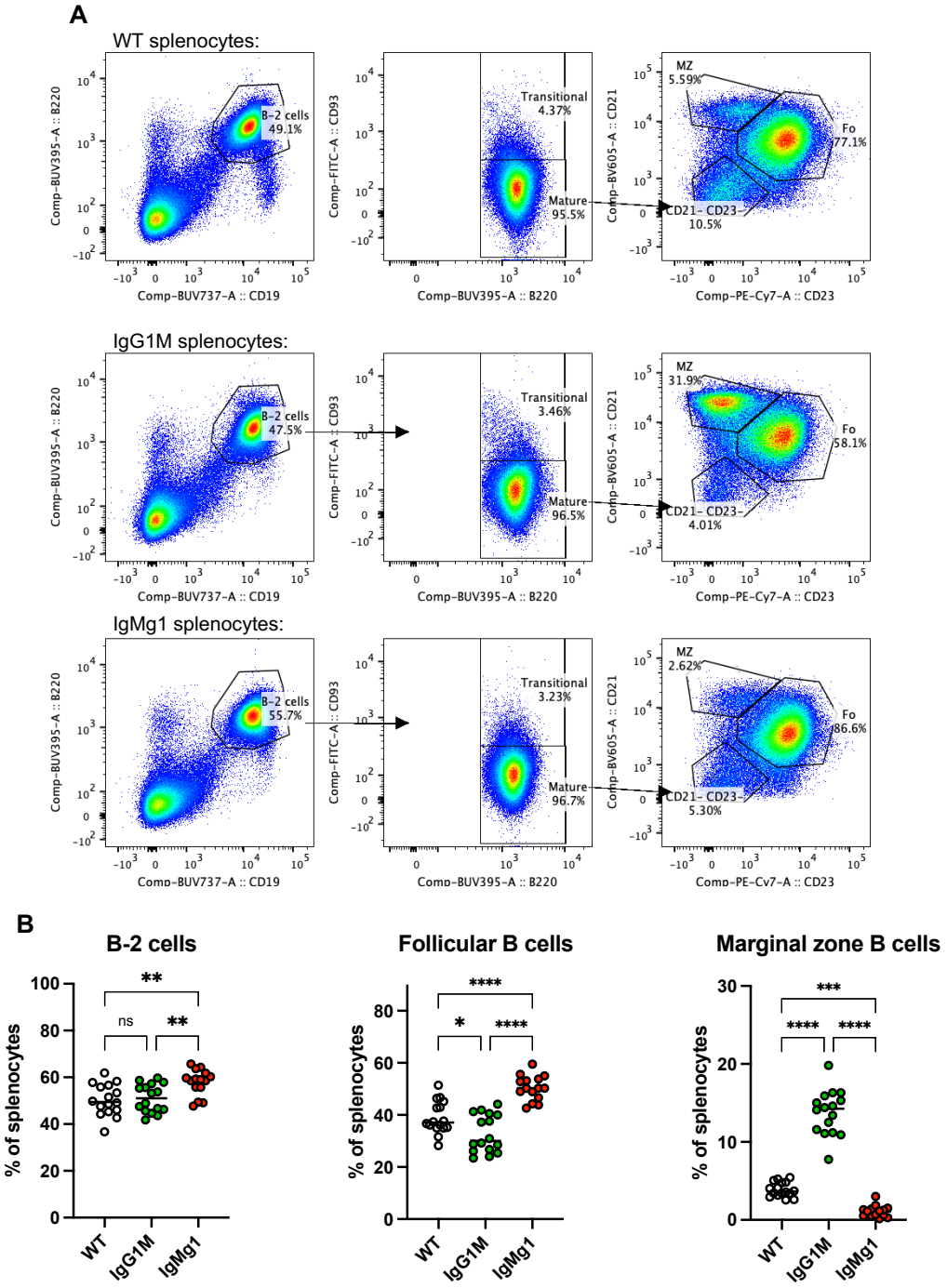

Figure 3.4 Spleen B cell maturation in IgMg1 and IgG1M mice.

Splenocytes from WT, IgMg1 and IgG1M mice were analysed by flow cytometry. (A) Representative gating for follicular (Fo) and marginal zone (MZ) B cells in WT, IgG1M and IgMg1 mice. B-2 cells were gated from splenocytes as $B220^{+}$ $CD19^{+}$; mature B cells were gated as $CD93^{-}$; MZ B cells were $CD21^{hi}$ $CD23^{-}$ and Fo B cells were gated as $CD23^{+}$ $CD21^{+}$. (B) Summary statistics showing frequencies of B-2 cells, Fo B cells and MZ B cells as percentage of splenocytes. Data combined from three independent experiments. Each symbol represents one mouse. Statistical tests were performed by ordinary one-way ANOVA with Tukey's multiple comparison test (ns, not significant; *, $p < 0.05$; **, $p < 0.01$; ***, $p < 0.001$; ****, $p < 0.0001$).

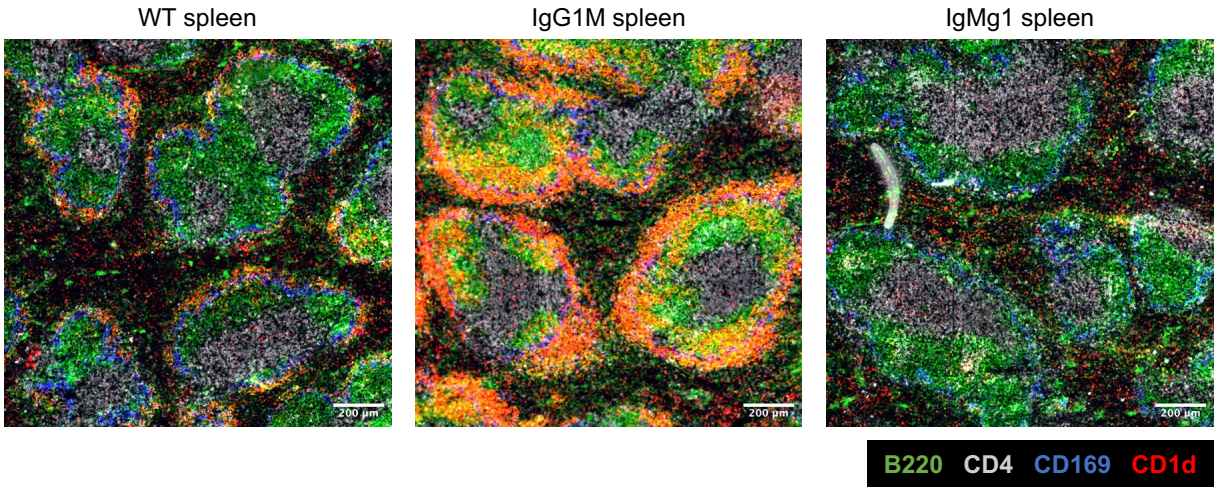

Figure 3.5 Immunofluorescent histology showing marginal zone in spleens of WT, IgG1M and IgMg1 mice

Spleens from mice were stained for B220 (green), CD4 (grey), CD169 (blue) and CD1d (red). Marginal zones can be identified as $CD1d^{+}$ area at edge of B cell follicles. Representative WT (left), IgG1M (centre) and IgMg1 spleens (right) are shown.

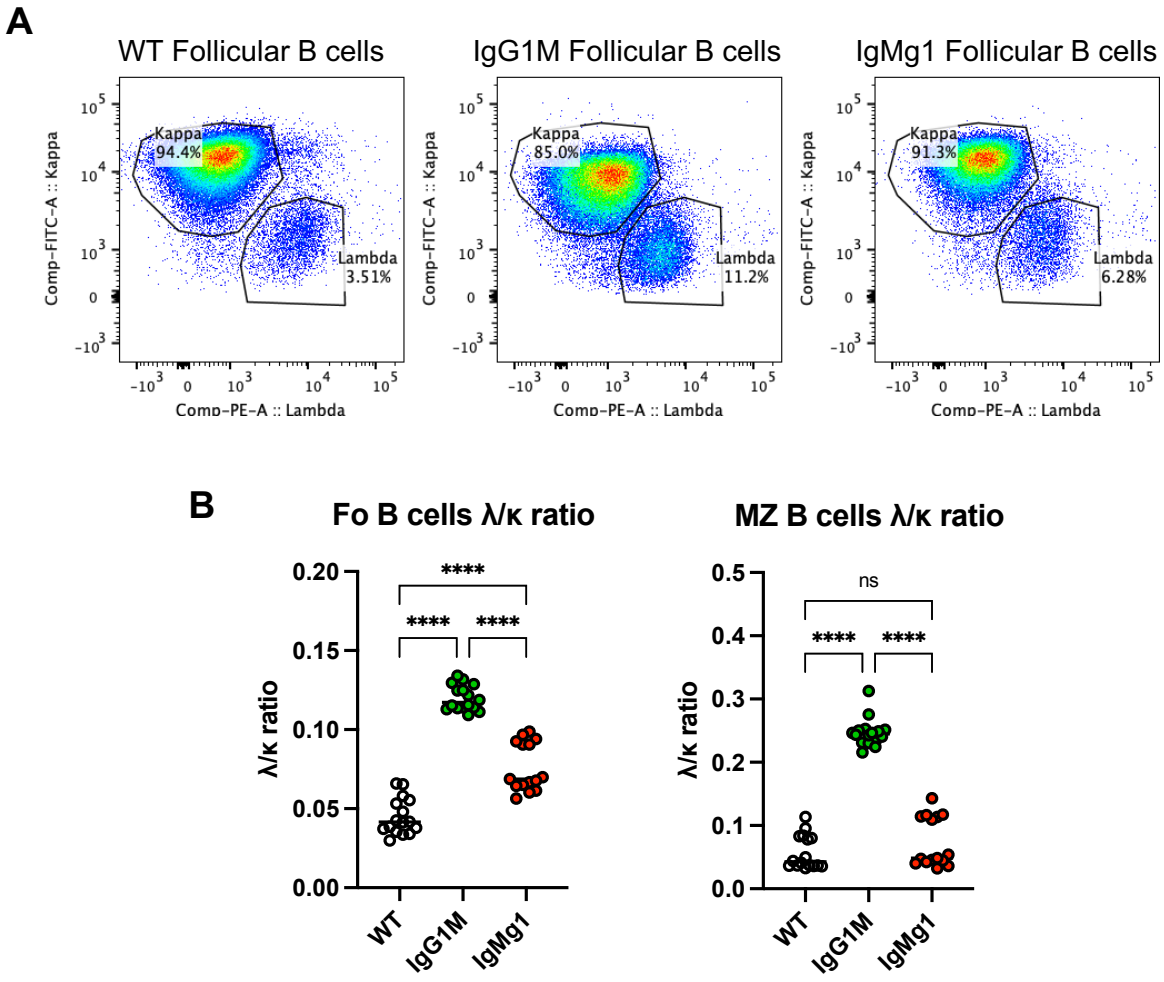

Figure 3.6 Lambda light chain usage in mature B cell populations

Follicular (Fo) and marginal zone (MZ) B cells were gated as shown in Figure 3.4 and analysed for lambda or kappa light chain usage. (A) Representative flow cytometry plots showing lambda and kappa light chain staining in Fo B cells of WT, IgMg1 and IgG1M mice. (B) Summaries of lambda/kappa (λ/κ) ratios from follicular B cells (left) and marginal zone B cells (right). Data combined from three independent experiments. Each symbol represents one mouse. Statistical tests were performed by ordinary one-way ANOVA with Tukey's multiple comparison test (ns, not significant; ****, $p < 0.0001$).

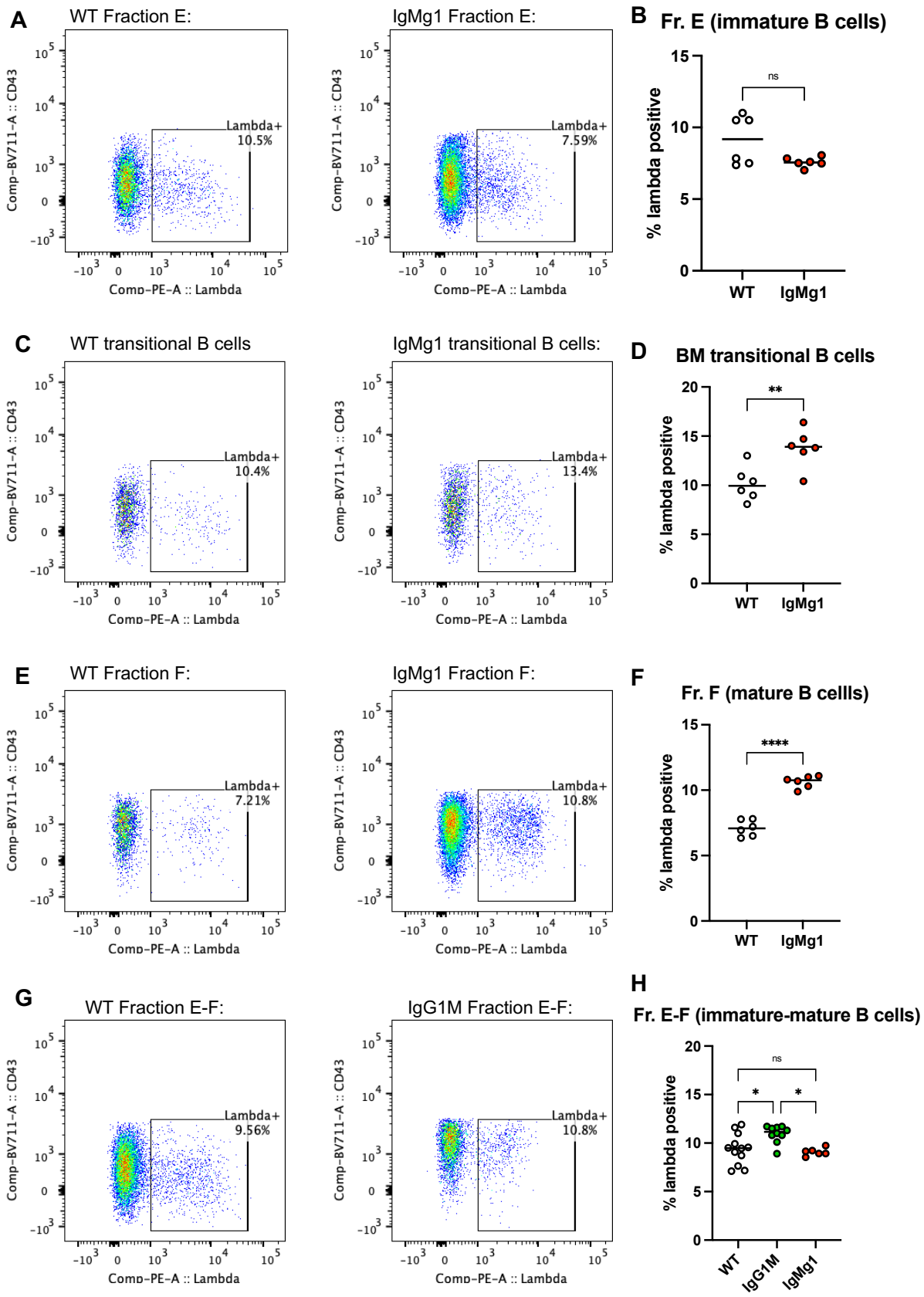
A
WT Fraction E:
Lambda+
10.5%
Comp-BV711-A :: CD43
Comp-PE-A :: Lambda
IgMg1 Fraction E:
Lambda+
7.59%
B
Fr. E (immature B cells)
% lambda positive
ns
WT
IgMg1
C
WT transitional B cells
Lambda+
10.4%
IgMg1 transitional B cells:
Lambda+
13.4%
D
BM transitional B cells
**
E
WT Fraction F:
Lambda+
7.21%
IgMg1 Fraction F:
Lambda+
10.8%
F
Fr. F (mature B cellls)
****
G
WT Fraction E-F:
Lambda+
9.56%
IgG1M Fraction E-F:
Lambda+
10.8%
H
Fr. E-F (immature-mature B cells)
*
IgG1M

Figure 3.7 Lambda light chain usage during bone marrow B cell development.

Bone marrow B cell fractions from immature B cells to mature B cells were analysed for expression of lambda light chain. Bone marrow cells were analysed by flow cytometry and immature B cells (fraction E), transitional B cells and mature B cells (fraction F) were gated as described in Figure 3.1. (A) Representative flow cytometry plots showing lambda expression in immature B cells (fraction E) in WT and IgMg1 mice. (B) Summary statistics for lambda expression in immature B cells in WT and IgMg1 mice. (C) Representative flow cytometry plots showing lambda expression in transitional B cells in WT and IgMg1 mice. (D) Summary statistics for lambda expression in transitional B cells in WT and IgMg1 mice. (E) Representative flow cytometry plots showing lambda expression in mature B cells (fraction F) in WT and IgMg1 mice. (F) Summary statistics for lambda expression in mature B cells in WT and IgMg1 mice. (G) Representative flow cytometry plots showing lambda expression in immature (fraction E) – mature B cells (fraction F) in WT and IgG1M mice. (H) Summary statistics for lambda expression in immature – mature B cells in WT and IgG1M mice. Data are combined from two experiments. Each symbol represents one mouse. Statistical tests performed by paired T-test for comparison of two groups (B, D, F), and ordinary one-way ANOVA with Tukey's multiple comparison test for comparison of three groups (H) (****, $p < 0.0001$; **, $p < 0.01$; *, $p < 0.05$, ns, not-significant).

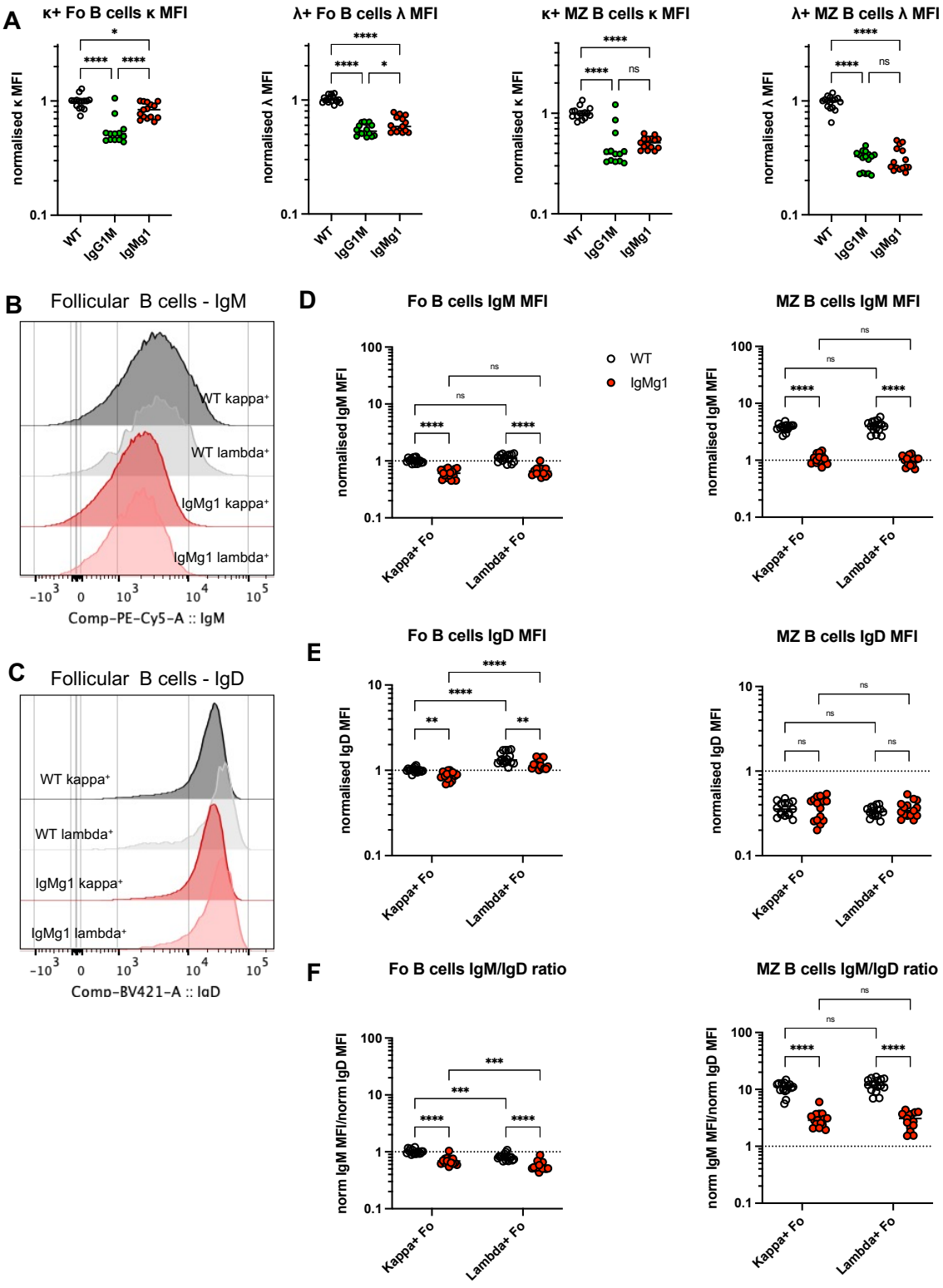
A
κ+ Fo B cells κ MFI
λ+ Fo B cells λ MFI
κ+ MZ B cells κ MFI
λ+ MZ B cells λ MFI
normalised κ MFI
normalised λ MFI
WT
IgG1M
IgMg1
B
Follicular B cells - IgM
WT kappa+
WT lambda+
IgMg1 kappa+
IgMg1 lambda+
Comp-PE-Cy5-A :: IgM
C
Follicular B cells - IgD
Comp-BV421-A :: IgD
D
Fo B cells IgM MFI
MZ B cells IgM MFI
normalised IgM MFI
Kappa+ Fo
Lambda+ Fo
E
Fo B cells IgD MFI
MZ B cells IgD MFI
normalised IgD MFI
F
Fo B cells IgM/IgD ratio
MZ B cells IgM/IgD ratio
norm IgM MFI/norm IgD MFI

Figure 3.8 Surface BCR expression in mature B cells

Kappa$^+$ (κ) and lambda$^+$ (λ) follicular (Fo) and marginal zone (MZ) B cells were gated as in Figure 3.6 and analysed for surface BCR expression by flow cytometry staining with anti-BCR antibodies. (A) Summaries of κ and λ expression in κ$^+$ and λ$^+$ Fo and MZ B cells in WT, IgG1M and IgMg1 spleens. (B-C) Representative histograms showing IgM (B) and IgD (C) expression in WT and IgMg1 κ$^+$ and λ+ Fo B cells. (D) Summaries of IgM expression in κ$^+$ and λ$^+$ Fo and MZ B cells in WT and IgMg1 spleens. (E) Summaries of IgD expression in κ$^+$ and λ$^+$ Fo and MZ B cells in WT and IgMg1 spleens. (F) Ratio between normalised IgM and IgD MFIs in κ$^+$ and λ$^+$ Fo and MZ B cells. Expression levels were determined by flow cytometry. Summary data are presented as geometric means normalised to the median geometric mean of WT (A) or WT κ$^+$ Fo B cells (B and C) to correct for differences between experiments. Data are combined from three independent experiments. Each symbol represents one mouse. Statistical tests were performed by ordinary one-way ANOVA with Tukey's multiple comparison test (A) or two-way ANOVA with Dunn's multiple comparison test (D-F) (ns, not significant; **, $p < 0.01$; ****, $p < 0.0001$).

3.2.3 B cell receptor-stimulated calcium flux is increased in IgG1M B cells but reduced in IgMg1 B cells

Previous work has shown that IgMg1 B cells have an anergic phenotype, as demonstrated by reduced calcium flux following BCR stimulation (Zhang, 2019). This raised the question of whether the anergy was simply a result of the reduced surface BCR density. IgG1M mice, as shown in section 3.2.2, also show evidence of increased negative selection during B cell development leading to reduced surface BCR expression and increased lambda/kappa ratio. To further investigate whether this would lead to an anergic phenotype, the calcium response was tested in B cells from IgG1M mice. Splenocytes taken from mice were calmed for 4 hours before loading with Indo-1 AM to allow tracking of intracellular calcium concentration. Cells were acquired by flow cytometry for 1 minute, before adding anti-BCR antibody as stimulation to evaluate the calcium response.

As expected, the IgMg1 B cells had a reduced calcium response compared to WT mice after stimulation with an anti-IgM $F(ab')_2$ (Figure 3.9A and B). In order to compare with B cells from the IgG1M mice that do not express IgM, cells were stimulated with a mixture of anti-kappa and anti-lambda antibodies (Figure 3.9C). As with the anti-IgM stimulation, there was a reduced calcium response in the IgMg1 mice following anti-kappa and lambda stimulation (Figure 3.9C), indicated by a reduced peak bound/unbound calcium ratio (Figure 3.9D). However, the IgG1M B cells had an increased response compared to both WT and IgMg1 B cells (Figure 3.9C), shown by an increased peak bound/unbound calcium ratio (Figure 3.9D). This suggests that, despite the partial block in B cell development and reduced BCR surface expression, the mature B cells in IgG1 expressing mice maintain hyperactive B cell receptor

signalling. In contrast, the IgMg1 mice develop B cells with an anergic phenotype. This shows further, that reduced BCR expression is unlikely to cause the anergic phenotype in IgMg1 B cells, and additional factors, for example altered BCR signalling, are likely to contribute to anergy in IgMg1 B cells.

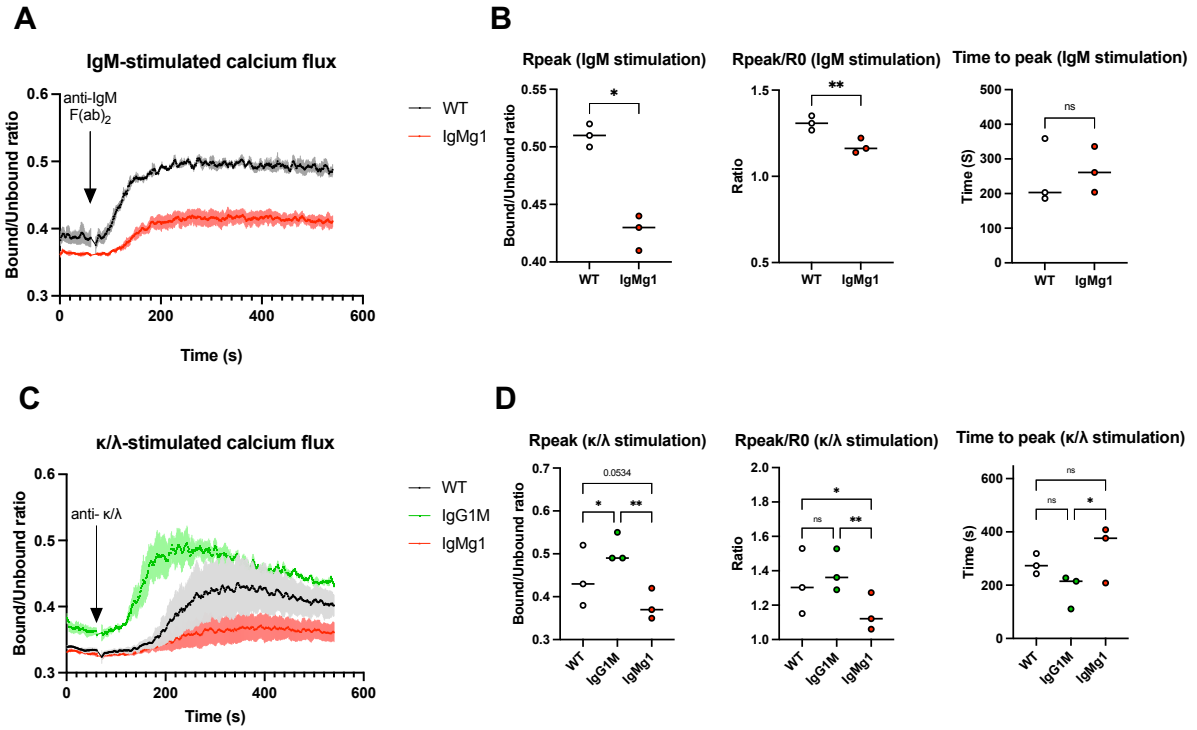

Figure 3.9 BCR stimulated calcium signalling in splenocytes

Splenocytes from WT, IgMg1 and IgG1M mice were rested for 4 hours and then loaded with Indo-1 AM and anti-CD43 PE. Cells were acquired by flow cytometry for 1 minute to collect baseline reading and then stimulated with anti-IgM or anti-kappa (κ) and lambda (λ) and acquired for 9 minutes. Cells were gated on $CD43^-$ cells and analysed in FlowJo to calculate bound/unbound calcium ratio. (A) IgM stimulated calcium flux in WT and IgMg1 splenocytes**.** Error bars represent standard error mean. (B) Summary statistics showing Rpeak (peak bound/unbound calcium ratio), Rpeak/R0 (ratio of Rpeak to R0 (baseline bound/unbound calcium ratio), and time to peak for WT and IgMg1 cells stimulated with anti-IgM. One spleen used per group, with each symbol representing one replicate. (C) Anti-Igκ/λ stimulated calcium flux in WT, IgG1M and IgMg1 splenocytes. Error bars represent standard error mean. (D) Summary statistics showing Rpeak, Rpeak/R0 and time to peak for WT, IgG1M and IgMg1 cells stimulated with anti-κ/λ. One spleen used per group, with each symbol representing one replicate. Statistical tests performed by paired T-test for comparison of two groups, and one-way repeated measure ANOVA with Tukey's multiple comparison test for comparison of three groups (**, $p < 0.01$; *, $p < 0.05$, ns, not-significant).

3.2.4 Spleen transitional B cells are reduced in IgMg1 mice and IgG1M mice

Although B cell development in the bone marrow of IgMg1 B cells appears relatively normal, there are increased mature B cells in the bone marrow, and in the spleen, there is an altered ratio of follicular to marginal zone B cells. Therefore, fate decisions during B cell maturation may be affected. To break this down further, transitional B cells in the spleen were analysed by flow cytometry. Transitional B cells in the spleen can be identified by CD93 expression and can be split into T1, T2 and T3 B cells based on levels of IgM and CD23 expression. T3 B cells ($CD23^{hi}$ IgM^{lo}) have been described as an anergic-like B cell subset (Merrell et al., 2006), and therefore it might be expected that these cells would be present in greater numbers in the IgMg1 mice due to anergy.

The overall number and percentage of $CD93^{+}$ transitional B cells were found to be decreased in IgMg1 spleens compared with wildtype spleens (Figure 3.10). This affected primarily T1 B cells with a reduction of 75%, but also T2 B cells with a 60% reduction. The percentages of T1 and T2 B cells were both reduced in IgMg1 mice, however there was an increase in the ratio of T2:T1 B cells. T3 B cells are defined phenotypically as being $CD23^{hi}$ IgM^{lo} within the $CD93^{+}$ transitional B cells (Allman et al., 2001). Due to the reduced IgM expression IgMg1 transitional B cells, T3 B cells in IgMg1 mice were increased by a factor of 2.

$CD93^{+}$ transitional B cells were also reduced in IgG1M mice (Figure 3.11A and B). As IgM expression could not be used to distinguish transitional cell subsets in IgG1M mice, only CD21 and CD23 could be used to separate T1 ($CD21^{lo}$ $CD23^{lo}$) from T2 and T3 cells ($CD21^{hi}$ $CD23^{hi}$). In IgG1M mice T1 cells were virtually absent, and T2 and T3 cells were reduced by 50%. A large proportion of the $CD93^{+}$ B cells had a $CD21^{hi}$ $CD23^{lo}$ phenotype. These were possibly contamination with marginal zone B cells.

However, when these cells were analysed for CD93 expression, they did not exclusively lie on the border between transitional $CD93^+$ and $CD93^-$ mature B cells (Figure 3.11C). Therefore, it is unclear if these cells are genuine transitional B cells with different expression of CD21 and CD23, or a contaminant with marginal zone B cells.

Overall, these data show that transitional cells are reduced in IgMg1, while they are severely reduced in IgG1M mice. This further demonstrates that B cell maturation is affected by B cell receptor signalling, and that signalling through complete IgG1 provides a different stimulus during transitional stage than IgMg1 BCR.

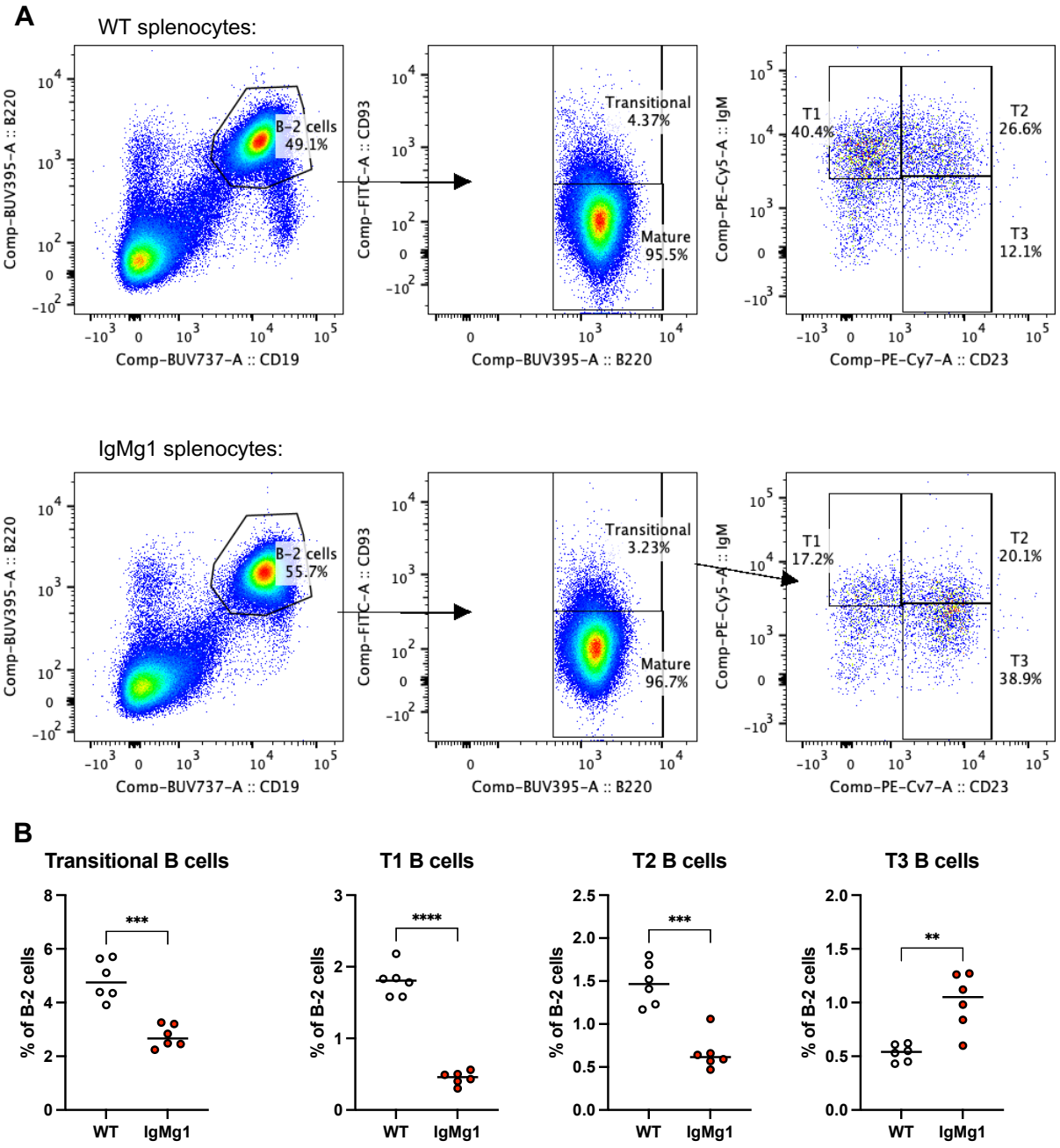

Figure 3.10 Transitional B cells in IgMg1 mice

Splenocytes from WT and IgMg1 mice were analysed by flow cytometry for transitional B cells. (A) Gating strategy for transitional, T1, T2 and T3 cells in representative WT and IgMg1 mice. From splenocytes, B-2 cells were gated as $B220^{+}$ $CD19^{+}$. From B-2 cells, transitional B cells were gated as $CD93^{hi}$. The position of this gate was set using a CD93 fluorescent minus one (FMO) control (not shown). From transitional cells, T1 cells were gated as $CD23^{lo}$ IgM^{hi}; T2 cells were gated as $CD23^{hi}$ IgM^{hi}; and T3 cells were gated as $CD23^{hi}$ IgM^{lo}. (B) Summaries of frequencies of transitional, T1, T2 and T3 cells in WT and IgMg1 mice as percentage of total B-2 cells. Data is shown from one experiment. Each symbol represents one mouse. Statistical tests were performed by two-tailed unpaired T-test. (****, $p < 0.0001$; ***, $p < 0.001$; **, $p < 0.01$; *, $p < 0.05$; ns, not significant).

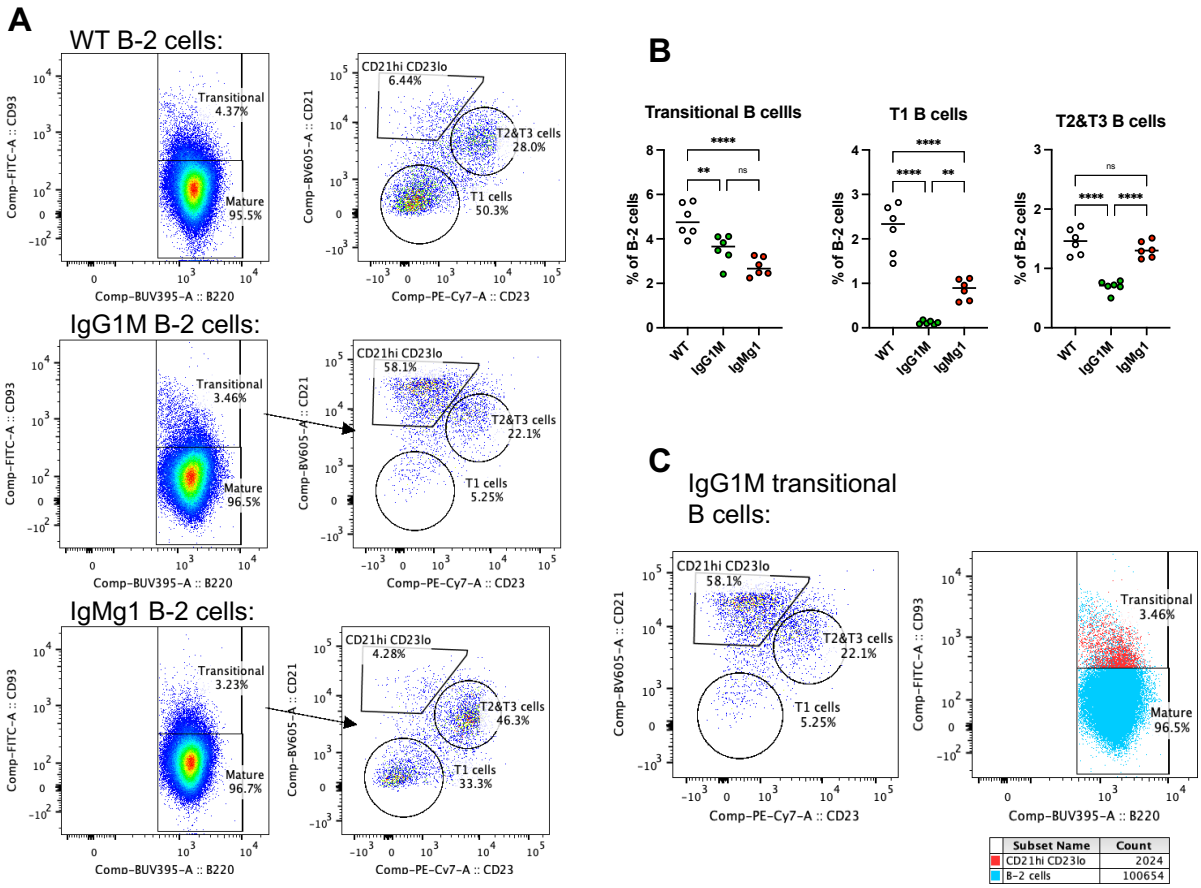

Figure 3.11 Transitional B cells in IgG1M and IgMg1 mice

Splenocytes from WT and IgMg1 mice were analysed by flow cytometry for transitional B cells using an alternative gating strategy. (A) Gating strategy for transitional, T1 and T2&T3 cells for representative WT, IgG1M and IgMg1 mice. B-2 cells were gated as shown in Figure 3.10. From B-2 cells, transitional B cells were gated as $CD93^{+}$. From transitional B cells, T1 B cells were gated as $CD21^{lo}$ $CD23^{lo}$ and $CD21^{hi}$ $CD23^{hi}$. (B) Summary of frequencies of transitional, T1 and T2&T3 cells in WT, IgG1M and IgMg1 mice as percentage within B-2 cells. Data are from one experiment. Statistical tests were performed by ordinary one-way ANOVA with Tukey's multiple comparison test. (****, $p < 0.0001$; **, $p < 0.01$; ns, not significant). (C) IgG1M $CD21^{hi}$ $CD23^{lo}$ population (red) shown on the flow cytometry plot of CD93 and B220 expression with total B-2 cells (blue).

3.2.5 B-1 cell development is impaired in IgMg1 and IgG1M mice

Although conventional B-2 B cells that develop in the bone marrow make up most B cells in mice, there is an additional mature subset of B cells: B-1 cells. These cells develop in the fetal liver and are a prominent cell type in the peritoneal and pleural cavities. To investigate the effect of altered BCR signalling on B-1 cell development, the peritoneal cavity cells of mice were analysed by flow cytometry (Figure 3.12).

B-1 cells are phenotypically described as $CD19^{+}$ $B220^{lo}$ and can be either $CD5^{+}$ (B-1a) or $CD5^{-}$ (B-1b). They are also $CD43^{+}$ and $CD23^{-}$ (Tung et al., 2004). Around half of the peritoneal cavity B cells in WT mice were found to be $B220^{lo}$, and the majority of these had the expected $CD43^{+}$ and $CD23^{-}$ phenotype of B-1 cells (Figure 3.12A). In both IgMg1 and IgG1M mice there was a much less distinct $B220^{lo}$ population, and the majority of these cells did not have the $CD43^{+}$ $CD23^{-}$ phenotype (Figure 3.12A). By defining B-1a and B-1b cells in this way, there was a clear reduction of B-1a cells in both IgMg1 and IgG1M mice (Figure 3.12C), and a reduction of B-1b cells in IgG1M mice (Figure 3.12D). However, B-1b cells in IgMg1 mice were not significantly affected (Figure 3.12D). $B220^{hi}$ $CD5^{lo}$ B-2 cells were not significantly altered in IgMg1 or IgG1M mice (Figure 3.12E). In the IgG1M peritoneal cavity, there was an expanded $B220^{hi}$ $CD5^{hi}$ population that was not present in WT mice (Figure 3.12F).

To further illustrate the altered phenotype of B cells in the peritoneal cavity of IgMg1 and IgG1M mice, a tSNE dimensionality reduction was performed on the $CD19^{+}$ cells using CD19, B220, CD5, CD11b, CD43, CD23 and CD21 expression as parameters. B-1a, B-1b and B-2 clusters were manually identified by back gating of the WT populations identified using the gating strategy described in Figure 3.12 (Figure 3.13A). These data confirm that the peritoneal cavity B cell populations in the IgMg1 and

IgG1M models are altered compared with WT mice. There is a clear reduction of cells in the B-1a and B-1b clusters located towards the bottom of the tSNE plot in both IgG1M and IgMg1 mice. In IgG1M mice there is an expanded cluster of $CD5^{hi}$ cells positioned at the top of the tSNE plot. However, despite their CD5 expression, they cluster closer to the B-2 cells and look more similar to B-2 cells with regards to expression of other markers such as CD43, CD23 and CD21, so may be an unusual population of $CD5^{hi}$ B2 cells (Figure 3.13B).

B-1 cells are also present at low abundance in the spleen. Splenocytes from WT, IgMg1 and IgG1M mice were analysed for B-1 cells by flow cytometry (Figure 3.14A). As in the peritoneal cavity, splenic B-1 cells were severely reduced in IgG1M and less in IgMg1 mice (Figure 3.14B). This was true for both B-1a (Figure 3.14C) and B-1b cells (Figure 3.14D). Similar to peritoneal cavity, spleen B-2 cells in IgG1M mice were found to have increased CD5 expression (Figure 3.14E and F), providing further evidence that the $B220^{hi}$ $CD5^{hi}$ cells in the peritoneal cavity may be B-2 cells, not B-1 cells.

Overall, these data show that in addition to affecting development of conventional B-2 cells, altered BCR signalling in IgG1M and IgMg1 mice results in impaired development of B-1 cells and altered peritoneal cavity B cell populations.

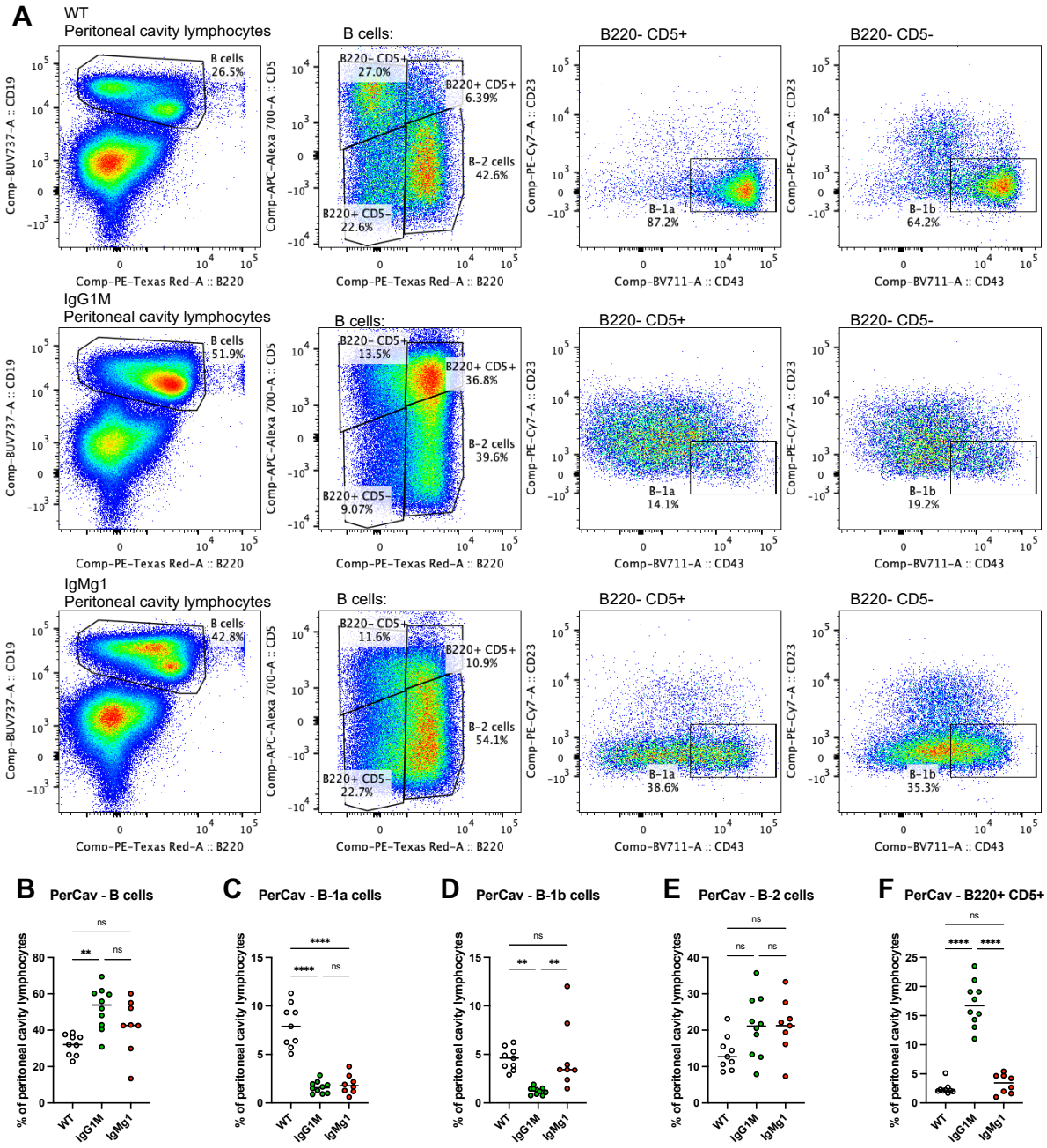

Figure 3.12 Peritoneal cavity B cells in IgMg1 and IgG1M mice

Peritoneal cavity cells were from WT, IgG1M and IgMg1 mice were analysed by flow cytometry. (A) Gating strategy shown for peritoneal cavity B cell phenotyping of representative WT, IgG1M and IgMg1 mice. From lymphocytes, B cells were gated as $CD19^{+}$. From B cells, B-2 cells were gated as $B220^{hi}$ $CD5^{lo}$; B-1a cells were gated as $B220^{lo}$ $CD5^{hi}$ $CD23^{-}$ $CD43^{+}$ and B-1b cells were gated as $B220^{lo}$ $CD5^{lo}$ $CD23^{-}$ $CD43^{+}$. $B220^{+}$ $CD5^{+}$ cells were also gated from B cells. (B-F) Summary statistics for (B) B cells, (C) B-1a cells, (D) B-1b cells, (E) B-2 cells and (F) $B220^{+}$ $CD5^{+}$ B cells as percentage of peritoneal cavity lymphocytes. Data are combined from two experiments. Each symbol represents one mouse. Statistical tests were performed by ordinary one-way ANOVA with Tukey's multiple comparison test. (****, $p < 0.0001$; **, $p < 0.01$; ns, not significant).

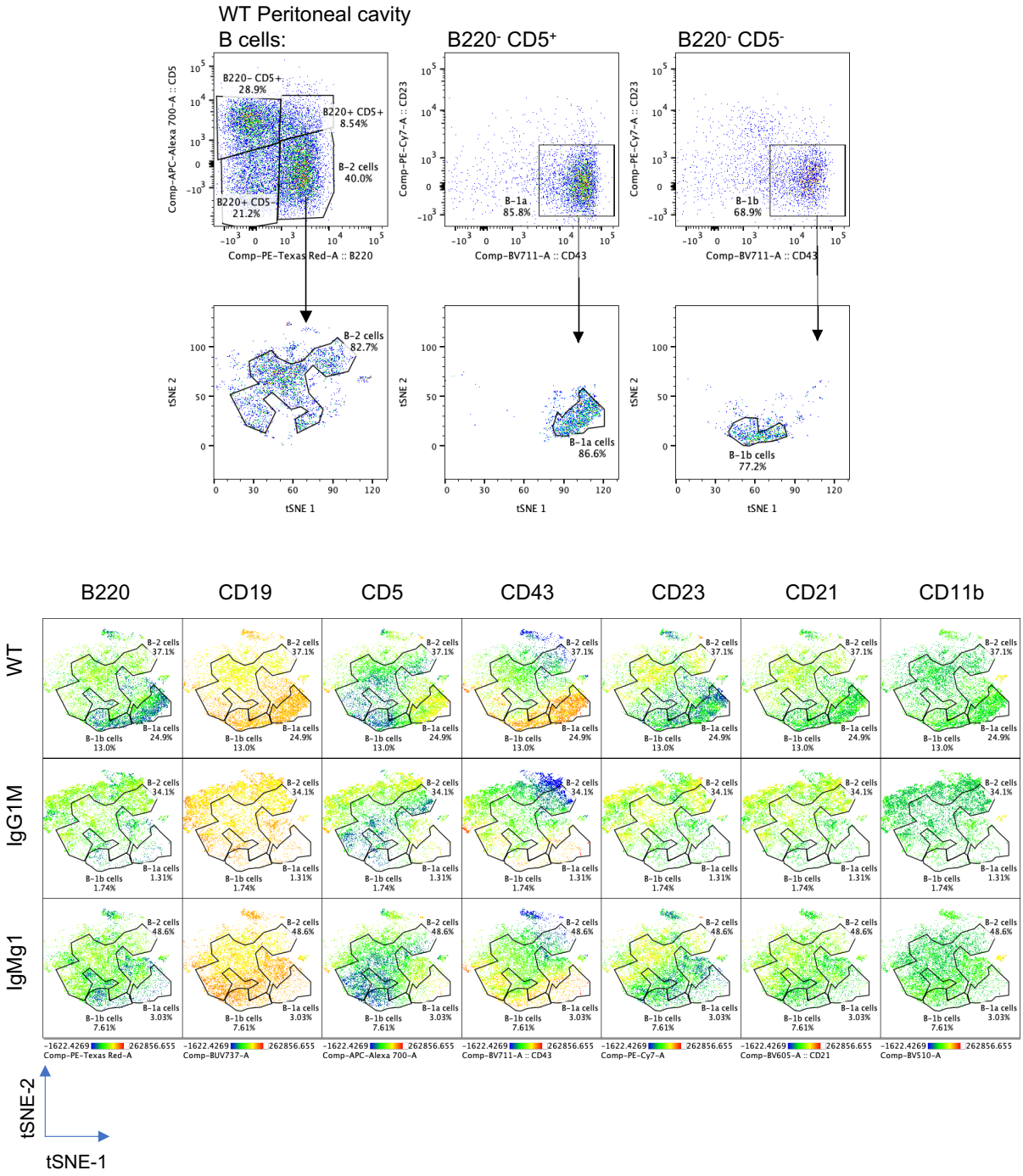

Figure 3.13 tSNE of peritoneal cavity B cells

tSNE algorithm was performed to reduce dimensionality of flow cytometry parameters B220, CD19, CD5, CD43, CD23, CD21 and CD11b in WT, IgG1M and IgMg1 peritoneal cavity B cells. (A) Gates for B-1a, B-1b and B-2 cells were manually drawn after back gating of WT populations identified using gating strategy in Figure 3.12. (B) tSNE plots coloured by heatmap statistic showing expression of the surface markers for each of 3 genotypes.

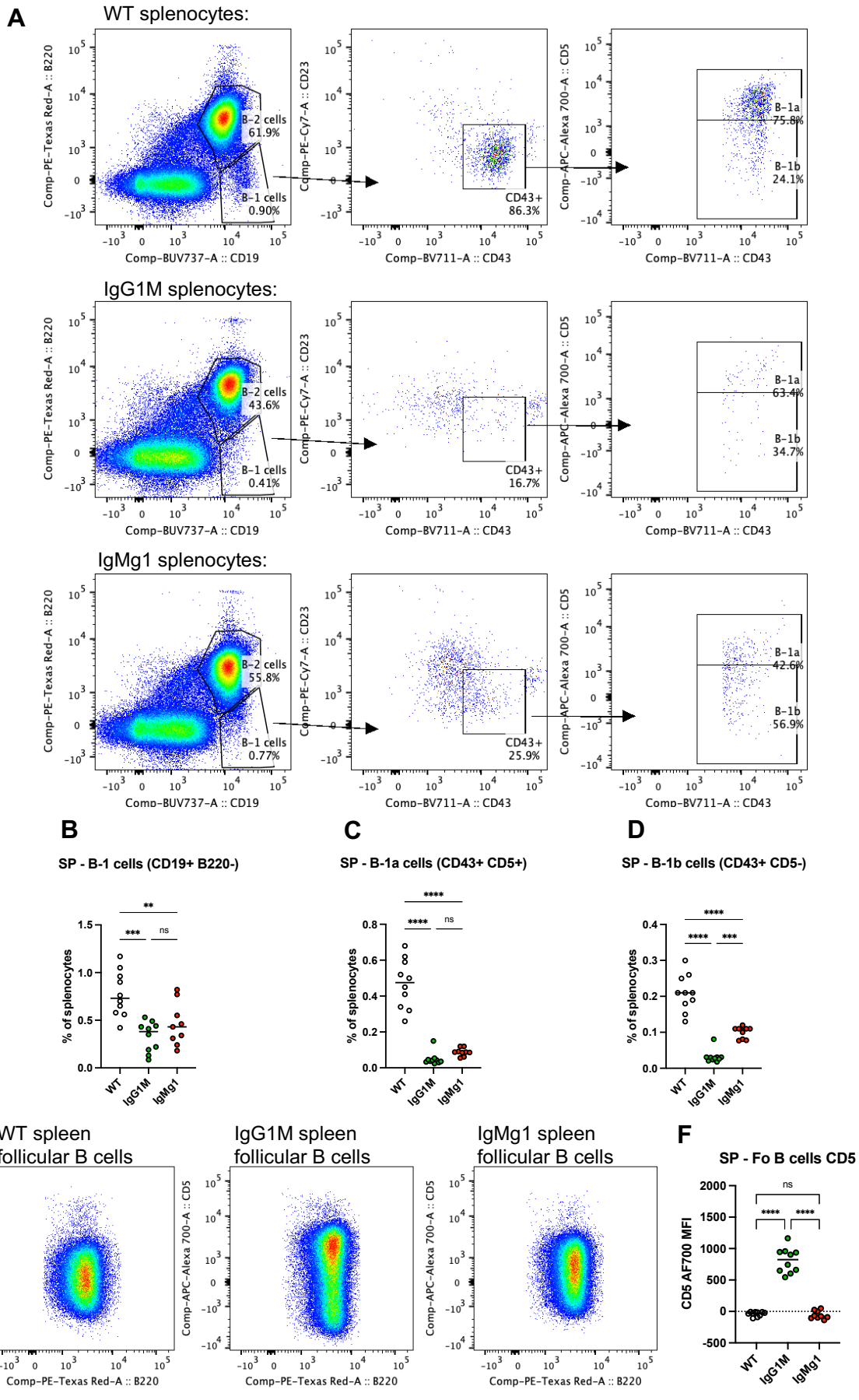
A
WT splenocytes:
B-2 cells
61.9%
B-1 cells
0.90%
CD43+
86.3%
B-1a
75.8%
B-1b
24.1%
IgG1M splenocytes:
B-2 cells
43.6%
B-1 cells
0.41%
CD43+
16.7%
B-1a
63.4%
B-1b
34.7%
IgMg1 splenocytes:
B-2 cells
55.8%
B-1 cells
0.77%
CD43+
25.9%
B-1a
42.6%
B-1b
56.9%
Comp-PE-Texas Red-A :: B220
Comp-BUV737-A :: CD19
Comp-PE-Cy7-A :: CD23
Comp-BV711-A :: CD43
Comp-APC-Alexa 700-A :: CD5
B
SP - B-1 cells (CD19+ B220-)
C
SP - B-1a cells (CD43+ CD5+)
D
SP - B-1b cells (CD43+ CD5-)
% of splenocytes
WT
IgG1M
IgMg1
E
WT spleen follicular B cells
IgG1M spleen follicular B cells
IgMg1 spleen follicular B cells
F
SP - Fo B cells CD5
CD5 AF700 MFI
ns

Figure 3.14 Spleen B-1 cell development

Splenocytes from WT, IgMg1 and IgG1M mice were analysed by flow cytometry. (A) Flow cytometry gating strategy shown for representative WT, IgG1M and IgMg1 mice. From splenocytes, B-1 cells were gated as $CD19^{+}$ $B220^{-}$; from B-1 cells, cells were gated as $CD43^{+}$ $CD23^{-}$; from $CD43^{+}$ $CD23^{-}$ cells, B-1a cells were gated as $CD5^{+}$ and B-1b cells were gated as $CD5^{-}$. (B-D) Summary statistics for frequencies of (B) splenic B-1 cells, (C) B-1a cells, and (D) B-1b cells, all shown as percentage of splenocytes. (E) Representative flow cytometry showing CD5 expression in follicular B cells in WT, IgG1M and IgMg1 mice. Follicular B cells were gated as shown in Figure 3.4. (F) Summary statistics for CD5 expression in B-2 cells. Data are combined from two experiments. Each symbol represents one mouse. Statistical tests were performed by ordinary one-way ANOVA with Tukey's multiple comparison test. (****, $p < 0.0001$; ***, $p < 0.001$; **, $p < 0.01$; ns, not significant).

3.2.6 Differential gene expression in IgMg1 follicular B cells

The above showed that IgMg1 B cells have an anergic phenotype. The data derived from IgG1M mice suggests that reduced surface BCR expression does not inevitably cause B cell anergy. To screen for other gene expression changes inducing the anergic phenotype, bulk RNA sequencing was done to analyse gene expression in follicular B cells from WT and IgMg1 mice. Follicular B cells ($B220^+$ $CD138^-$ Fas^- $CD38^+$ $CD19^+$ $GL7^-$ $CD93^-$ $CD21^+$ $CD23^+$) were sorted by fluorescent activated cell sorting (FACS) from the popliteal lymph node on the opposite side from injection site with NP-CGG, and bulk RNA sequencing was performed to monitor gene expression. A principal components analysis (PCA) was performed to reduce dimensionality of the gene expression data and assess variability between the samples (Figure 3.15A). This showed that there is a difference between WT and IgMg1 B cells as they separated on principal component 1. There was also some variation within each genotype on principal component 2. Using an adjusted p-value threshold of 0.05 and at least 2-fold difference in gene expression, 89 genes were identified that were differentially expressed between WT and IgMg1 B cells: 53 were upregulated in IgMg1, and 36 were downregulated (Figure 3.15B and Figure 3.16A). An additional, 29 significantly upregulated and 18 significantly downregulated genes were identified with a lower than 2-fold change (Figure 3.16B).

Some of the genes identified were expected: upregulation of *Iglv1*, *Iglc1* and *Iglv2* reflects the increased usage of lambda light chain observed by flow cytometry; upregulation of *Ighc1* may reflect the presence of the section of gene coding the IgG1 cytoplasmic tail on the IgMg1 BCR. To further investigate the function of some of the

other genes, functional analyses were performed. The lists of differentially expressed genes were analysed for enriched gene ontology (GO) terms using g:Profiler. This showed that immune system process (GO:0002376), immune response (GO:0006955), response to stimulus (GO:0050896) and cell activation (GO:0001775) were amongst the GO terms enriched in the list of IgMg1 upregulated genes (Figure 3.17A and B). Differentially expressed genes from the immune system process GO term (GO:0002376) include *Apoe*, *Jchain*, *Ackr2* (all upregulated in IgMg1), *Ccr6*, *Slamf1* and *Ifi208* (all downregulated in IgMg1) (Figure 3.17C). Gene set enrichment analysis (GSEA) was performed using the whole expression dataset to identify gene sets that were significantly enriched in IgMg1 or WT follicular B cells (Figure 3.18). Of the hallmark gene sets, oxidative phosphorylation was found to be significantly enriched (false discovery rate (FDR) q-value < 0.05) in IgMg1 follicular B cells (Figure 3.18 and Figure 3.19A). Genes that made up the leading edge for this gene set included *Casp7* (encoding caspase 7) (Figure 3.19C), *Fxn* (encoding frataxin) (Figure 3.19D), *Nqo2* (encoding NAD(P)H dehydrogenase, quinone 2) (Figure 3.19E) and *Decr1* (encoding 2,4 Dienoyl-CoA reductase) (Figure 3.19F). GSEA was also performed using the gene ontology biological process gene sets, pre-filtered for gene sets related to immune function (Figure 3.20). Although none of the gene sets in this analysis reached significance with FDR q-value below 0.05, several gene sets had a nominal p-value of less than 0.05 (Figure 3.20A). Gene sets related to humoral immune response were enriched in IgMg1 follicular B cells (Figure 3.20B), whereas gene sets related to immune cell activation (Figure 3.20C) and negative regulation (Figure 3.20D) of immune response were enriched in WT follicular B cells.

Overall, these data indicate that there were a relatively small number of genes identified that were differentially expressed in IgMg1 follicular B cells compared with WT follicular B cells.

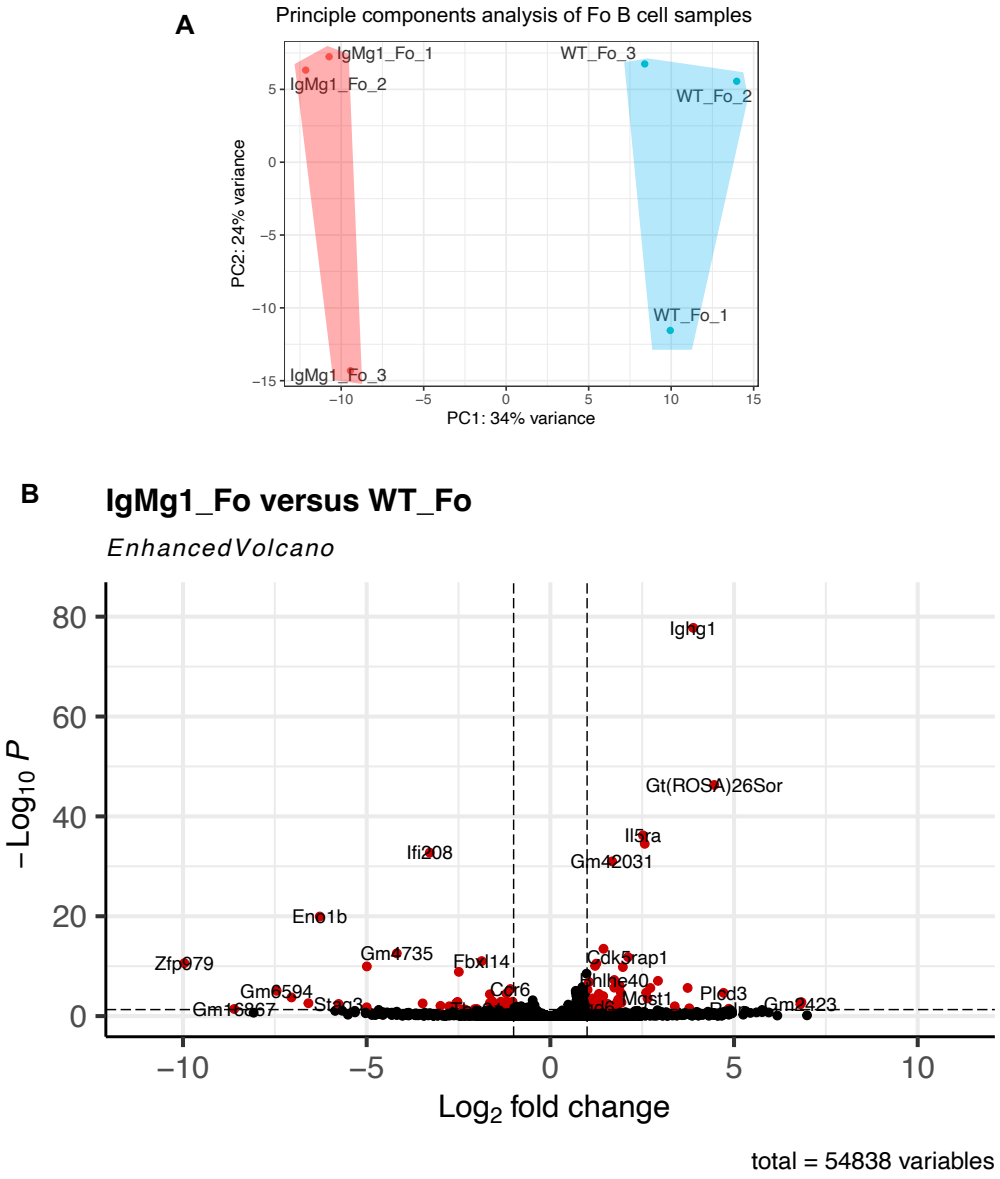

Figure 3.15 Bulk RNA sequencing comparing WT and IgMg1 follicular B cells

Follicular B cells from WT and IgMg1 mice were sequenced by bulk RNA sequencing. (A) Expression data had dimensionality reduced using principal components analysis to assess variance between samples. (B) Differentially expressed genes were identified using DESeq2 package on R. Volcano plot shows differentially expressed genes (2-fold change and adjusted p value < 0.05) indicated in red. Horizontal dashed line represents p value of 0.05 and vertical dashed lines represent $\log_2$ fold-change of 1 and -1.

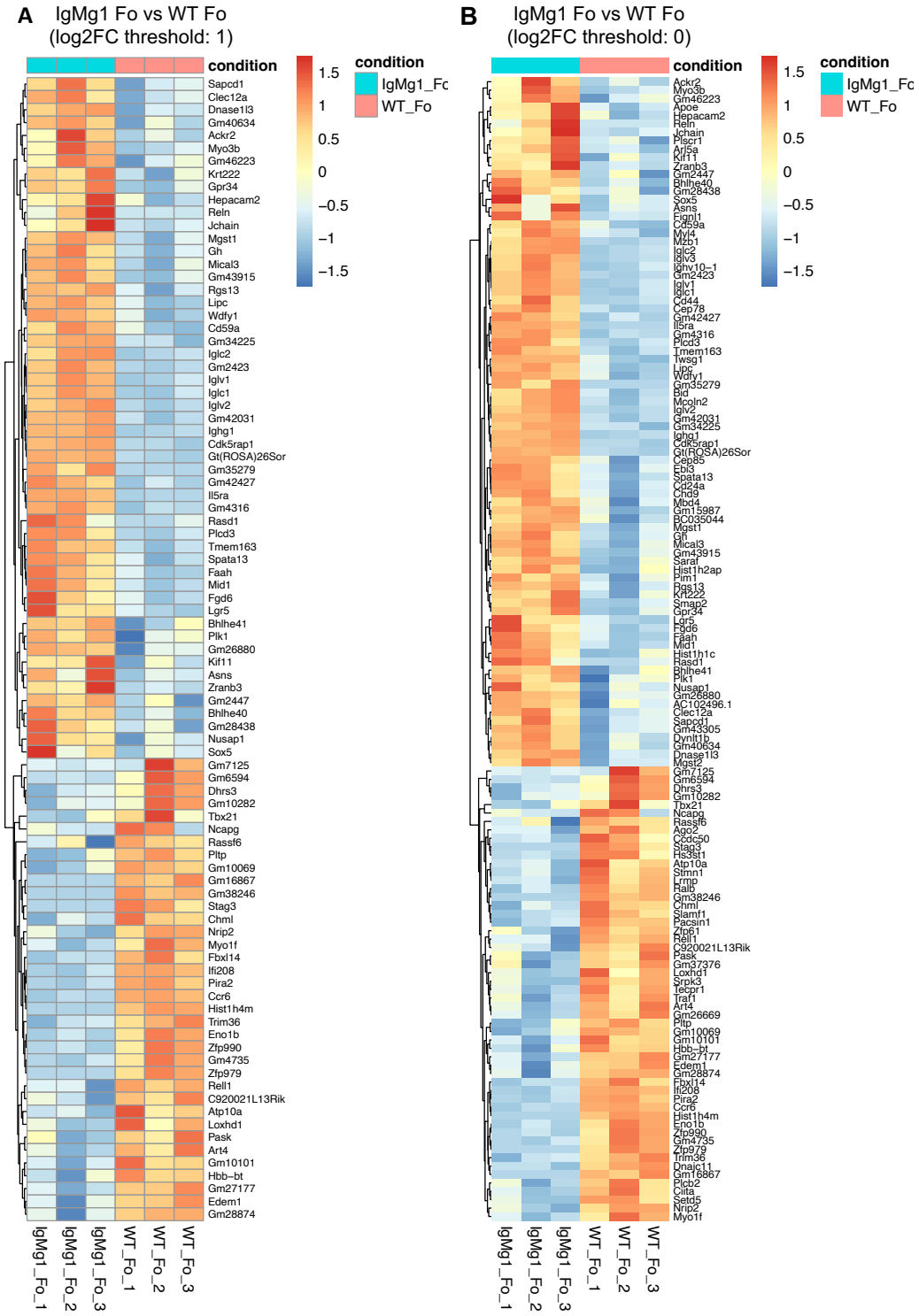

Figure 3.16 Heatmaps showing differentially expressed genes

Heatmaps produced to show relative expression of differentially expressed genes identified in IgMg1 follicular B cells compared with WT follicular B cells. (A) Significantly differentially expressed genes (adjusted p value < 0.05) with a log2FC threshold of 1 (at least 2-fold difference in gene expression). (B) Significantly differentially expressed genes (adjusted p value < 0.05) with no threshold for log2FC used. Colour scale represents gene Z-score.

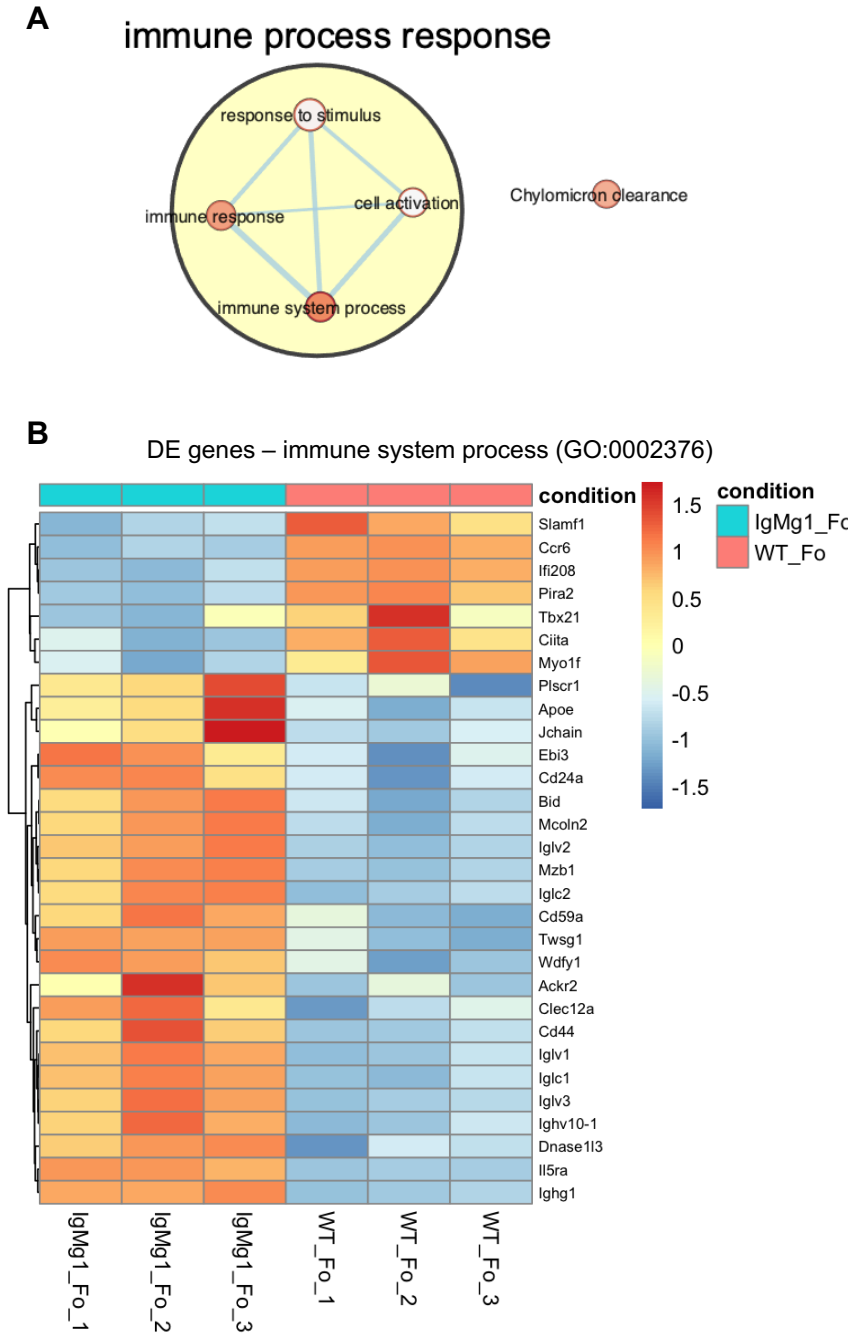

Figure 3.17 Immune process response genes enriched within upregulated IgMg1 follicular B cell genes

Genes identified as upregulated in IgMg1 follicular B cells compared with WT follicular B cells were analysed for gene ontology (GO) term enrichment using g:profiler (Reimand et al., 2019). (A) Enrichment map showing enriched GO terms (adjusted p value < 0.05) from biological processes and reactome GO terms. Each circle represents a GO term enriched in IgMg1 follicular B cells. GO terms connected by a line contain overlapping genes. Clusters of GO terms containing similar genes have been grouped together in a large circle. (B) Heatmap showing relative expression of differentially expressed genes contained in GO term immune system process (GO:002376). Colour scale represents gene Z-score.

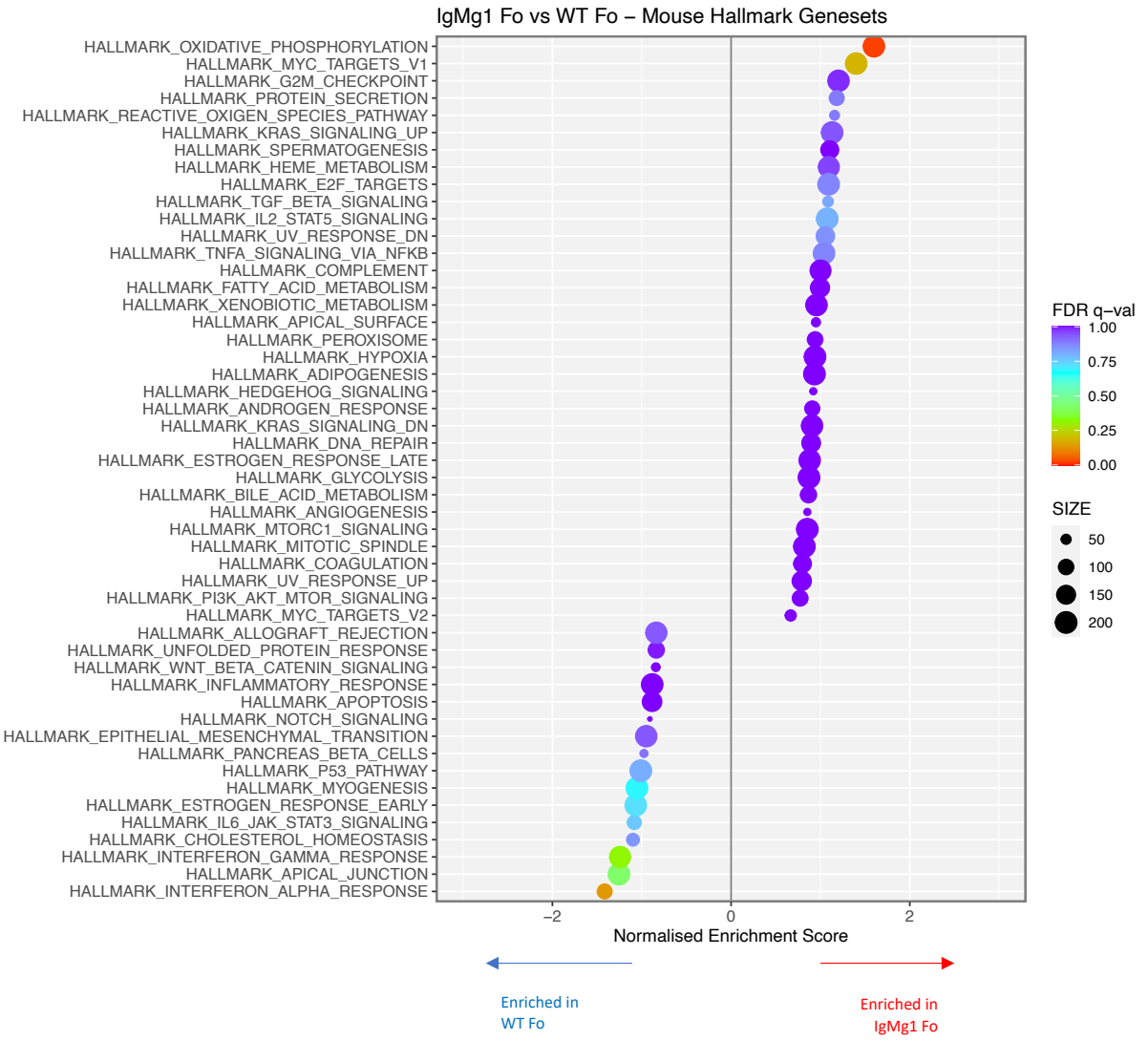

Figure 3.18 Gene set enrichment analysis for hallmark gene sets

Gene set enrichment analysis (GSEA) was performed on IgMg1 and WT follicular B cell expression data, comparing to mouse hallmark gene sets. Plot shows normalised enrichment scores for hallmark gene sets for GSEA performed between IgMg1 and WT follicular B cells. Size of circle represents number of genes in set. Colour represents false discovery rate (FDR) q-value.

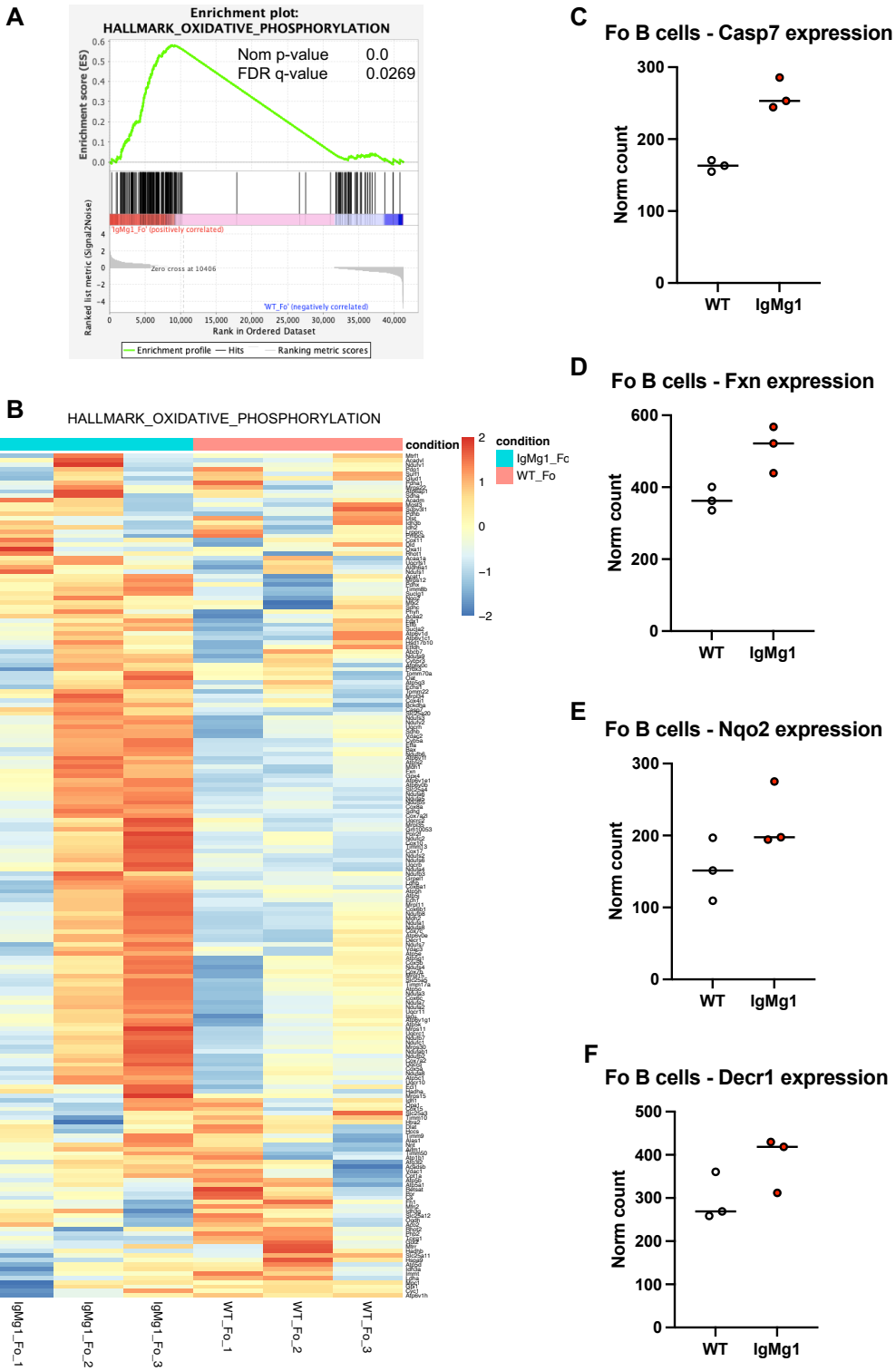

Figure 3.19 Oxidative phosphorylation enriched in IgMg1 follicular B cells compared to WT

(A) Gene set enrichment analysis for hallmark oxidative phosphorylation gene set. (B) Heatmap showing relative gene expression for genes in hallmark oxidative phosphorylation gene set. Colour scale represents gene Z-score. (C-F) Gene expression for four genes in leading edge: (C) *Casp7*, (D) *Fxn*, (E) *Nqo2*, (F) *Decr1*. Expression is shown as normalised count.

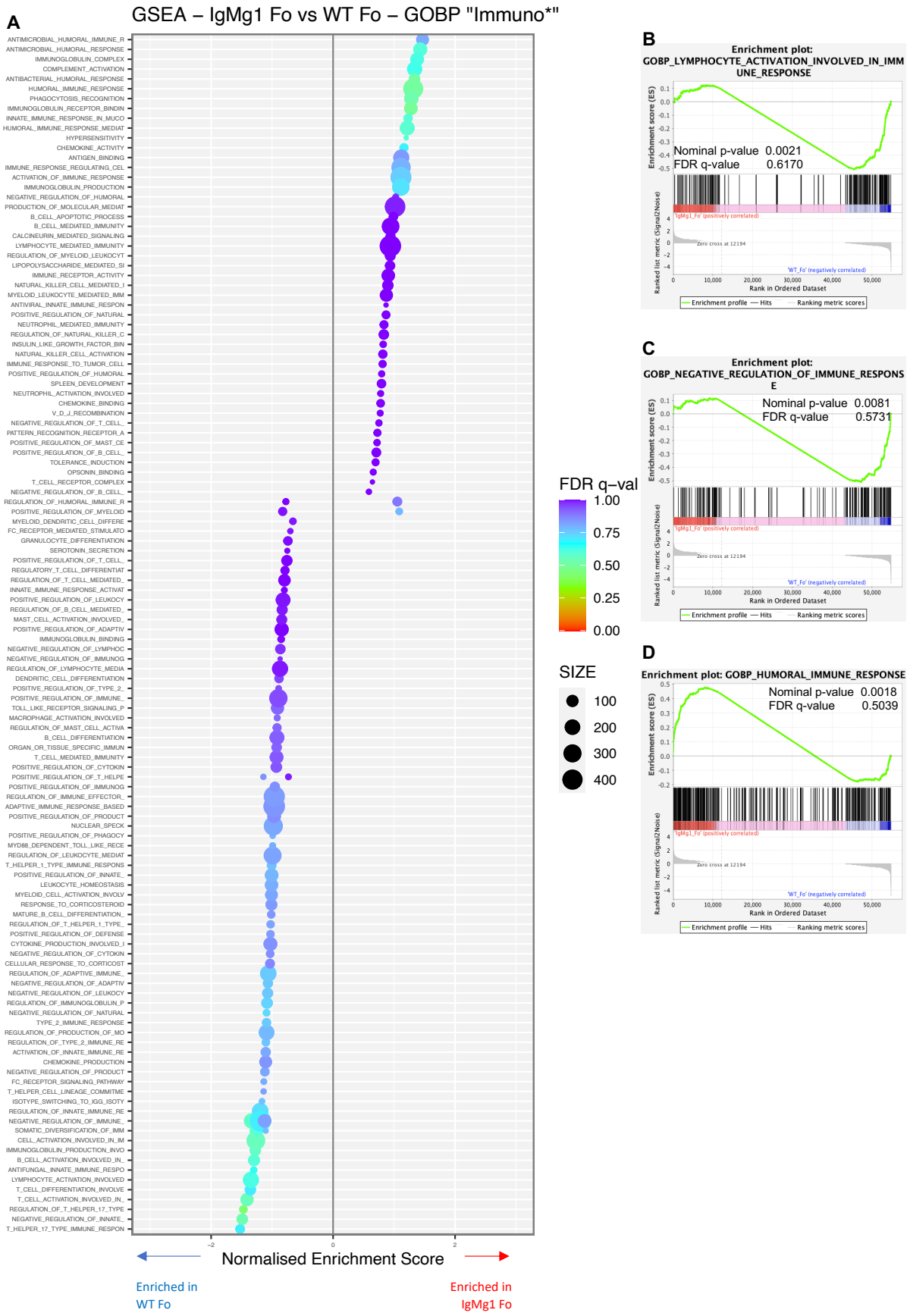
A
GSEA – IgMg1 Fo vs WT Fo – GOBP "Immuno*"
ANTIMICROBIAL_HUMORAL_IMMUNE_R
ANTIMICROBIAL_HUMORAL_RESPONSE
IMMUNOGLOBULIN_COMPLEX
COMPLEMENT_ACTIVATION
ANTIBACTERIAL_HUMORAL_RESPONSE
HUMORAL_IMMUNE_RESPONSE
PHAGOCYTOSIS_RECOGNITION
IMMUNOGLOBULIN_RECEPTOR_BINDIN
INNATE_IMMUNE_RESPONSE_IN_MUCO
HUMORAL_IMMUNE_RESPONSE_MEDIAT
HYPERSENSITIVITY
CHEMOKINE_ACTIVITY
ANTIGEN_BINDING
IMMUNE_RESPONSE_REGULATING_CEL
ACTIVATION_OF_IMMUNE_RESPONSE
IMMUNOGLOBULIN_PRODUCTION
NEGATIVE_REGULATION_OF_HUMORAL
PRODUCTION_OF_MOLECULAR_MEDIAT
B_CELL_APOPTOTIC_PROCESS
B_CELL_MEDIATED_IMMUNITY
CALCINEURIN_MEDIATED_SIGNALING
LYMPHOCYTE_MEDIATED_IMMUNITY
REGULATION_OF_MYELOID_LEUKOCYT
LIPOPOLYSACCHARIDE_MEDIATED_SI
IMMUNE_RECEPTOR_ACTIVITY
NATURAL_KILLER_CELL_MEDIATED_I
MYELOID_LEUKOCYTE_MEDIATED_IMM
ANTIVIRAL_INNATE_IMMUNE_RESPON
POSITIVE_REGULATION_OF_NATURAL_
NEUTROPHIL_MEDIATED_IMMUNITY
REGULATION_OF_NATURAL_KILLER_C
INSULIN_LIKE_GROWTH_FACTOR_BIN
NATURAL_KILLER_CELL_ACTIVATION
IMMUNE_RESPONSE_TO_TUMOR_CELL
POSITIVE_REGULATION_OF_HUMORAL
SPLEEN_DEVELOPMENT
NEUTROPHIL_ACTIVATION_INVOLVED
CHEMOKINE_BINDING
V_D_J_RECOMBINATION
NEGATIVE_REGULATION_OF_T_CELL_
PATTERN_RECOGNITION_RECEPTOR_A
POSITIVE_REGULATION_OF_MAST_CE
POSITIVE_REGULATION_OF_B_CELL_
TOLERANCE_INDUCTION
OPSONIN_BINDING
T_CELL_RECEPTOR_COMPLEX
NEGATIVE_REGULATION_OF_B_CELL_
REGULATION_OF_HUMORAL_IMMUNE_R
POSITIVE_REGULATION_OF_MYELOID
MYELOID_DENDRITIC_CELL_DIFFERE
FC_RECEPTOR_MEDIATED_STIMULATO
GRANULOCYTE_DIFFERENTIATION
SEROTONIN_SECRETION
POSITIVE_REGULATION_OF_T_CELL_
REGULATORY_T_CELL_DIFFERENTIAT
REGULATION_OF_T_CELL_MEDIATED_
INNATE_IMMUNE_RESPONSE_ACTIVAT
POSITIVE_REGULATION_OF_LEUKOCY
REGULATION_OF_B_CELL_MEDIATED_
MAST_CELL_ACTIVATION_INVOLVED_
POSITIVE_REGULATION_OF_ADAPTIV
IMMUNOGLOBULIN_BINDING
NEGATIVE_REGULATION_OF_LYMPHOC
NEGATIVE_REGULATION_OF_IMMUNOG
REGULATION_OF_LYMPHOCYTE_MEDIA
DENDRITIC_CELL_DIFFERENTIATION
POSITIVE_REGULATION_OF_TYPE_2_
POSITIVE_REGULATION_OF_IMMUNE_
TOLL_LIKE_RECEPTOR_SIGNALING_P
MACROPHAGE_ACTIVATION_INVOLVED
REGULATION_OF_MAST_CELL_ACTIVA
B_CELL_DIFFERENTIATION
ORGAN_OR_TISSUE_SPECIFIC_IMMUN
T_CELL_MEDIATED_IMMUNITY
POSITIVE_REGULATION_OF_CYTOKIN
POSITIVE_REGULATION_OF_T_HELPE
POSITIVE_REGULATION_OF_IMMUNOG
REGULATION_OF_IMMUNE_EFFECTOR_
ADAPTIVE_IMMUNE_RESPONSE_BASED
POSITIVE_REGULATION_OF_PRODUCT
NUCLEAR_SPECK
POSITIVE_REGULATION_OF_PHAGOCY
MYD88_DEPENDENT_TOLL_LIKE_RECE
REGULATION_OF_LEUKOCYTE_MEDIAT
T_HELPER_1_TYPE_IMMUNE_RESPONS
POSITIVE_REGULATION_OF_INNATE_
LEUKOCYTE_HOMEOSTASIS
MYELOID_CELL_ACTIVATION_INVOLV
RESPONSE_TO_CORTICOSTEROID
MATURE_B_CELL_DIFFERENTIATION_
REGULATION_OF_T_HELPER_1_TYPE_
POSITIVE_REGULATION_OF_DEFENSE
CYTOKINE_PRODUCTION_INVOLVED_I
NEGATIVE_REGULATION_OF_CYTOKIN
CELLULAR_RESPONSE_TO_CORTICOST
REGULATION_OF_ADAPTIVE_IMMUNE_
NEGATIVE_REGULATION_OF_ADAPTIV
NEGATIVE_REGULATION_OF_LEUKOCY
REGULATION_OF_IMMUNOGLOBULIN_P
NEGATIVE_REGULATION_OF_NATURAL
TYPE_2_IMMUNE_RESPONSE
REGULATION_OF_PRODUCTION_OF_MO
REGULATION_OF_TYPE_2_IMMUNE_RE
ACTIVATION_OF_INNATE_IMMUNE_RE
CHEMOKINE_PRODUCTION
NEGATIVE_REGULATION_OF_PRODUCT
FC_RECEPTOR_SIGNALING_PATHWAY
T_HELPER_CELL_LINEAGE_COMMITME
ISOTYPE_SWITCHING_TO_IGG_ISOTY
REGULATION_OF_INNATE_IMMUNE_RE
NEGATIVE_REGULATION_OF_IMMUNE_
SOMATIC_DIVERSIFICATION_OF_IMM
CELL_ACTIVATION_INVOLVED_IN_IM
IMMUNOGLOBULIN_PRODUCTION_INVO
B_CELL_ACTIVATION_INVOLVED_IN_
ANTIFUNGAL_INNATE_IMMUNE_RESPO
LYMPHOCYTE_ACTIVATION_INVOLVED
T_CELL_DIFFERENTIATION_INVOLVE
T_CELL_ACTIVATION_INVOLVED_IN_
REGULATION_OF_T_HELPER_17_TYPE
NEGATIVE_REGULATION_OF_INNATE_
T_HELPER_17_TYPE_IMMUNE_RESPON
−2
0
2
Normalised Enrichment Score
Enriched in WT Fo
Enriched in IgMg1 Fo
FDR q−val
1.00
0.75
0.50
0.25
0.00
SIZE
100
200
300
400
B
Enrichment plot: GOBP_LYMPHOCYTE_ACTIVATION_INVOLVED_IN_IMMUNE_RESPONSE
Nominal p-value 0.0021
FDR q-value 0.6170
Enrichment score (ES)
Ranked list metric (Signal2Noise)
IgMg1_Fo' (positively correlated)
Zero cross at 12194
'WT_Fo' (negatively correlated)
Rank in Ordered Dataset
Enrichment profile
Hits
Ranking metric scores
C
Enrichment plot: GOBP_NEGATIVE_REGULATION_OF_IMMUNE_RESPONSE
Nominal p-value 0.0081
FDR q-value 0.5731
D
Enrichment plot: GOBP_HUMORAL_IMMUNE_RESPONSE
Nominal p-value 0.0018
FDR q-value 0.5039

Figure 3.20 Gene set enrichment analysis of immune gene sets

Gene set enrichment analysis (GSEA) was performed with mouse gene ontology biological process gene sets pre-filtered for gene sets including search term “immun*”. (A) Normalised enrichment scores for all immune gene set. Size of circle represents number of genes in set. false discovery rate (FDR) q-value (B-D) GSEA enrichment plots for: (B) “lymphocyte activation involved in immune response” gene set, (C) “negative regulation of immune response” gene set; and (D) “humoral immune response” gene set.

3.2.7 Identification of an anergic gene signature

A number of the differentially expressed genes and gene sets identified in IgMg1 B cells appear to be related to hyperactive signalling as a result of the cytoplasmic IgG1 tail on the BCR. However, it is unclear which genes are important for the anergic phenotype of IgMg1 B cells. Gene expression analysis has been performed in the literature for the classical B cell anergy model, the MD4 x ML5 mouse. This mouse model expresses soluble HEL as a self-antigen, and has B cells with an HEL-specific BCR (Goodnow et al., 1988). Comparison of MD4 x ML5 gene expression data with the expression data from IgMg1 B cells could potentially identify key genes for maintaining anergy. The two MD4 x ML5 studies used had similarities. Sabouri et al., (2016) performed a microarray study of mature ($CD93^-$ $CD23^+$) MD4 x ML5 B cells, and by including all genes with an adjusted p-value of below 0.05 there were 2000 differentially expressed genes compared with non-anergic mature B cells from MD4 mice, which are transgenic for the HEL-specific BCR but do not express HEL as a self-antigen (Sabouri et al., 2016). Schwickert et al. (2019) performed RNA sequencing to compare anergic MD4 x ML5 follicular B cells with MD4 follicular B cells. They reported a much smaller gene signature of 59 upregulated and 50 downregulated genes (Schwickert et al., 2019). However, most of the genes they identified overlapped with the Sabouri et al., (2016) study, with 51 out of the 59 (86.4 %) upregulated (Figure 3.21A) and 36 out of the 50 (72 %) downregulated genes (Figure 3.21B) being the same. There was very limited overlap between the differentially expressed genes from IgMg1 B cells, and those identified in MD4 x ML5 B cells. Only 12 out of the 82 (14.6 %) upregulated IgMg1 genes (Figure 3.21A) and 4 out of the 54 (7.4 %) downregulated IgMg1 genes (Figure 3.21B) were also identified in at least one of the MD4 x ML5

studies. GSEA was used to compare the IgMg1 follicular B cell expression data with gene sets generated from the two MD4 x ML5 studies (strong up, strong down, strong-moderate up and strong-moderate down from Sabouri et al., (2016); up and down from Schwickert et al. (2019)) with no evidence of enrichment found for any of the gene sets (Figure 3.21C-F).

The 12 upregulated genes that overlapped (Figure 3.22A-L) were *Lgr5* (encoding Leucine-rich repeat-containing G-protein coupled receptor 5, or LGR5)), *Krt222* (encoding Keratin 222), *Bhlhe41* (encoding Basic Helix-Loop-Helix Family Member E41), *Apoe* (encoding Apolipoprotein E), *Bhlhe40* (encoding Basic Helix-Loop-Helix Family Member E40) *Iglv1* (encoding immunoglobulin lambda variable 1), *Mcoln2* (encoding Mucolipin-2, also known as TRPML2 (transient receptor potential cation channel, mucolipin subfamily, member 2), *Faah* (encoding Fatty acid amide hydrolase), *Sapcd1* (encoding Suppressor APC Domain-Containing Protein 1), *Twsg1* (encoding Twisted gastrulation protein homolog 1), *Gm2447* (predicted gene 24447), and *Rgs13* (encoding Regulator Of G Protein Signalling 13). The four downregulated genes that overlapped (Figure 3.22M-P) were *Pltp* (encoding Phospholipid transfer protein), *Trim36* (encoding Tripartite Motif Containing 36), *Ralb* (encoding RAS Like Proto-Oncogene B) and *Traf1* (encoding TNF receptor-associated factor 1). It is possible that some of these genes may be important in maintaining B cell anergy. For example BHLHE40 has been described as having a role in restraining germinal centre (GC) reactions (Rauschmeier et al., 2021), and RGS13 has been reported to have a role in control of early activation of B cells and GCs (Hwang et al., 2013).

Overall, these data indicate that IgMg1 gene expression is very different to the signature reported for the classical MD4 x ML5 B cell anergy model. However, some genes in common were identified, and these may be key genes for control of the anergic phenotype.

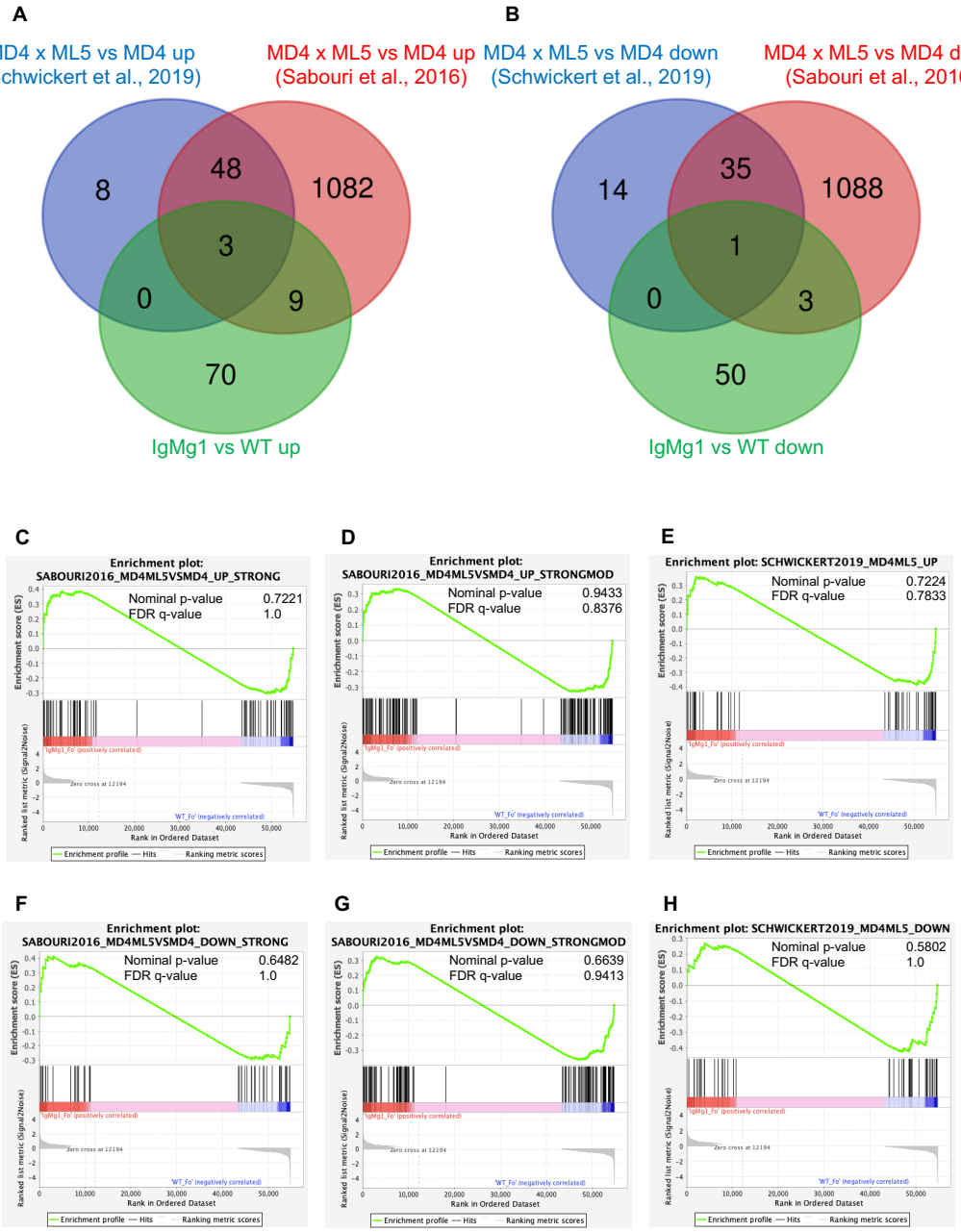

Figure 3.21 IgMg1 differentially expressed genes have very little overlap with MD4 x ML5 differentially expressed genes.

(A) Venn diagram comparing IgMg1 upregulated genes with genes identified in anergic MD4 x ML5 vs MD4 anergy signature published RNAseq data (Schwickert et al., 2019) and gene microarray data (with adjusted p value < 0.05) (Sabouri et al., 2016). (B) Venn diagram comparing IgMg1downregulated genes with downregulated genes identified in anergic MD4 x ML5 vs MD4 anergy signature published RNAseq data (Schwickert et al., 2019) and microarray data (with adjusted p value < 0.05) (Sabouri et al., 2016). (C-H) Gene set enrichment analysis performed with IgMg1 follicular B cells vs WT B cells data comparing to 6 gene sets created from previously published analysis of gene expression in MD4 x ML5 compared with MD4. Gene sets: (C) Sabouri et al., 2016 Strong up; (D) Sabouri et al., 2016 Strong and moderate up; (E) Schwickert et al., 2019 Up; (F) Sabouri et al., 2016 Strong down; (G) Sabouri et al., 2016 Strong and moderate down; (H) Schwickert et al., 2019 down.

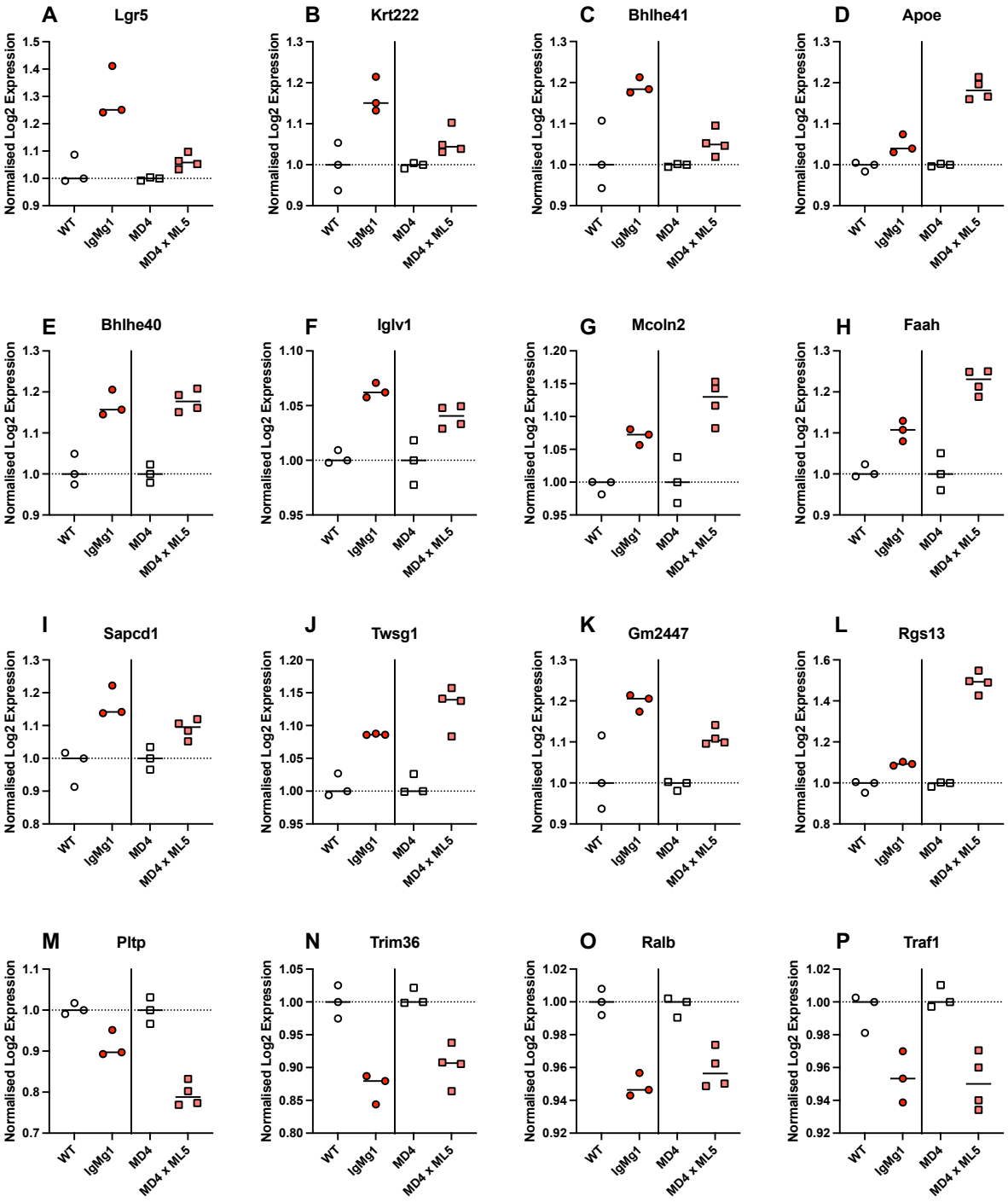

Figure 3.22 IgMg1 differentially expressed genes in common with MD4 x ML5 differentially expressed genes

Differentially expressed genes in IgMg1 B cells that overlapped with MD4 x ML5 B cells were identified. (A-L) IgMg1 upregulated genes also identified as upregulated in MD4 x ML5 (M-P) IgMg1 upregulated genes also identified as downregulated in MD4 x ML5. Rlog transformed data (Love et al., 2014) used for IgMg1 and WT and normalised relative to WT expression values. Microarray data published by Sabouri et al. 2014 used for MD4 x ML5 and MD4 (log2 expression) and normalised relative to MD4 expression values.

3.2.8 Identification of surface markers for anergic IgMg1 B cells

The work in this thesis regarding IgMg1 B cells has been performed with homozygous IgMg1 mice. Previous work from our lab has also looked at the behaviour of IgMg1 B cells in congenitally marked bone marrow chimeras. It would be useful to perform analysis of anergic IgMg1 B cells in competition with wildtype IgM (IgMwt) B cells in heterozygous mice, where allelic exclusion would ensure approximately 50% of the cells were IgMg1 and 50% were IgMwt. However, this would require identification of surface markers to allow reliable identification of the cells. Such a marker may also be useful to identify anergic cells in healthy and diseased WT mice. To identify surface markers which are differentially expressed, the bulk RNA sequencing data was filtered for genes included in the GO term for cell surface expression (GO:0009986). Ten differentially expressed genes were identified with at least a two-fold change in expression (Figure 3.23A and B): two genes were identified that were expressed higher in WT follicular B cells, and eight genes were identified that were expressed higher in IgMg1 follicular B cells. This included *Ighg1*, *Iglc2* and *Iglc1*. Of the remaining genes (Figure 3.23C-I), *Eno1b* (Figure 3.23D) and *Il5ra* (Figure 3.23G) were concluded to be the best options for flow cytometry due to relatively high expression levels, or having a large fold-change.

Antibodies for these markers were tested by flow cytometry and histology. However, neither of the markers identified proved to be usable. Eno1 expression could not be identified in any splenocytes by flow cytometry (Figure 3.24A) and there was no difference between WT and IgMg1 follicular B cells (Figure 3.24C and E). IL5Rα expression was mainly detected on non-B cells ($CD19^-$) by flow cytometry (Figure 3.24B), and no difference was observed between WT and IgMg1 follicular B cells

(Figure 3.24D and F). Similarly, analysis of spleen sections by immunofluorescent histology showed that Eno1 expression could not be detected in B cells, and IL5Rα expression was restricted to extrafollicular cells, with none being observed on IgD^+ B cells within the follicles (Figure 3.25A and B).

Therefore, surface markers allowing identification of IgMg1 B cells from WT B cells could not be identified.

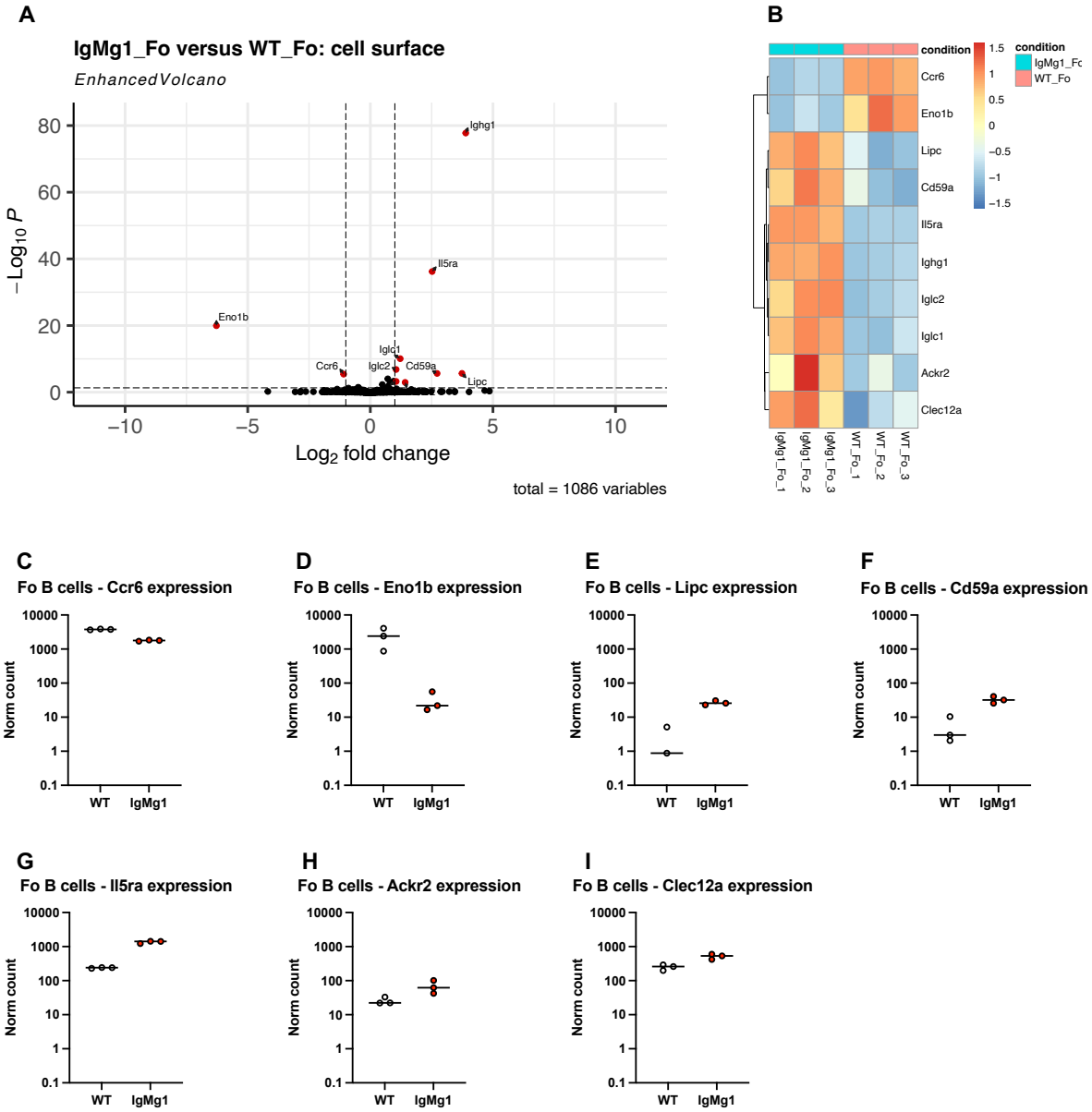

Figure 3.23 Identification of differentially expressed cell surface-expressed genes

Differentially expressed genes were filtered for genes included in gene ontology term for cell surface expression. (A) Volcano plot showing only genes that are in GO term cell surface (GO:009986). Differentially expressed genes are marked in red (2-fold change and adjusted p-value < 0.05). Horizontal dashed line represents p value of 0.05 and vertical dashed lines represent $\log_2$ fold-change of 1 and -1. (B) Heatmap showing relative expression of differentially expressed surface expressed genes in IgMg1 and WT follicular B cells. Colour scale represents gene Z-score. (C-I) Summary of expression data (normalised count) for surface expressed genes: (C) *Ccr6*, (D) *Eno1b*, (E) *Lipc*, (F) *Cd59a*, (G) *Il5ra*, (H) *Ackr2*, (I) *Clec12a.*

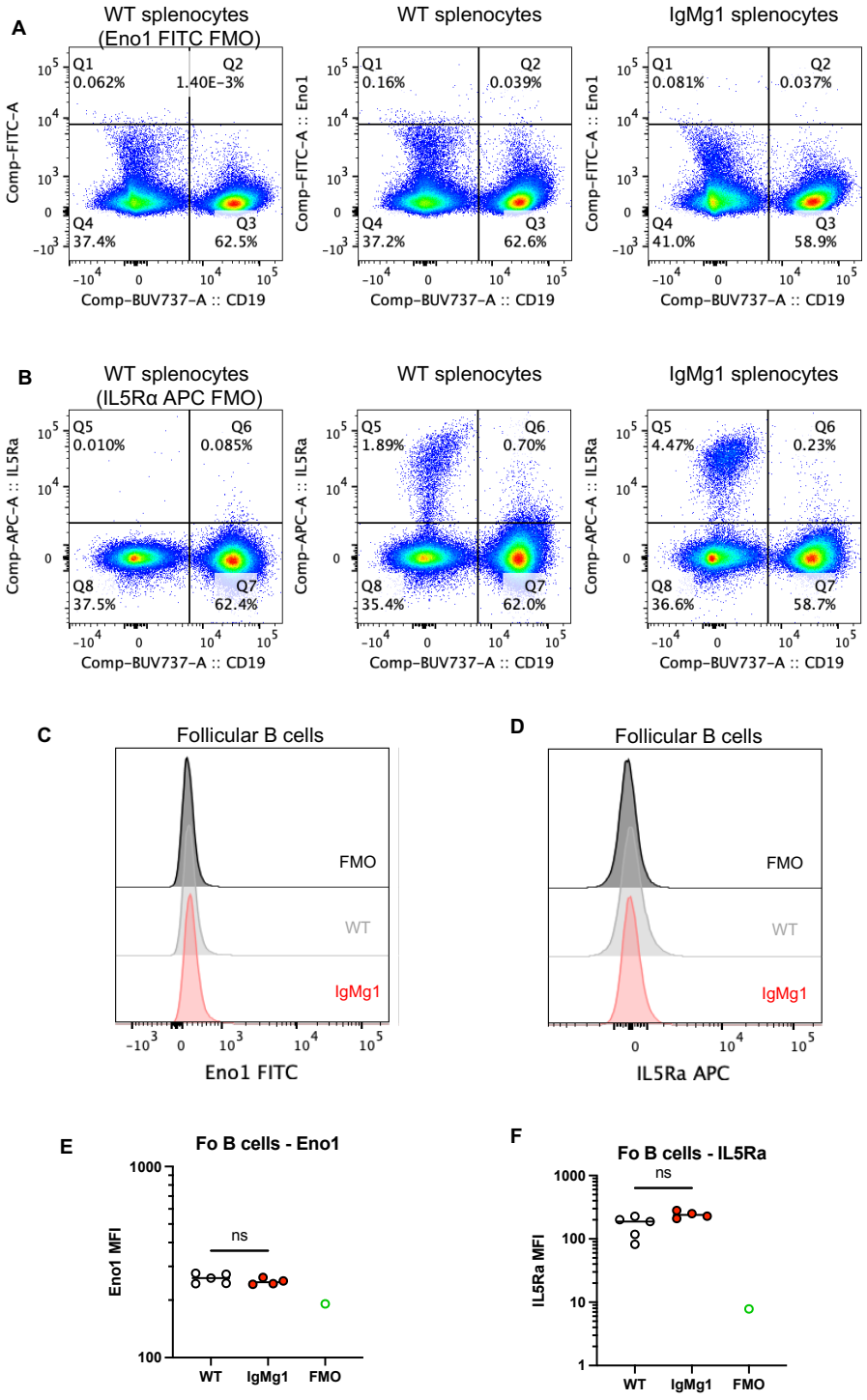

Figure 3.24 Flow cytometry analysis of Eno1 and IL5Rα expression in WT and IgMg1 splenocytes

Splenocytes from WT and IgMg1 mice were analysed by flow cytometry. (A) Flow cytometry showing Eno1-FITC staining in WT and IgMg1 splenocytes. (B) Flow cytometry showing IL5Rα-APC antibody staining in WT and IgMg1 splenocytes. (C) Histogram showing Eno1-FITC staining in follicular B cells (gated as in Figure 3.4). (D) Histogram showing IL5Rα antibody staining in follicular B cells (gated as in Figure 3.4). (E) Summary statistics for Eno1 expression in follicular B cells determined by flow cytometry. (F) Summary statistics for IL5Rα expression in follicular B cells determined by flow cytometry. Statistics determined by two-tailed T-test (ns, not-significant).

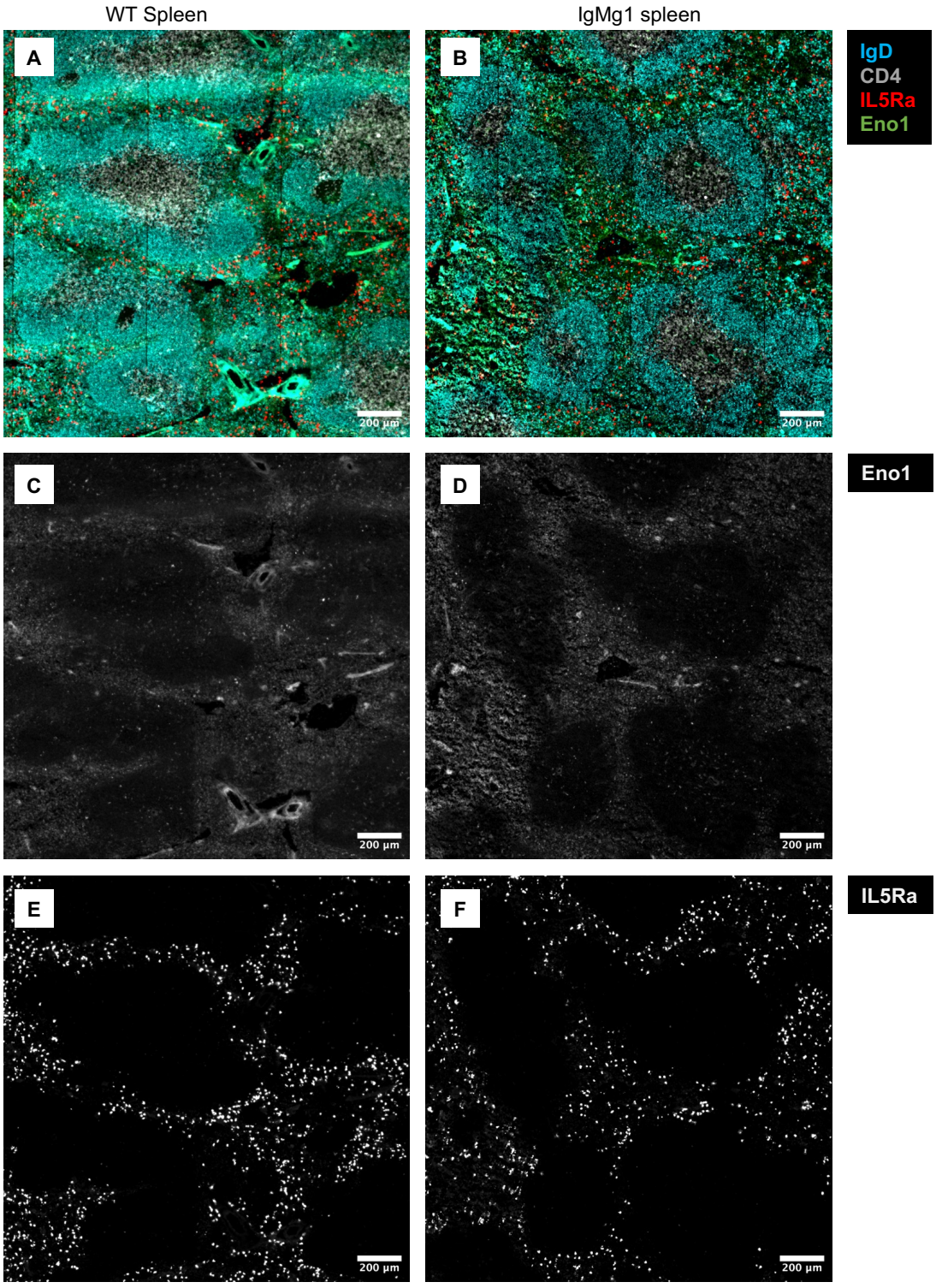

Figure 3.25 IL5Rα and Eno1 staining in WT and IgMg1 spleen

(A and B) Spleen sections from WT (A) and IgMg1 (B) mice were stained by immunofluorescence histology for IgD (B cell follicles, cyan), CD4 (T cell zone, grey), IL5Rα (red) and Eno1 (green). (C and D) The same frame of WT (C) and IgMg1 (D) spleen section showing only Eno1 staining. (E and F) The same frame of WT (E) and IgMg1 (F) spleen section showing only IL5Rα staining. Scale bars represent 200 µm.

3.2.9 Analysis of splenic B cells by single cell RNA sequencing

The data shown here suggests that altered BCR signalling on IgMg1 B cells results in alterations to B cell development and B cell subsets, with bulk RNA sequencing revealing some subtle gene expression changes to follicular B cells. To further evaluate the gene expression changes in all splenic B cell subsets at a higher resolution, single cell RNA sequencing was performed to compare total spleen B cells from WT and IgMg1 mice.

Splenic B cells were purified by negative enrichment using magnetic beads and then single cell RNA sequencing and VDJ sequencing was performed with a 10x chromium kit. Following quality control of the data, cells were clustered in an unsupervised manner. This resulted in 12 B cell clusters being identified (Figure 3.26A). Gene expression analysis was performed between the 12 clusters to identify genes that were upregulated in each cluster (Figure 3.26B).

The cells were separated based on whether they were WT or IgMg1, showing that cells from both genotypes fell into all 12 B cell clusters (Figure 3.27A). Further analysis of the 12 clusters within each genotype showed that there were differences between the distributions of the cells within the clusters (Figure 3.27B and C). Clusters 1, 5, 11 and 12 were enriched within WT splenic B cells, and clusters 2, 3, 8 and 9 being enriched within IgMg1 splenic B cells. Cluster 11 is enriched for expression of genes expressed in marginal zone B cells (for example *Cr2*, *Dtx1*, *Plac8*, *Pdia4*) (Figure 3.26B) so this is consistent with the reduction in marginal zone B cells in IgMg1 mice observed by flow cytometry and histology. These data reproduce that the IgMg1 BCR results in alterations to B cell development.

Figure 3.26 Splenic B cell clusters identified using single cell RNA sequencing

Splenic B cells from WT and IgMg1 mice were sequenced by 10X single cell RNA sequencing, and cells were clustered based on gene expression. (A) tSNE plot showing clustering of total B cells (WT and IgMg1 combined). (B) Heatmap showing differentially expressed genes identifying each cluster. Colour scale represents $\log_2$ fold change relative to the other clusters.

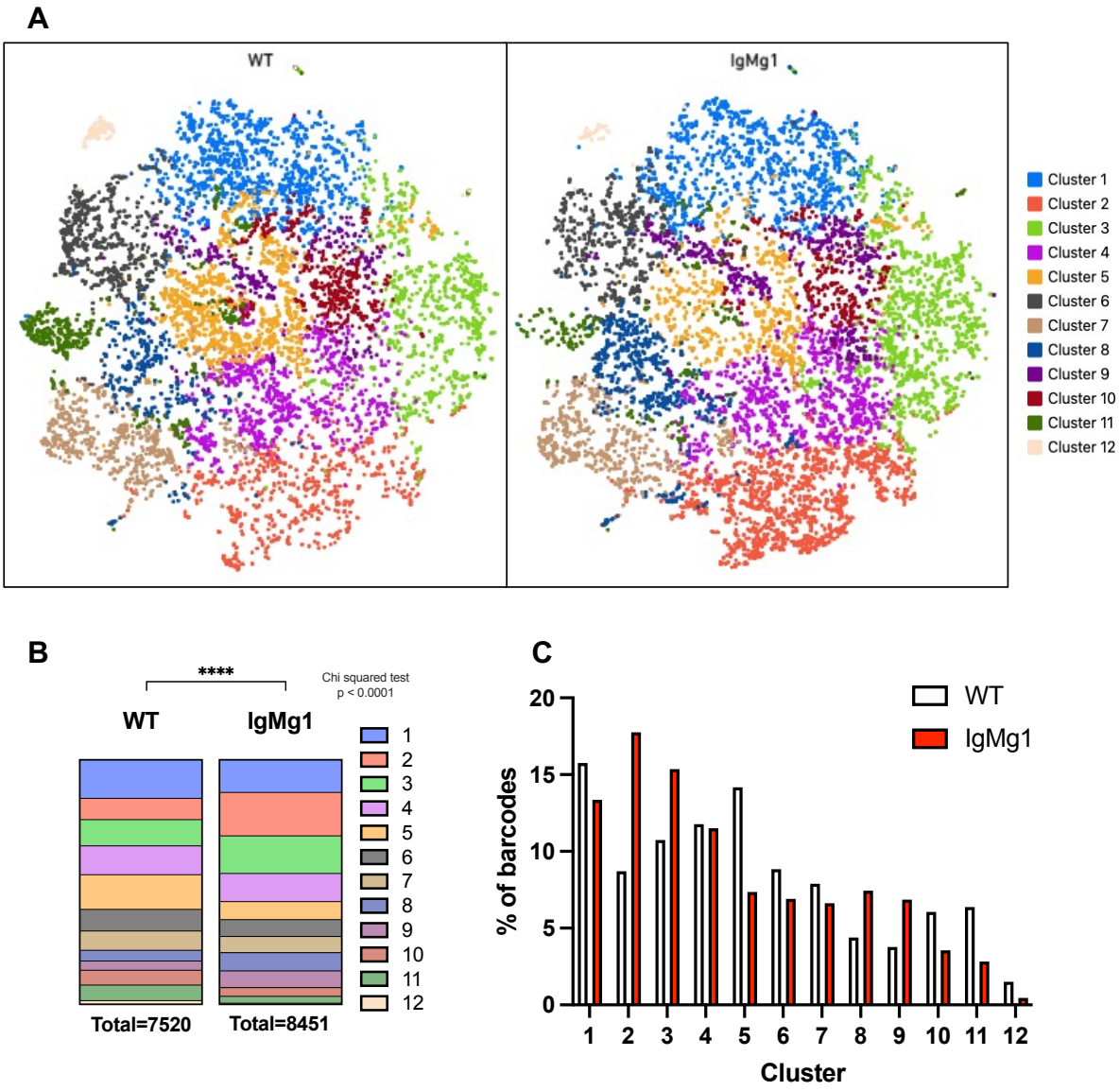

Figure 3.27 Clustering of WT and IgMg1 splenic B cells based on single cell RNA sequencing

The single cell sequenced B cells were separated by genotype (WT or IgMg1). (A) tSNE plot showing clustering of cells in WT (left) and IgMg1 (right) B cells. (B) Comparison of number of cells in each of B cell clusters in WT and IgMg1 mice. Statistical significance determined by Chi squared test. (C) Comparison of percentage of cells in each of clusters in WT and IgMg1 mice.

3.2.10 IgMg1 B cells have a wildtype-like BCR repertoire

One of the main limitations with study of B cell anergy using the classical MD4 x ML5 anergy model is that it is a monoclonal transgenic BCR model, where all B cells develop with an identical BCR. On the other hand, IgMg1 mice possess a polyclonal BCR repertoire generated as normal during B cell development, which may allow anergic B cells response to a range of antigens to be investigated. Although bone marrow B cell development appears normal in IgMg1 mice, there is evidence that cells may undergo some negative selection during development, which may have an effect on the BCR repertoire.

To address this question, the bulk RNA sequencing data was filtered to only look at Immunoglobulin heavy variable (IGHV) genes. A PCA showed that there were differences in IGHV gene expression between WT and IgMg1 follicular B cells (Figure 3.28A). However, a volcano plot showed that none of the genes were differentially expressed at an adjusted p-value of less than 0.05 and a greater than 2-fold change (Figure 3.28B). A heat map showing expression of all IGHV genes within all samples showed that the IgMg1 and WT follicular B cells looked very similar to each other with similar IGHV genes being preferentially expressed in both genotypes (Figure 3.28C).

To confirm these results, the single cell RNA sequencing dataset described in section 3.2.9 was analysed for frequencies of different IGHV, immunoglobulin kappa variable (IGKV) and lambda variable (IGLV) genes within splenic B cells. This showed that the majority of the IGHV genes were used to a similar degree in both genotypes (Figure 3.29A). Similarly, apart from *IGLV2* (which was used by a much higher frequency of IgMg1 B cells, reflecting the higher usage of lambda light chain) most of the light chain IGKV and IGLV genes had similar frequencies in both genotypes (Figure 3.29B). While

some IGHV genes were underrepresented in IgMg1 B cells (Figure 3.29A), these may represent difference in usage due to underrepresented populations. For example, *IGHV11-2* had a lower frequency in IgMg1 B cells than in WT B cells, but this is a IGHV gene associated with B-1 cells (Kreslavsky et al., 2018) which are reduced among IgMg1 B cells (section 3.2.5). However, it cannot be ruled out that these differences in IGHV gene useage are due to altered B cell selection during B cell development.

Overall, these data indicate that IgMg1 B cells develop with a wildtype-like BCR repertoire, broadly unaffected by altered BCR signalling.

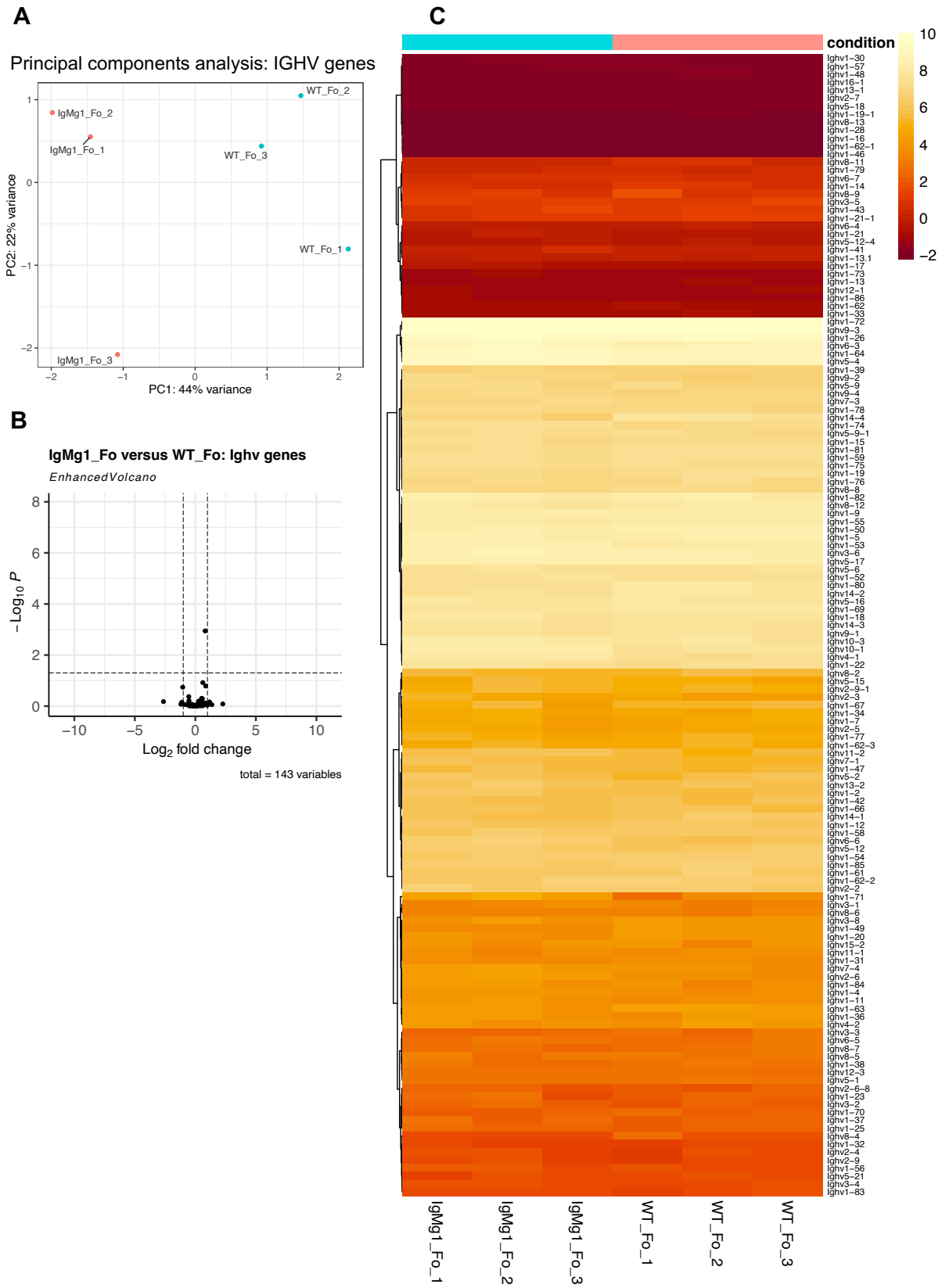
A
Principal components analysis: IGHV genes
WT_Fo_2
IgMg1_Fo_2
IgMg1_Fo_1
WT_Fo_3
WT_Fo_1
IgMg1_Fo_3
PC2: 22% variance
PC1: 44% variance
B
IgMg1_Fo versus WT_Fo: Ighv genes
EnhancedVolcano
−Log10 P
Log2 fold change
total = 143 variables
C
condition
IgMg1_Fo_1
IgMg1_Fo_2
IgMg1_Fo_3
WT_Fo_1
WT_Fo_2
WT_Fo_3

Figure 3.28 IGHV gene usage in IgMg1 and WT follicular B cells from bulk RNA sequencing

Bulk RNA sequencing gene expression data for WT and IgMg1 follicular B cells was filtered for IGHV genes. (A) IGHV expression data had dimensionality reduced using principal components analysis to assess variance between samples. (B) Volcano plot showing $\log_2$ fold-change between WT and IgMg1 follicular B cells and $-\log_{10}$ adjusted p-value for all IGHV genes. Horizontal dashed line represents p value of 0.05 and vertical dashed lines represent $\log_2$ fold-change of 1 and -1. (C) Heatmap showing IGHV gene expression in WT and IgMg1 follicular B cells. Colour scale represents rlog-transformed gene expression (Love et al., 2014).

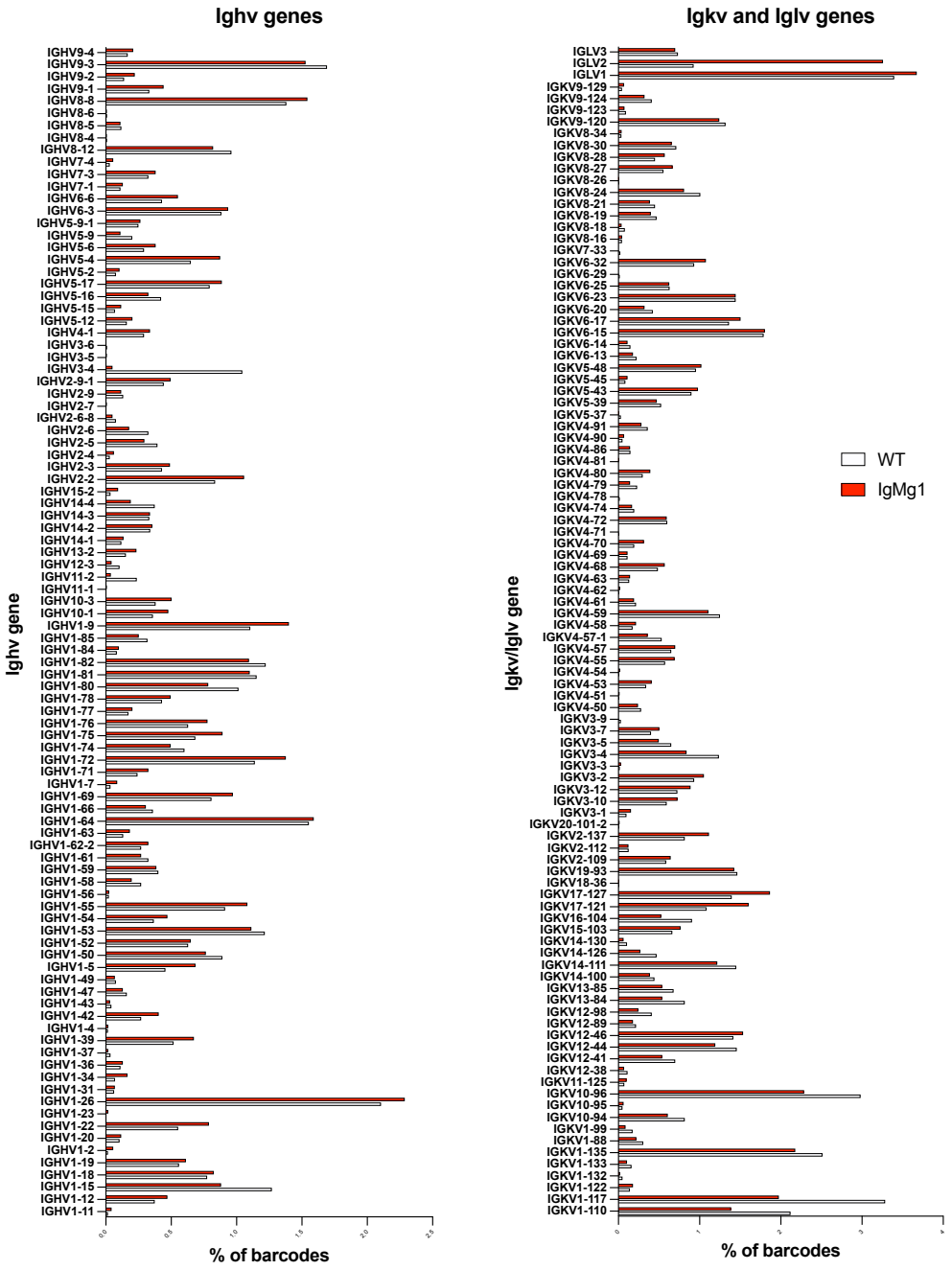

Figure 3.29 Variable gene usage in IgMg1 and WT B cells from single cell RNA sequencing analysis

BCR sequencing was performed on splenic B cells from WT and IgMg1 mice by single cell 10X RNA sequencing. (A-B) Percentage of cells carrying each (A) IGHV gene and (B) IGLV or IGKV gene in WT and IgMg1 splenic B cells

3.3 Discussion

3.3.1 Impact of BCR signalling on B cell development

The results presented in this chapter show that the BCRs in both the IgMg1 and IgG1M mice result in B cell development being altered. The IgG1M mice have a partial block in B cell development in the bone marrow, reduced transitional B cells, increased marginal zone B cells and a reduction in B-1 cells. The IgMg1 mice have no observed blocks in B cell development in the bone marrow, reduced transitional T1 and T2 cells, but an increase in T3 cells, reduced marginal zone B cells and reduced B-1 cells. Both genotypes have increased lambda light chain usage, and reduced BCR cell surface expression. Despite similar changes in BCR expression, the IgG1M mice have increased calcium flux in response to *in vitro* BCR stimulation, while the IgMg1 B cells have reduced calcium flux consistent with an anergic B cell as phenotype previously described (Zhang, 2019).

The partial block in B cell development observed in the IgG1M mice at the pre-B cell stage is as described previously (Waisman et al., 2007). This is a less extreme version of the phenotype seen in mice deficient in pre-BCR assembly (Shimizu et al., 2002). This suggests that the IgM heavy chain is required for optimal pairing with the surrogate light chain to form the pre-BCR (Waisman et al., 2007). As this block is not observed in the IgMg1 mice, it suggests that it is the IgM extracellular region which is required for the efficient pre-BCR assembly. However, the fact that there is not a complete block at the pre-B cell stage as observed in the μMT mouse (disrupted IgM heavy chain membrane exon) (Kitamura et al., 1991), shows that the IgG1 heavy chain is still able to form a pre-BCR complex to some extent, but not as efficiently as the IgM heavy chain.

Both IgG1M and IgMg1 models have an increase in lambda light chain usage. This can be observed in the IgMg1 mice from the bone marrow transitional B cell stage (where cells have low to intermediate IgD expression) onwards. Lambda light chain usage has been used as a marker for increased receptor editing by others (Tiegs et al., 1993; Hertz and Nemazee, 1997; Bai et al., 2007) and this is consistent with the stage at which the BCR mediates negative selection, resulting in increased secondary light chain gene rearrangements or receptor editing (Nemazee, 2006). The IgG1M late-stage bone marrow B cells ($B220^+$ $CD43^-$ $IgG1^+$) cannot be further divided into immature, transitional and mature B cells as they do not express IgD. However, lambda light chain usage is increased in the total late-stage bone marrow B cells in IgG1M mice, and it's probable that this is also a result of stronger negative selection occurring at the same stage as in IgMg1 mice. This suggests that in the bone marrow, the IgG1 cytoplasmic tail present on the BCR in IgMg1 and IgG1M B cells mediates stronger BCR signalling and mimics self-reactivity, leading to increased receptor editing.

As shown in this chapter, and previously (Zhang, 2019), IgMg1 mice appear to undergo strong negative selection during bone marrow development, resulting in increased receptor editing and mature B cells which have an anergic phenotype. However, this increased negative selection does not also result in increased apoptosis or blocks in B cell development due to clonal deletion. Increased active caspase-3 staining was not observed at any point during bone marrow B cell development in IgMg1 mice. There were also no decreases in any of the IgMg1 bone marrow B cell subsets and B cells were not developmentally arrested, further supporting that there was not increased death in IgMg1 B cells due to negative selection. This may reflect the possibility that receptor editing and clonal anergy are preferred outcomes for B cells that are

negatively selected. It has been reported that cells reactive to membrane expressed self-antigens will undergo receptor editing, and only default to clonal deletion if receptor editing fails to relieve the B cell of self-reactivity (Halverson et al., 2004). Clonal anergy may also be preferable over clonal deletion to avoid having gaps in the BCR repertoire (Burnett et al., 2019). Alternatively, the tendency of B cells in this system to undergo receptor editing or become anergic may reflect the strength of BCR signalling. The choice between anergy and clonal deletion may depend on the nature of the self-antigen, and the strength of BCR signalling. Immature B cells in the periphery that receive strong BCR signals through extensive cross-linking with membrane antigen undergo apoptosis, whereas moderate BCR signalling through binding to a soluble antigen induces anergy (Hartley et al., 1991). The hyperactive tonic BCR signalling provided by the IgG1 cytoplasmic tail may be enough to induce receptor editing and anergy, but not be strong enough to induce clonal deletion.

Splenic B cells from both mouse models were tested for their ability to mobilise calcium in response to BCR stimulation. As shown in section 3.2.3, IgG1M B cells have enhanced calcium flux following anti-kappa and lambda stimulation, whereas IgMg1 B cells have impaired calcium flux following either anti-IgM or anti-kappa and lambda stimulation. This shows that IgG1M mature B cells have hyperactive BCR signalling, whereas IgMg1 mature B cells have dampened BCR signalling. Reports of the effects of BCR signalling strength on B cell maturation and fate decision between differentiation into either follicular B cell or marginal zone B cell in various mouse models reported in the literature are mixed, with conflicting reports of both strong and weak BCR signalling favouring marginal zone B cell development (Cariappa et al., 2001, 2009; Samardzic et al., 2002; Setz et al., 2018; Härzschel et al., 2021; Wen et

al., 2005; Kanayama et al., 2005; Horikawa et al., 2007; Geier et al., 2018; Ottens and Satterthwaite, 2021). In the results shown in this chapter, consistent strong BCR signalling in the IgG1M model led to increased marginal zone B cells. This was described previously by Waisman et al. (2007). The nature of the IgMg1 BCR signalling is not as clear. The fact that there was evidence of increased negative selection in the bone marrow transitional cells indicates hyperactive BCR signalling at that stage, but the in vitro stimulation of mature splenocytes indicated dampened BCR signalling. The overall result of this was a reduced or almost-complete absence of marginal zone B cells. This is similar to the phenotype of transgenic B cell anergy models reported in the literature, as the MD4 x ML5 model also has a reduction in marginal zone B cells (Mason et al., 1992; Phan et al., 2003). It is possible that similarly to what seems to happen with the IgMg1 B cells, the contradictory reports of the effect of BCR signalling strength on marginal zone B cell development reflects that mutations that introduce strong BCR signalling will often result in negative feedback generated during development that causes mature B cells to have apparently weaker signalling.

Both models investigated in this chapter have reduced BCR surface expression. In the case of IgG1M mice which only express IgG1, this could be detected using anti-kappa and lambda antibodies. The IgMg1 mice had reduced IgM expression as detected with an anti-IgM antibody. However, total BCR was also reduced, even considering that IgD expression was much less severely affected. Downregulation of BCR expression is a defining feature of anergic B cells, induced during B cell development as a result of the strong self-reactive BCR signalling (Cambier et al., 2007). This mechanism is seen in several B cell anergy models driven by exposure to a self-antigen, indicating that there is a mechanism driving downregulation of IgM BCRs due to strong BCR signalling. It

is possible that the mechanism driving this is increased internalisation of the BCR in response to BCR signalling (Nemazee, 2017). However, in the IgG1M and IgMg1 models it is also worth noting that the BCRs in these models bear the IgG1 cytoplasmic tail. It has been reported that presence of this region drives downregulation of the BCR via an independent mechanism. The IgG1 cytoplasmic tail is a target for ubiquitination, causing degradation and downregulation of the receptor (Kodama et al., 2020; Sundling et al., 2021). Therefore, downregulation of the BCR by this mechanism in IgMg1 and IgG1M mice cannot be ruled out.

In IgG1M mice, despite the evidence of strong negative selection during bone marrow development, and the reduced BCR surface expression on mature B cells, there is no evidence that the IgG1M B cells have an anergic phenotype. The fact that the reduced BCR expression does not result in reduced ability to mobilise calcium in response to BCR stimulation is interesting, and indicates that additional, perhaps genetic, changes must be present in IgMg1 B cells to cause the anergic phenotype. However, the increased BCR signalling during B cell development does not result in anergy in the IgG1M mice. This may indicate that the IgM extracellular region plays a role in negative regulation of signalling, especially in response to antigen. The IgM hinge region is less flexible than the IgG1 hinge region (Ma et al., 2022) which may effectively reduce the contact between the BCR and antigen. Alternatively, it may be because IgG1M B cells do not express IgD. Anergic B cells (both naturally occurring, and in transgenic BCR anergy models) have high IgD expression, despite their reduced IgM expression (Goodnow et al., 1989; Merrell et al., 2006; Burnett et al., 2019). This may reflect an important role for IgD in maintenance of anergy. The function of IgD has been largely unknown, however work in recent years has started to reveal roles in B cell anergy.

Cross-linking of IgD has been shown to inhibit cell survival compared to cross-linking of IgM which enhances cell survival (Yasuda et al., 2018). Experiments with a Nur77-GFP BCR signalling reporter introduced into cells expressing either IgM or IgD alone showed that BCR signalling is transmitted less efficiently by IgD-only expressing cells, and IgD-only B cells make reduced autoantibody response in the lupus-prone *Lyn*$^{-/-}$ model (Noviski et al., 2018). Experiments looking at anergic B cells co-expressing IgM and IgD, or expressing IgM alone showed that expression of IgD promoted the accumulation of anergic B cells (Sabouri et al., 2016). High expression of IgD may therefore be important for maintenance of anergy. A better model system for these experiments may be one where B cells express the full IgG1 BCR, but also co-express IgD.

Kappa^{+} and lambda^{+} cells in WT and IgMg1 mice were separately analysed for expression of IgM and IgD. Surprisingly, there was a statistically significant increase in IgD expression in lambda^{+} follicular B cells compared with kappa^{+} follicular B cells, in both WT and IgMg1 mice. This suggests that cells which undergo strong negative selection during B cell development and undergo receptor editing, later increase IgD expression. To our knowledge, this has not been previously reported in the literature. The function of this is unclear, but it may be mechanism for regulating potentially self-reactive B cells. In humans, lambda^{+} cells are enriched in some autoantibody driven autoimmune diseases such as rheumatoid arthritis (Slot et al., 2021), which suggests that autoreactivity is not always completely eliminated by receptor editing. Therefore, a separate means of regulating them may be useful.

Although overall transitional B cells were reduced in IgMg1 mice, there was an increase in B cells with the $CD93^+$ $CD23^+$ IgM^{lo} T3 phenotype. This is consistent with the anergy of the IgMg1 B cells, as T3 cells have been identified in literature as a natural subset of anergic B cells in WT mice (Merrell et al., 2006). However, most of the IgMg1 B cells are not T3 cells. It has been reported that the majority of the B cells in the MD4 x ML5 and ArsA1 anergy models have a T3 phenotype (Merrell et al., 2006). However, data from a different publication about MD4 x ML5 B cells shows that although $CD93^+$ cells were expanded they were still a relatively minor subset of all B cells (Sabouri et al., 2016). The anergic T3 cells have been shown to be relatively short-lived so may not survive long enough to accumulate as the main population. Another natural anergic B cell subset has been identified which is a mature $CD93^-$ subset and is longer-lived (Nojima et al., 2020), so these may make up the majority of anergic cells.

B-1 cells were apparently reduced in both IgMg1 and IgG1M mice. This was surprising as B-1a cells are thought to be positively selected during development (Hayakawa et al., 1999; Casola et al., 2004) so stronger BCR signalling was predicted to lead to an increase in B-1a cells. It has also been shown that inefficient assembly of the pre-BCR affects B-1 cell development. VH11, a heavy chain gene that pairs less effectively with the surrogate light chain to form the pre-BCR, is overrepresented in B-1 cells, and a model has been proposed where poor pre-BCR assembly results in cell proliferation in the fetal liver during B-1 cell development (Hardy, 2006). Therefore, it is unclear why IgG1M B cells, that appear to have stronger BCR signalling and inefficient pre-BCR assembly, do not efficiently develop as B-1 cells. In IgMg1 mice peritoneal cavity there were $B220^{lo}$ cells that did not phenotypically resemble B-1 cells due to not having the

expected $CD23^{lo}$ $CD43^{+}$ phenotype. However, it is possible that they are still functionally B-1 cells but with altered expression of key activation markers. To confirm if these cells are or are not B-1 cells, typical B-1 cell characteristics could be evaluated experimentally, for example CpG1680-induced differentiation to antibody secreting cells (Genestier et al., 2007) or high-frequency of B-1 enriched heavy chain genes such as VH11 (Nguyen et al., 2015).

3.3.2 Identification of an anergic gene signature

Bulk RNA sequencing was performed on IgMg1 follicular B cells to analyse gene expression in anergic B cells. Compared with WT follicular B cells, differentially expressed genes were identified. However, the overall number of differentially expressed genes were relatively low. This may be because of high variability between samples of the same genotype. Additional samples may have been useful to increase statistical power and allow identification of a larger number of genes.

GSEA identified oxidative phosphorylation as an upregulated gene set in IgMg1 B cells, which is a process associated with B cell stimulation (Waters et al., 2018). Given the anergic phenotype of these cells, this is slightly counter-intuitive. However, it may reflect hyperactive BCR signalling due to the presence of the IgG1 cytoplasmic tail which has inherent signalling capabilities such as the immunoglobulin tail tyrosine motif (Martin and Goodnow, 2002; Horikawa et al., 2007; Waisman et al., 2007; Engels et al., 2009), possibly leading to hyperactivation of this particular pathway without activation of other pathways downstream of the BCR. Other pathways may not be

activated by the IgG1 cytoplasmic chain or may have become exhausted from continuous stimulation.

The differentially expressed genes identified here were compared with genes identified in two published analyses of gene expression in the classical B cell anergy model, MD4 x ML5 mice (Sabouri et al., 2016; Schwickert et al., 2019). There were very few overlapping genes identified, and GSEA performed using gene sets created from the published MD4 x ML5 data showed these genes were not enriched in IgMg1 follicular B cells. It is not clear why expression in anergic IgMg1 B cells is so different to gene expression in anergic MD4 x ML5 B cells. Although the IgMg1 B cells have a clear anergic phenotype as shown by reduced surface BCR expression and reduced calcium flux in response to BCR stimulation, as well as reduced BCR-stimulation induced phosphorylation of proteins downstream of the BCR (Zhang, 2019), it is a very different model to the MD4 x ML5 mouse. Anergy in the MD4 x ML5 model, as well as many other transgenic BCR models of anergy, is driven primarily by chronic stimulation by a specific self-antigen during B cell development and in the periphery (Goodnow et al., 1988). However, in IgMg1 mice it has been proposed that enhanced tonic BCR signalling replicates self-antigen trigged BCR signalling of self-reactive B cells during B cell development, and results in downregulation of the BCR and induction of the anergic phenotype. Antigens driving the BCR signalling in the IgMg1 model are likely to be seen by B cells only occasionally during B cell development, whereas antigen in the MD4 x ML5 model is soluble and present at high concentrations (Goodnow et al., 1988).

Despite the clear differences between the models, a small number of genes were identified as being differentially regulated in both IgMg1 and MD4 x ML5 models. It is possible that genes that play a critical role in regulation of anergy are among them. For example, *Bhlhe40* encodes a transcription factor which has recently been shown to have a role in restraining generation of early germinal centre B cells. B cells deficient in Bhlhe40 have a competitive advantage in the early germinal centre reaction. Although Bhlhe40 has been shown to negatively regulate proliferation in B-1 cells (Kreslavsky et al., 2017), no effect was found on proliferation of B-2 cells. It may function by negatively regulating genes involved in the germinal centre response (Rauschmeier et al., 2021). *Bhlhe41*, a related gene, was also identified as upregulated in IgMg1 and MD4 x ML5 B cells. There are no reports of its function in B-2 cells, but it has a similar function to Bhlhe40 in regulating B-1 cells (Kreslavsky et al., 2017).

Rgs13 was also upregulated. It encodes a protein that binds to G_i proteins and inhibits signalling through G-protein coupled receptors (GPCRs), including chemokine receptors CXCR4 and CXCR5 (Shi et al., 2002). Knockdown of Rgs13 mRNA in a Burkitt's lymphoma cell line increased calcium mobilisation in response to CXCR4 and CXCR5 ligands CXCL12 and CXCL13 (Han, 2006). Rgs13-deficient mice had an increased germinal centre response, and in mixed bone marrow chimeras Rgs13-deficient B cells expanded more rapidly at the T-B cell border (Hwang et al., 2013). This shows that increased expression of *Rgs13* in anergic IgMg1 and MD4 x ML5 B cells may function to restrain the B cell response.

Another upregulated gene, *Apoe*, is involved in lipid metabolism but has been shown to be involved in regulation of immune cell function. In dendritic cells it has been shown

that Apoe-deficiency results in accumulation of cholesterol in the cell membrane, resulting in enhanced MHC class II presentation (Bonacina et al., 2018). Cholesterol is an important component of lipid rafts which act as specialised environments on the cell membrane where BCRs localise for signalling to take place (Pierce, 2002), and reduced cholesterol in immature B cells has been linked with reduced ability to respond to BCR signalling (Karnell et al., 2005). Therefore, this could be a mechanism by which increased Apoe expression in anergic B cells inhibits BCR signalling.

Twsg1 encodes an extracellular regulator of bone morphogenetic protein (BMP) signalling (Tsalavos et al., 2011). BMP signalling has been shown to affect the germinal centre response (Tomayko et al., 2021). Twsg1-deficient B cells are hyperproliferative in response to BCR stimulation, and Twsg1-deficient mice make an increased antibody response following immunisation with TI-I antigen 2,4-Dinitrophenyl Lipopolysaccharide (DNP-LPS). Therefore Twsg1 may have a role in regulating B cell response (Tsalavos et al., 2011).

Traf1 was identified as being downregulated in IgMg1 and MD4 x ML5 B cells. This has been shown to co-operate with Traf2 in CD40-mediated activation of B cells (Xie et al., 2006). Although Traf1-deficient mice do not have a significant defect in humoral immunity or CD40-induced B cell proliferation (Tsitsikov et al., 2001), reduced Traf1 expression in anergic B cells may play a role in reduced B cell activation.

Altogether, there is clear published evidence of the role of a number of identified genes in regulation of B cell activation, and these genes may warrant further investigation for a role in B cell anergy.

In addition to the bulk RNA sequencing analysis, 10x single cell RNA sequencing was utilised to further examine splenic naive B cell populations in IgMg1 mice. The cells were clustered based on gene expression, and this showed that the distribution of IgMg1 B cells within the clusters was significantly altered, confirming the flow cytometry data showing significant differences in splenic B cell populations. Further interrogation of this data will be necessary to determine the biological relevance of the changes to gene expression at a single cell level.

3.3.3 Conclusions

The results presented in this chapter show that different BCRs can affect B cell development. In the IgMg1 model, the chimeric IgMg1 BCR induces stronger negative selection, leading to reduced BCR expression and an anergic B cell phenotype in mature B cells. Gene expression has been analysed to identify genes that may be important in regulating anergic B cells in a polyclonal B cell environment, but further analysis and investigation is required. In the IgG1M model, B cells that express IgG1 instead of co-expressing IgM and IgD have a partial block at the pre-B cell stage. However, cells that develop into mature B cells do not have an anergic phenotype despite strong negative selection and reduced BCR expression. Instead, cells develop as mature B cells with hyperactive BCR signalling.

Chapter 4. B cell response in mouse models with altered BCR signalling

4.1 Introduction

4.1.1 Role of BCR signalling in B cell activation

BCR recognition of antigen and BCR signalling are critical for B cell activation and participation in the germinal centre (GC) response. Entry into the GC is regulated to some extent by BCR affinity (Schwickert et al., 2011). The main role of the BCR for GC B cells is to capture antigen so it can be processed and presented to T follicular helper (Tfh) cells in order to receive T cell help. The amount of antigen captured is dependent on BCR affinity for the antigen (Batista and Neuberger, 2000; Victora et al., 2010). It has been shown that most proliferating GC B cells do not actively undergo BCR signalling (Khalil et al., 2012) and have reduced phosphorylation of proteins in the BCR signalling pathway (Khalil et al., 2012; Nowosad et al., 2016). However, BCR signalling is important for extraction of membrane-presented antigen, as treatment of GC B cells with inhibitors of BCR signalling resulted in reduced antigen extraction in an *in vitro* assay (Nowosad et al., 2016). Use of a Nur77-GFP reporter of BCR signalling showed that although overall BCR signalling was reduced in GC B cells compared with naïve cells, there was a small population of light zone (LZ) GC B cells which were strongly GFP^+ suggesting that BCR signalling was active in a subset of GC B cells (Mueller et al., 2015). BCR signalling works synergistically with CD40 signalling, induced by CD40L on Tfh cells, to efficiently promote Myc expression and cell cycle entry in positively selected GC B cells (Luo et al., 2018). Additionally, $IgG1^+$ GC B cells are able to outcompete IgM^+ GC B cells, indicating that there is BCR involvement in

positive selection (Sundling et al., 2021). BCR signalling also plays a role in apoptosis in the GC, as in mice where Shp-1, a negative regulator of BCR signalling, was deleted shortly after B cell activation there was increased apoptosis (Yam-Puc et al., 2021). Therefore, BCR signalling is important in GC B cells for antigen capture, positive selection, and apoptosis.

BCR signalling is also involved in T cell-independent (TI) B cell responses. It is required for *in vitro* B cell proliferation in response to stimulation by toll-like receptor (TLR) ligands CpG and lipopolysaccharide (LPS) (Otipoby et al., 2015). LPS stimulates both the BCR and TLR4, which synergistically induce BCR signalling and expression of AID, critical for class-switch recombination (Pone et al., 2012). Defects in proteins involved in BCR signalling result in an impaired TI B cell response (Khan et al., 1995; Xu et al., 2000).

4.1.2 BCR signalling and Tfh cells

BCR signalling affects the ability of GC B cells to present antigen to Tfh cells. B cells with high affinity BCRs have stronger interactions with Tfh cells, resulting in them receiving more help. This is due to higher affinity B cells capturing more antigen, and thus presenting more antigen to T cells via MHC class II (Liu et al., 2015). Recently, it has been shown that during a GC response, Tfh cells undergo clonal selection, with increased antigen presentation resulting in increased Tfh cell proliferation (Merkenschlager et al., 2021). Sustained antigen presentation from B cells is required to maintain the Tfh cell phenotype (Baumjohann et al., 2013).

Interactions between ICOS on T cells and ICOSL on B cells induces calcium signalling and cytokine expression by Tfh cells and increased CD40 signalling which induces higher ICOSL expression on B cells, creating a feed-forward loop (Liu et al., 2015). However, stronger BCR signalling itself results in downregulation of ICOSL on B cells (Liu et al., 2015; Sacquin et al., 2017), and, in *in vitro* co-cultures, was shown to result in decreased Tfh cell differentiation independently of amount of antigen presented (Sacquin et al., 2017). Furthermore, in *in vivo* experiments, immunisation with a high-affinity antigen resulted in fewer Tfh cells 5 days after immunisation compared to immunisation with a low-affinity antigen, and treatment with an anti-ICOSL antibody blocked these differences (Sacquin et al., 2017). Therefore, the link between BCR signalling and Tfh cells is complex.

4.1.3 Reactivation of anergic B cells

There is clear evidence that B cell anergy is reversable and cells can become reactivated. Inappropriate activation of anergic B cells can contribute to autoimmunity. For example, in healthy humans autoreactive 9G4 (N-acetyllactosamine-specific) B cells have been shown to be functionally anergic and excluded from GCs, whereas in SLE patients they are not anergic and are expanded within GCs (Cappione et al., 2005). In B cell anergy models, anergic B cells have been reactivated *in vivo* in certain conditions. In an experimental system where T cell help was provided, anergic hen egg lysozyme (HEL)-specific B cells in MD4 x ML5 mice expanded and secreted HEL-specific antibodies following immunisation with membrane-bound HEL, but not soluble HEL (Cooke et al., 1994). In a similar model, anergic HEL-specific B cells could not take part in GCs when immunised with sheep red blood cells (SRBCs) coupled to HEL

at a density equivalent to self-antigen on mouse red blood cells, but could enter GCs when immunised with SRBCs coupled to HEL at a 30-fold higher density (Burnett et al., 2018). Anergic double stranded DNA-specific B cells could be activated and formed antibody-secreting cells in a model system where T cell help was provided (Seo et al., 2002). This suggests a crucial role for T cell help in activation of anergic B cells, but also that the nature of the antigen cross-linking with the BCR may be important.

Recently, it has been proposed that the reason for having a pool of self-reactive B cells in a state of anergy is so that they can be reactivated in the event of encountering a foreign antigen that mimics self-antigen. This process has been named 'clonal redemption' (Burnett et al., 2019) and was demonstrated in experiments using bone marrow chimeric mice in which HEL-specific B cells were present in a state of anergy because of expression of HEL as a self-antigen. In this model, HEL-specific anergic B cells could be recruited into GCs following immunisation with a foreign antigen with high similarity to HEL, duck egg lysozyme (DEL). In the GC they were selected for mutations that reduced affinity to the self-antigen HEL and gained affinity for the foreign antigen DEL (Burnett et al., 2018).

However, most of the previously published work on reactivation of anergic B cell comes from transgenic BCR models with known specificity. Little is known about polyclonal anergic B cell participation in GCs.

4.1.4 Chapter aims

In the previous chapter it was established that the IgMg1 and IgG1M models have altered BCR signalling resulting in some defects in B cell development. IgMg1 B cells

appear to have an anergic phenotype, whereas B cells in IgG1M mice have enhanced BCR signalling. This chapter aims to investigate how the altered BCR signalling in these mouse models affects the B cell response to model TI-II and TD antigens, and analyse impact on Tfh cells. It will be particularly interesting to investigate participation of the anergic IgMg1 B cells in the GC in a polyclonal B cell environment.

The aims of this chapter are as follows:

iv. Analysis of B cell response to model TI-II antigen NP-Ficoll in IgMg1 and IgG1M mice.
v. Analysis of B cell response to model TD antigen NP-KLH in IgMg1 and IgG1M mice.
vi. Analysis of gene expression changes in GC B cells in IgMg1 mice by bulk RNA sequencing.
vii. Analysis of Tfh cells and Tfh cell activation during GC B cell responses.

4.2 Results

4.2.1 IgG1M mice have a severely impaired response to TI-II antigen while IgMg1 response is moderately impaired

As shown in chapter 3, IgMg1 and IgG1M mice both have evident defects in B cell development as a result of altered BCR signalling. Mature IgMg1 B cells have dampened calcium flux in response to BCR stimulation, while IgG1M mice have hyperactive calcium flux in response to altered BCR signalling. IgMg1 mice have a reduction in marginal zone B cells and B-1 cells. IgG1M mice also have reduced B-1 cells but have increased marginal zone B cells. To determine how these changes would impact on the B cell response to a TI-II antigen, mice were immunised i.p. with 50 µg NP-Ficoll and analysed 6 days later (Figure 4.1A). Splenocytes were analysed by flow cytometry to assess the frequency of NP-specific B cells and plasma cells (Figure 4.1B). Plasma cells were reduced as a percentage of splenocytes by 46% in IgG1M mice, with hardly any of the cells having detectable binding to NP (Figure 4.1C and D). Absolute numbers of NP-specific plasma cells in IgG1M mice were also reduced (Figure 4.1G). IgMg1 mice had a slight reduction in total plasma cells ($p=0.2546$) and a 40% reduction in NP-specific cells as a percentage of plasma cells ($p=0.0223$) compared with WT mice (Figure 4.1C and D), but the absolute number of NP-specific plasma cells per spleen was not significantly reduced (Figure 4.1F and G). NP-specific B cells were reduced in IgMg1 mice and reduced even further in IgG1M mice (Figure 4.1E and H).

To confirm the flow cytometry results, NP-specific antibody secreting cells were analysed by ELISpot (Figure 4.2) and fluorescent immunohistology (Figure 4.3). As shown by flow cytometry, ELISpot showed there was a large reduction in the frequency of NP-specific IgG secreting cells in the spleens of IgG1M mice 6 days after

immunisation with NP-Ficoll (Figure 4.2B), and as expected there were no NP-specific IgM secreting cells (Figure 4.2C). For IgMg1 mice there were no significant differences in either NP-specific IgG (Figure 4.2B) or IgM secreting cells (Figure 4.2C) compared with WT mice. The severe reduction in NP-specific plasma cells in IgG1M mice spleens was also evident by fluorescent immunohistology, whereas IgMg1 mice were not significantly different from WT (Figure 4.3). However, ELISpot analysis of NP-specific antibody secreting cells in the bone marrow 6 days after immunisation with NP-Ficoll showed very little difference compared to WT mice (Figure 4.2D and E)

NP-binding ELISAs were performed to quantify relative amounts of NP-specific antibody from the sera of mice 6 days after immunisation with NP-Ficoll (Figure 4.4). Compared to WT mice, there was a slight but non-significant reduction in NP-specific IgG (Figure 4.4A and B) and IgM (Figure 4.4C and D) in IgMg1 mice. However, there was a large reduction in NP-specific IgG (Figure 4.4A and B) in IgG1M mice, and NP-specific IgM was undetectable as expected (Figure 4.4C and D).

Overall, these data show that the B cell response to a model TI-II antigen in IgMg1 mice was slightly reduced at day 6 after immunisation. A larger reduction in the TI-II plasma cell response had been previously observed in IgMg1 mice (Zhang, 2019). However, in that experiment analysis was performed at day 5 after immunisation, suggesting that the TI-II response in IgMg1 mice may be delayed. Relative to IgMg1 mice, IgG1M mice had a more severely impaired TI-II response.

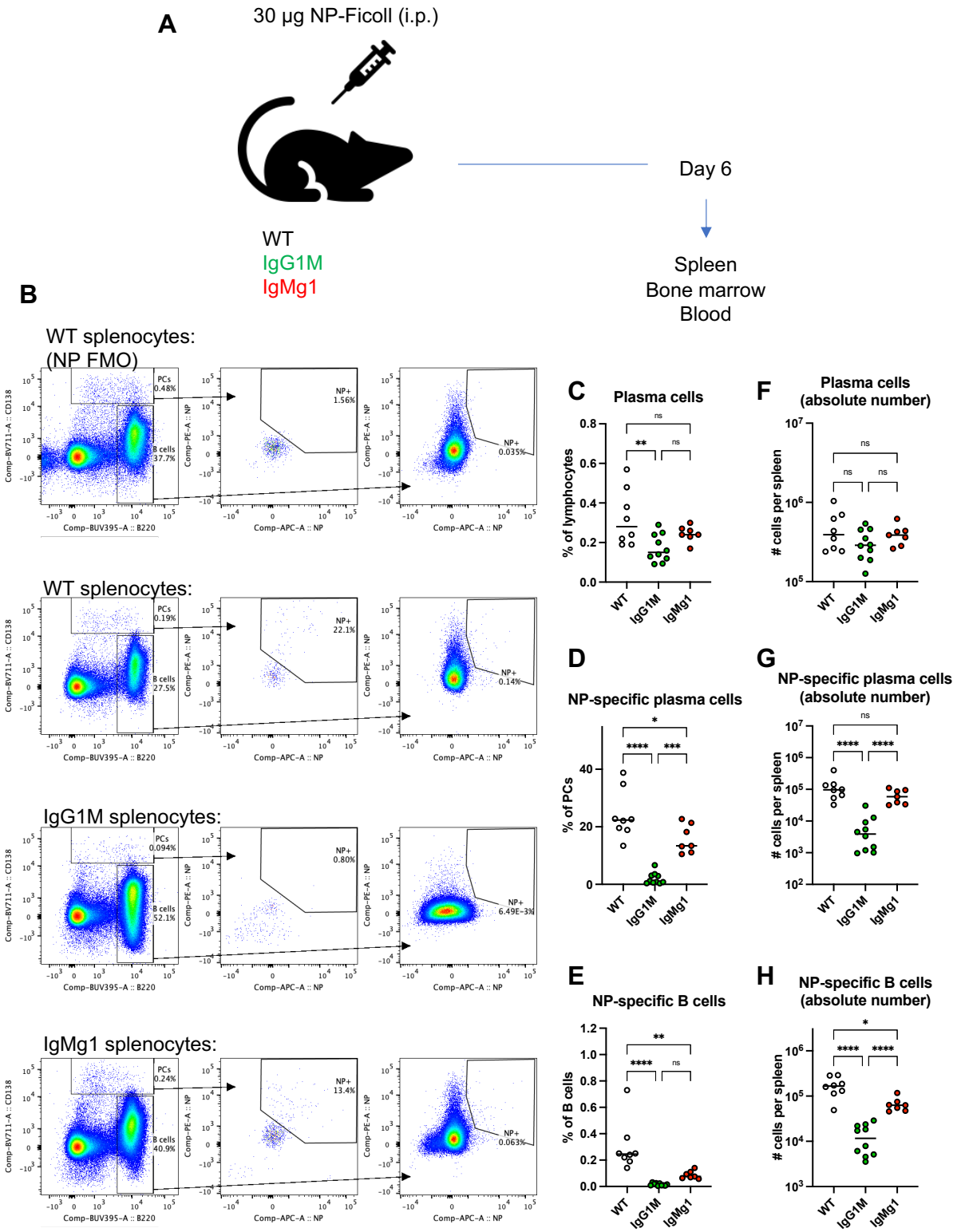
A
30 µg NP-Ficoll (i.p.)
Day 6
WT
IgG1M
IgMg1
Spleen
Bone marrow
Blood
B
WT splenocytes:
(NP FMO)
WT splenocytes:
IgG1M splenocytes:
IgMg1 splenocytes:
C
Plasma cells
% of lymphocytes
F
Plasma cells
(absolute number)
cells per spleen
D
NP-specific plasma cells
% of PCs
G
NP-specific plasma cells
(absolute number)
cells per spleen
E
NP-specific B cells
% of B cells
H
NP-specific B cells
(absolute number)
cells per spleen
WT
IgG1M
IgMg1

Figure 4.1 Analysis of response to TI-II antigen NP-Ficoll by flow cytometry

(A) Schematic showing immunisation with NP-Ficoll. Mice were immunised i.p. with 50 µg NP-Ficoll. Tissues were analysed at day 6. (B) Gating strategy for NP-specific plasma cells and NP-specific B cells from spleens of immunised mice, with representative plots shown for WT, IgMg1 and IgG1M mice. From live splenocytes, plasma cells (PCs) were gated as CD138+ and B cells were gated as B220+ CD138-. NP-specific cells were gated as NP-APC+ NP-PE+. Gates for NP-specific cells set using WT cells stained without NP-APC or NP-PE (shown top row). (C) Summary statistics for frequency of plasma cells as percentage of lymphocytes. (D) Summary statistics for frequency of NP-specific plasma cells as percentage of plasma cells. (E) Summary statistics for frequency of NP-specific B cells as percentage of B cells. (F-H) Summary statistics for absolute numbers of: (F) plasma cells, (G) NP-specific plasma cells and (H) NP-specific B cells per spleen. Data were combined from two experiments. Each symbol represents one mouse. Statistical tests were performed by ordinary one-way ANOVA with Tukey's multiple comparison test (****, $p < 0.0001$; ***, $p < 0.001$; **, $p < 0.01$; *, $p < 0.05$; ns, not significant).

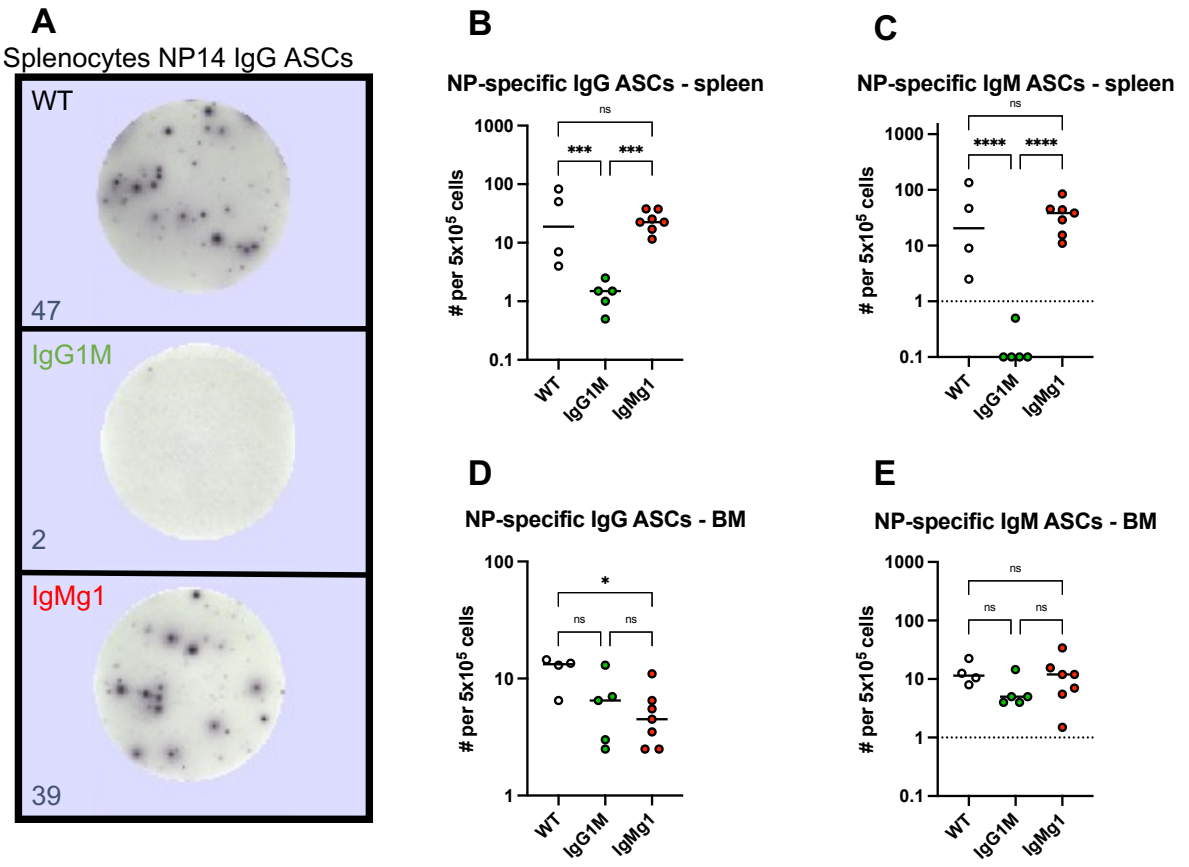

Figure 4.2 ELISpot quantification of NP-specific antibody secreting cells 6 days after immunisation with TI-II antigen NP-Ficol

NP-specific plasma cells in spleen and bone marrow were analysed 6 days after immunisation with NP-Ficoll by ELISpot. Mice were immunised as in Figure 4.1. (A) Representative wells from splenocytes of WT, IgMg1 and IgG1M mice analysed by ELISpot for NP-specific IgG secreting cells. Each spot represents one antibody-secreting cell (ASC). Spots were counted using ELISpot plate reader. (B-E) Summary statistics for number of: (B) NP-specific IgG ASCs in spleen; (C) NP-specific IgM ASCs in spleen; (D) NP-specific IgG ASCs in bone marrow (BM); (E) NP-specific IgM ASCs in BM; All data is plotted as number of ASCs per 5x105 cells. Data are from one experiment. Each symbol represents one mouse. Statistical tests were performed by ordinary one-way ANOVA with Tukey's multiple comparison test (****, $p < 0.0001$; ***, $p < 0.001$; *, $p < 0.05$; ns, not significant).

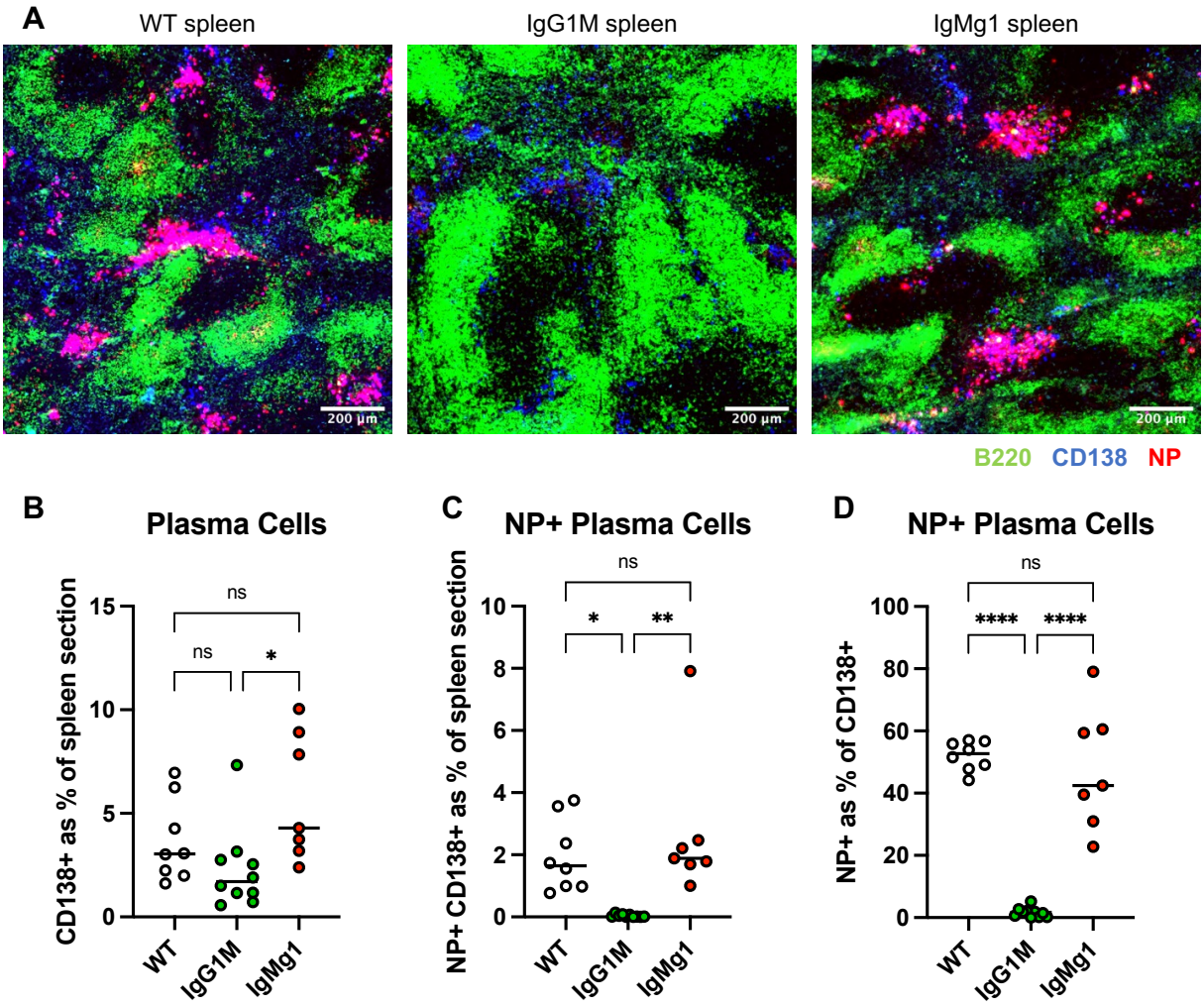

Figure 4.3 Fluorescent immunohistology analysis of NP-specific plasma cells in the spleen 6 days after immunisation with TI-II antigen NP-Ficoll

NP-specific plasma cells in spleen were analysed 6 days after immunisation with NP-Ficoll by fluorescent immunohistology. Mice were immunised as in Figure 4.1. (A) Representative spleen sections stained with anti-B220 (green), anti-CD138 (blue) and NP (red). NP-specific plasma cells are magenta-coloured. Scale bars represent 200 µm. (B-D) Images were analysed using Fiji to quantify area covered by plasma cells ($CD138^+$) and NP-specific plasma cells (NP^+ $CD138^+$). Summary statistics for: (B) plasma cells ($CD138^+$) as percentage of spleen section (C) NP-specific plasma cells (NP^+ $CD138^+$) as percentage of spleen section; (D) NP-specific plasma cells (NP^+ $CD138^+$) as percentage of plasma cells ($CD138^+$). Data are combined from two experiments. Each symbol represents one mouse. Statistical tests were performed by ordinary one-way ANOVA with Tukey's multiple comparison test (****, $p < 0.0001$; **, $p < 0.01$; *, $p < 0.05$; ns, not significant).

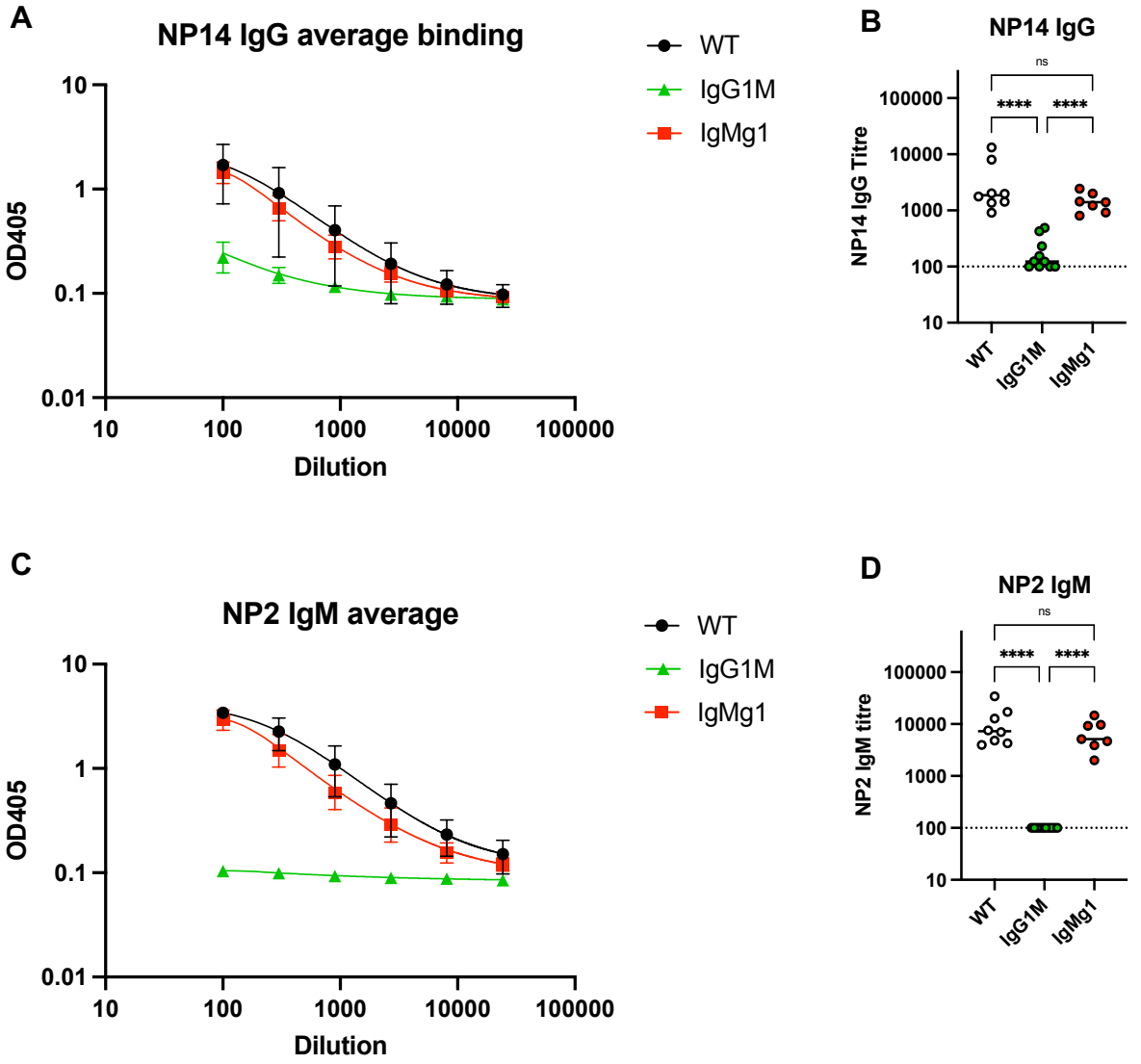

Figure 4.4 NP-specific antibody titres 6 days after immunisation with TI-II antigen NP-Ficoll

Mice were immunised with NP-Ficoll as in Figure 4.1 and serum samples were collected at day 6. Anti-NP sera titres were determined by ELISA using plates coated with NP_2-BSA or NP_{14}-BSA. (A) Binding curves for NP_{14}-specific IgG in sera of WT, IgMg1 and IgG1M mice. Mean data points plotted with error-bars representing standard deviation. (B) Summary statistics for relative NP_{14}-specific IgG sera titres. (C) Binding curves for NP_2-specific IgM in sera of WT, IgMg1 and IgG1M mice. Mean data points plotted with error-bars representing standard deviation. (D) Summary statistics for relative NP_2-specific IgM sera titres. Data combined from two experiments. Each symbol represents one mouse. Statistical tests were performed by ordinary one-way ANOVA with Tukey's multiple comparison test (****, $p < 0.0001$; ns, not significant).

4.2.2 IgG1M mice have an impaired plasma cell response to the TD antigen NP-KLH but response in IgMg1 mice is not impaired

Next, in order to assess the ability of IgMg1 and IgG1M B cells to take part in GC responses, mice were immunised with model TD antigen NP-KLH. Mice were immunised s.c. on the plantar surface of the foot with 10 µg alum precipitated antigen, with heat inactivated *Bordetella pertussis* included as an additional adjuvant. At day 8 mice were culled by schedule 1 method (Figure 4.5A) and the draining popliteal lymph node was analysed by flow cytometry (Figure 4.5B).

IgMg1 mice made a plasma cell response that was equivalent with WT mice. The overall frequency of plasma cells (Figure 4.6B) and the frequency of NP-specific plasma cells were not significantly changed from the WT mice (Figure 4.6C and D). However, in the IgG1M mice the plasma cell response was impaired. The overall frequency of plasma cells was significantly reduced (Figure 4.6B). Although the percentage of NP-specific cells within plasma cells was not significantly reduced compared with the WT plasma cells (Figure 4.6D), there was a significant reduction of NP-specific plasma cells as a percentage of lymphocytes (Figure 4.6C). As the size of the draining lymph node can vary greatly depending on the magnitude of the immune response, the absolute number of lymphocytes in each lymph node was estimated by using counting beads. This showed that the number of plasma cells and NP-specific plasma cells were reduced in IgG1M lymph nodes but were not significantly different from WT in IgMg1 lymph nodes (Figure 4.6D and E).

Serum samples taken at day 8 after immunisation with NP-KLH were analysed for NP-specific antibodies by ELISA. For NP-specific IgG, high-affinity antibodies were detected on plates coated with NP_2-BSA (Figure 4.7B), whereas total NP-specific

antibodies were detected on plates coated with the higher valency NP_{14}-BSA (Figure 4.7A). The ratio of the high-affinity titre to total titre gives an estimate of relative affinity. The total NP-specific IgG titre was similar in WT and IgMg1 mice but was significantly reduced in IgG1M mice (Figure 4.7D). High affinity fraction of NP-specific IgG was also similar in WT and IgMg1 mice (Figure 4.7E), and IgG affinity was not significantly different (Figure 4.7F). High affinity NP-specific IgG could not be detected in IgG1M mice, even at a serum dilution of 1/30 (Figure 4.7E). This supports the flow cytometry data that showed a reduction in plasma cells in the IgG1M mice. Although the anti-NP IgG was not significantly different in IgMg1 mice, there was a significantly lower titre for anti-NP IgM showing the IgM response in IgMg1 mice was reduced (Figure 4.7C and F).

Overall, these data suggest that at day 8 after immunisation with NP-KLH the plasma cell response was strongly impaired in IgG1M mice, while there was little impact on IgMg1 mice.

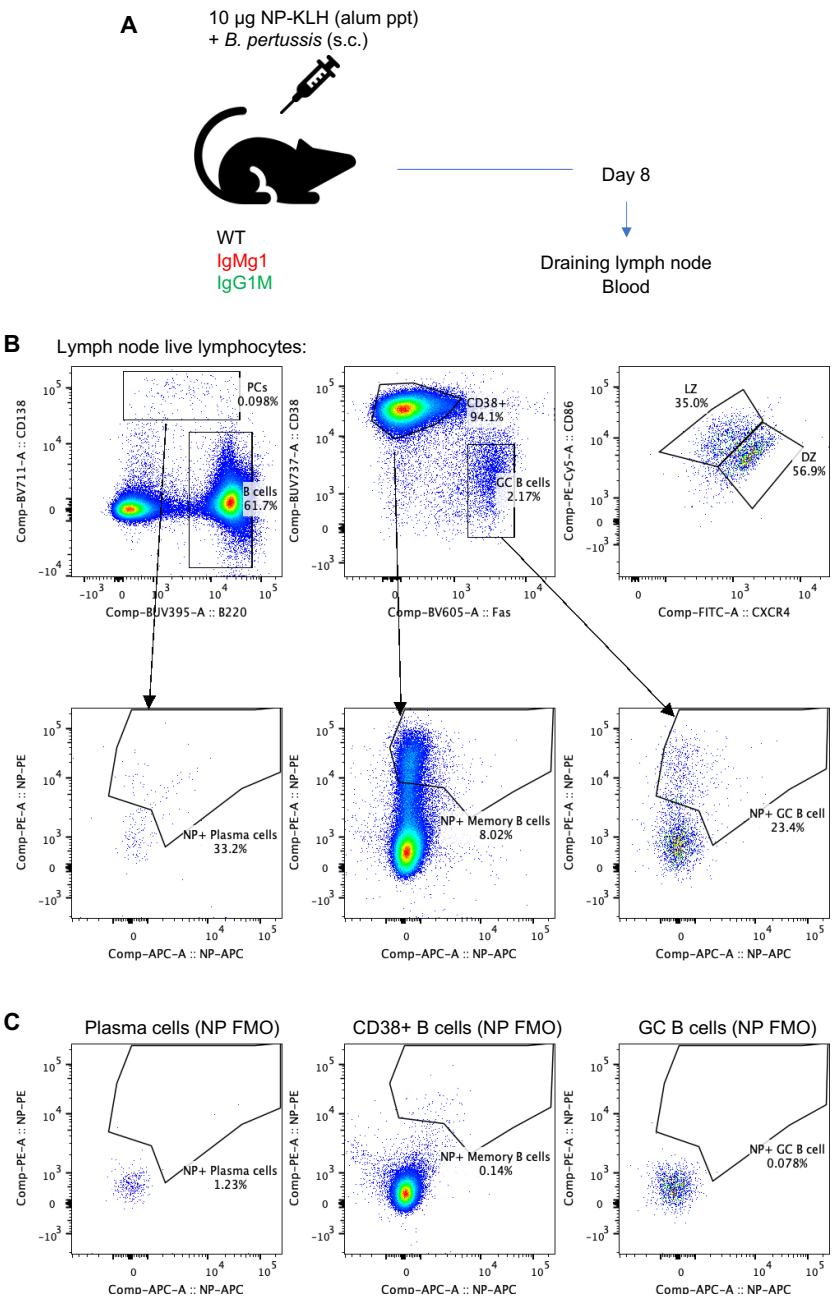

Figure 4.5 Immunisation with model TD antigen NP-KLH and flow cytometry gating strategy

(A) Schematic showing immunisation with NP-KLH. Mice were immunised s.c. on the plantar surface of the foot with 10 µg NP-KLH (alum ppt) and heat-inactivated *Bordetella pertussis*. Tissues were collected at day 8. (B) Gating strategy for plasma cells, NP-specific plasma cells, GC B cells, NP-specific GC B cells and NP-specific memory B cells (NP-specific $CD38^+$ B cells) from draining lymph nodes of immunised mice. From live lymphocytes, plasma cells (PCs) were gated as $CD138^+$ and B cells were gated as $B220^+$ $CD138^-$. From B cells, GC B cells were gated as Fas^+ $CD38^-$. NP-specific cells were gated as $NP\text{-}PE^+$ $NP\text{-}APC^+$. (C) Gates for NP-specific cells set using WT cells stained without NP-APC or NP-PE.

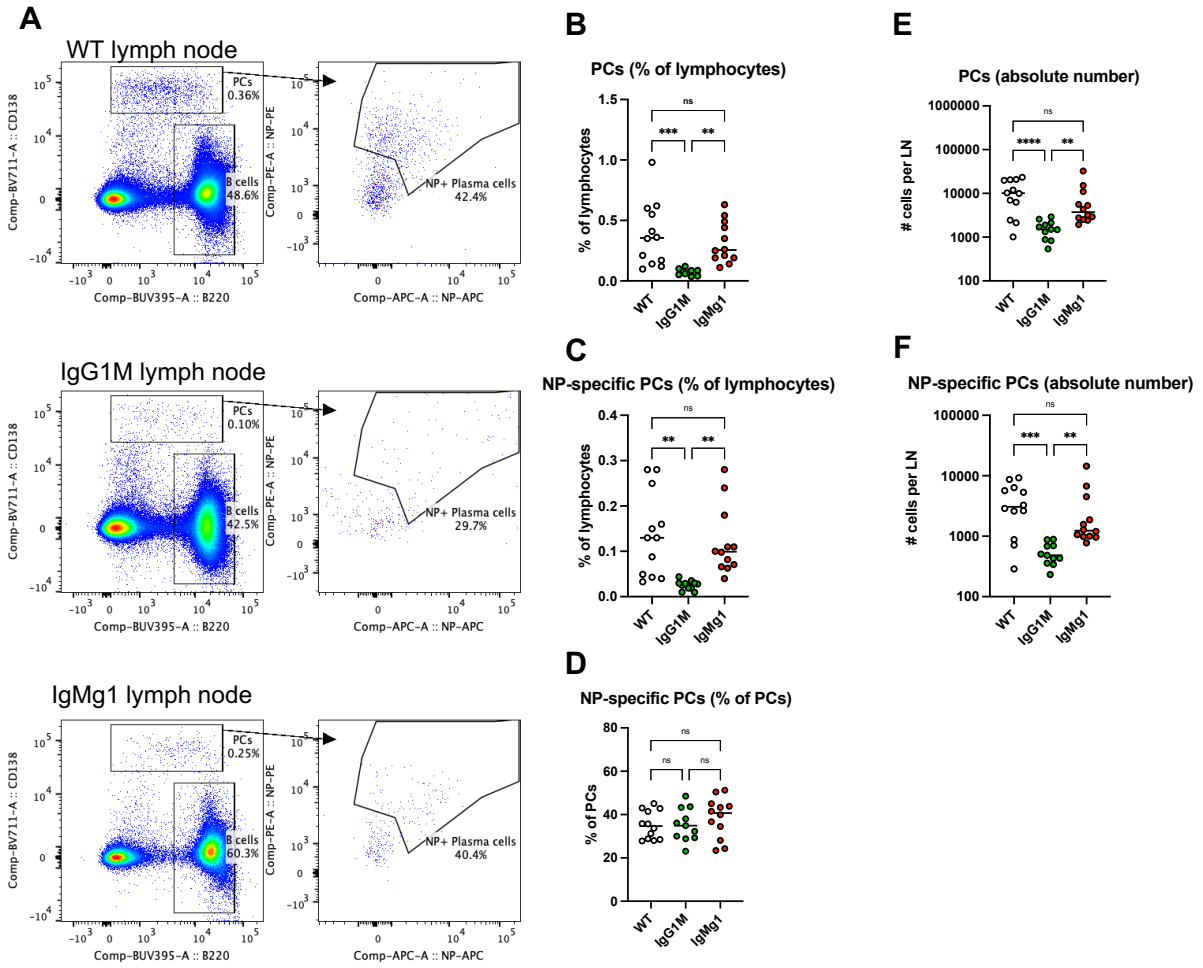

Figure 4.6 Analysis of plasma cells 8 days after immunisation with NP-KLH

Mice were immunised with NP-KLH described in Figure 4.5 and lymph nodes were analysed by flow cytometry at day 8. (A) Representative flow cytometry plots showing plasma cells (PCs) and NP-specific PCs in WT, IgG1M and IgMg1 mice. Gating was as described in Figure 4.5. (B-E) Summary statistics showing (B) PCs as percentage of lymphocytes; (C) NP-specific PCs as percentage of lymphocytes; (D) NP-specific PCs as percentage of total PCs; (E) absolute number of PCs per lymph node; (F) absolute number of NP-specific PCs per lymph node. Data combined from two experiments. Each symbol represents one mouse. Statistical tests were performed by ordinary one-way ANOVA with Tukey's multiple comparison test (****, $p < 0.0001$; ***, $p < 0.001$; **, $p < 0.01$; ns, not significant).

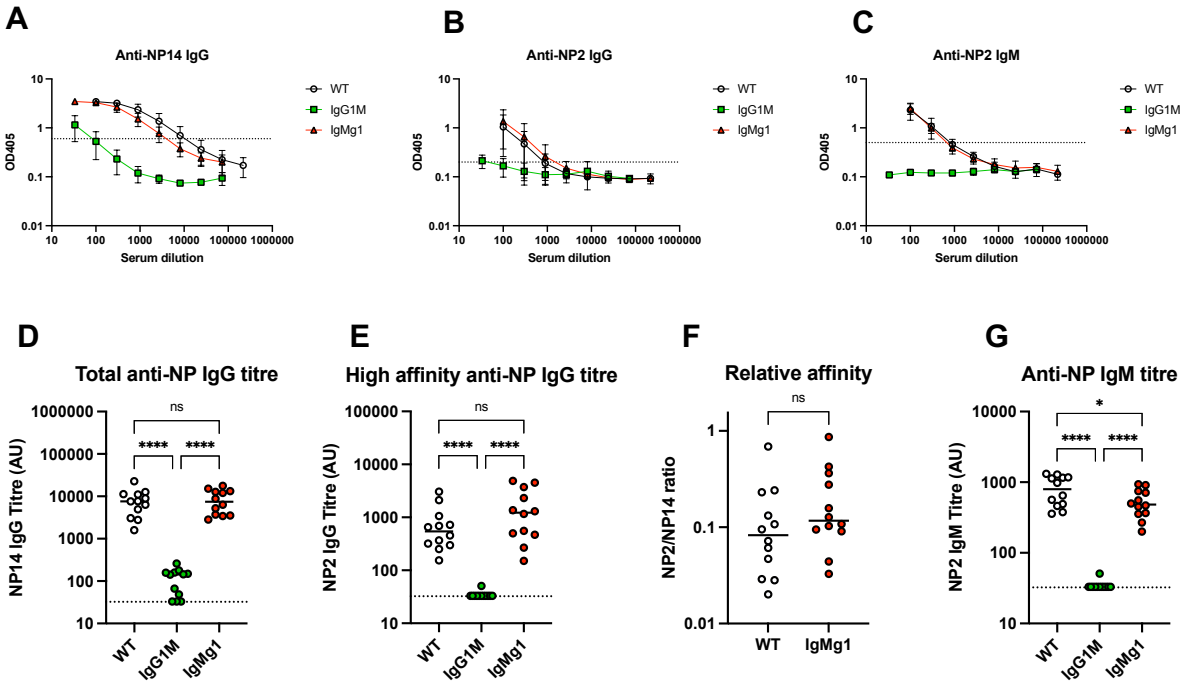

Figure 4.7 Analysis of serum NP-specific antibodies 8 days after NP-KLH immunisation

Mice were immunised with NP-KLH described in Figure 4.5 and serum samples were collected. Anti-NP sera titres were determined by ELISA using plates coated with NP_2-BSA or NP_{14}-BSA. (A) Binding curves for NP_{14}-specific IgG in sera of WT, IgMg1 and IgG1M mice. Mean data points plotted with error-bars representing standard deviation. (B) Binding curves for NP_2-specific IgG in sera of WT, IgMg1 and IgG1M mice. Mean data points plotted with error-bars representing standard deviation. (C) Binding curves for NP_2-specific IgM in sera of WT, IgMg1 and IgG1M mice. Mean data points plotted with error-bars representing standard deviation. (D) Summary statistics for relative NP_{14}-specific IgG sera titres. (E) Summary statistics for relative affinity (NP_2/NP_{14} ratio). (F) Summary statistics for relative NP_{14}-specific IgG sera titres. (G) Summary statistics for relative NP_2-specific IgG sera titres. Data combined from two experiments. Each symbol represents one mouse. Statistical tests were performed by ordinary one-way ANOVA with Tukey's multiple comparison test for comparison of three groups, and two-tailed unpaired T-test for comparison of two groups (****, $p < 0.0001$; *, $p < 0.05$; ns, not significant).

4.2.3 IgG1M and IgMg1 B cells can take part in GCs, but IgMg1 GCs have more antigen-specific cells, and IgG1M GCs have fewer antigen-specific cells

The GC B cell response was analysed by flow cytometry at day 8 after immunisation with NP-KLH (Figure 4.8A). GC B cells were reduced in IgMg1 mice, as a percentage of B cells and lymphocytes (Figure 4.8B and C). The absolute number of GC B cells was also reduced (Figure 4.8D). However, within the GC B cells, the frequency of NP-specific cells was increased so that the absolute number of NP-specific GC B cells, and the frequency within the lymphocytes, were overall comparable to those observed in WT mice (Figure 4.8E-G). In IgG1M mice, the frequency of GC B cells within the B cells was elevated (Figure 4.8B-D), although absolute number and frequency within the lymphocytes were similar to WT mice, and the frequency of NP-specific GC B cells was similar to WT mice (Figure 4.8E-G).

Therefore, there was an apparent increase in NP-specific cells within the IgMg1 GC and a reduction in NP-specific cells in the IgG1M GC. It is likely that flow cytometry detects antigen binding only in higher affinity B cells (Viant et al., 2020). To further evaluate the affinity of BCRs in the GC B cells, a ratio was taken of the frequency of NP^{hi} cells relative to NP^{int} cells, with a higher ratio indicating higher affinity (Figure 4.9A and B). Analysis in this way showed that $IgG1^+$ GC B cells in IgMg1 mice had higher average NP staining compared with WT GC B cells, indicating higher affinity (Figure 4.9C). However, IgM^+ GC B cells had comparable NP staining to WT, indicating similar affinity (Figure 4.9D). $IgG1^+$ GC B cells in IgG1M GCs on the other hand appeared to have a reduced proportion of NP^{hi} cells, indicating lower average BCR affinity of GC B cells in this model (Figure 4.9C).

Positioning of the B cells within the light zone (LZ) and dark zone (DZ) can be estimated by flow cytometry using CD86 and CXCR4 staining (Figure 4.10A). The ratio of $CXCR4^{hi}$ $CD86^{lo}$ dark zone (DZ) GC B cells to $CXCR4^{lo}$ $CD86^{hi}$ light zone (LZ) GC B cells can inform on B cell selection dynamics within the GC. GC B cells in the IgG1M mice had similar DZ/LZ ratio to WT mice. However, IgMg1 GC B cells had a significantly higher DZ/LZ ratio, indicating that more of the GC B cells were positioned within the DZ (Figure 4.10B).

GC B cells undergo apoptosis in the LZ if they are not selected, and in the DZ if somatic hypermutation results in a damaged BCR (Mayer et al., 2017). Intracellular active Caspase-3 staining was used to identify apoptotic cells by flow cytometry (Figure 4.11A). The frequency of active Caspase-3^{+} GC B cells was significantly higher in IgMg1 mice than in WT mice. In IgG1M mice, the frequency of active Caspase3^{+} GC B cells trended towards a reduction compared to WT mice but did not reach significance. This suggested that apoptosis may be increased in GC B cells in IgMg1 mice, but not in IgG1M mice (Figure 4.11C). Analysis of active Caspase-3 staining in DZ and LZ cells (Figure 4.11B) showed that apoptosis may be higher in both GC compartments in IgMg1 mice (although not significant in DZ B cells) (Figure 4.11D and E). This suggests that BCR signalling may be important in both these apoptosis decisions. A caveat with this data is that the CXCR4 and CD86 staining for this experiment was not optimal so these results may not be correct.

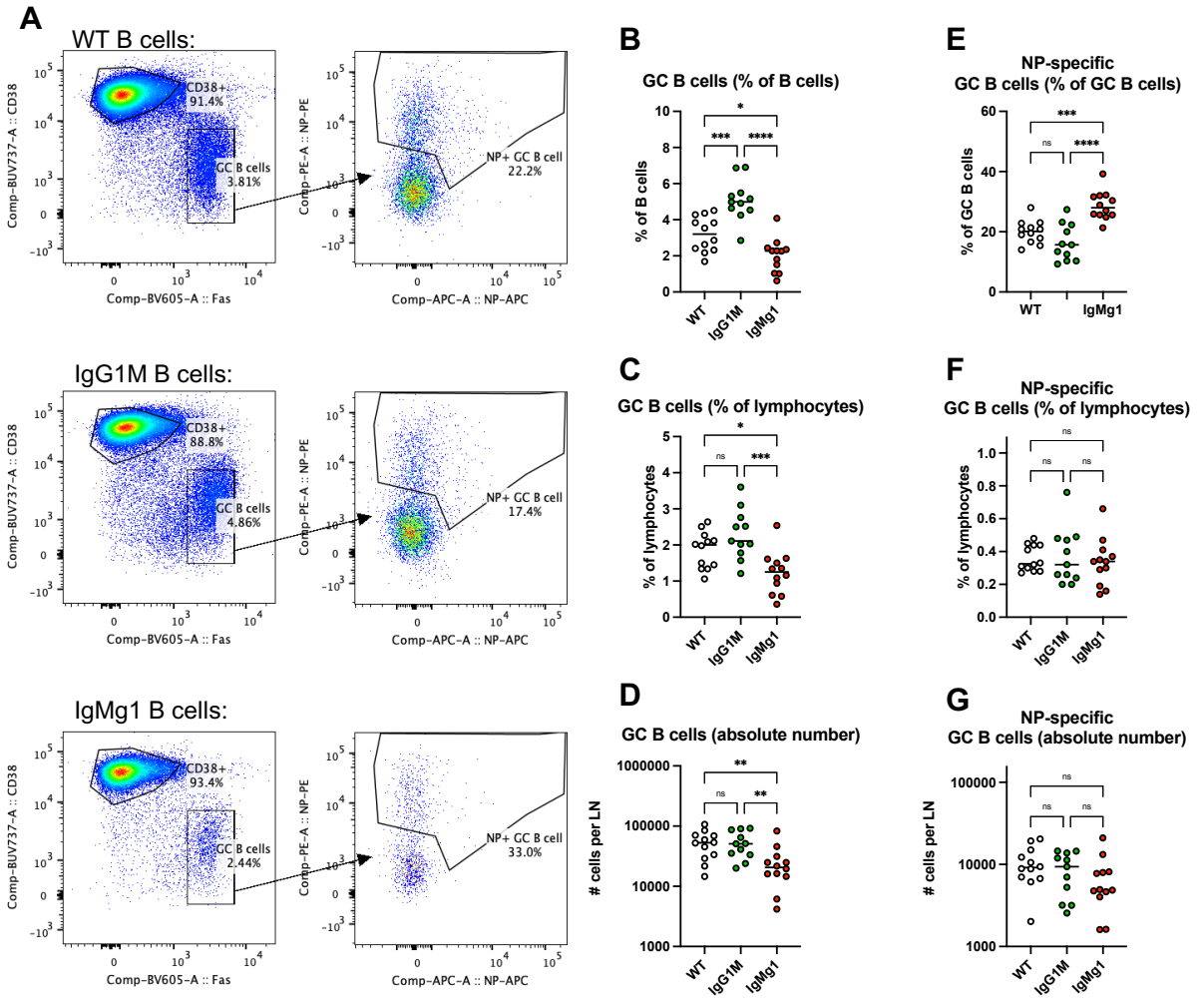

Figure 4.8 Flow cytometry analysis of GC B cells 8 days after NP-KLH immunisation

Mice were immunised with NP-KLH described in Figure 4.5 and lymph nodes were analysed by flow cytometry at day 8. (A) Representative flow cytometry plots showing GC B cells and NP-specific GC B cells for WT, IgG1M and IgMg1 mice. Gating was as described in Figure 4.5. (B-G) Summary statistics showing: (B) GC B cells as percentage of B cells; (C) GC B cells as percentage of lymphocytes; (D) absolute number of GC B cells (E) NP-specific GC B cells as percentage of GC B cells; (F) NP-specific GC B cells as percentage of lymphocytes; (G) absolute number of NP-specific GC B cells. Data combined from two experiments. Each symbol represents one mouse. Statistical tests were performed by ordinary one-way ANOVA with Tukey's multiple comparison test (****, $p < 0.0001$; ***, $p < 0.001$; **, $p < 0.01$; *, $p < 0.05$; ns, not significant).

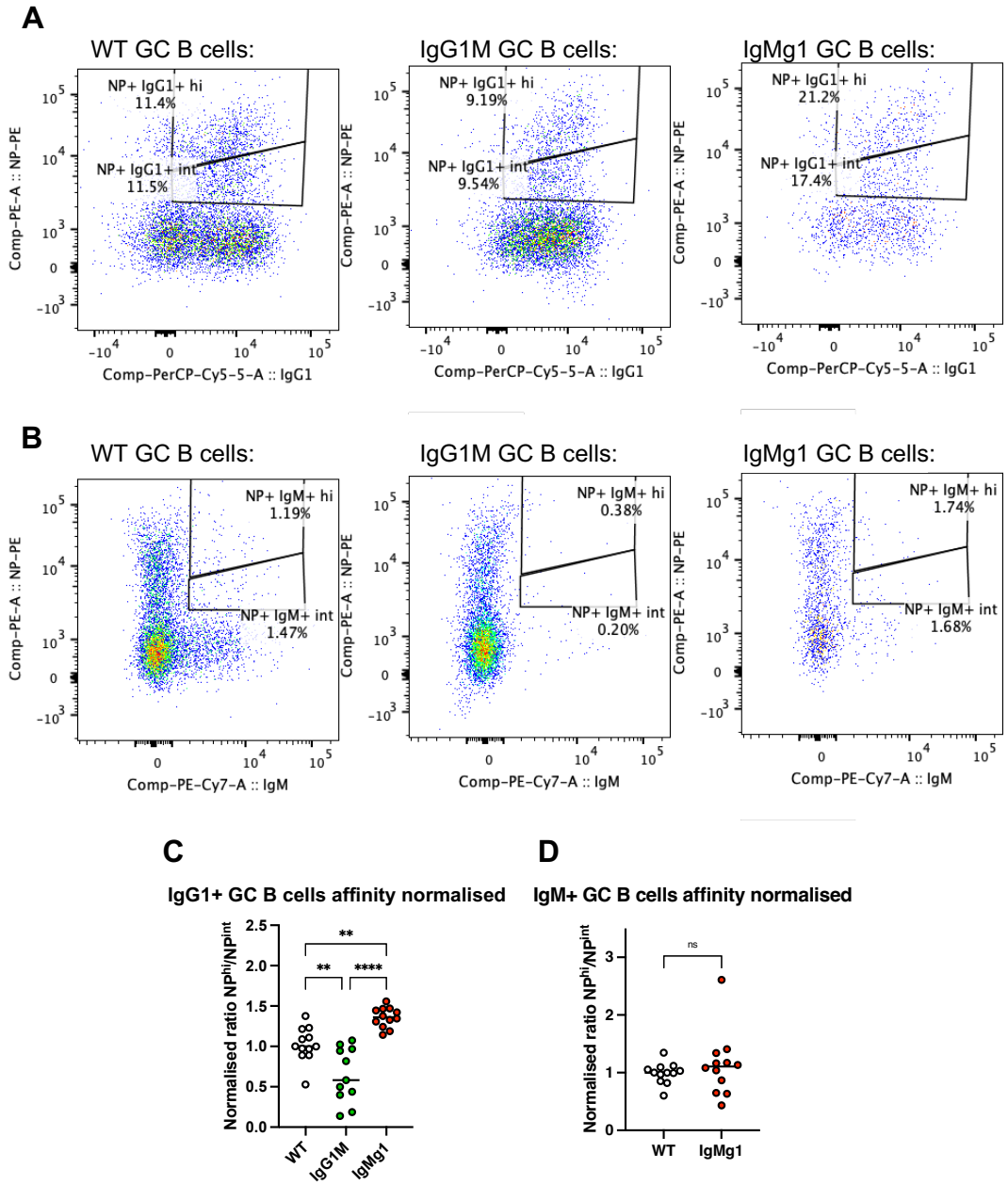

Figure 4.9 BCR NP-affinity assessed by flow cytometry

Mice were immunised with NP-KLH described in Figure 4.5 and lymph nodes were analysed by flow cytometry at day 8. (A) Representative gating for NP^{hi} and NP^{int} $IgG1^+$ GC B cells in WT, IgG1M and IgMg1 mice. GC B cells were gated as described in Figure 4.5. From GC B cells, NP^{hi} cells were gated as NP-PE^{hi} $IgG1^+$ cells and NP^{int} cells were gated as NP-PE^{int} $IgG1^+$. (B) Representative gating for NP^{hi} and NP^{int} IgM^+ GC B cells in WT, IgG1M and IgMg1 mice. GC B cells were gated as described in Figure 4.5. From GC B cells, NP^{hi} cells were gated as NP-PE^{hi} IgM^+ cells and NP^{int} cells were gated as NP-PE^{int} IgM^+. (C-D) Summary statistics for: (C) $IgG1^+$ GC B cell BCR affinity (NP^{hi}/NP^{int} ratio) for WT, IgG1M and IgMg1 mice; (D) IgM^+ GC B cell BCR affinity (NP^{hi}/NP^{int} ratio) for WT and IgMg1 mice. Data were normalised to median WT ratio to allow comparison between experiments. Data combined from two experiments. Each symbol represents one mouse. Statistical tests were performed by ordinary one-way ANOVA with Tukey's multiple comparison test for comparison of three groups, and two-tailed unpaired T-test for comparison of two groups (****, $p < 0.0001$; **, $p < 0.01$; ns, not significant).

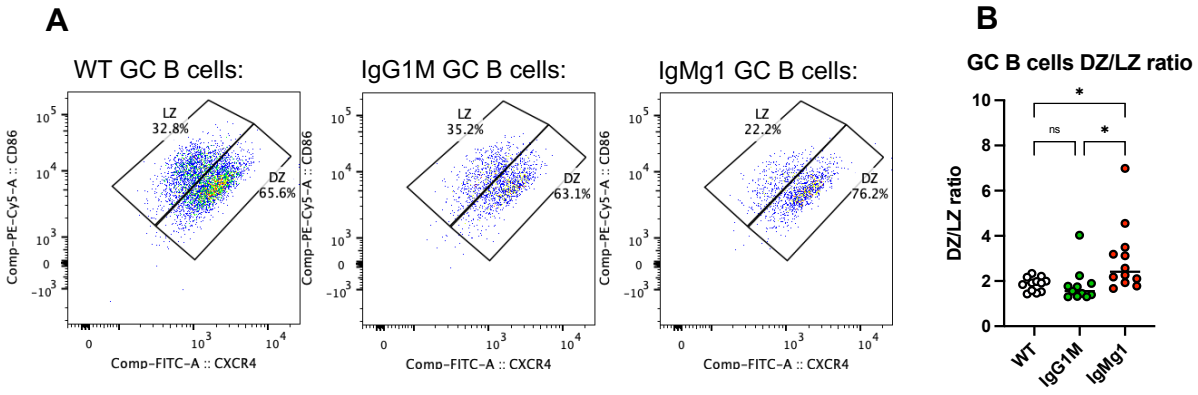

Figure 4.10 Dark zone/light zone ratio

Mice were immunised with NP-KLH described in Figure 4.5 and lymph nodes were analysed by flow cytometry at day 8. (A) Representative flow cytometry plots showing dark zone (DZ) and light zone (LZ) GC B cells for WT, IgG1M and IgMg1 mice. GC B cells were gated as described Figure 4.5. From GC B cells, DZ cells were gated as $CXCR4^{hi}$ $CD86^{lo}$ and LZ B cells were gated as $CXCR4^{lo}$ $CD86^{hi}$. (B) Summary statistics showing DZ/LZ ratio. Data combined from two experiments. Each symbol represents one mouse. Statistical tests were performed by ordinary one-way ANOVA with Tukey's multiple comparison test (*, $p < 0.05$; ns, not significant).

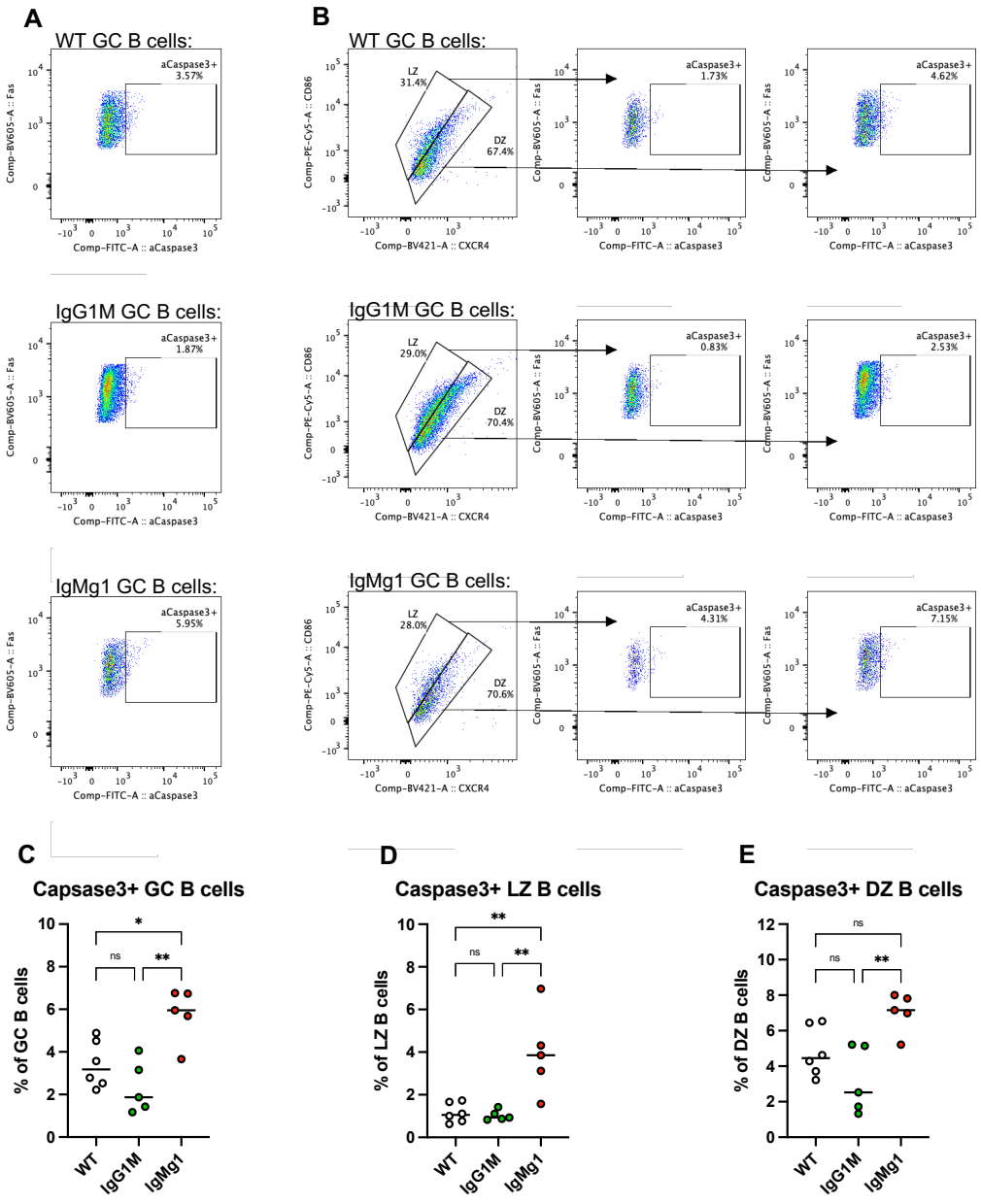

Figure 4.11 Identification of apoptotic cells by intracellular active Caspase-3 staining

Mice were immunised with NP-KLH described in Figure 4.5 and lymph nodes were analysed by flow cytometry at day 8. (A) Representative flow cytometry plots showing active Caspase-3 staining in WT, IgG1M and IgMg1 GC B cells. Mice were immunised with NP-KLH described in Figure 4.5 and lymph nodes were analysed by flow cytometry at day 8. Active Caspase-3$^+$ gate was set using an FMO control. (B) Representative flow cytometry plots showing active Caspase-3 staining in WT, IgG1M and IgMg1 LZ and DZ GC B cells. GC B cells were gated in a similar way to in Figure 4.4. From GC B cells, DZ cells were gated as CXCR4^{hi} CD86^{lo} and LZ B cells were gated as CXCR4^{lo} CD86^{hi}. Active Caspase-3$^+$ gate was set using an FMO control. (C-E) Summary statistics showing: (C) active Caspase-3$^+$ GC B cells as a percentage of GC B cells; (D) active Caspase-3$^+$ LZ GC B cells as a percentage of LZ GC B cells; (E) active Caspase-3$^+$ DZ GC B cells as a percentage of DZ GC B cells. Data from one experiment. Each symbol represents one mouse. Statistical tests were performed by ordinary one-way ANOVA with Tukey's multiple comparison test (**, $p < 0.01$; *, $p < 0.05$; ns, not significant).

4.2.4 GCs of IgMg1 mice contain fewer non-class-switched B cells

The IgMg1 B cells can undergo class-switching as normal during an immune response, switching to other isotypes such as IgG1. Once class-switched, these cells would no longer bear the chimeric IgMg1 BCR, but would instead express normal BCRs of the appropriate isotype. To investigate how class switching affects the GC B cell response in WT and IgMg1 mice, IgM^+ and $IgG1^+$ GC B cells were analysed separately (Figure 4.12A). This showed that the GCs in IgMg1 mice were dominated by class-switched B cells, with IgM^+ GC B cells being significantly reduced (Figure 4.12B). As a percentage of GC B cells, $IgG1^+$ GC B cells were significantly increased in IgMg1 mice (Figure 4.12C) confirming that the apparent reduction in IgM^+ cells was not simply due to IgM expression being too low to detect. Overall $IgG1^+$ GC B cell numbers in IgMg1 mice were not significantly different to WT mice (Figure 4.12E), showing that the overall GC B cell reduction in IgMg1 mice is predominantly due to the significant reduction in non-class-switched IgM^+ GC B cells (Figure 4.12D). The frequency of NP-specific cells was higher in $IgG1^+$ GC B cells in IgMg1 mice (Figure 4.12G) but not significantly different as a percentage of B cells (Figure 4.12I). Whereas NP-specific cells were found at the same frequency amongst IgM^+ GC B cells in IgMg1 and WT mice (Figure 4.12F), but were reduced overall in IgMg1 mice because of the overall reduction of IgM^+ GC B cells (Figure 4.12H). Analysis of BCR density on GC B cells showed that class switching to IgG1 did not change the reduced BCR expression in IgMg1 B cells (Figure 4.12J and K). In summary, there was a reduction of IgM^+ GC B cells in IgMg1 mice, with most of the GC B cells being class-switched.

To further investigate if the reduction of IgM$^+$ GC B cells in IgMg1 mice was due to altered selection, DZ/LZ ratio was analysed for IgM$^+$ and IgG1$^+$ GC B cells separately (Figure 4.13A). This showed that on average DZ/LZ ratio was higher in IgMg1 B cells regardless of isotype (Figure 4.13B and C), suggesting that class-switching did not affect IgMg1 B cells' ability to be selected into the DZ pool. To investigate if differential survival could explain the reduction in IgM$^+$ GC B cells in IgMg1 mice, IgG1$^+$ and IgM$^+$ GC B cells were also analysed for intracellular active caspase-3 staining to identify apoptotic cells (Figure 4.14A). IgG1$^+$ GC B cells in IgMg1 mice were around twice as often active caspase-3 positive compared with IgG1$^+$ GC B cells in WT mice (Figure 4.14B). This was similar for IgM$^+$ GC B cells but was not statistically significant (Figure 4.14C. There was no difference in the ratio of caspase-3$^+$ IgM$^+$ to IgG1$^+$ B cells in IgMg1 mice (Figure 4.14D) which suggested that the reduction in IgM$^+$ GC B cells in IgMg1 mice was not due to the increase in apoptosis in IgM$^+$ cells, as otherwise IgG1$^+$ GC cells would also be similarly reduced in IgMg1 mice. Furthermore, as previously described in section 4.2.2, there was no difference in plasma cell output (Figure 4.6) and a slight decrease in NP-specific IgM (Figure 4.7C and G) in IgMg1 mice, which suggests the reduction in IgM$^+$ GC B cells in IgMg1 mice was not due to increased output of IgM$^+$ plasma cells.

Overall, these data show that there is a reduction of IgM$^+$ B cells taking part in germinal centres in IgMg1 mice at day 8 after immunisation with NP-KLH. The reason for this reduction requires further investigation.

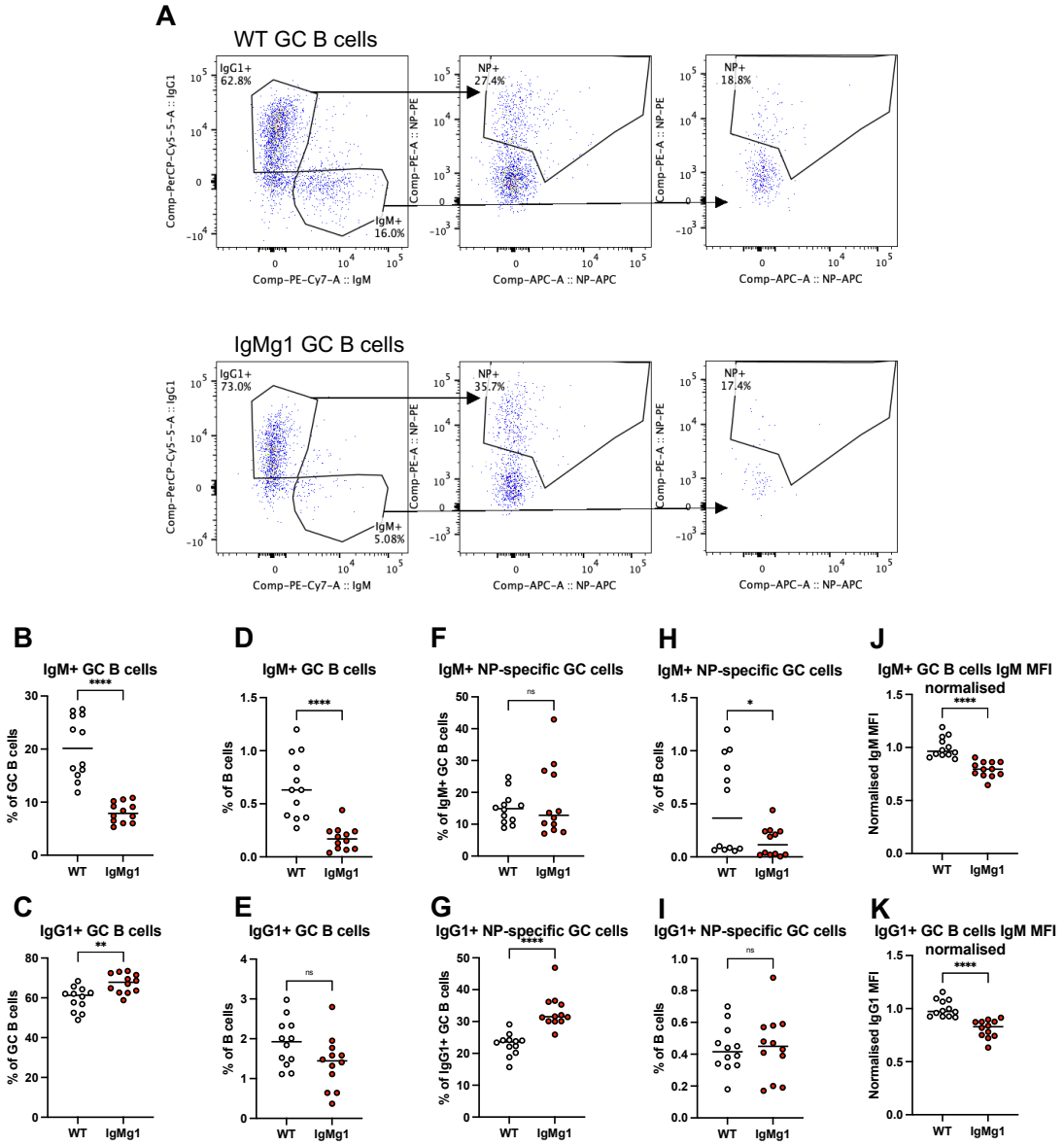

Figure 4.12 IgG1⁺ and IgM⁺ GC B cells in WT and IgMg1 mice 8 days after NP-KLH immunisation

Mice were immunised with NP-KLH described in Figure 4.5 and lymph nodes were analysed by flow cytometry at day 8. (A) Representative flow cytometry plots showing IgM⁺ and IgG1⁺ GC B cells and NP-specific IgM⁺ and IgG1⁺ GC B cells in WT and IgMg1 mice. GC B cells were gated as described in Figure 4.5. From GC B cells, IgG1⁺ GC B cells were gated as IgG1⁺ IgM⁻ and IgM⁺ GC B cells were gated as IgM⁺ IgG1⁻. NP-specific cells were gated as NP-PE⁺ NP-APC⁺. Gate was set using cells stained without NP-PE or NP-APC. (B-K) Summary statistics showing: (B) IgG1⁺ GC B cells as a percentage of GC B cells; (C) IgM⁺ GC B cells as a percentage of GC B cells; (D) IgG1⁺ GC B cells as a percentage of B cells; (E) IgM⁺ GC B cells as a percentage of B cells; (F) IgG1⁺ NP-specific GC B cells as a percentage of IgG1⁺ GC B cells; (G) IgM⁺ NP-specific GC B cells as a percentage of IgM⁺ GC B cells; (H) IgG1⁺ NP-specific GC B cells as a percentage of B cells; (I) IgM⁺ NP-specific GC B cells as a percentage of B cells; (J) IgG1 MFI in IgG1⁺ GC B cells. MFI normalised to the median MFI of the WT cells for comparison between separate experiments. (K) IgM MFI in IgM⁺ GC B cells. MFI normalised to the median MFI of the WT cells for comparison between separate experiments. Data combined from two experiments. Each symbol represents one mouse. Statistical tests were performed by two-tailed unpaired T-test (****, $p < 0.0001$; **, $p < 0.01$; *, $p < 0.05$; ns, not significant).

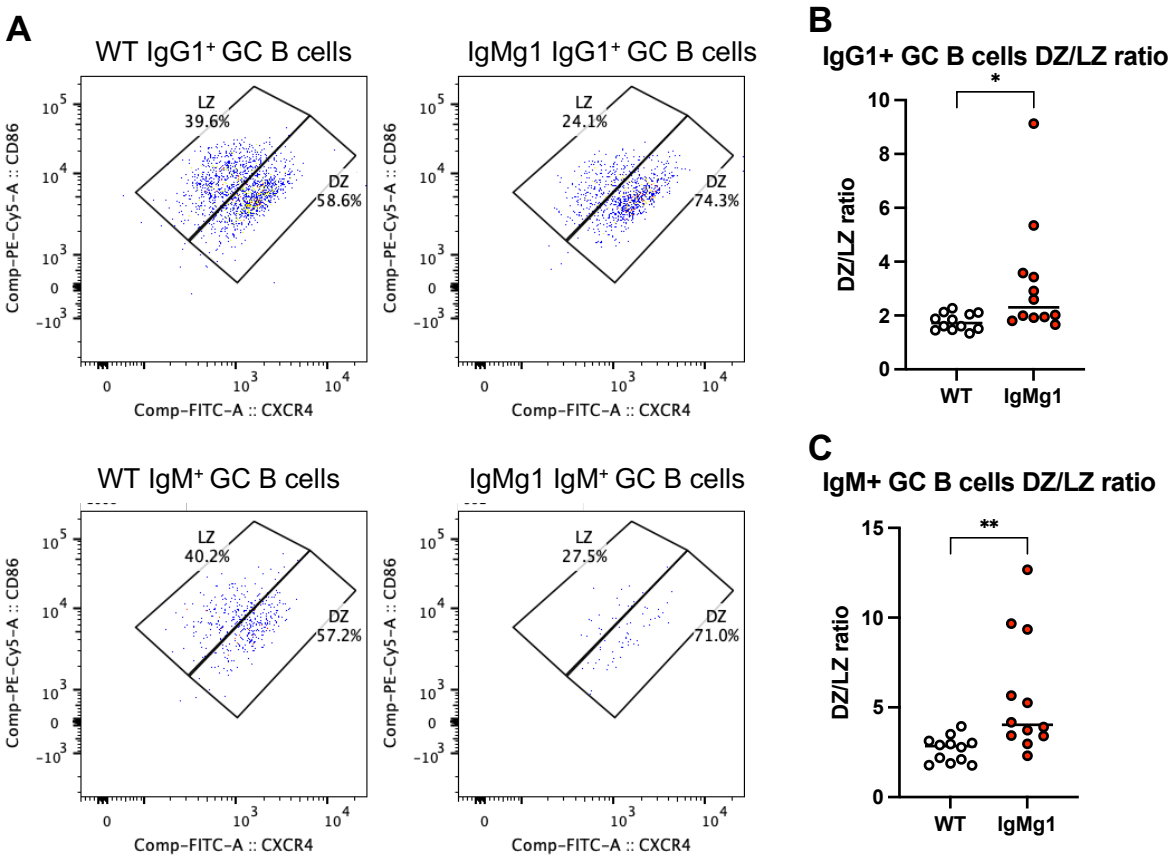

Figure 4.13 DZ/LZ ratio in IgG1$^+$ and IgM$^+$ GC B cells

Mice were immunised with NP-KLH described in Figure 4.5 and lymph nodes were analysed by flow cytometry at day 8. (A) Representative flow cytometry plots showing LZ and DZ staining in IgG1$^+$ and IgM$^+$ GC B cells in WT and IgMg1 mice. IgG1$^+$ and IgM$^+$ GC B cells were gated as described in Figure 4.12, and then DZ cells were gated as CXCR4^{hi} CD86^{lo} and LZ B cells were gated as CXCR4^{lo} CD86^{hi}. (B-C) Summary statistics showing DZ/LZ ratio in (A) IgG1$^+$ GC B cells and (C) IgM$^+$ GC B cells. Data is combined from two experiments. Each symbol represents one mouse. Statistical tests were performed by two-tailed unpaired T-test (**, $p < 0.01$; *, $p < 0.05$; ns, not significant).

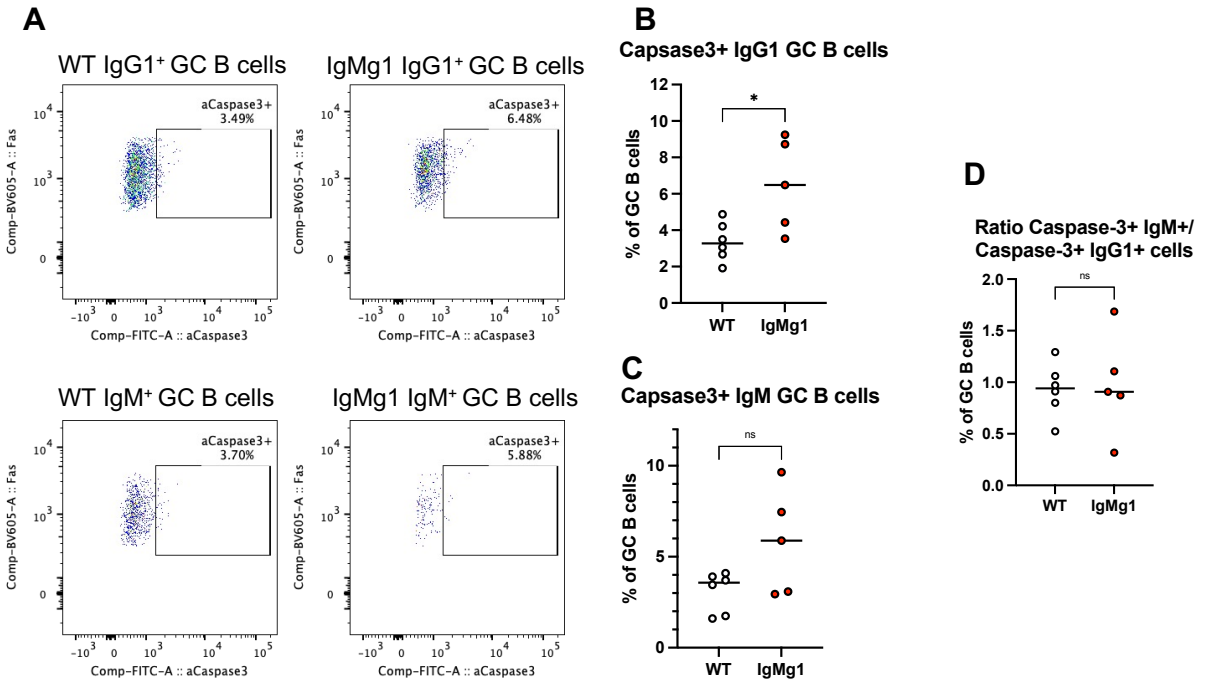

Figure 4.14 Intracellular active capase-3 staining in IgG1$^+$ and IgM$^+$ GC B cells

Mice were immunised with NP-KLH described in Figure 4.5 and lymph nodes were analysed by flow cytometry at day 8. (A) Representative flow cytometry plots showing active-Caspase-3 staining in IgG1$^+$ and IgM$^+$ GC B cells in WT and IgMg1 mice. IgG1$^+$ and IgM$^+$ GC B cells were gated as described in Figure 4.12, and then active-Caspase-3$^+$ cells were gated using an FMO control. (B-C) Summary statistics showing frequency of active Caspase-3$^+$ ratio in (B) IgG1$^+$ GC B cells and (C) IgM$^+$ GC B cells. (D) Summary statistics for ratio of active Caspase-3$^+$ IgM$^+$ GC B cells/active Caspase-3$^+$ IgG1$^+$ GC B cells. Data is from one experiment. Each symbol represents one mouse. Statistical tests were performed by two-tailed unpaired T-test (*, $p < 0.05$; ns, not significant).

4.2.5 Similar gene expression in GC B cells of WT and IgMg1 mice

IgMg1 B cells can take part in GCs despite their anergic phenotype. However, they maintain reduced surface BCR expression. Also, if clonal redemption of anergic B cells is linked to GC differentiation, entering GC differentiation of IgMg1 B cells would be expected to lead to a change in the gene expression profile. We therefore hypothesised that changes in gene expression may differentiate GC B cells in WT mice and IgMg1 mice in early GCs. Bulk RNA sequencing was therefore performed on FACS sorted GC B cells ($B220^+$ $CD138^-$ Fas^+ $CD38^-$) from draining popliteal lymph node 8 days after immunisation with NP-CGG s.c. in the plantar surface of the foot. This was performed in parallel with the sequencing of follicular B cells presented in chapter 3, allowing a comparison between gene expression between follicular B cells and GC B cells in both IgMg1 and WT mice. A comparison of all samples by PCA showed that most of the gene expression variability was between follicular and GC B cells regardless of genotype, separated on principal component 1 which accounted for 97% of the variation. However, there was separation between IgMg1 and WT B cells on principal component 2 which accounted for 3% of the variation (Figure 4.15). This suggested that there are a relatively small number of differences in gene expression between IgMg1 and WT B cells, and that these differences may be maintained even after differentiation into GC B cells.

Differential gene expression analysis was performed comparing WT GC B cells with WT follicular B cells to identify the normal gene expression profile of GC B cells (Figure 4.16A). There were 2017 genes identified as upregulated and 2312 genes identified as downregulated in WT GC B cells (with at least a 2-fold change and an adjusted p-value of less than 0.05) (Figure 4.16B). Gene set enrichment analysis (GSEA) with

hallmark gene sets showed that several gene sets were significantly enriched in either GC B cells or follicular B cells at a false discovery rate (FDR) q-value of below 0.05 (Figure 4.17A). Gene sets enriched in GC B cells included E2F targets (Figure 4.17B), Myc targets (Figure 4.17C) and cell cycle G2M checkpoint (Figure 4.17D), whereas gene sets enriched in follicular B cells included Interferon-α response (Figure 4.17E), Interferon-γ response (Figure 4.17F) and TNFα signalling via NFκB (Figure 4.17G).

The same analysis was then performed comparing IgMg1 GC B cells with IgMg1 follicular B cells to identify the gene expression changes in GC B cells in IgMg1 mice (Figure 4.18A). This identified 1952 genes that were upregulated in IgMg1 GC B cells and 2218 genes that were downregulated in IgMg1 GC B cells (Figure 4.18B). The majority of the differentially expressed genes identified in IgMg1 GC B cells were also differentially expressed in WT GC B cells (Figure 4.19A). Of the identified IgMg1 GC B cell differentially expressed genes, 1555 out of 1952 (79.7%) of the upregulated (Figure 4.19B) and 1555 out of 2218 (72.1%) of the downregulated genes (Figure 4.19C) were identified in the WT analysis. GSEA on the IgMg1 GC B cells using hallmark gene sets showed a very similar profile to WT GC B cells, with the same gene sets being significantly enriched (Figure 4.20).

These data showed that the overall gene expression programme in IgMg1 GC B cells, as well as the changes in gene expression from follicular B cell to GC B cell stage, appear to be similar to the overall gene expression changes in WT B cells.

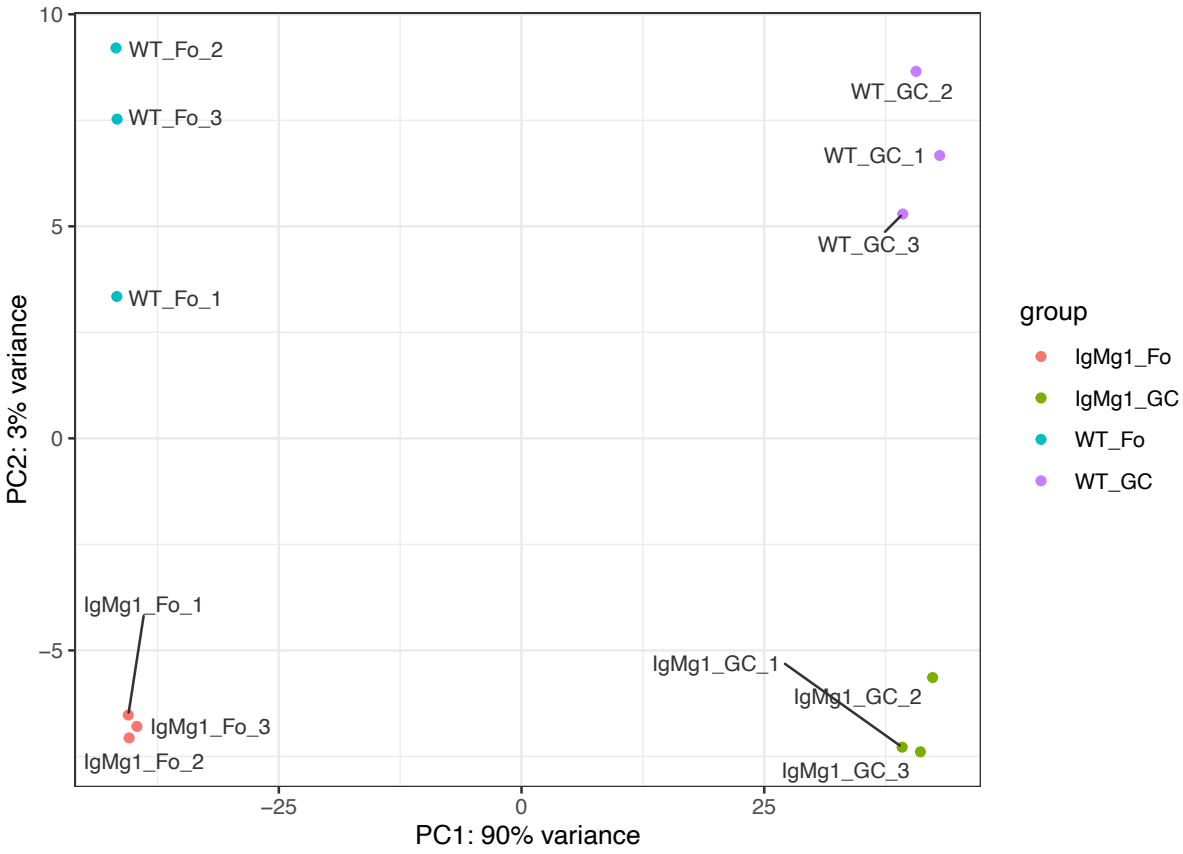

Figure 4.15 Principal components analysis of WT and IgMg1 follicular and GC B cell gene expression data

WT and IgMg1 follicular and GC B cells were sequenced by bulk RNA sequencing. Principal components analysis was performed to reduce dimensionality of gene expression data and visualise variance between samples.

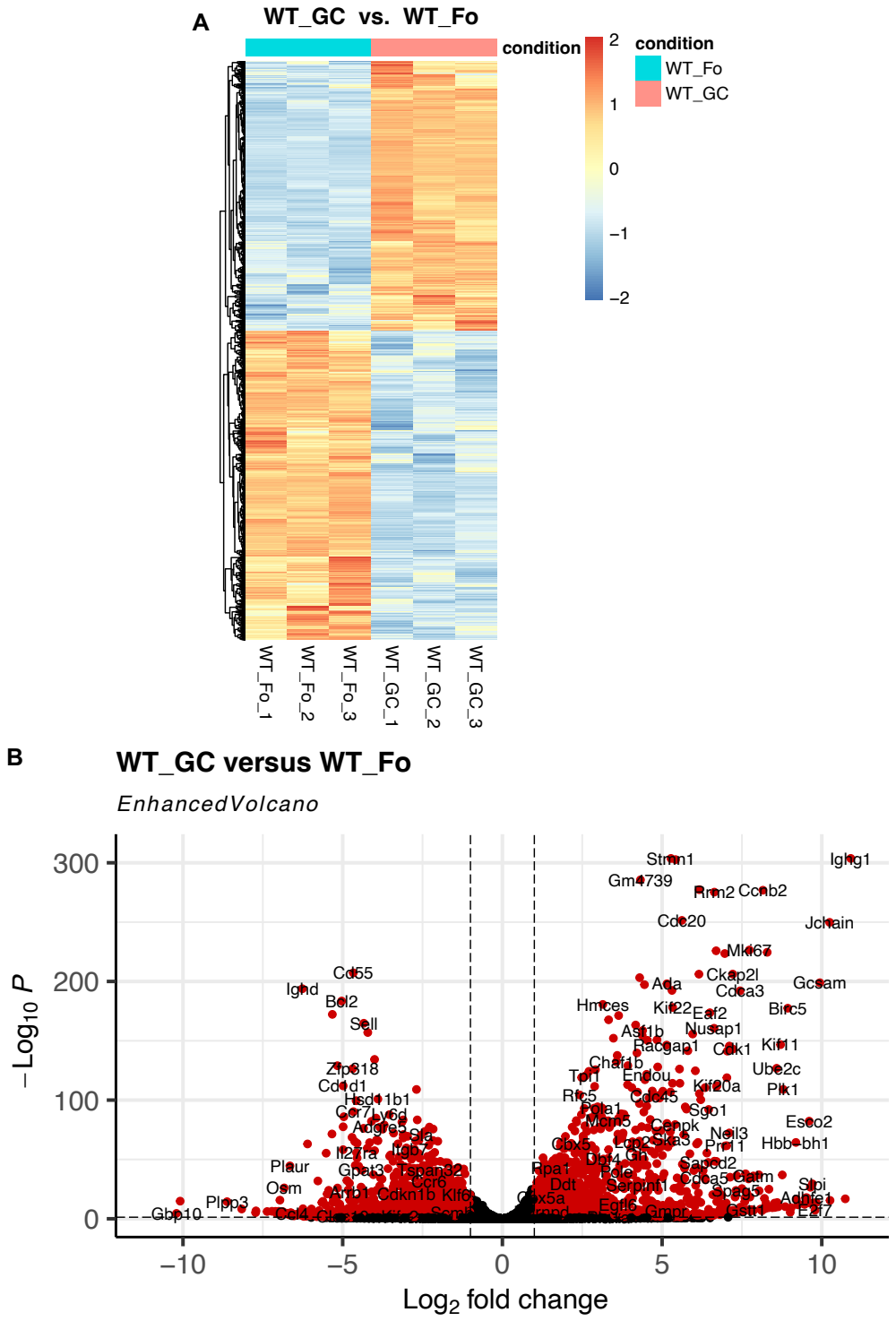

Figure 4.16 Differential gene expression in WT GC B cells compared with WT follicular B cells

Genes were identified that were differentially expressed in WT GC B cells compared with WT follicular B cells using DESeq2 package on R. (A) Heatmap showing expression of differentially expressed genes in WT GC B cells compared with WT follicular B cells (at least 2-fold change and adjusted p value < 0.05). Colour scale represents gene Z-score. (B) Volcano plot showing differentially expressed genes (at least 2-fold change and adjusted p value < 0.05) indicated in red. Horizontal dashed line represents adjusted p-value of 0.05 and vertical dashed lines represent $\log_2$-fold change of 1 and -1.

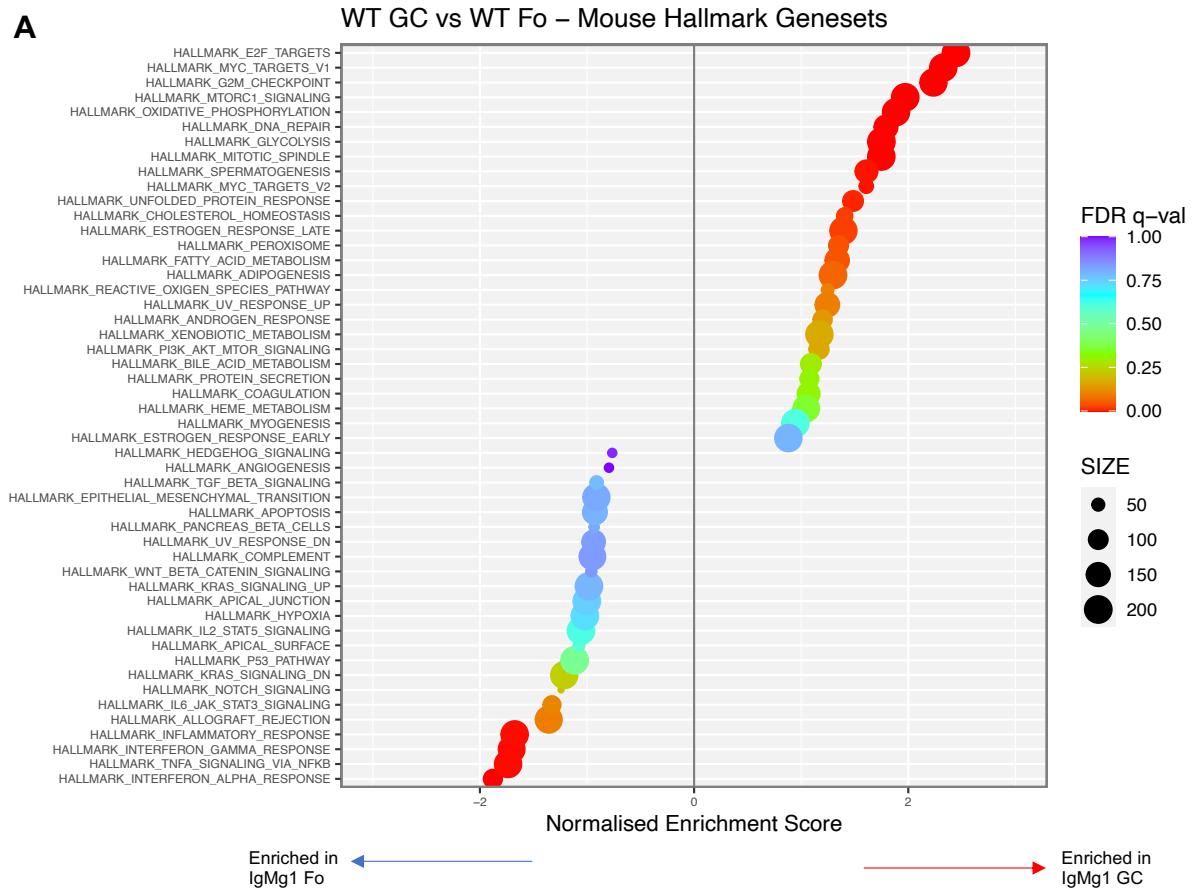
A
WT GC vs WT Fo – Mouse Hallmark Genesets
HALLMARK_E2F_TARGETS
HALLMARK_MYC_TARGETS_V1
HALLMARK_G2M_CHECKPOINT
HALLMARK_MTORC1_SIGNALING
HALLMARK_OXIDATIVE_PHOSPHORYLATION
HALLMARK_DNA_REPAIR
HALLMARK_GLYCOLYSIS
HALLMARK_MITOTIC_SPINDLE
HALLMARK_SPERMATOGENESIS
HALLMARK_MYC_TARGETS_V2
HALLMARK_UNFOLDED_PROTEIN_RESPONSE
HALLMARK_CHOLESTEROL_HOMEOSTASIS
HALLMARK_ESTROGEN_RESPONSE_LATE
HALLMARK_PEROXISOME
HALLMARK_FATTY_ACID_METABOLISM
HALLMARK_ADIPOGENESIS
HALLMARK_REACTIVE_OXIGEN_SPECIES_PATHWAY
HALLMARK_UV_RESPONSE_UP
HALLMARK_ANDROGEN_RESPONSE
HALLMARK_XENOBIOTIC_METABOLISM
HALLMARK_PI3K_AKT_MTOR_SIGNALING
HALLMARK_BILE_ACID_METABOLISM
HALLMARK_PROTEIN_SECRETION
HALLMARK_COAGULATION
HALLMARK_HEME_METABOLISM
HALLMARK_MYOGENESIS
HALLMARK_ESTROGEN_RESPONSE_EARLY
HALLMARK_HEDGEHOG_SIGNALING
HALLMARK_ANGIOGENESIS
HALLMARK_TGF_BETA_SIGNALING
HALLMARK_EPITHELIAL_MESENCHYMAL_TRANSITION
HALLMARK_APOPTOSIS
HALLMARK_PANCREAS_BETA_CELLS
HALLMARK_UV_RESPONSE_DN
HALLMARK_COMPLEMENT
HALLMARK_WNT_BETA_CATENIN_SIGNALING
HALLMARK_KRAS_SIGNALING_UP
HALLMARK_APICAL_JUNCTION
HALLMARK_HYPOXIA
HALLMARK_IL2_STAT5_SIGNALING
HALLMARK_APICAL_SURFACE
HALLMARK_P53_PATHWAY
HALLMARK_KRAS_SIGNALING_DN
HALLMARK_NOTCH_SIGNALING
HALLMARK_IL6_JAK_STAT3_SIGNALING
HALLMARK_ALLOGRAFT_REJECTION
HALLMARK_INFLAMMATORY_RESPONSE
HALLMARK_INTERFERON_GAMMA_RESPONSE
HALLMARK_TNFA_SIGNALING_VIA_NFKB
HALLMARK_INTERFERON_ALPHA_RESPONSE
−2
0
2
Normalised Enrichment Score
FDR q−val
1.00
0.75
0.50
0.25
0.00
SIZE
50
100
150
200
Enriched in IgMg1 Fo
Enriched in IgMg1 GC

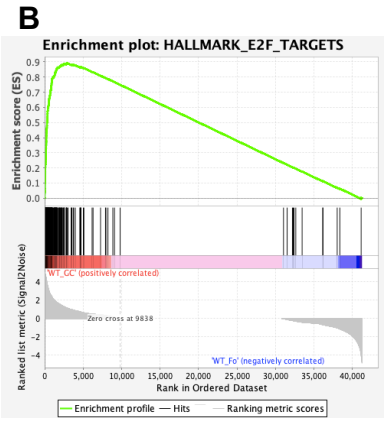
B
Enrichment plot: HALLMARK_E2F_TARGETS
Enrichment score (ES)
Ranked list metric (Signal2Noise)
'WT_GC' (positively correlated)
Zero cross at 9838
'WT_Fo' (negatively correlated)
Rank in Ordered Dataset
Enrichment profile
Hits
Ranking metric scores

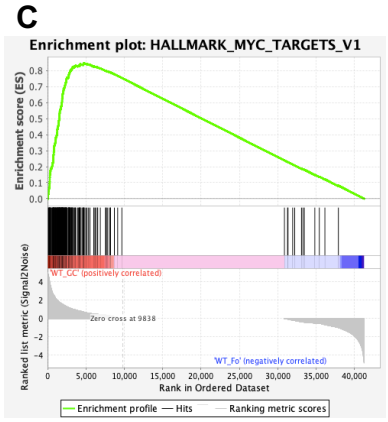
C
Enrichment plot: HALLMARK_MYC_TARGETS_V1
Enrichment score (ES)
Ranked list metric (Signal2Noise)
'WT_GC' (positively correlated)
Zero cross at 9838
'WT_Fo' (negatively correlated)
Rank in Ordered Dataset
Enrichment profile
Hits
Ranking metric scores

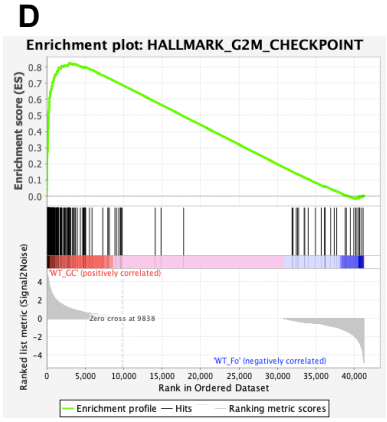
D
Enrichment plot: HALLMARK_G2M_CHECKPOINT
Enrichment score (ES)
Ranked list metric (Signal2Noise)
'WT_GC' (positively correlated)
Zero cross at 9838
'WT_Fo' (negatively correlated)
Rank in Ordered Dataset
Enrichment profile
Hits
Ranking metric scores

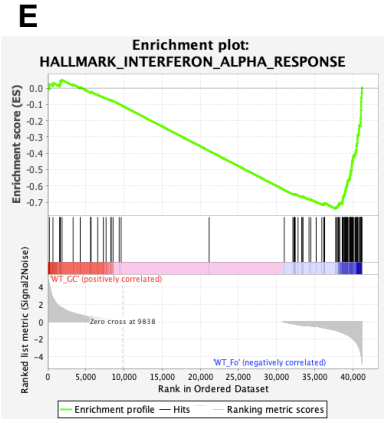
E
Enrichment plot:
HALLMARK_INTERFERON_ALPHA_RESPONSE
Enrichment score (ES)
Ranked list metric (Signal2Noise)
'WT_GC' (positively correlated)
Zero cross at 9838
'WT_Fo' (negatively correlated)
Rank in Ordered Dataset
Enrichment profile
Hits
Ranking metric scores

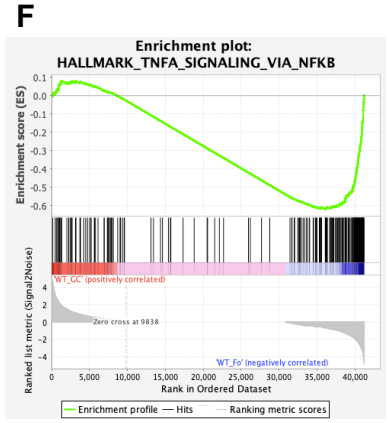
F
Enrichment plot:
HALLMARK_TNFA_SIGNALING_VIA_NFKB
Enrichment score (ES)
Ranked list metric (Signal2Noise)
'WT_GC' (positively correlated)
Zero cross at 9838
'WT_Fo' (negatively correlated)
Rank in Ordered Dataset
Enrichment profile
Hits
Ranking metric scores

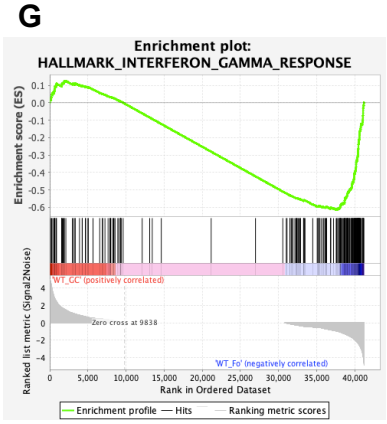
G
Enrichment plot:
HALLMARK_INTERFERON_GAMMA_RESPONSE
Enrichment score (ES)
Ranked list metric (Signal2Noise)
'WT_GC' (positively correlated)
Zero cross at 9838
'WT_Fo' (negatively correlated)
Rank in Ordered Dataset
Enrichment profile
Hits
Ranking metric scores

Figure 4.17 GSEA of mouse hallmark gene sets in WT GC B cells compared with WT follicular B cells

(A) Gene set enrichment analysis (GSEA) was performed on WT follicular B cell and GC B cell expression data, comparing to mouse hallmark gene sets. Plot shows normalised enrichment scores for hallmark gene sets for GSEA performed between WT follicular and GC B cells. Size of circle represents number of genes in set. Colour represents FDR q-value. (B-G) GSEA enrichment plots for some of enriched gene sets: (B) E2F targets; (C) Myc targets v1; (D) G2M checkpoint; (E) Interferon α response; (F) TNFa signalling via NFκB; (G) Interferon γ response.

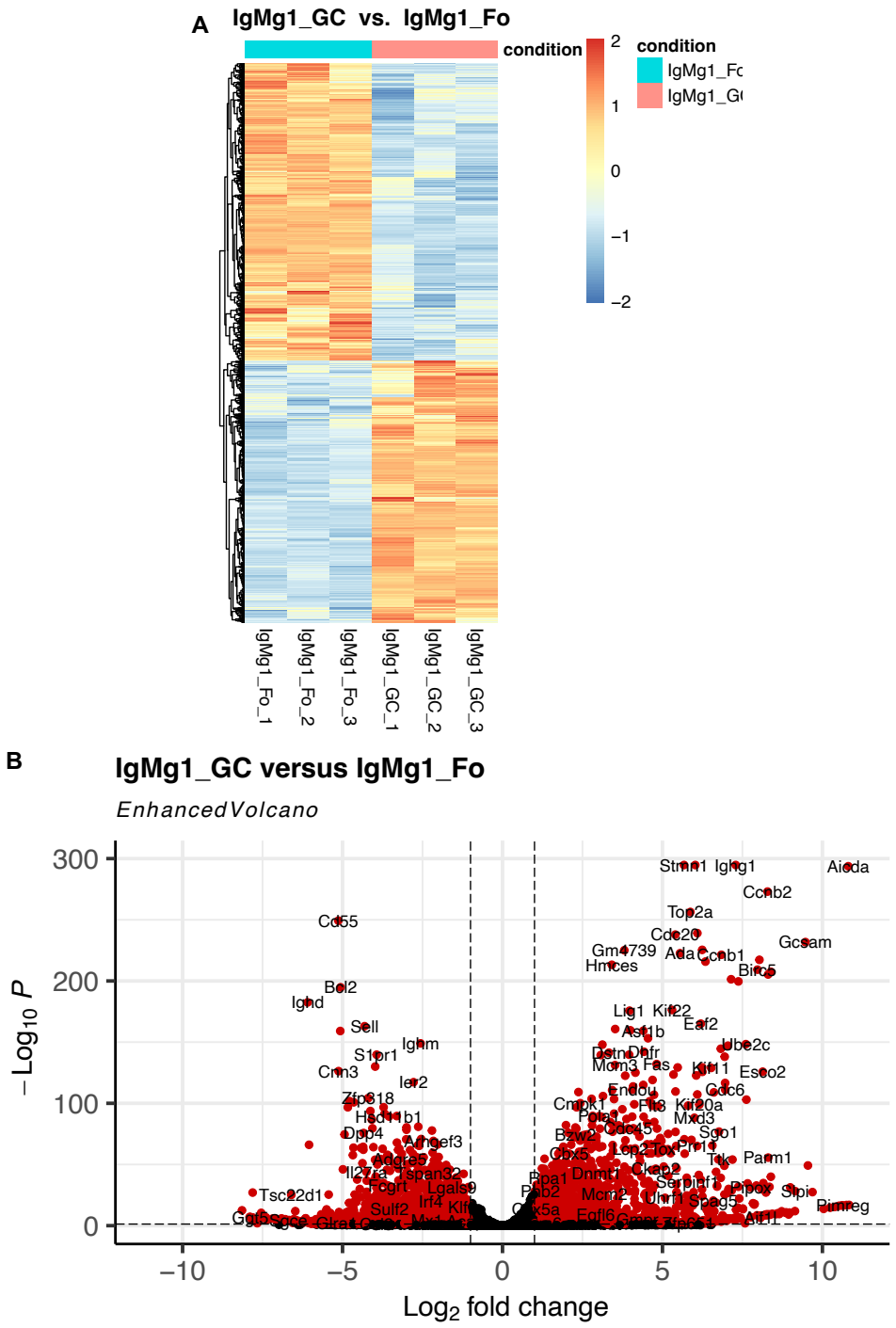

Figure 4.18 Differential gene expression in IgMg1 GC B cells compared with IgMg1 follicular B cells

Genes were identified that were differentially expressed in IgMg1 GC B cells compared with IgMg1 follicular B cells using DESeq2 package on R. (A) Heatmap showing expression of differentially expressed genes in IgMg1 GC B cells compared with IgMg1 follicular B cells (at least 2-fold change and adjusted p value < 0.05). Colour scale represents gene Z-score. (B) Volcano plot showing differentially expressed genes (at least 2-fold change and adjusted p value < 0.05) indicated in red. Horizontal dashed line represents adjusted p-value of 0.05 and vertical dashed lines represent $\log_2$-fold change of 1 and -1.

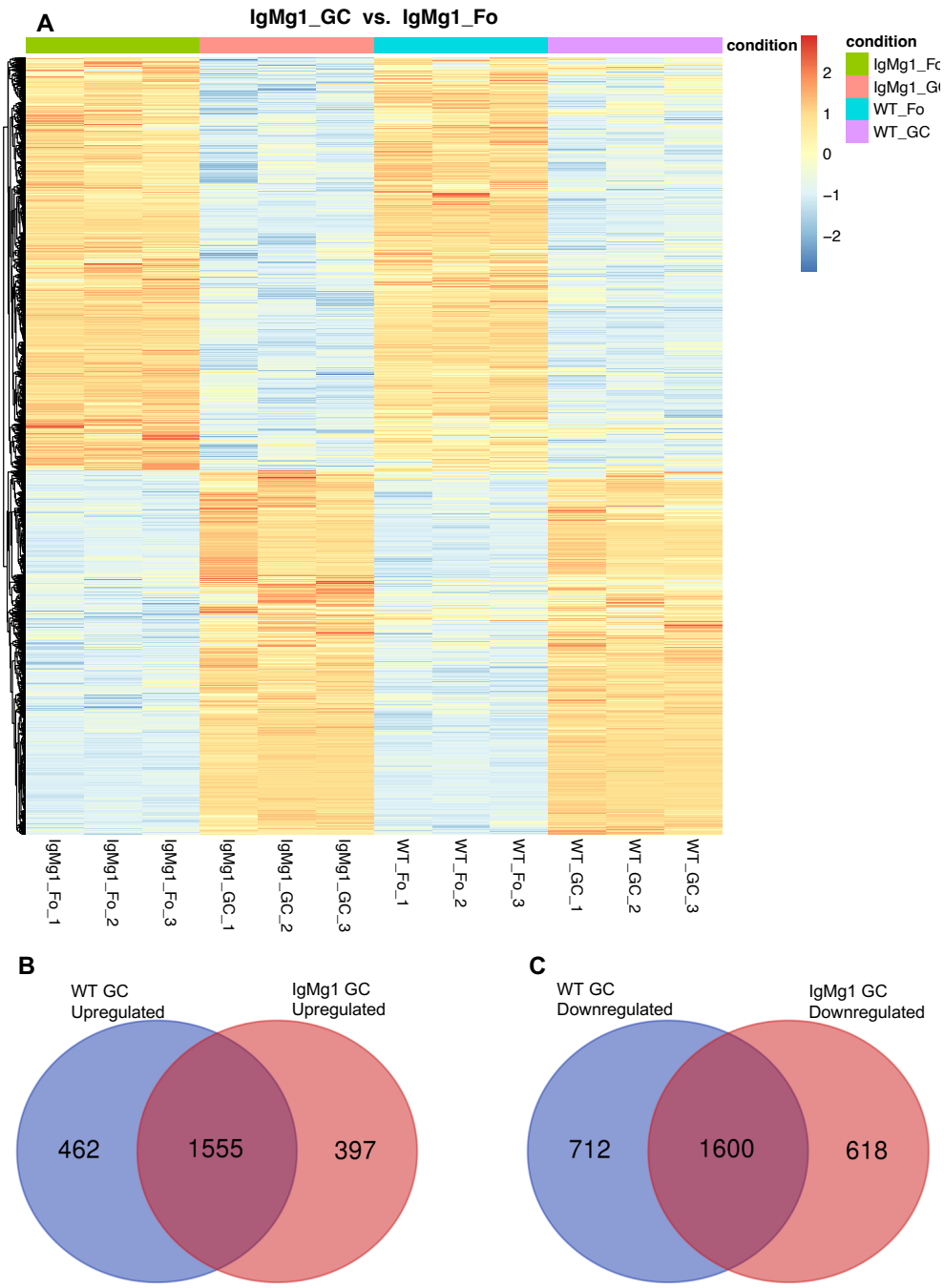

Figure 4.19 Comparison of genes differentially expressed in GC vs follicular B cells in IgMg1 and WT mice

The differentially expressed genes in GC B cells compared with follicular B cells were compared in IgMg1 and WT mice. (A) Heatmap showing relative expression of genes identified as differentially expressed in IgMg1 GC B cells compared with IgMg1 follicular B cells (at least 2-fold change and adjusted p value < 0.05) across all WT and IgMg1 samples. Colour scale represents gene Z-score. (B) Venn diagram showing overlap of identified upregulated genes in WT GC B cells compared with WT follicular B cells, with upregulated genes in IgMg1 GC B cells compared with IgMg1 follicular B cells. (C) Venn diagram showing overlap of identified downregulated genes in WT GC B cells compared with WT follicular B cells, with downregulated genes in IgMg1 GC B cells compared with IgMg1 follicular B cells.

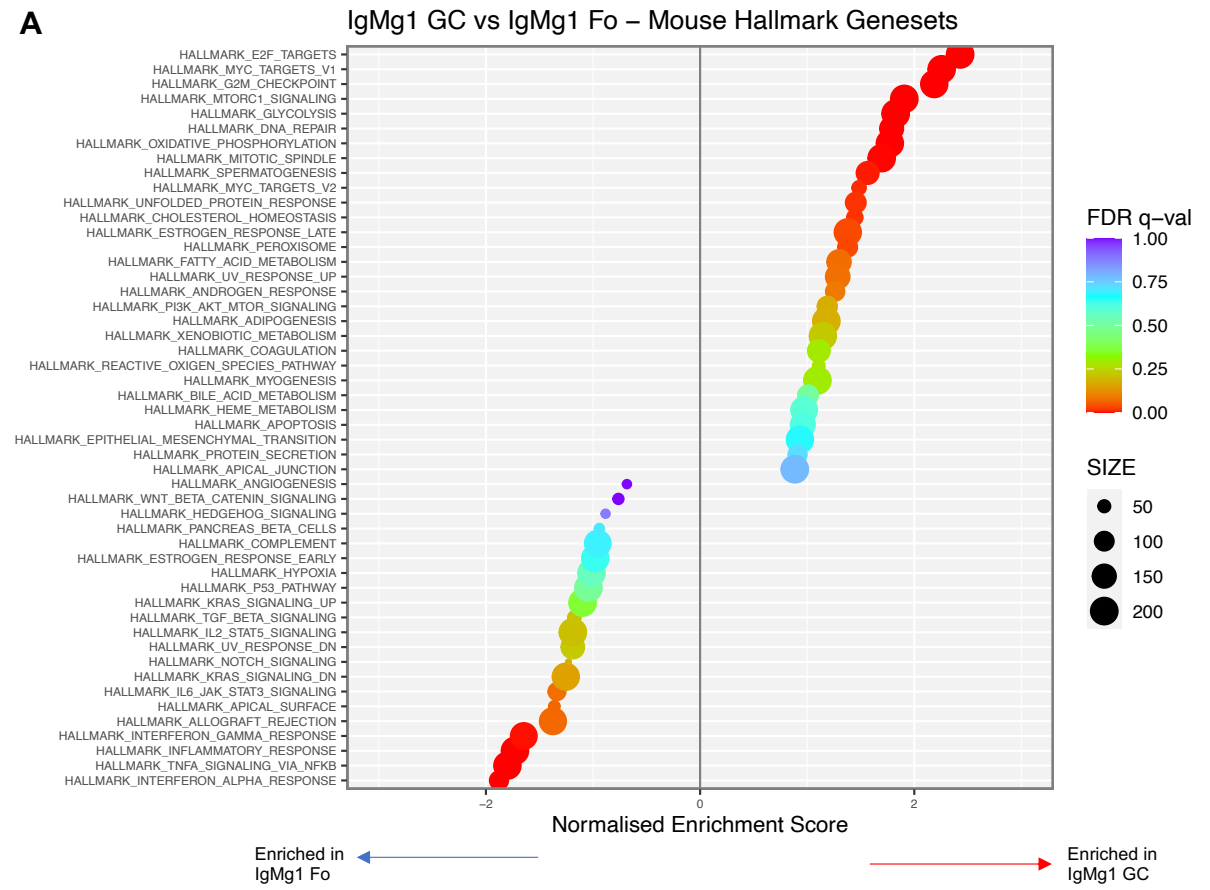
A
IgMg1 GC vs IgMg1 Fo – Mouse Hallmark Genesets
HALLMARK_E2F_TARGETS
HALLMARK_MYC_TARGETS_V1
HALLMARK_G2M_CHECKPOINT
HALLMARK_MTORC1_SIGNALING
HALLMARK_GLYCOLYSIS
HALLMARK_DNA_REPAIR
HALLMARK_OXIDATIVE_PHOSPHORYLATION
HALLMARK_MITOTIC_SPINDLE
HALLMARK_SPERMATOGENESIS
HALLMARK_MYC_TARGETS_V2
HALLMARK_UNFOLDED_PROTEIN_RESPONSE
HALLMARK_CHOLESTEROL_HOMEOSTASIS
HALLMARK_ESTROGEN_RESPONSE_LATE
HALLMARK_PEROXISOME
HALLMARK_FATTY_ACID_METABOLISM
HALLMARK_UV_RESPONSE_UP
HALLMARK_ANDROGEN_RESPONSE
HALLMARK_PI3K_AKT_MTOR_SIGNALING
HALLMARK_ADIPOGENESIS
HALLMARK_XENOBIOTIC_METABOLISM
HALLMARK_COAGULATION
HALLMARK_REACTIVE_OXIGEN_SPECIES_PATHWAY
HALLMARK_MYOGENESIS
HALLMARK_BILE_ACID_METABOLISM
HALLMARK_HEME_METABOLISM
HALLMARK_APOPTOSIS
HALLMARK_EPITHELIAL_MESENCHYMAL_TRANSITION
HALLMARK_PROTEIN_SECRETION
HALLMARK_APICAL_JUNCTION
HALLMARK_ANGIOGENESIS
HALLMARK_WNT_BETA_CATENIN_SIGNALING
HALLMARK_HEDGEHOG_SIGNALING
HALLMARK_PANCREAS_BETA_CELLS
HALLMARK_COMPLEMENT
HALLMARK_ESTROGEN_RESPONSE_EARLY
HALLMARK_HYPOXIA
HALLMARK_P53_PATHWAY
HALLMARK_KRAS_SIGNALING_UP
HALLMARK_TGF_BETA_SIGNALING
HALLMARK_IL2_STAT5_SIGNALING
HALLMARK_UV_RESPONSE_DN
HALLMARK_NOTCH_SIGNALING
HALLMARK_KRAS_SIGNALING_DN
HALLMARK_IL6_JAK_STAT3_SIGNALING
HALLMARK_APICAL_SURFACE
HALLMARK_ALLOGRAFT_REJECTION
HALLMARK_INTERFERON_GAMMA_RESPONSE
HALLMARK_INFLAMMATORY_RESPONSE
HALLMARK_TNFA_SIGNALING_VIA_NFKB
HALLMARK_INTERFERON_ALPHA_RESPONSE
−2
0
2
Normalised Enrichment Score
FDR q−val
1.00
0.75
0.50
0.25
0.00
SIZE
50
100
150
200
Enriched in IgMg1 Fo
Enriched in IgMg1 GC

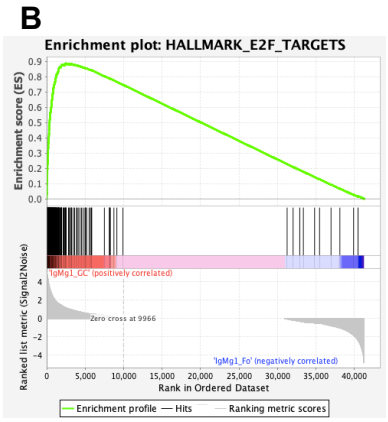
B
Enrichment plot: HALLMARK_E2F_TARGETS
Enrichment score (ES)
Ranked list metric (Signal2Noise)
'IgMg1_GC' (positively correlated)
Zero cross at 9966
'IgMg1_Fo' (negatively correlated)
Rank in Ordered Dataset
Enrichment profile
Hits
Ranking metric scores

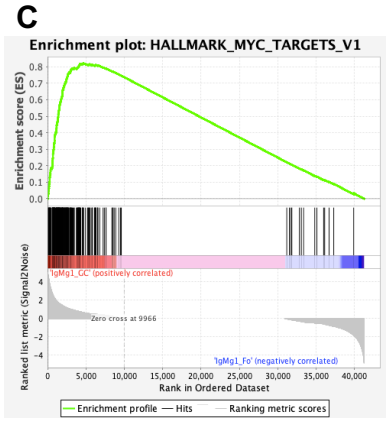
C
Enrichment plot: HALLMARK_MYC_TARGETS_V1
Enrichment score (ES)
Ranked list metric (Signal2Noise)
'IgMg1_GC' (positively correlated)
Zero cross at 9966
'IgMg1_Fo' (negatively correlated)
Rank in Ordered Dataset
Enrichment profile
Hits
Ranking metric scores

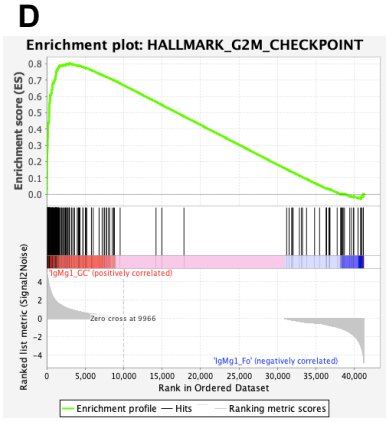
D
Enrichment plot: HALLMARK_G2M_CHECKPOINT
Enrichment score (ES)
Ranked list metric (Signal2Noise)
'IgMg1_GC' (positively correlated)
Zero cross at 9966
'IgMg1_Fo' (negatively correlated)
Rank in Ordered Dataset
Enrichment profile
Hits
Ranking metric scores

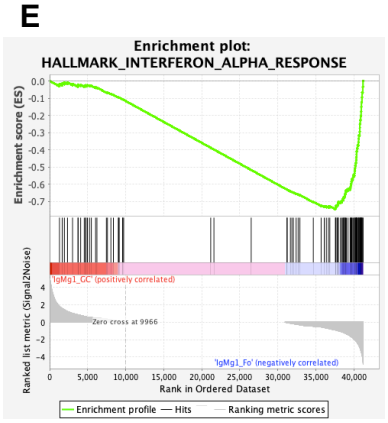
E
Enrichment plot:
HALLMARK_INTERFERON_ALPHA_RESPONSE
Enrichment score (ES)
Ranked list metric (Signal2Noise)
'IgMg1_GC' (positively correlated)
Zero cross at 9966
'IgMg1_Fo' (negatively correlated)
Rank in Ordered Dataset
Enrichment profile
Hits
Ranking metric scores

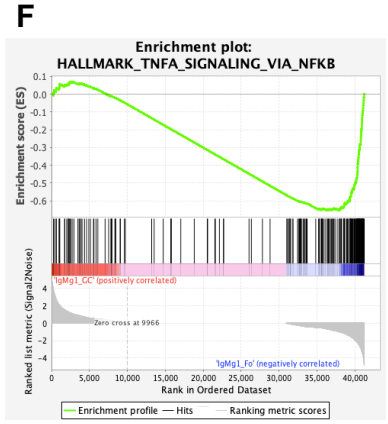
F
Enrichment plot:
HALLMARK_TNFA_SIGNALING_VIA_NFKB
Enrichment score (ES)
Ranked list metric (Signal2Noise)
'IgMg1_GC' (positively correlated)
Zero cross at 9966
'IgMg1_Fo' (negatively correlated)
Rank in Ordered Dataset
Enrichment profile
Hits
Ranking metric scores

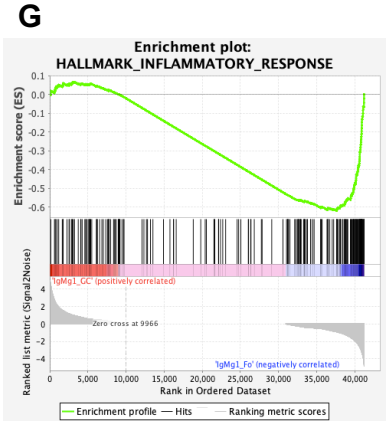
G
Enrichment plot:
HALLMARK_INFLAMMATORY_RESPONSE
Enrichment score (ES)
Ranked list metric (Signal2Noise)
'IgMg1_GC' (positively correlated)
Zero cross at 9966
'IgMg1_Fo' (negatively correlated)
Rank in Ordered Dataset
Enrichment profile
Hits
Ranking metric scores

Figure 4.20 GSEA of mouse hallmark gene sets in IgMg1 GC B cells compared with IgMg1 follicular B cells

(A) Gene set enrichment analysis (GSEA) was performed on IgMg1 follicular B cell and IgMg1 GC B cell expression data, comparing to mouse hallmark gene sets. Plot shows normalised enrichment scores for hallmark gene sets for GSEA performed between WT follicular and GC B cells. Size of circle represents number of genes in set. Colour represents FDR q-value. (B-G) GSEA enrichment plots for some of enriched gene sets: (B) E2F targets; (C) Myc targets v1; (D) G2M checkpoint; (E) Interferon α response; (F) TNFa signalling via NFκB; (G) Inflammatory response.

4.2.6 A small number of genes have differential expression in IgMg1 GC B cells compared with WT GC B cells

To better understand the differences in the GC B cell response in IgMg1 mice, differential gene expression analysis was performed comparing GC B cells from WT mice with GC B cells from IgMg1 mice. As expected from the PCA (Figure 4.15) there was a relatively small number of genes that were differentially expressed between IgMg1 GC B cells and WT GC B cells (Figure 4.21A). Using a log2-fold change threshold of over 1 or below -1, 34 genes were identified with significantly increased expression and 51 genes were identified with significantly reduced expression in IgMg1 GC B cells (Figure 4.21B). An additional 10 upregulated genes and 10 downregulated genes were identified with a lower fold-change (Figure 4.21C).

GSEA was performed using the gene expression data from GC B cells in IgMg1 and WT mice (Figure 4.22A). From the hallmark mouse gene sets, E2F targets (Figure 4.22B), G2M checkpoint (Figure 4.22C), Myc targets v1 (Figure 4.22D) and Myc targets v2 (Figure 4.22E) were all found to be significantly enriched in WT GC B cells at an FDR q-value of less than 0.05. These were also the amongst the leading gene sets enriched in GC B cells compared with follicular B cells (Figure 4.17 and Figure 4.20), indicating that they are upregulated during T cell-dependent B cell activation. They are associated with proliferation and cell-cycle progression (Liberzon et al., 2015; Cuitiño et al., 2019). Additionally, Myc and targets of Myc have been reported to be expressed in B cells that have been positively selected in the GC (Calado et al., 2012; Dominguez-Sola et al., 2012).

The up and downregulated genes were analysed using g:profiler to identify gene ontology (GO) terms that were statistically enriched within the differentially expressed

genes. Immunoglobulin variable (V)-genes were highly enriched in the list of genes with reduced expression in IgMg1 GC B cells compared with WT GC B cells, resulting in significant enrichment of several GO terms related to immunity such as immune response (GO:0006955) (adjusted p-value = 5.877×10^{-16}) (Figure 4.23A). Repeating the GO term enrichment analysis with only the differentially expressed non-immunoglobulin V-genes, showed that negative regulators of kinase signalling (GO:0006469) were enriched in IgMg1 GC B cells (adjusted p-value = 0.06923). These genes were *Cdk5rap1*, *Dusp16*, *Cdkn1b* and *Cep85* (Figure 4.23B).

Overall, these data show that relatively few genes were differentially expressed in IgMg1 GC B cells compared with WT GC B cells. However, gene sets associated with B cell activation, positive selection, and proliferation were significantly enriched in WT GC B cells, and negative regulators of kinase signalling were overrepresented in the genes with high expression in IgMg1 GC B cells.

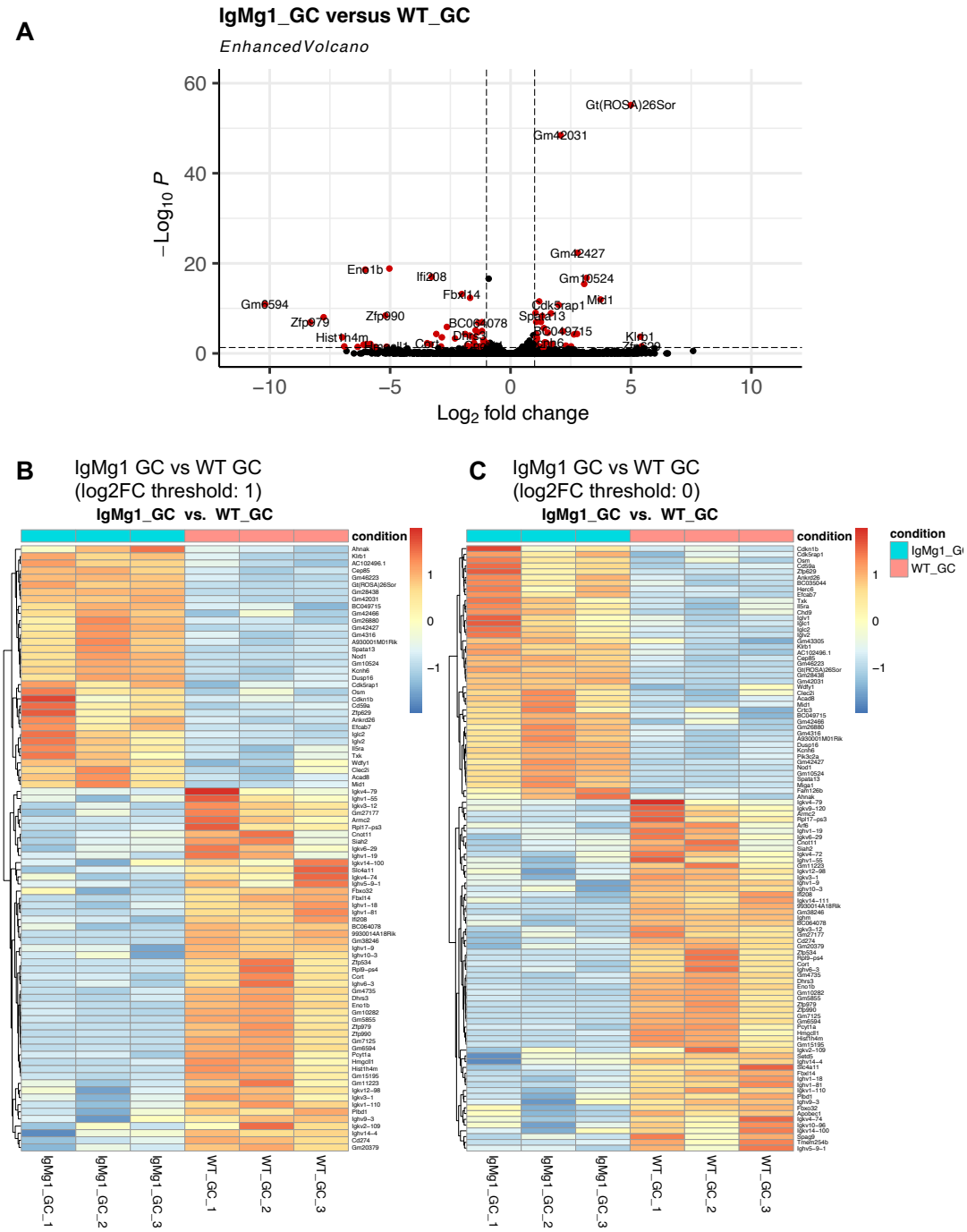

Figure 4.21 Differential gene expression in IgMg1 GC B cells compared with WT GC B cells

Genes were identified that were differentially expressed in IgMg1 GC B cells compared with WT GC B cells using DESeq2 package on R. (A) Volcano plot showing differentially expressed genes (2-fold change and adjusted p value < 0.05) indicated in red. Horizontal dashed line indicates adjusted p-value of 0.05 and vertical dashed lines represent log_2-fold change of 1 and -1. (B) Heatmap showing expression of differentially expressed genes in IgMg1 GC B cells compared with WT GC B B cells (at least a 2-fold change and adjusted p value < 0.05). (C) Heatmap showing expression of differentially expressed genes in IgMg1 GC B cells compared with WT GC B cells (adjusted p value < 0.05 but no fold change threshold). Colour scale represents gene Z-score.

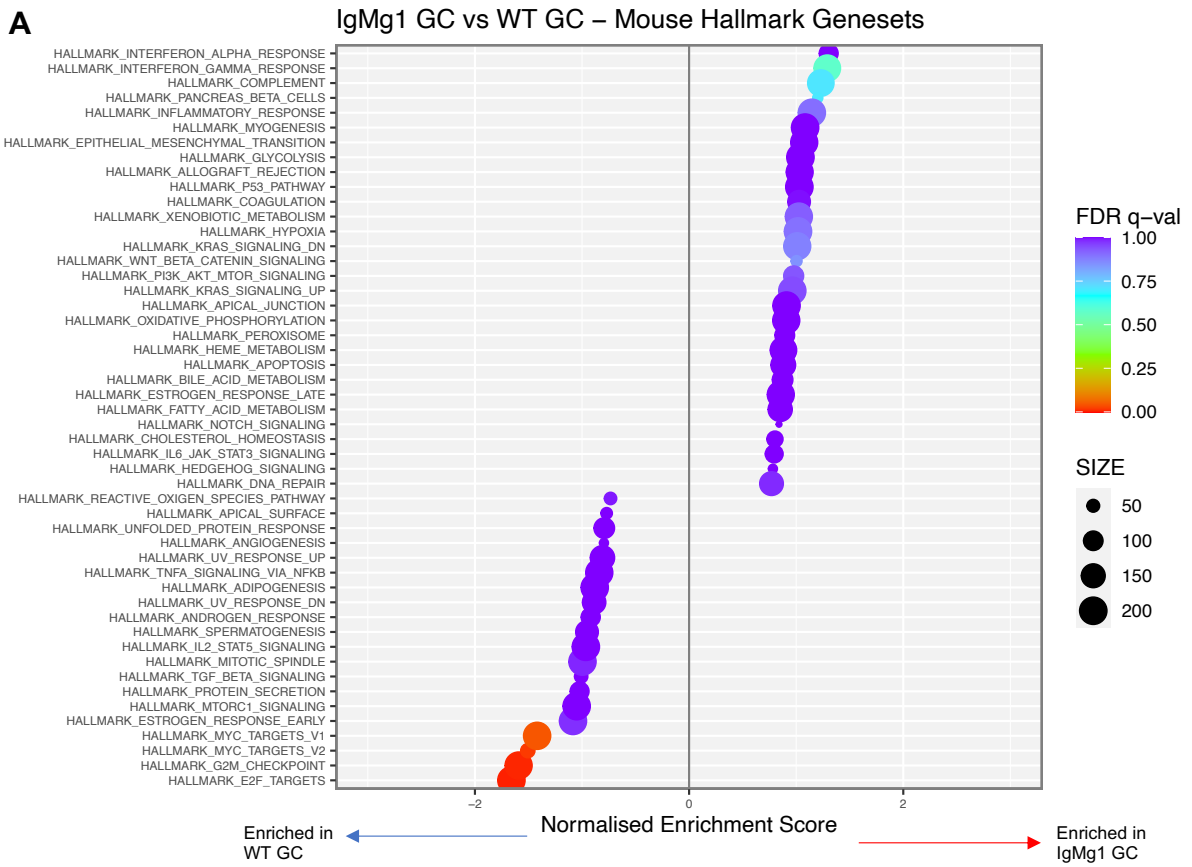
A
IgMg1 GC vs WT GC – Mouse Hallmark Genesets
HALLMARK_INTERFERON_ALPHA_RESPONSE
HALLMARK_INTERFERON_GAMMA_RESPONSE
HALLMARK_COMPLEMENT
HALLMARK_PANCREAS_BETA_CELLS
HALLMARK_INFLAMMATORY_RESPONSE
HALLMARK_MYOGENESIS
HALLMARK_EPITHELIAL_MESENCHYMAL_TRANSITION
HALLMARK_GLYCOLYSIS
HALLMARK_ALLOGRAFT_REJECTION
HALLMARK_P53_PATHWAY
HALLMARK_COAGULATION
HALLMARK_XENOBIOTIC_METABOLISM
HALLMARK_HYPOXIA
HALLMARK_KRAS_SIGNALING_DN
HALLMARK_WNT_BETA_CATENIN_SIGNALING
HALLMARK_PI3K_AKT_MTOR_SIGNALING
HALLMARK_KRAS_SIGNALING_UP
HALLMARK_APICAL_JUNCTION
HALLMARK_OXIDATIVE_PHOSPHORYLATION
HALLMARK_PEROXISOME
HALLMARK_HEME_METABOLISM
HALLMARK_APOPTOSIS
HALLMARK_BILE_ACID_METABOLISM
HALLMARK_ESTROGEN_RESPONSE_LATE
HALLMARK_FATTY_ACID_METABOLISM
HALLMARK_NOTCH_SIGNALING
HALLMARK_CHOLESTEROL_HOMEOSTASIS
HALLMARK_IL6_JAK_STAT3_SIGNALING
HALLMARK_HEDGEHOG_SIGNALING
HALLMARK_DNA_REPAIR
HALLMARK_REACTIVE_OXIGEN_SPECIES_PATHWAY
HALLMARK_APICAL_SURFACE
HALLMARK_UNFOLDED_PROTEIN_RESPONSE
HALLMARK_ANGIOGENESIS
HALLMARK_UV_RESPONSE_UP
HALLMARK_TNFA_SIGNALING_VIA_NFKB
HALLMARK_ADIPOGENESIS
HALLMARK_UV_RESPONSE_DN
HALLMARK_ANDROGEN_RESPONSE
HALLMARK_SPERMATOGENESIS
HALLMARK_IL2_STAT5_SIGNALING
HALLMARK_MITOTIC_SPINDLE
HALLMARK_TGF_BETA_SIGNALING
HALLMARK_PROTEIN_SECRETION
HALLMARK_MTORC1_SIGNALING
HALLMARK_ESTROGEN_RESPONSE_EARLY
HALLMARK_MYC_TARGETS_V1
HALLMARK_MYC_TARGETS_V2
HALLMARK_G2M_CHECKPOINT
HALLMARK_E2F_TARGETS
−2
0
2
Normalised Enrichment Score
Enriched in WT GC
Enriched in IgMg1 GC
FDR q−val
1.00
0.75
0.50
0.25
0.00
SIZE
50
100
150
200

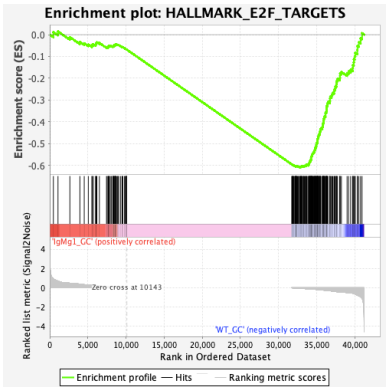
B
Enrichment plot: HALLMARK_E2F_TARGETS
Enrichment score (ES)
Ranked list metric (Signal2Noise)
'IgMg1_GC' (positively correlated)
Zero cross at 10143
'WT_GC' (negatively correlated)
Rank in Ordered Dataset
Enrichment profile
Hits
Ranking metric scores

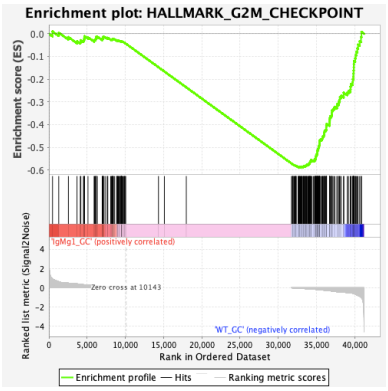
C
Enrichment plot: HALLMARK_G2M_CHECKPOINT
Enrichment score (ES)
Ranked list metric (Signal2Noise)
'IgMg1_GC' (positively correlated)
Zero cross at 10143
'WT_GC' (negatively correlated)
Rank in Ordered Dataset
Enrichment profile
Hits
Ranking metric scores

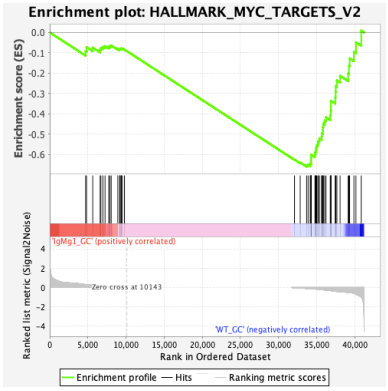
D
Enrichment plot: HALLMARK_MYC_TARGETS_V2
Enrichment score (ES)
Ranked list metric (Signal2Noise)
'IgMg1_GC' (positively correlated)
Zero cross at 10143
'WT_GC' (negatively correlated)
Rank in Ordered Dataset
Enrichment profile
Hits
Ranking metric scores

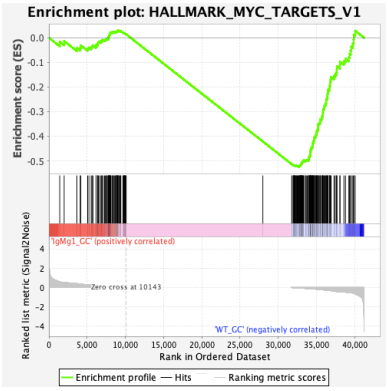
E
Enrichment plot: HALLMARK_MYC_TARGETS_V1
Enrichment score (ES)
Ranked list metric (Signal2Noise)
'IgMg1_GC' (positively correlated)
Zero cross at 10143
'WT_GC' (negatively correlated)
Rank in Ordered Dataset
Enrichment profile
Hits
Ranking metric scores

Figure 4.22 GSEA of mouse hallmark gene sets in IgMg1 GC B cells compared with WT GC B cells

(A) Gene set enrichment analysis (GSEA) was performed on IgMg1 GC B cell and WT GC B cell expression data, comparing to mouse hallmark gene sets. Plot shows normalised enrichment scores for hallmark gene sets for GSEA performed between IgMg1 GC B cells and WT GC B cells. Size of circle represents number of genes in set. Colour represents FDR q-value. (B-E) GSEA enrichment plots for some of enriched gene sets: (B) E2F targets; (C) G2M checkpoint; (D) Myc targets v2; (E) Myc targets v2.

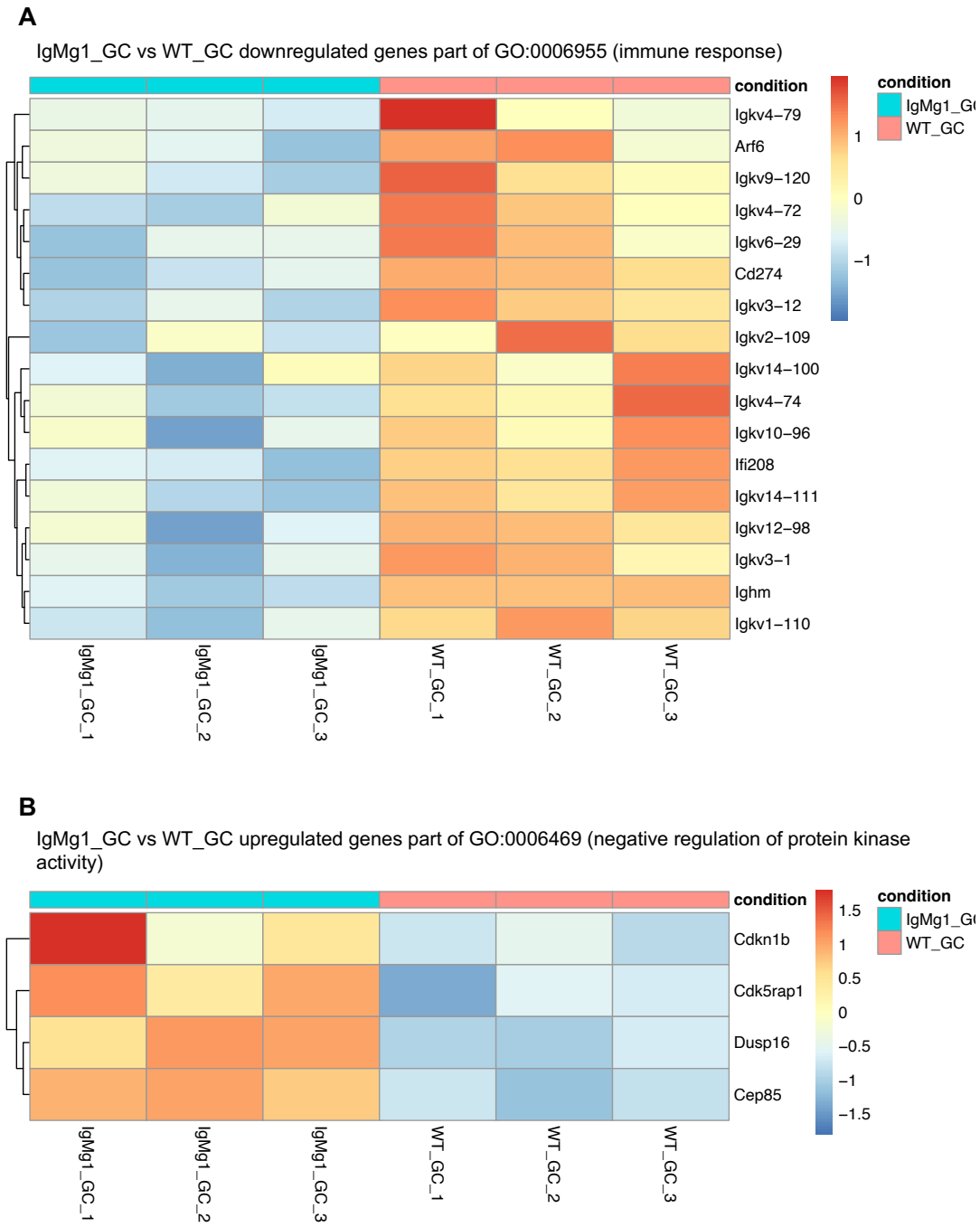

Figure 4.23 Heatmaps showing expression of genes part of enriched gene ontology terms

Genes identified as up or down-regulated in IgMg1 GC B cells compared with WT GC B Cells were analysed for enrichment of gene ontology (GO) terms using g:profiler. (A) Heatmap showing expression of IgMg1 GC upregulated genes that are part of GO:000955 (immune response). Colour scale represents gene Z-score. (B) Heatmap showing expression of IgMg1 upregulated genes that are part of GO:0006469 (negative regulation of protein kinase activity). Colour scale represents gene Z-score.

4.2.7 IGHV gene expression in GC B cells is altered in IgMg1 mice

As shown in chapter 3, during B cell development, apart from changes in kappa and lambda expression due to receptor editing, there were no major changes in immunoglobulin variable genes between IgMg1 follicular B cells compared with WT follicular B cells. However, the fact that immunoglobulin genes were highly enriched in the list of genes with lower expression in IgMg1 GC B cells compared with WT GC B cells (Figure 4.23A) suggested that B cells bearing certain immunoglobulin variable genes may be less able to participate in GCs in IgMg1 mice. To further investigate this, the gene expression data was filtered to only include the immunoglobulin heavy variable (IGHV) genes. Several IGHV genes that were differentially expressed between GC B cells and follicular B cells in WT and IgMg1 mice were identified. In both IgMg1 and WT mice a similar number of IGHV genes are up and downregulated by GC B cells (Figure 4.24A-C). The canonical NP-specific IGHV gene *Ighv1-72* (also known as V186.2) was highly upregulated in both genotypes, as was *Ighv14-3* which has been previously reported as the canonical anti-NP IGHV gene in Balb/c mice (Loh et al., 1983; Dale et al., 2019). This suggests that in both WT and IgMg1 mice, similar B cell clones dominate the anti-NP response.

The IGHV genes in IgMg1 GC B cells were also compared with WT GC B cells. As expected from the overall gene expression analysis (Figure 4.23), a number of IGHV genes were identified with reduced expression by IgMg1 GC B cells, but none were increased (Figure 4.24D). A heatmap showing relative expression of these genes, showed that in WT mice these genes tended to have moderate to high expression in both WT and IgMg1 follicular B cells. In WT GC B cells they continue to be expressed at moderate levels, whereas in IgMg1 GC B cells they had low expression (Figure

4.24E). This suggested that follicular B cells bearing these BCRs were unable to take part in the GC in IgMg1 mice.

Therefore, although the predominant B cells taking part in the GC in IgMg1 mice seem to use similar IGHV genes to the ones that dominate in WT mice, there are some other IGHV genes which are used less in GC B cells in IgMg1 mice than in WT mice.

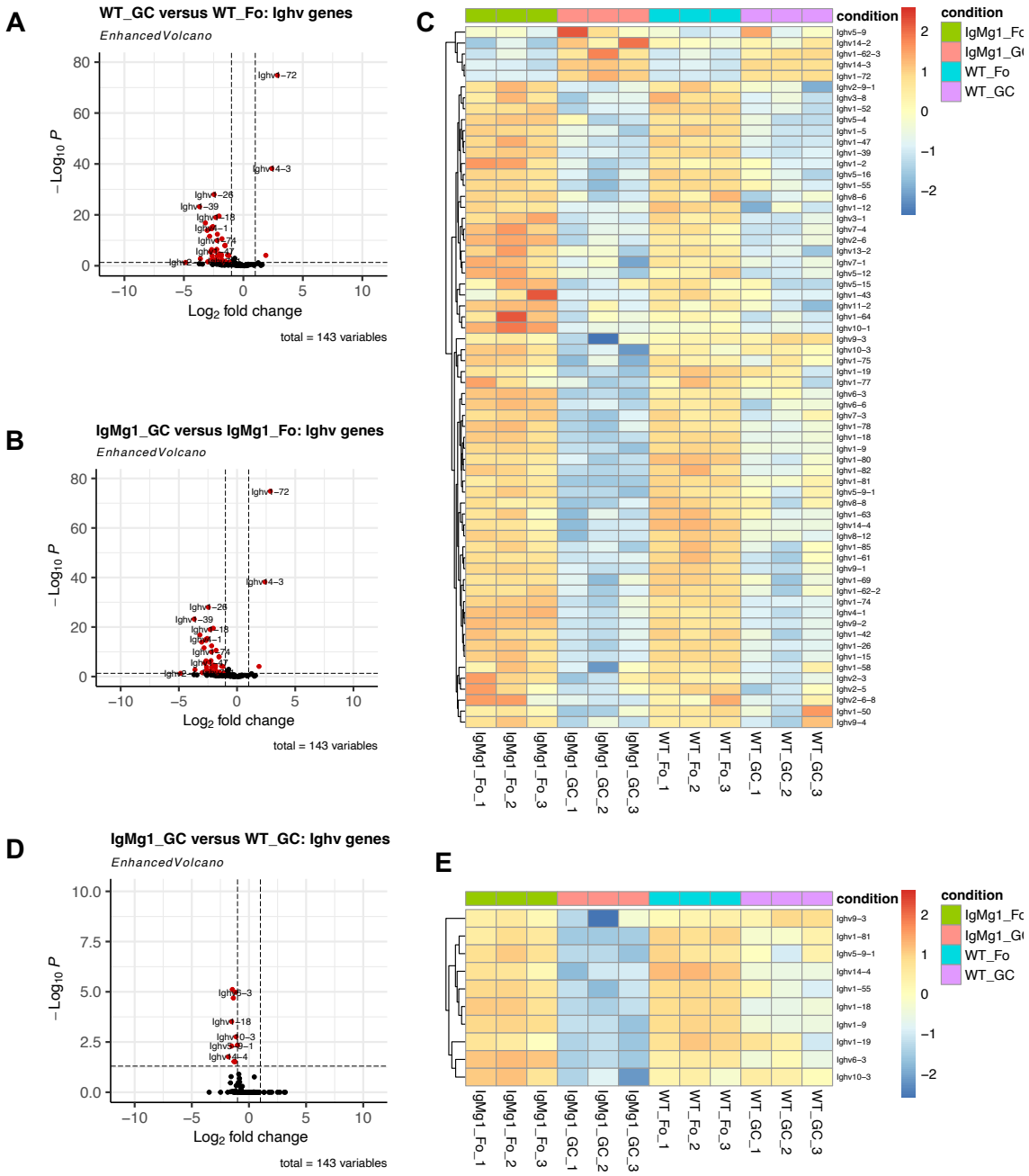

Figure 4.24 Differentially expressed IGHV genes in WT and IgMg1 GC B cells

Differential gene expression analysis was filtered to only show IGHV genes to allow analysis of IGHV gene usage. (A) Volcano plot showing IGHV genes compared in WT GC B cells and WT follicular B cells, with differentially expressed genes (at least a 2-fold change and adjusted p value < 0.05) marked in red. (B) Volcano plot showing IGHV genes compared in IgMg1 GC B cells and IgMg1 follicular B cells, with differentially expressed genes (at least a 2-fold change and adjusted p value < 0.05) marked in red. (C) Heatmap showing expression of IGHV genes identified as differentially expressed in IgMg1 GC B cells compared with follicular B cells across all samples. Colour scale represents gene Z-score. (D) Volcano plot showing IGHV genes compared in IgMg1 GC B cells and WT GC B cells, with differentially expressed genes (at least a 2-fold change and adjusted p value < 0.05) marked in red. (E) Heatmap showing expression of IGHV genes identified as differentially expressed in IgMg1 GC B cells compared with WT GC B cells across all samples. Colour scale represents gene Z-score.

4.2.8 Identification of differences in GC gene expression programme

The GC gene expression programme looked very similar in IgMg1 mice as in WT mice, but there were still 20-30% of the IgMg1 GC B cell differentially expressed genes which were not identified as differentially expressed in WT GC B cells (Figure 4.19B and C). To further investigate differences in the gene expression programme, the differences in gene expression on transition from follicular B cells to GC B cell were compared between IgMg1 mice and WT. Genes that were differentially expressed in GC B cells in only one of the genotypes were identified. These were defined as having a log2-fold change over 1 and adjusted p-value below 0.05 in one of the genotypes and a log2-fold change of below 0.5 in the other genotype. In this way, 81 genes were identified that were upregulated in IgMg1 GC B cells and 110 genes that were downregulated in IgMg1 GC B cells compared with IgMg1 follicular B cells, but which were not differentially expressed in WT GC B cells compared with WT follicular B cells. Additionally, there were 83 genes that were upregulated and 147 genes that were downregulated in WT GC B cells, but that weren't differentially expressed in IgMg1 GC B cells.

These individual lists of genes were analysed for enriched GO terms (with immunoglobulin genes removed). The genes upregulated in GC B cells in IgMg1 mice but not differentially expressed in GC B cells in WT mice mostly functioned in biological regulation (GO:0065007) (adjusted p-value = 0.0186). This group of genes were mainly expressed at low levels in IgMg1 follicular B cells, and became upregulated in IgMg1 GC B cells. In WT follicular B cells they had higher expression than IgMg1 follicular B cells but they were not upregulated in WT GC B cells (Figure 4.26A). Genes that were downregulated in WT GC B cells compared to WT follicular B cells but not

differentially expressed in IgMg1 GC B cells compared to IgMg1 follicular B cells were found to be enriched for positive regulators of signal transduction (GO:0009967) (adjusted p-value = 0.000412) (Figure 4.26B).

Overall, although most of the gene expression changes on transit from follicular B cell to GC B cell were the same in WT and IgMg1 mice. This suggests that some additional gene expression changes take place when anergic B cells take part in a GC reaction.

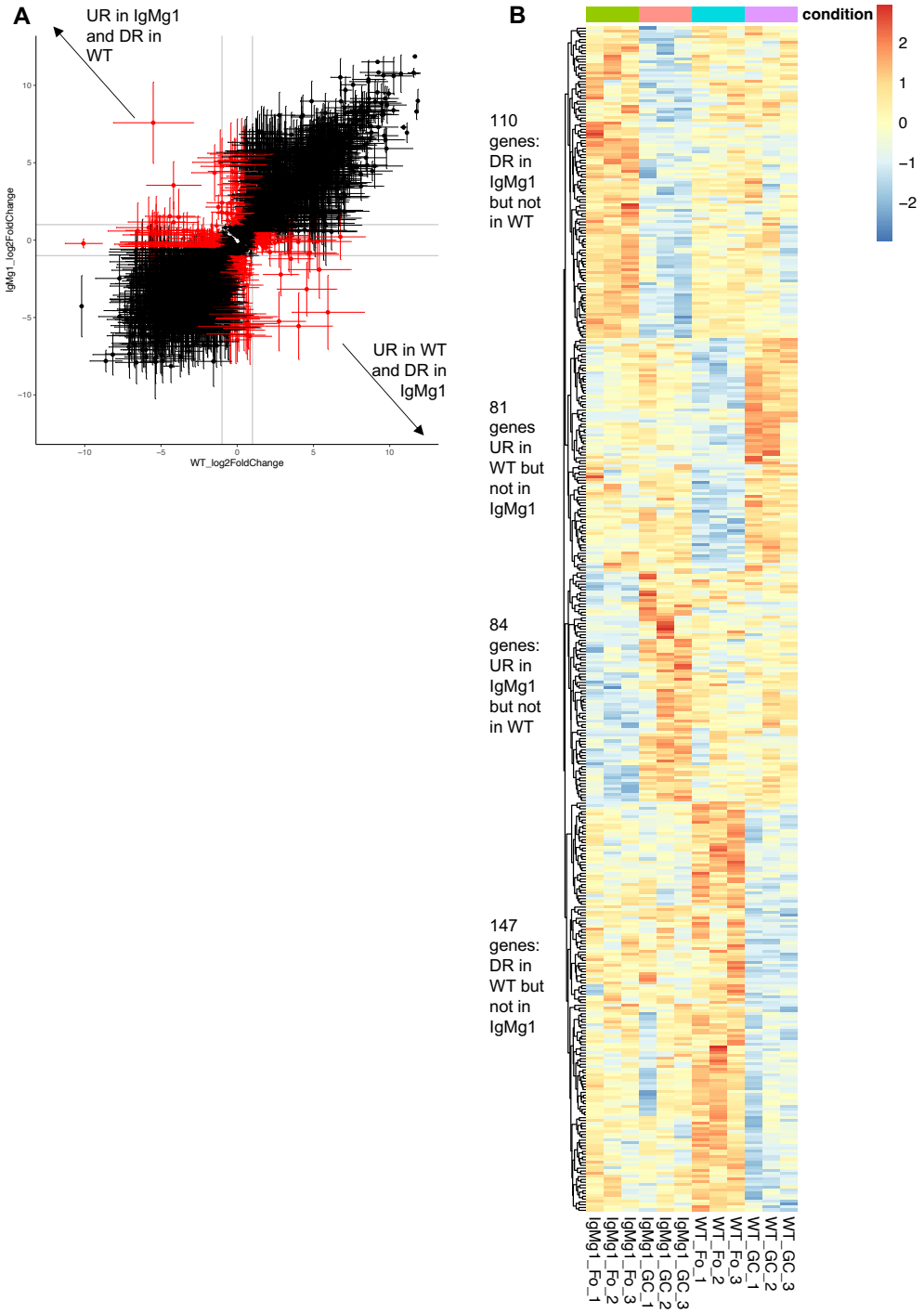

Figure 4.25 Identification of genes differentially regulated between GC B cells and follicular B cells in only one of genotypes

Differential gene expression data between GC B cells and follicular B cells were compared for WT and IgMg1 mice. (A) Plot comparing log2-fold changes in WT with log2-fold changes in IgMg1 mice (log2-fold change in GC B cells compared with follicular B cells). Error bars represent log2-fold change standard error. Points marked in red represent genes differentially expressed in only one of the genotypes. (B) Heatmap showing relative expression of genes identified in this analysis across all samples. Gene expression scaled by gene.

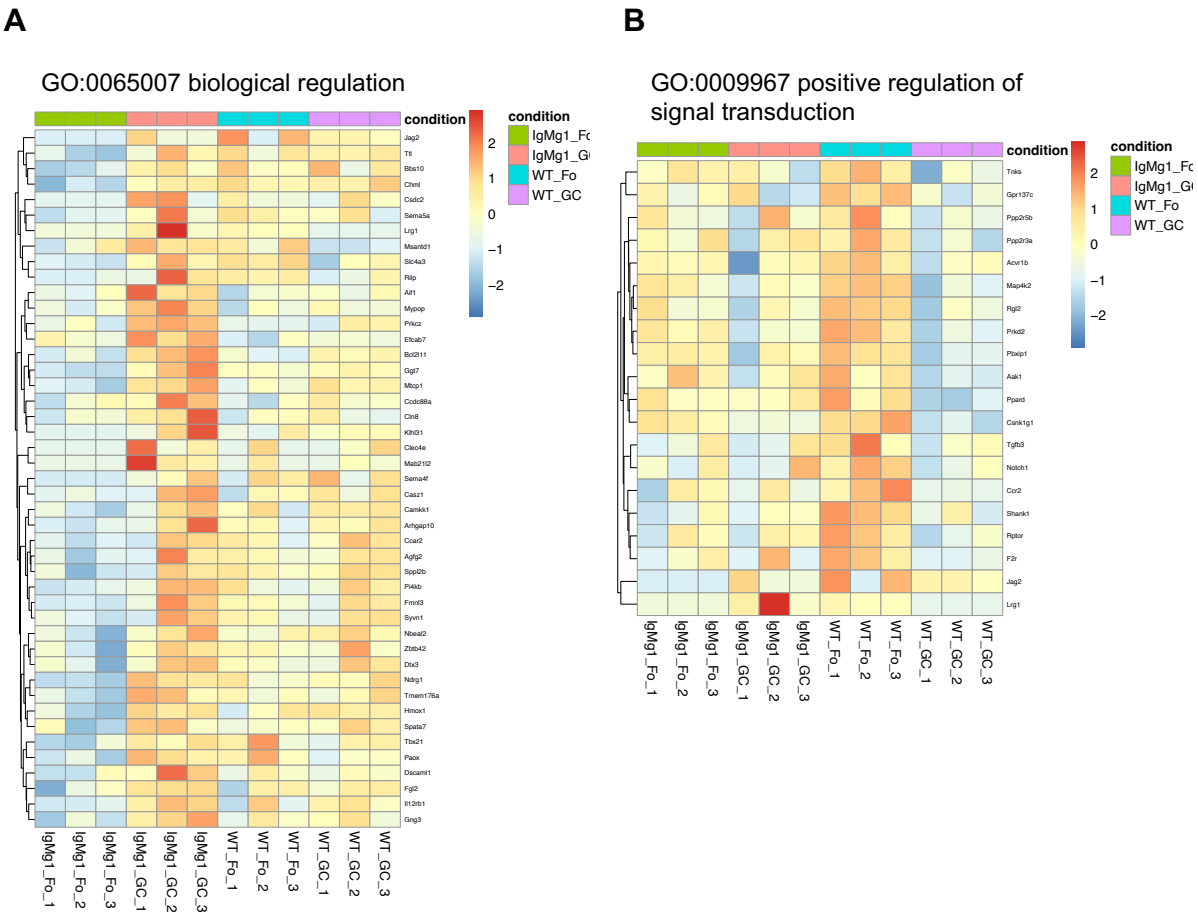

Figure 4.26 Heatmaps showing expression of genes part of enriched gene ontology terms

Genes identified as differentially regulated in only one of the genotypes in Figure 4.25 were analysed for enrichment of GO terms using g:profiler. (A) Heatmap showing expression of genes in GO:0065007 (biological regulation) that are upregulated in IgMg1 GC B cells compared with IgMg1 follicular B cells but not in WT GC B cells compared with WT follicular B cells. (B) Heatmap showing expression of genes in GO:0009967 (positive regulation of signal transduction) that are downregulated in WT GC B cells compared with WT follicular B cells but not in IgMg1 GC B cells compared with IgMg1 follicular B cells. Colour scales represent gene Z-score.

4.2.9 Identification of maintained IgMg1 differentially expressed genes

The gene expression data were next analysed to identify genes that continued to be differentially expressed in B cells from IgMg1 mice compared with WT mice, when transiting from follicular to GC B cell compartment. These genes may represent regulators of B cell anergy maintaining anergy within the GC.

This was approached in two separate ways. The first was to identify the overlapping genes from the individual comparisons of IgMg1 GC B cells vs WT GC B cells and IgMg1 follicular B cells vs WT follicular B cells. From this approach, 22 genes were identified that were upregulated and 14 genes that were downregulated in IgMg1 B cells in both follicular and GC B cells (Figure 4.27A-C). The second approach was to perform a separate gene expression analysis comparing all IgMg1 samples with all the WT samples regardless of which type of B cells they were. This approach identified 19 genes upregulated and 20 genes that were downregulated in IgMg1 B cells compared with WT B cells (Figure 4.27D and E). The two approaches in total identified 30 genes upregulated in IgMg1 B cells and 23 genes downregulated in WT B cells (Figure 4.28A-D). However, GO term enrichment for biological processes and KEGG pathways identified no enriched terms within the genes. GSEA of mouse hallmark gene sets for comparison of all IgMg1 samples with all WT samples did not identify any gene sets significantly enriched with FDR q-values below 0.05 (Figure 4.29A), although oxidative phosphorylation was enriched in IgMg1 B cells (Figure 4.29B) and G2M checkpoint (Figure 4.29C) and Myc targets (Figure 4.29D) were enriched in WT B cells with nominal p-values below 0.05.

Altogether, these data indicated that a small number of genes were maintained as differentially expressed in IgMg1 B cells even in the GC response. However, the

biological function of the maintained gene signature is unknown. Further analysis of the identified genes identified may be useful.

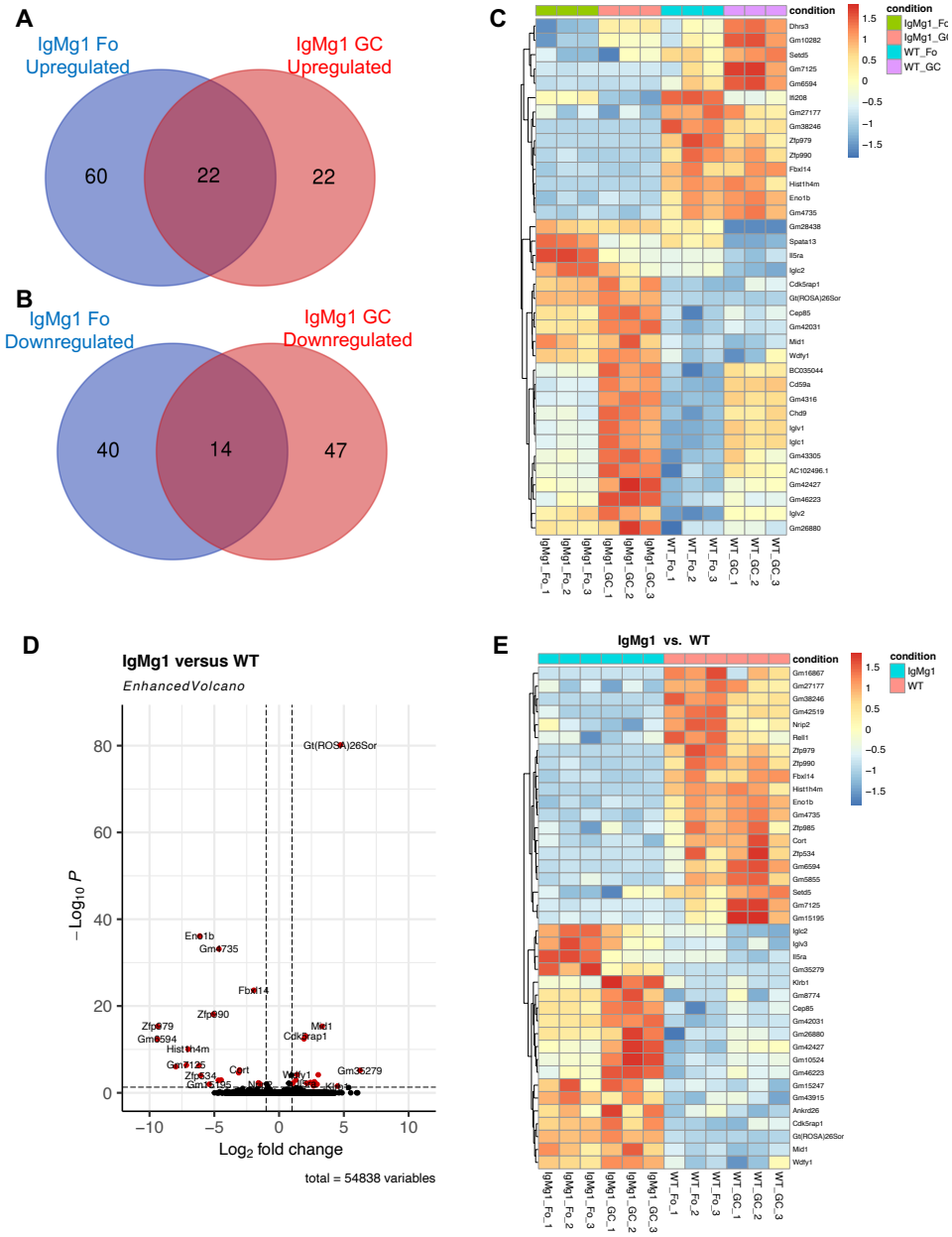

Figure 4.27 Identification of maintained IgMg1 gene expression signature

Analysis of gene expression to identify genes differentially expressed in IgMg1 B cells compared with WT B cells in both follicular B cells and GC B cells. Two approaches were used. (A-C) Approach 1. Overlap between IgMg1 GC vs WT GC and IgMg1 follicular vs WT follicular comparisons. (A) Venn diagram showing overlap of genes upregulated in IgMg1 GC B cells vs WT GC B cells and genes upregulated in IgMg1 follicular B cells vs WT follicular B cells. (B) Venn diagram showing overlap of genes downregulated in IgMg1 GC B cells vs WT GC B cells and genes downregulated in IgMg1 follicular B cells vs WT follicular B cells. (C) Heatmap showing expression of overlapping genes from (A) and (B). Colour scale represents gene Z-score. (D-E) Approach 2: analysis of differentially expressed genes in all 6 IgMg1 samples compared with all 6 WT samples using DESeq2 package on R. (D) Volcano plot showing differentially expressed genes in IgMg1 B cells compared with WT B cells (log2FC>1 or <(-1) and adjusted p value < 0.05) marked in red. (E) Heatmap showing relative expression of genes identified as differentially expressed in IgMg1 B cells compared with WT B cells (adjusted p value < 0.05). Colour scale represents gene Z-score.

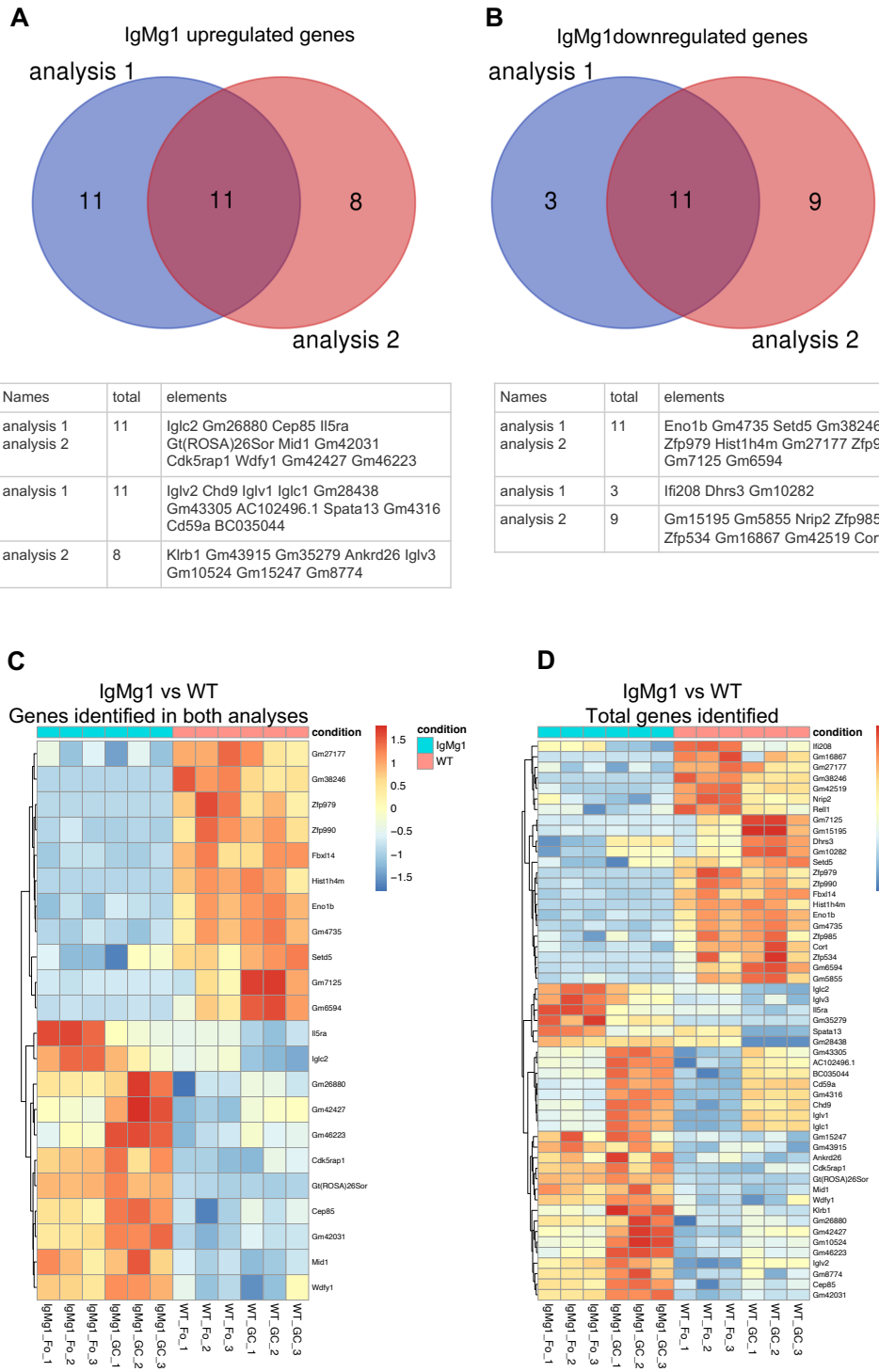

Names	total	elements
analysis 1 analysis 2	11	Iglc2 Gm26880 Cep85 Il5ra Gt(ROSA)26Sor Mid1 Gm42031 Cdk5rap1 Wdfy1 Gm42427 Gm46223
analysis 1	11	Iglv2 Chd9 Iglv1 Iglc1 Gm28438 Gm43305 AC102496.1 Spata13 Gm4316 Cd59a BC035044
analysis 2	8	Klrb1 Gm43915 Gm35279 Ankrd26 Iglv3 Gm10524 Gm15247 Gm8774

Names	total	elements
analysis 1 analysis 2	11	Eno1b Gm4735 Setd5 Gm38246 Fbxl14 Zfp979 Hist1h4m Gm27177 Zfp990 Gm7125 Gm6594
analysis 1	3	Ifi208 Dhrs3 Gm10282
analysis 2	9	Gm15195 Gm5855 Nrip2 Zfp985 Rell1 Zfp534 Gm16867 Gm42519 Cort

Figure 4.28 Combination of two approaches for identification of maintained IgMg1 genes

The two approaches for identification of maintained genes as shown in Figure 4.27 were compared. (A) Venn diagram showing IgMg1 upregulated genes identified by two approaches and table showing genes. (B) Venn diagram showing IgMg1 downregulated genes identified by two approaches and table showing genes. (C) Heatmap showing relative expression of overlapping genes across all samples. Gene expression scaled by gene. (D) Heatmap showing relative expression of all genes identified in two approaches across all samples. Gene expression scaled by gene.

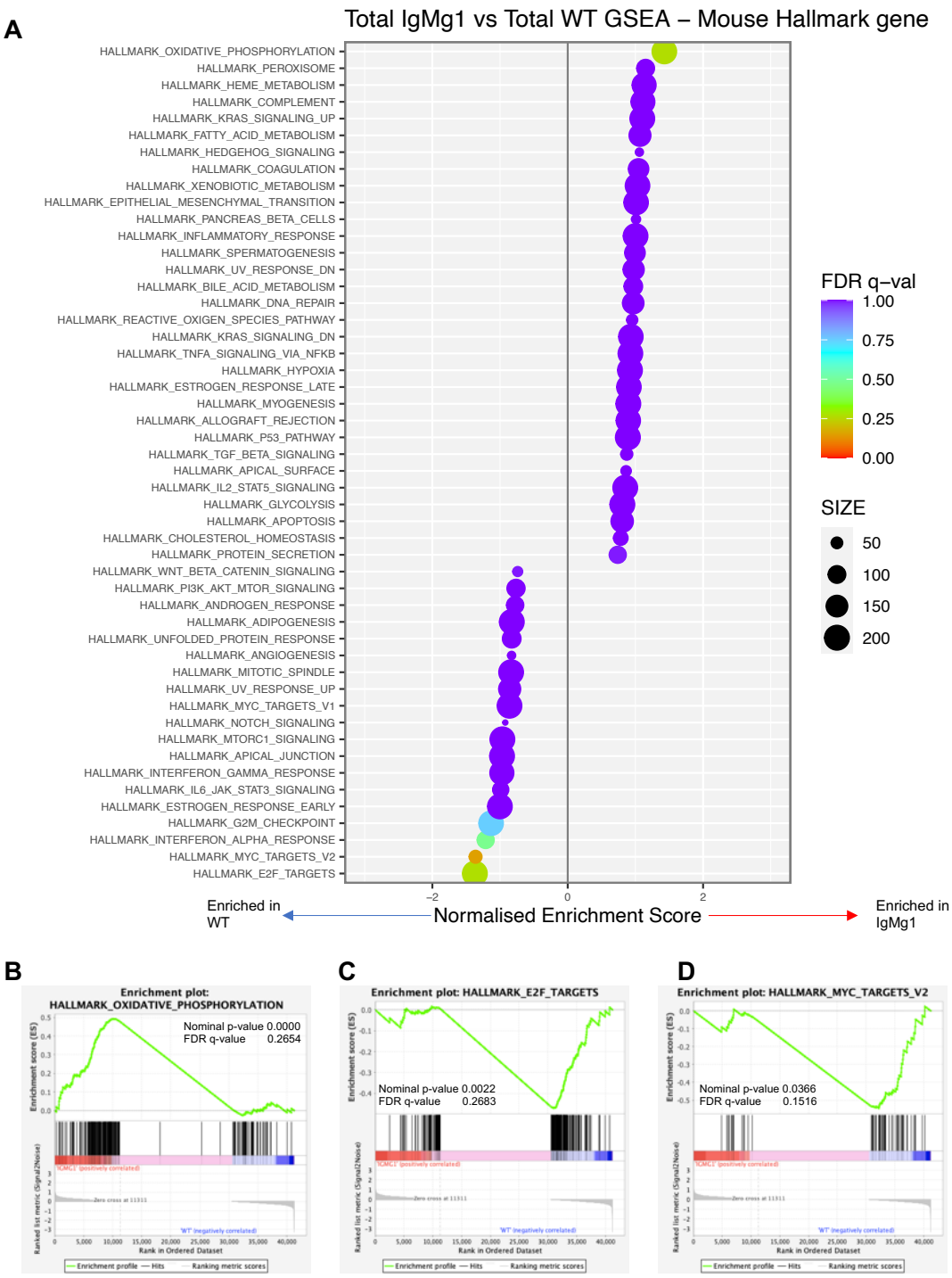

Figure 4.29 GSEA of mouse hallmark gene sets in total IgMg1 B cells compared with total WT B cells

(A) Gene set enrichment analysis (GSEA) was performed on total IgMg1 B cell vs total WT B cell expression data, comparing to mouse hallmark gene sets. Plot shows normalised enrichment scores for hallmark gene sets for GSEA performed between IgMg1 B cells and WT B cells. Size of circle represents number of genes in set. Colour represents FDR q-value. (B-D) GSEA enrichment plots for gene sets enriched at nominal p-value < 0.05: (B) oxidative phosphorylation; (C) E2F targets; (D) Myc targets v2.

4.2.10 Tfh cells are increased in IgMg1 mice during GC response

Besides B cells, other immune cells in the GC are critical for GC function. For example, Tfh cells provide signals for B cells to enter the DZ for expansion (Victora et al., 2010) and for plasma cell generation (Zhang, 2018). BCR signalling may be important in B cell ability to interact with Tfh cells. Therefore, 8 days after immunisation with NP-KLH, Tfh cells were analysed by flow cytometry. Tfh cells can be identified as $CXCR5^{hi}$ $PD\text{-}1^{hi}$ cells from within the activated ($CD44^{+}$ $CD62L^{-}$) CD4 T cells (Figure 4.30A).

Although there was no significant change in $CD4^{+}$ T cell numbers, IgMg1 mice showed a significant increase in Tfh cells (Figure 4.30C and D). In contrast, IgG1M mice showed a significant decrease in Tfh cells as a percentage of lymphocytes (Figure 4.30D). The ratio of Tfh cells to GC B cells was also calculated to give an indication of how much Tfh cell help should be available per GC B cell. The Tfh/GC B cell ratio was significantly higher in IgMg1 lymph nodes with an approximately 2-fold increase compared with WT lymph nodes. The Tfh/GC B cell ratio in IgG1M mice trended to a reduction but was not statistically significance (Figure 4.30E).

Chronic GCs occur in Peyer's patches in the guts, in response to gut microbiota. To assess whether Tfh cells were increased in chronic IgMg1 GCs, Peyer's patches from mice were analysed by flow cytometry (Figure 4.31A). $CD4^{+}$ T cells were found to be significantly increased in IgMg1 Peyer's patches (Figure 4.31C), and the frequency of Tfh cells within Peyer's patch lymphocytes were significantly increased (Figure 4.31E). This shows that the increase in Tfh cells in IgMg1 mice can also be seen in ongoing GC responses to complex bacterial antigens and is not specific to early TD vaccine induced GCs.

In summary, the data shown here suggest that altered BCR signalling in IgMg1 B cells increases the number of Tfh cells within the GC. Whether this is due to changes in Tfh activation will be investigated in the following.

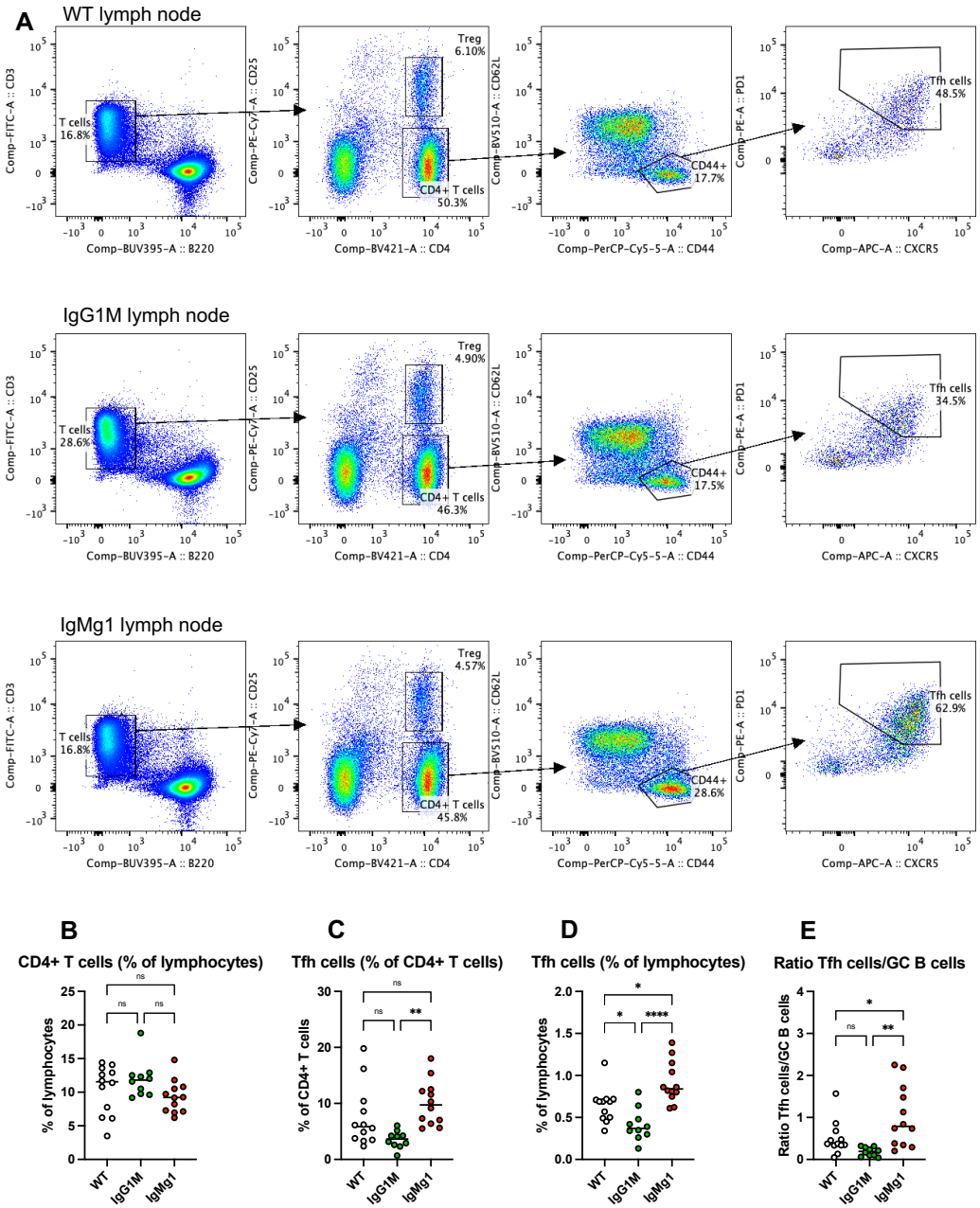

Figure 4.30 Tfh cells in draining lymph node 8 days after NP-KLH immunisation

WT, IgG1M and IgMg1 mice were immunised with NP-KLH as shown in Figure 4.5 and at day 8 lymph nodes were analysed by flow cytometry. (A) Gating strategy for Tfh cells shown for representative WT, IgG1M and IgMg1 mice. From live lymphocytes, T cells were gated as $CD3^+$ $B220^-$. From T cells, conventional $CD4^+$ T cells were gated as $CD4^+$ $CD25^-$. From conventional $CD4^+$ T cells, activated cells were identified as $CD44^+$ $CD62L^-$. From activated cells, Tfh cells were identified as $PD\text{-}1^{hi}$ $CXCR5^{hi}$. (B-E) Summary statistics showing: (B) frequency of $CD4^+$ T cells as percentage of lymphocytes; (C) frequency of Tfh cells as percentage of $CD4^+$ T cells; (D) frequency of Tfh cells as percentage of lymphocytes; (E) Ratio of Tfh cells to GC B cells (GC B cells gated as described in Figure 4.5). Data combined from two experiments. Each symbol represents one mouse. Statistical tests were performed by ordinary one-way ANOVA with Tukey's multiple comparison test (****, $p < 0.0001$; **, $p < 0.01$; *, $p < 0.05$; ns, not significant).

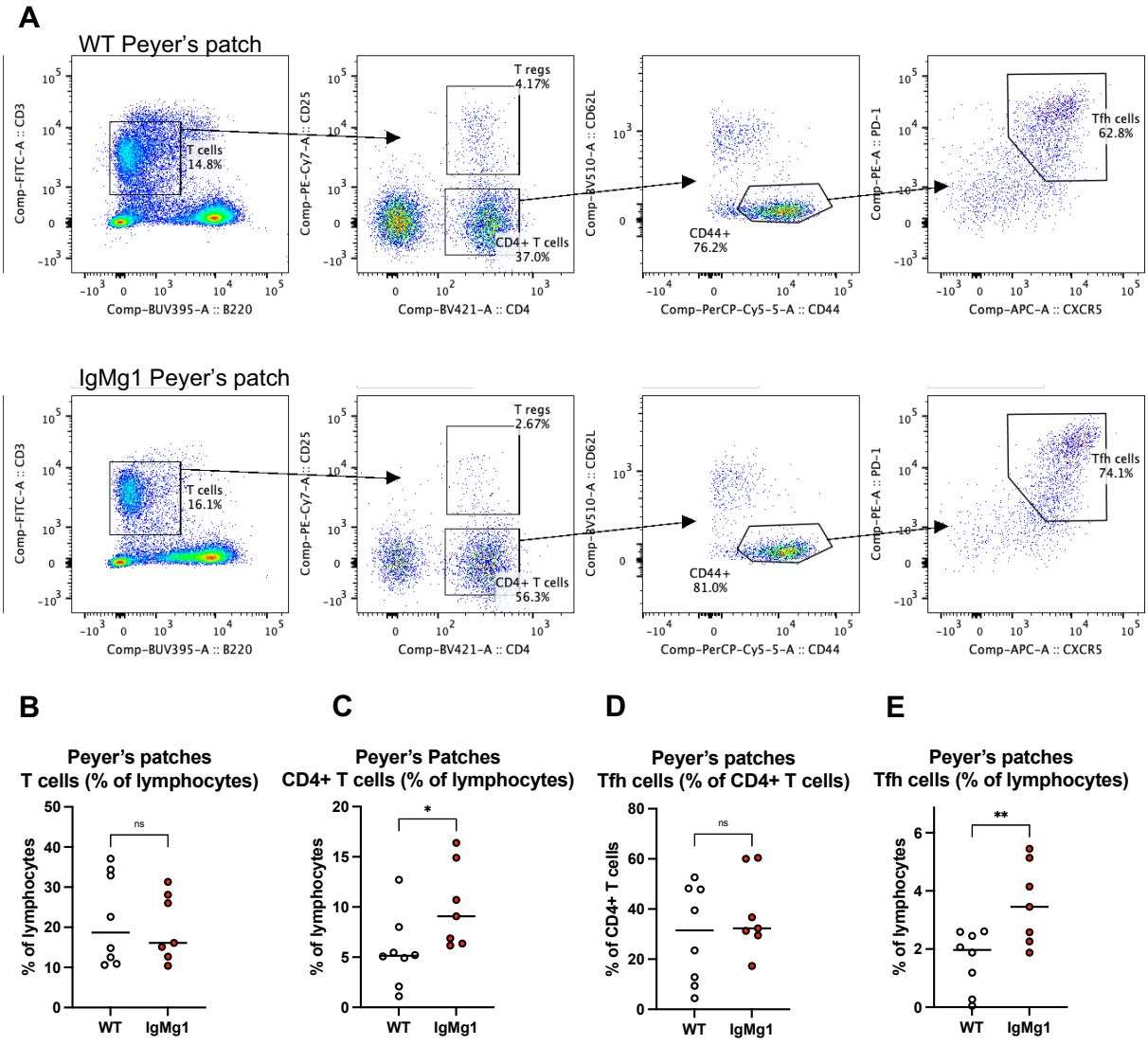

Figure 4.31 Tfh cells in Peyer's patches

Peyer's patches from WT and IgMg1 mice were analysed by flow cytometry. (A) Gating strategy for Tfh cells shown for representative WT and IgMg1 mice. From live lymphocytes, T cells were gated as $CD3^+$ $B220^-$. From T cells, conventional $CD4^+$ T cells were gated as $CD4^+$ $CD25^-$. From conventional $CD4^+$ T cells, activated cells were identified as $CD44^+$ $CD62L^-$. From activated cells, Tfh cells were identified as $PD\text{-}1^{hi}$ $CXCR5^{hi}$. (B-E) Summary statistics showing: (B) frequency of T cells as percentage of lymphocytes; (C) frequency of $CD4^+$ T cells as percentage of lymphocytes; (D) frequency of Tfh cells as percentage of $CD4^+$ T cells; (E) frequency of Tfh cells as percentage of lymphocytes. Data combined from two experiments. Each symbol represents one mouse. Statistical tests were performed by two-tailed unpaired T-test (**, $p < 0.01$; *, $p < 0.05$; ns, not significant).

4.2.11 Analysis of Tfh cell activation with Nr4a3-Tocky mice

To further investigate the interaction between B cells and Tfh cells during a TD response, Nr4a3-Tocky, a fluorescent timer reporter of T cell receptor (TCR) signalling was introduced. Nr4a3 expression in T cells is rapidly upregulated following TCR stimulation with an anti-CD3 antibody. Tocky uses a fluorescent timer protein that initially emits blue fluorescence, which decays with a half-life of approximately 7 hours, and later emits red fluorescence, allowing analysis of the kinetics of signalling. This means that recently activated cells will emit blue fluorescence, and less-recently activated cells will emit red fluorescence (Bending et al., 2018).

To determine if Nr4a3-expression could be observed in Tfh cells in Nr4a3-Tocky mice, heterozygous Nr4a3-Tocky mice were immunised with NP-KLH and draining popliteal lymph nodes were analysed by flow cytometry 8 days later (Figure 4.32A). Tfh cells represented a mix of Nr4a3-blue, Nr4a3-red, and double-positive cells (Figure 4.32B), indicating that Tfh cells showed signs of TCR activation at various stages, and that this system could be useful to analyse Tfh cell activation.

Next, IgMg1 mice that had been crossed with Nr4a3-Tocky mice were immunised with NP-KLH to compare Tfh cell activation with that of WT Nr4a3-Tocky mice. Homozygous Nr4a3-Tocky mice were used for optimal expression of the fluorescent reporters. The mice were immunised with NP-KLH, and lymph nodes were analysed at day 8 (Figure 4.33A). There was a trend (not significant) towards a higher frequency of Nr4a3^{+} Tfh cells in IgMg1 mice (Figure 4.33B-F). There were also increased blue MFI in Nr4a3-blue^{+} red^{-} Tfh cells and increased red MFI in Nr4a3-blue^{-} red^{+} Tfh cells in IgMg1 mice (Figure 4.33G and H). These results indicated that Tfh cells in IgMg1 mice underwent stronger TCR signalling.

To attempt to synchronise antigen processing and presentation to TCR cells, mice were boosted with soluble antigen 8 days after primary immunisation. The mice were then left for 4 hours, before Tfh cell activation was measured by flow cytometry (Figure 4.34A). An initial experiment in WT Nr4a3-Tocky heterozygous mice showed that boosting with soluble antigen 4 hours before the mice were culled, gave a boost in Nr4a3 expression, specific to Tfh cells rather than non-Tfh ($CD44^-$ $CD62L^+$) $CD4^+$ T cells or $CD4^-$ T cells (Figure 4.34B-D). The increase in $Nr4a3^+$ cells was primarily in the recently activated $blue^+$ cells, with no increase in $blue^-$ red^+ cell frequency (Figure 4.34F-H).

As Tfh cells are predominantly activated by B cell antigen presentation, it is likely that the increase in Nr4a3-expression induced by the boost 4 hours before cull involves BCR-mediated antigen capture by B cells. Therefore, to assess the impact of the IgMg1 BCR on antigen capture and presentation to Tfh cells, IgMg1 or WT Nr4a3-Tocky homozygous mice were immunised with NP-KLH, and at day 8 were boosted with soluble antigen 4 hours before being culled (Figure 4.35A). Again, in this experiment the frequency of $Nr4a3^+$ Tfh cells was higher in IgMg1 mice compared with WT mice (Figure 4.35B and G). There was a significant increase in the frequency of $blue^+$ red^+ cells and $blue^-$ red^+ cells, although no significant difference in recently activated $blue^+$ red^- cells (Figure 4.35D-F). Additionally, the blue MFI of Nr4a3-$blue^+$ Tfh cells and the red MFI of Nr4a3-red^+ Tfh cells were significantly increased in IgMg1 mice, suggesting more Nr4a3 expression in the $Nr4a3^+$ cells (Figure 4.35H and I).

Overall, these data suggest that IgMg1 B cells are more efficient at capturing and presenting antigen to Tfh cells, resulting in increased Tfh cell activation. Whether this

is due to the IgG1 cytoplasmic tail linking to antigen uptake or processing, or differences in BCR signalling remains to be investigated.

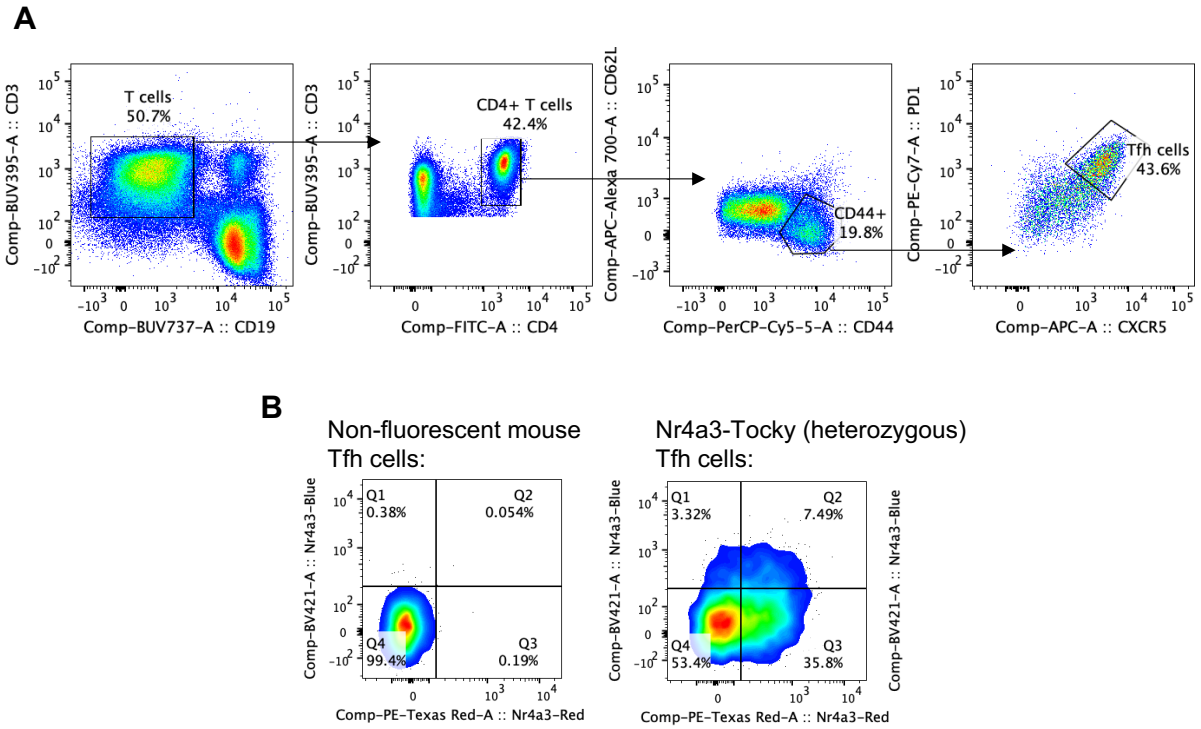

Figure 4.32 Nr4a3-Tocky expression in Tfh cells in Nr4a3-Tocky mice 8 days after NP-KLH immunisation

Nr4a3-Tocky mice or non-fluorescent WT mice were immunised with NP-KLH as shown in Figure 4.5 and at day 8 lymph nodes were analysed by flow cytometry. (A) Gating strategy for identification of Tfh cells in Nr4a3-Tocky mice. From lymphocytes, T cells were gated as $CD3^+$ $CD19^-$. From T cells, $CD4^+$ T cells were gated as $CD4^+$. From $CD4^+$ T cells, activated $CD4^+$ T cells were gated as $CD44^+$ $CD62L^-$. From activated $CD4^+$ T cells, Tfh cells were gated as PD-1^{hi} $CXCR5^{hi}$. (B) Representative flow cytometry plot showing Nr4a3-Blue and Nr4a3-Red expression in Tfh cells from non-fluorescent (WT) mouse and Nr4a3-Tocky (heterozygous) mouse.

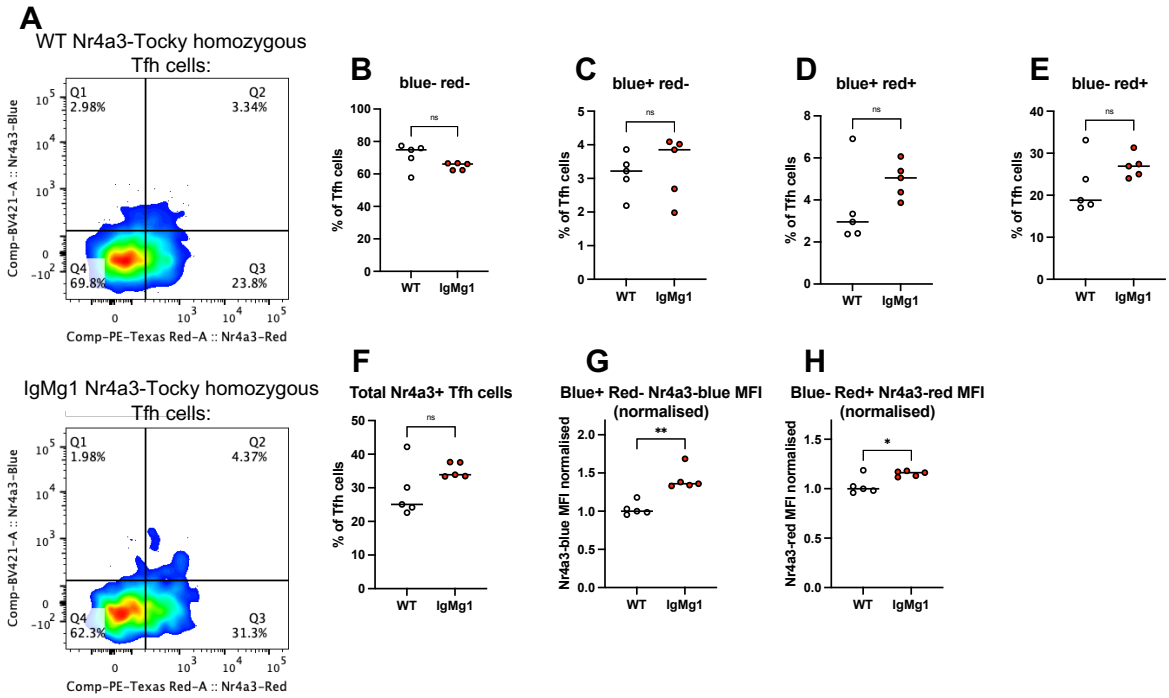

Figure 4.33 Nr4a3-Tocky expression in WT and IgMg1 Tfh cells 8 days after NP-KLH immunisation of Nr4a3-Tocky homozygous mice

WT Nr4a3-Tocky homozygous and IgMg1 Nr4a3-Tocky homozygous mice were immunised with NP-KLH as shown in Figure 4.5 and at day 8 lymph nodes were analysed by flow cytometry. Tfh cells were gated as shown in Figure 4.32. (A) Representative flow cytometry plots showing Nr4a3-blue and Nr4a3-red expression in WT Nr4a3-Tocky homozygous mice and IgMg1 Nr4a3-Tocky homozygous mice. (B-H) Summary statistics showing: (B) Frequency of Nr4a3-blue$^-$ red$^-$ Tfh cells as percentage of Tfh cells; (C) Frequency of Nr4a3-blue$^+$ red$^-$ Tfh cells as percentage of Tfh cells; (D) Frequency of Nr4a3-blue$^+$ red$^+$ Tfh cells as percentage of Tfh cells; (E) Frequency of Nr4a3-blue$^-$ red$^+$ Tfh cells as percentage of Tfh cells; (E) Frequency of total Nr4a3$^+$ cells as percentage of Tfh cells; (F) Nr4a3-blue MFI in Nr4a3-blue$^+$ red$^-$ Tfh cells (normalised to median MFI of WT); (G) Nr4a3-red MFI in Nr4a3-blue$^-$ red$^+$ Tfh cells (normalised to median MFI of WT). Data from one experiment. Each symbol represents one mouse. Statistical tests were performed by two-tailed unpaired T-test (**, $p < 0.01$; *, $p < 0.05$; ns, not significant).

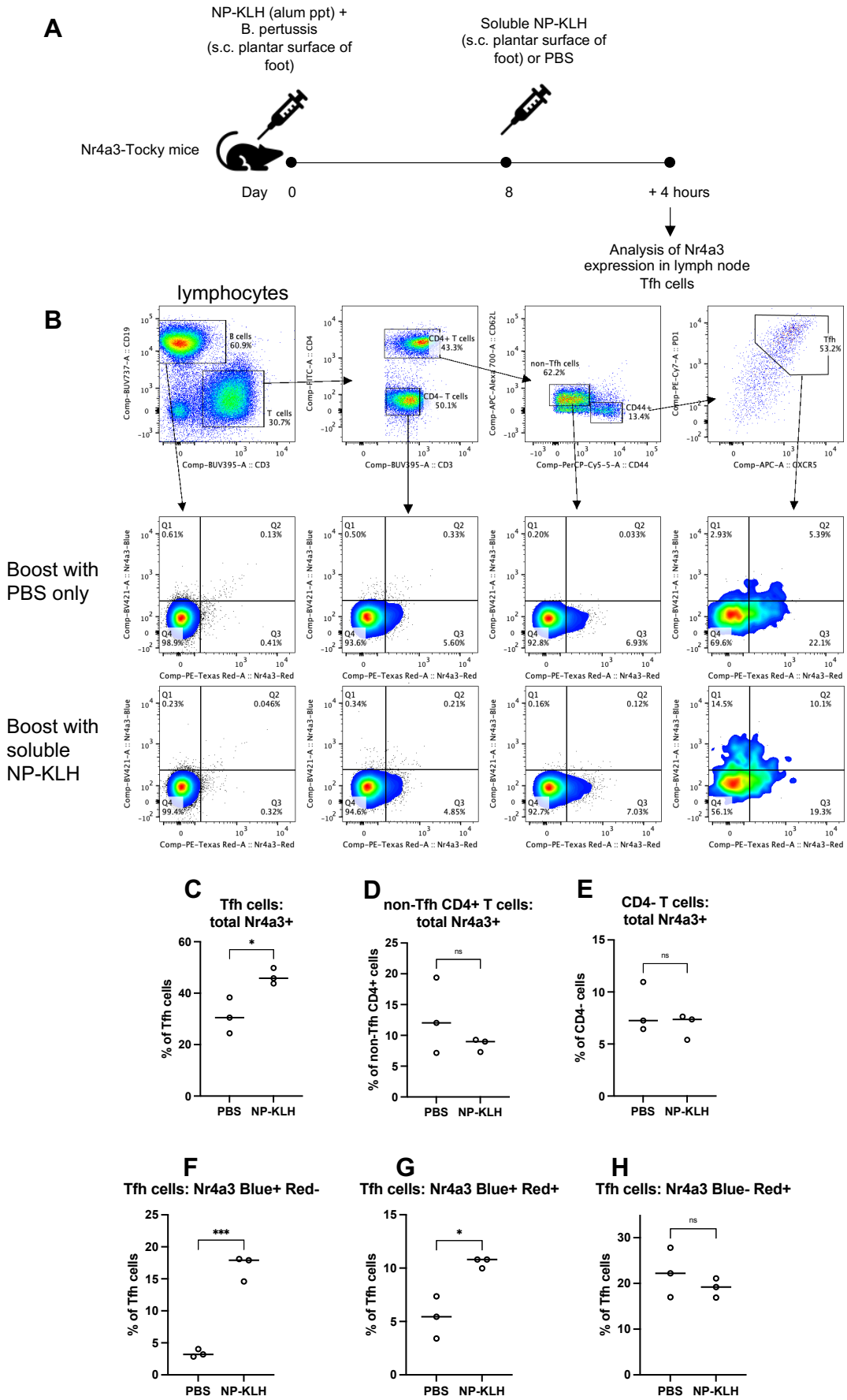
A
NP-KLH (alum ppt) + B. pertussis (s.c. plantar surface of foot)
Soluble NP-KLH (s.c. plantar surface of foot) or PBS
Nr4a3-Tocky mice
Day 0
8
+ 4 hours
Analysis of Nr4a3 expression in lymph node Tfh cells
B
lymphocytes
B cells 60.9%
T cells 30.7%
CD4+ T cells 43.3%
CD4- T cells 50.1%
non-Tfh cells 62.2%
CD44+ 13.4%
Tfh 53.2%
Boost with PBS only
Boost with soluble NP-KLH
C
Tfh cells: total Nr4a3+
% of Tfh cells
PBS NP-KLH
D
non-Tfh CD4+ T cells: total Nr4a3+
% of non-Tfh CD4+ cells
E
CD4- T cells: total Nr4a3+
% of CD4- cells
F
Tfh cells: Nr4a3 Blue+ Red-
G
Tfh cells: Nr4a3 Blue+ Red+
H
Tfh cells: Nr4a3 Blue- Red+

Figure 4.34 Nr4a3 expression 4 hours after boost with soluble antigen is increased specifically in Tfh cells rather than non-Tfh cells

(A) Heterozygous Nr4a3-Tocky mice were immunised with NP-KLH (alum ppt) and B. pertussis s.c. on the plantar surface of one foot. At day 8 mice were boosted with either soluble NP-KLH or PBS only. Mice were culled 4 hours later, and lymph nodes analysed by flow cytometry. (B) Gating strategy and representative flow cytometry plots showing Nr4a3-blue and Nr4a3-red expression in B cells, CD4- T cells, non-Tfh CD4+ T cells and Tfh cells. From lymphocytes, B cells were gated as CD19+ CD3- and T cells were gated as CD3+ CD19-. From T cells, CD4+ T cells were gated as CD4+. From CD4+ T cells, non-Tfh cells were gated as CD62L+ CD44- and activated cells were gated as CD44+ CD62L-. From activated cells, Tfh cells were gated as PD-1hi CXCR5hi. (C-H) Summary statistics showing: (C) total frequency of Nr4a3+ Tfh cells as percentage of Tfh cells; (D) total frequency of Nr4a3+ non-Tfh CD4+ T cells as percentage of non-Tfh CD4+ T cells; (E) total frequency of Nr4a3+ CD4- T cells as percentage of CD4- T cells; (F) frequency of Nr4a3-blue+ red- Tfh cells as percentage of Tfh cells; (G) frequency of Nr4a3-blue+ red+ Tfh cells as percentage of Tfh cells; (H) frequency of Nr4a3-blue- red+ Tfh cells as percentage of Tfh cells. Data are from one experiment. Each symbol represents one mouse. Statistical tests were performed by two-tailed unpaired T-test (***, $p < 0.001$; *, $p < 0.05$; ns, not significant).

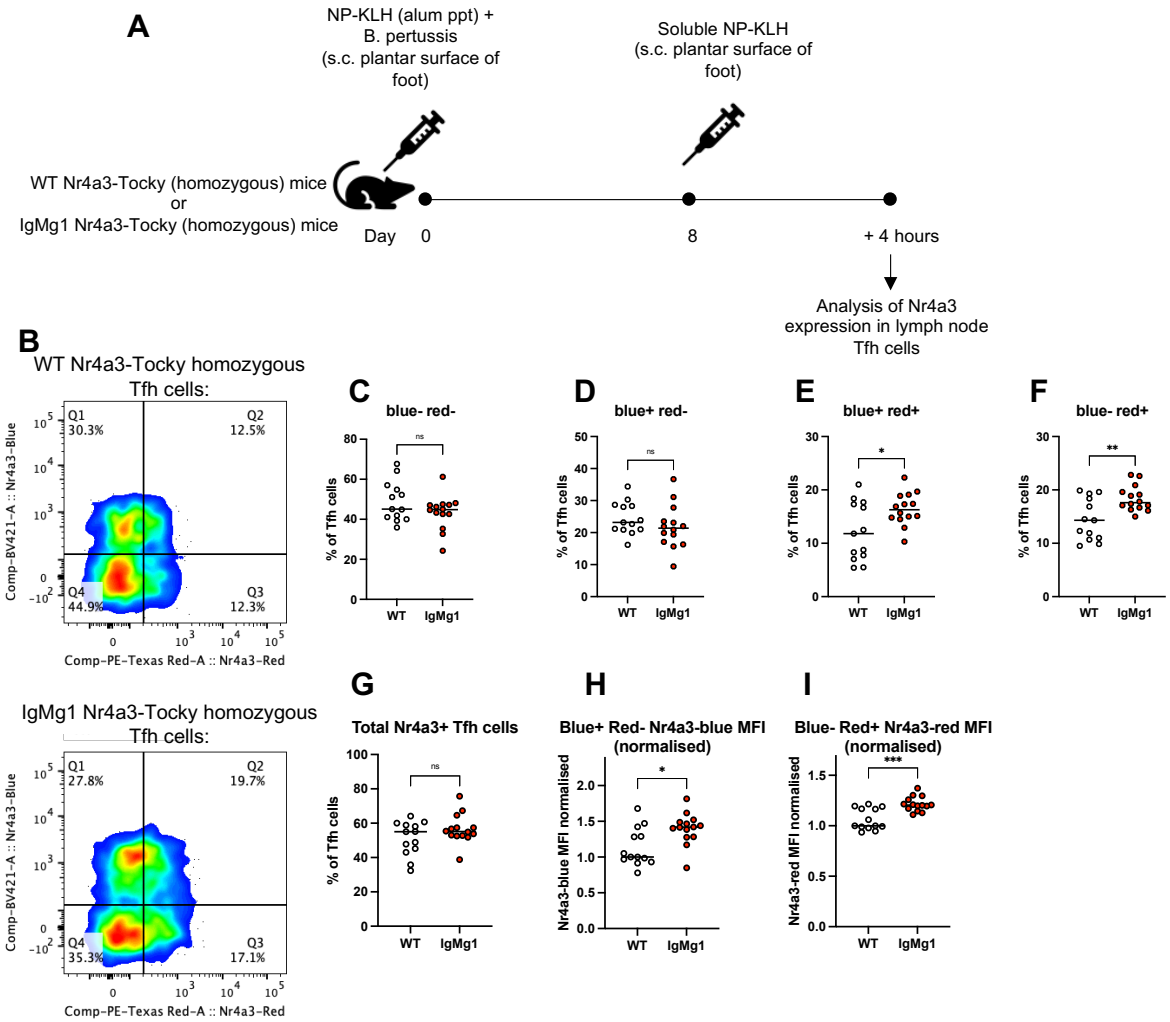

Figure 4.35 Nr4a3-Tocky expression in WT and IgMg1 Tfh cells 4 hours after boost with soluble antigen

(A) WT Nr4a3-Tocky (homozygous) and IgMg1 Nr4a3-Tocky (homozygous) mice were immunised with NP-KLH (alum ppt) and *B. pertussis* s.c. on the plantar surface of one foot. At day 8 mice were boosted with either soluble NP-KLH. Mice were culled 4 hours later, and lymph nodes analysed by flow cytometry. (B) Representative flow cytometry plots showing Nr4a3-blue and Nr4a3-red expression in WT Nr4a3-Tocky homozygous mice and IgMg1 Nr4a3-Tocky homozygous mice. (C-I) Summary statistics showing: (C) Frequency of Nr4a3-blue$^-$ red$^-$ Tfh cells as percentage of Tfh cells; (D) Frequency of Nr4a3-blue$^+$ red$^-$ Tfh cells as percentage of Tfh cells; (E) Frequency of Nr4a3-blue$^+$ red$^+$ Tfh cells as percentage of Tfh cells; (F) Frequency of Nr4a3-blue$^-$ red$^+$ Tfh cells as percentage of Tfh cells; (G) Frequency of total Nr4a3$^+$ cells as percentage of Tfh cells; (H) Nr4a3-blue MFI in Nr4a3-blue$^+$ red$^-$ Tfh cells (normalised to median MFI of WT); (I) Nr4a3-red MFI in Nr4a3-blue$^-$ red$^+$ Tfh cells (normalised to median MFI of WT). Data combined from two experiments. Each symbol represents one mouse. Statistical tests were performed by two-tailed unpaired T-test (***, $p < 0.001$; **, $p < 0.01$; *, $p < 0.05$; ns, not significant).

4.3 Discussion

4.3.1 Participation of anergic IgMg1 B cell in the germinal centre reaction

The data presented in this chapter show that anergic IgMg1 B cells can take part in GCs as efficiently as WT B cells. Although the total frequency of GC B cells was reduced in IgMg1 mice, there was a significant increase in the frequency of GC B cells where binding to antigen could be detected. Additionally, plasma cell output was similar, with comparable antibody serum titres.

In other models of B cell anergy, B cells can be activated and take part in GCs if they receive sufficient T cell help (Cooke et al., 1994; Seo et al., 2002; Sabouri et al., 2014; Burnett et al., 2018). Notably, recent work has shown that anergic B cells can be recruited into GCs when the self-reactive BCR cross-reacts with a foreign antigen. Within the GCs they may gain mutations that reduce affinity for self-antigen and increase affinity for the foreign antigen. It is thought that this process of “clonal redemption” can preserve responses to pathogens that hide from the immune system by molecular mimicry, being cross-reactive with self. Specificities of self-reactive B cells can be preserved by deactivating such B cells through anergy. Once infection with a pathogen cross-reactive happens, these anergic B cells can be activated by T cell help, and through clonal redemption evolve their antigen-specificity away from self-reactivity and towards specific reactivity with the pathogen (Burnett et al., 2018, 2019).

Crucially, in the model by Burnett et al., anergy of a monoclonal B cell repertoire is driven by constant exposure to a specific self-antigen. In the IgMg1 model, on the other hand, hyperactive BCR signalling from the IgG1 cytoplasmic tail results in negative selection during B cell development and an anergic phenotype. However, it has a polyclonal BCR repertoire. This allowed immunisation with any antigen to analyse the

B cell response, including the well characterised model TD antigen, NP-KLH (Jacob et al., 1991a; Jacob and Kelsoe, 1992; Jacob et al., 1993; Han et al., 1995b; Takahashi et al., 1998). As there is no increased negative selection affecting T cell development, sufficient cognate Tfh cell help should be available, but with the experiments presented here, it is not possible to analyse if somatic hypermutation resulted in loss of affinity for a cognate self-antigen.

Bulk RNA sequencing analysis of WT and IgMg1 GC B cells showed that the gene expression programme in IgMg1 GC B cells was very similar to WT GC B cells. Comparison of the differentially expressed genes between GC and follicular B cells showed that there was extensive overlap in both mouse genotypes. Additionally, GSEA showed almost identical results with similar GC-typical gene sets being enriched in GC B cells of both genotypes. These included E2F targets and G2M checkpoint, both associated with cell cycle progression and proliferation (Liberzon et al., 2015; Cuitiño et al., 2019). They also included Myc targets. Myc expression marks positively selected GC B cells (Calado et al., 2012; Dominguez-Sola et al., 2012). When gene expression in IgMg1 GC B cells was directly compared with WT GC B cells there were relatively few differentially expressed genes. However, GSEA found that Myc targets, E2F targets and G2M checkpoint were all significantly enriched in WT GC B cells compared with IgMg1 GC B cells. This suggested that relative to WT GC B cells, IgMg1 GC B cells may have fewer signs of positive selection, and are less proliferative.

Antigen binding detected by flow cytometry using fluorescently-labelled NP could be seen in a higher proportion of the IgMg1 GC B cells compared with WT B cells. In a recent study, Viant et al. analysed the affinity of GC B cells using biolayer

interferometry. It was found that antigen binding could be detected in around 30% of GC B cells by flow cytometry. When antibodies from single GC B cells were expressed and tested by biolayer interferometry in a monovalent assay they found similar frequency of binders, but by increasing the valency to detect lower affinity binders they could detect antigen binding in around 50% of GC B cells (Viant et al., 2020). This suggests only high affinity binders are detected by flow cytometry. Additionally, when the NP^{+} cells were split into NP^{hi} and NP^{int} cells, the NP^{hi}/NP^{int} ratio was significantly higher in IgMg1 GC B cells. Overall, this suggested that the average affinity for NP was higher in IgMg1 GC B cells. One explanation for these results is that, due to the reduced surface BCR density on anergic B cells, there is a higher affinity threshold for GC participation. Higher affinity may be required for B cells to be able to capture and present enough antigen to receive sufficient T cell help. This higher affinity threshold is consistent with the requirement for high BCR crosslinking for efficient B cell activation in other anergy models. Membrane-bound HEL, but not soluble HEL, could raise a response from anergic B cells in MD4 x ML5 mice (Cooke et al., 1994). Similarly, a high density of HEL cross-linked to sheep red blood cells was required to make a HEL-specific GC B cell response from anergic B cells in a chimeric bone marrow model where soluble HEL was expressed as a self-antigen (Burnett et al., 2018).

The increased affinity threshold could explain the differences in IGHV gene usage observed from the bulk RNA sequencing of GC B cells following immunisation with NP-CGG. In both WT and IgMg1 GC B cells there was generally a similar pattern of IGHV gene expression, including an increase in the BL/6 canonical anti-NP IGHV gene, IGHV1-72 (also known as V186.2), associated with high-affinity NP-response (Jacob

et al., 1991b, 1993). However, a comparison of the IGHV gene expression in IgMg1 GC B cells compared with WT GC B cells showed that several IGVH genes had reduced frequency of expression in IgMg1 GC B cells. These genes had similar frequency in follicular B cells, suggesting that they are selected against when IgMg1 transition to GC stage. These genes have no published association with NP-binding, and likely represent B cells with low-affinity for NP. For example, IGHV1-81 was found to be the predominant IGHV gene amongst anti-phycoerythrin (PE) antibodies (Pape et al., 2018). These appear to be used at lower frequency by IgMg1 GC B cells than WT GC B cells following immunisation with NP-CGG.

The DZ/LZ ratio was higher in IgMg1 B cells which suggests that more GC B cells are being selected into the DZ and proliferating (Victora et al., 2010). However, as described above, GSEA of the bulk RNA sequencing analysis shows that positive selection and proliferation may be negatively enriched in IgMg1 GC B cells. Therefore, there may be an alternative reason for the increased DZ/LZ ratio. Active-Caspase 3 staining showed that apoptosis is increased in IgMg1 GC B cells, and this seemed more prominent in the LZ B cells. Apoptosis in LZ B cells is associated with weak BCR signalling and failure to compete for sufficient T cell help (Mayer et al., 2017). This is compatible with less positive selection in the IgMg1 GC. It is possible that the lower affinity B cells undergo apoptosis due to being unable to capture and present enough antigen to compete for T cell help, and this contributes to higher average BCR affinity and more stringent selection of the IGHV repertoire. This indicates that this may happen at LZ stage inside GCs, rather than during B cell recruitment during the initial extrafollicular activation.

The GCs in IgMg1 mice are predominantly made up of class-switched B cells, with a reduced percentage of unswitched IgM$^+$ GC B cells compared to WT mice. IgG1$^+$ GC B cells have a competitive advantage over IgM$^+$ GC B cells in terms of positive selection (Sundling et al., 2021). However, in IgMg1 mice, IgG1$^+$ B cells appear to be even more dominant. Although active-Caspase-3 staining was higher in IgMg1 GC B cells than WT B cells, this was observed in both IgG1$^+$ and IgM$^+$ GC B cells, so it is unlikely that the lower frequency of IgM$^+$ cells is due to increased apoptosis. There were also similarly increased DZ/LZ ratios in IgG1$^+$ and IgM$^+$ GC B cells of IgMg1 mice compared with WT, suggesting that the IgG1M IgM$^+$ B cells were not less likely to be selected into the DZ. Further, there was no overall difference in plasma cells, and there was a slight but significantly reduced IgM anti-NP serum response, suggesting that the loss of IgM$^+$ GC B cells was not due to increased IgM$^+$ plasma cell output. It is therefore likely that either increased class-switching or reduced ability of IgM$^+$ IgMg1 B cells to enter the GC are explanations for the reduction in IgM$^+$ GC B cells. It is feasible that altered BCR signalling could have an impact on class-switching. BCR signalling has been shown to act in synergy with TLR signalling to promote class-switching (Pone et al., 2012). However, BCR signalling is unable to induce class-switching alone (Chen et al., 2020) but requires T cell help and cytokines that promote class-switching (Snapper and Mond, 1993; Kawabe et al., 1994). Therefore, it is possible that the increase in Tfh cells in IgMg1 mice results in an environment that promotes increased class-switching. Alternatively, IgM$^+$ GC B cells bearing the IgMg1 chimeric BCR may be unable to enter the GC due to their anergic state. Class-switching could allow the B cell to escape anergy by switching from the chimeric IgMg1 BCR to IgG. However, even after class-switching, reduced surface BCR expression compared to WT IgG1$^+$

B cells could still be observed, indicating some features of anergy remain. To further investigate this in the future, IgMg1 mice are being crossed with AID-deficient AID Cre mice which would allow the IgMg1 GC response to be studied in a system where B cells are unable to class-switch.

4.3.2 IgMg1 GC B cells present more antigen to Tfh cells

As described above, Tfh cells were increased in IgMg1 mice. This was the case in the draining lymph node 8 days after immunisation and could also be observed in Peyer's patches where chronic GC reactions take place. Tfh cells have been shown to proliferate during a GC response, with the amount of proliferation dependent on the amount of antigen they are presented (Merkenschlager et al., 2021). This raised the possibility that IgMg1 B cells were presenting more antigen to Tfh cells, resulting in more Tfh cell differentiation and proliferation.

The Nr4a3-Tocky reporter system allows analysis of TCR signalling in Tfh cells (Bending et al., 2018), as Nr4a3 is expressed transiently following TCR activation (Odagiu et al., 2021). This system was used to analyse antigen presentation to Tfh cells by IgMg1 GC B cells compared with WT GC B cells. Classically, antigen presentation by B cells to T cells has been analysed with *in vitro* co-cultures of antigen-specific B and T cells (Batista and Neuberger, 2000), but the advantage of the Nr4a3-Tocky system was that it allows analysis during an *in vivo* immune response. Mice were immunised with NP-KLH with adjuvants, and then at day 8 were boosted with soluble NP-KLH 4 hours before the mice were culled and draining lymph nodes analysed. This boost specifically induced Nr4a3-blue expression in Tfh cells rather

than non-Tfh $CD4^+$ or $CD4^-$ T cells, suggesting that the activation induced by the boost would be influenced by antigen presentation by B cells. Additionally, the boost with soluble antigen allowed synchronisation of antigen capture by B cells to this timepoint. Previously it has been shown that injection of soluble antigen at the peak of the GC response induces apoptosis within GC B cells, but it was noted that B-T cell interactions were not disrupted (Han et al., 1995b). The results shown here appear to show that injection of soluble antigen results in increased B cell antigen presentation to T cells, and increased Tfh activation. It is possible that there are not enough T cells to sustain interactions with all antigen-presenting B cells able to capture antigen, resulting in the increased apoptosis observed by Han et al. (1995).

Following the boost with soluble antigen there was a significant increase in the percentage of Tfh cells expressing Nr4a3-blue in IgMg1 mice. The average Nr4a3-expression in the $Nr4a3^+$ cells also appeared to be higher. Overall, this suggests antigen-presentation by IgMg1 B cells to Tfh cells increased. This may relate to the higher average affinity of the B cells in the GC, allowing the cells to capture more antigen and thus present more to the Tfh cells. It is not clear if this would also be the case in anergic B cells reactivated through clonal redemption in the classical models of anergy (Burnett et al., 2018).

It is unclear how increased antigen presentation and increased availability and activation of Tfh cells in the GC in IgMg1 mice fits with increased apoptosis of GC B cells and reduced positive selection and proliferation. It is thought that increased T cell help results in B cell positive selection into the DZ, or output from the GC as plasma cells or memory B cells (Nakagawa and Calado, 2021). Apoptosis is thought to be the

fate of cells that fail to receive T cell help (Liu et al., 1989, 1991; Mayer et al., 2017). The results shown here suggest that receiving T cell help may not be enough to result in positive selection and prevent apoptosis. Strength of BCR signalling may be an important contributing factor, independently of ability to capture and present antigen to Tfh cells.

Although Nr4a3-expression is also induced in B cells following BCR stimulation (Tan et al., 2020), Nr4a3-red or blue expression could not be detected on B cells in Nr4a3-Tocky mice. Use of an alternative marker Nr4a1 (Nur77) reporter would allow simultaneous analysis of BCR and TCR signalling (Moran et al., 2011; Zikherman et al., 2012; Elliot et al., 2022) as Nr4a1 has around 6-fold higher expression in B cells following BCR stimulation than Nr4a3 (Tan et al., 2020). Additionally, it is a more sensitive marker of TCR signalling (Elliot et al., 2022). This can be done by crossing Nur77-tempo mice (Elliot et al., 2022) with IgMg1 mice in the future. In this chapter Tfh cells have been analysed at day 8 after primary immunisation. However, the Tfh cell phenotype has been shown to be transient (Baumjohann et al., 2013), so analysis at different time points will be important for insight on how interaction between the IgMg1 GC B cells and Tfh cells affects the dynamics of Tfh cells throughout an immune response.

4.3.3 IgG1M mice have impaired TI and TD antibody response

The B cell responses to model TI-II and TD antigens were also assessed in IgG1M mice which have B cells expressing only IgG1 as a BCR. $IgG1^+$ cells have stronger BCR signalling and outcompete IgM^+ B cells in GCs (Sundling et al., 2021). $IgG1^+$

memory B cells are also rapidly reactivated in response to re-exposure to antigen (Pape et al., 2011). As shown in chapter 3, the B cells in IgG1M mice had stronger calcium flux in response to BCR stimulation. Therefore, it was predicted that there would be an enhanced B cell response to immunisations in these mice. Surprisingly, it was found that IgG1M mice had a severely impaired antibody response to model TI-II antigen NP-Ficoll at day 6 post-immunisation, with reduced plasma cells and reduced NP-specific antibody titre.

The IgG1M mice also had an impaired antibody response to TD antigen NP-KLH at day 8 post-immunisation, with reduced plasma cells and reduced antibody titre. However, they were able to form GC B cells and NP-specific GC B cells at a similar level to WT mice, suggesting that the defect was in plasma cell output from the GC. The DZ/LZ ratio of IgG1M GC B cells was similar to WT GC B cells suggesting that there was no defect in B cell selection into the DZ. Although strong BCR signalling has been shown to induce apoptosis in GC B cells and plasmablasts (Yam-Puc et al., 2021), there was no observed increase in apoptosis in IgG1M GC B cells. The NP^{hi}/NP^{int} ratio of GC B cells was significantly reduced, indicating that the average affinity of the BCRs were reduced. There was also a slight reduction in Tfh cells.

It is not clear why the IgG1M mice have an impaired antibody response despite the B cells having hyperactive BCR signalling. One possible explanation could be absence of secreted IgM in IgG1M mice, which can play an important role in regulation of GCs by formation of immune complex with the antigen (Zhang et al., 2013) and trapping antigen on follicular dendritic cells (Boes et al., 1998). Consistent with this, several studies have shown that soluble IgM-deficient mice immunised with carrier-conjugated

NP had an impaired IgG1 response (Ehrenstein et al., 1998; Boes et al., 1998; Zhang et al., 2013), and similarly in an influenza infection model, soluble IgM-deficient mice had reduced IgG2a titres, viral clearance, and survival (Baumgarth et al., 2000). Injection of naïve serum IgM rescued the antibody response, showing its importance (Ehrenstein et al., 1998; Baumgarth et al., 2000). However, this soluble IgM-deficient model made a stronger response to TI-II antigen NP-Ficoll (Ehrenstein et al., 1998; Boes et al., 1998), whereas the IgG1M mouse have an impaired anti-NP-Ficoll response, so soluble IgM deficiency cannot fully explain the results for the IgG1M mice. This may be because the soluble IgM-deficient mice had an increased B-1 cell population (Ehrenstein et al., 1998; Boes et al., 1998), whereas, as shown in chapter 3, IgG1M mice have a reduced B-1 population.

Another potential factor is that IgG1M mice may have gaps in their BCR repertoire. As shown in chapter 3, IgG1M mice had a block during B cell development at the pre-B cell stage and increased apoptosis in pre-B cells, likely due to inefficient pairing of the IgG1 heavy chain with the surrogate light chain to form the pre-BCR. Although B cells that progressed through this stage appeared to continue their development to mature B cells as normal, it is possible that this block in development created a bottleneck resulting in a less diverse mature B cell population, less able to respond to immunisation. One way to test this could be to perform BCR sequencing of naïve B cells and compare diversity with normal BCR repertoires.

4.3.4 Conclusions

Overall, the results in this chapter show that alterations to the BCR can have different impacts on B cell activation. In IgG1M mice, there is impaired plasma cell differentiation and antibody production in response to TI-II and TD antigens, despite the B cells having hyperactive BCR signalling. However, in anergic IgMg1 B cells, the chimeric IgMg1 BCR allows normal participation in GCs and plasma cell differentiation, and increased antigen presentation to Tfh cells.

Chapter 5. Testing the development of autoimmunity in the IgMg1 model of B cell anergy

5.1 Introduction

5.1.1 B cells and autoimmunity

A crucial aspect of immunity is the ability to distinguish from foreign- and self-antigens. Several controls and regulatory mechanisms, including B cell tolerance, are in place to prevent the cells of the immune system from becoming activated to self. When these mechanisms fail, it may result in autoimmunity. There is a well-established link between ageing and development of autoimmunity. Autoimmune disease has increased incidence with increased age. For example, rheumatoid arthritis (RA) is most prevalent in males and females over 75 years of age (Hasler and Zouali, 2005). Peak incidence of systemic lupus erythematosus (SLE) occurs at 50-54 years for females and 70-74 years for males (Somers et al., 2007). Aged WT C57BL/6 mice spontaneously develop autoimmunity in multiple organs (Hayashi et al., 1989).

Defective B cell tolerance and production of autoantibodies is implicated in several autoimmune diseases. In RA, autoantibodies are present in serum several years before development of symptoms and autoreactive B cells fail to be removed as they are in healthy people (Samuels et al., 2005). Defective tolerance is also observed in patients with Sjogren's syndrome. Polyreactive B cell receptors (BCRs) are increased among newly emigrant and transitional B cells, and self-reactive BCRs are increased in mature B cells in patients compared with healthy controls (Glauzy et al., 2017). SLE patients also have increased mature B cells that are self-reactive (Yurasov et al., 2005).

Genome wide association studies have found links between components of the BCR signalling pathway and increased risk of autoimmunity, suggesting that there may be a role of altered BCR signalling in driving disease (Jackson et al., 2015; Rawlings et al., 2017). One example of this is protein tyrosine phosphatase nonreceptor 22 (PTPN22), a negative regulator of BCR and T cell receptor (TCR) signalling. A variant of human PTPN22 with a single nucleotide polymorphism (R620W) has been linked to an increased risk of development of autoimmune diseases (Kyogoku et al., 2004; Bottini et al., 2004; Begovich et al., 2004). In a mouse knock-in model it was found that B cells bearing the murine homologue of the variant, PEP-R619W, had hyperactive BCR signalling. Although PEP affects both B and T cell signalling, it was found that a model with B cell-restricted expression of PEP-R619W developed autoimmunity, showing a role for BCR signalling in autoimmunity (Dai et al., 2013).

During B cell development BCR signalling plays a role in both positive and negative selection and therefore altered BCR signalling can result in increased autoreactive B cells in the mature B cell repertoire. Mice with Wiskott-Aldrich syndrome (WAS) protein-deficient B cells have increased BCR and toll-like receptor (TLR) signalling. Transitional B cells in these mice have increased proliferation suggesting increased positive selection, and self-reactivity is enriched in B cells at the transitional to mature B cell stages (Kolhatkar et al., 2015). However, it is thought that an increased self-reactive repertoire is not sufficient for development of autoimmunity, as additional signals are required for B cell activation and differentiation into autoantibody-secreting plasma cells (Rawlings et al., 2017). Short-lived extrafollicular plasma cells, and germinal centre (GC)-derived long-lived plasma cells may both contribute to autoimmunity. Autoreactive B cells in the lupus prone MRL.Fas^{lpr} mouse model are

primarily located at the border of the T zone and red pulp, not in GCs (William et al., 2002). However, evidence that GCs contribute to autoantibodies comes from the fact that SLE B cells have extensive somatic hypermutation (Wellmann et al., 2005). GCs are frequently found in mouse models of autoimmunity including T1D and lupus models (Luzina et al., 2001).

Additionally, autoreactive GC B cells may contribute to autoimmunity by activating and inducing proliferation of cognate Tfh cells (Rawlings et al., 2017). In humans there is evidence that Tfh cells are dysregulated or play a role in development of several autoimmune diseases. For example, Tfh cells have been found to be elevated in RA patients (Ma et al., 2012; Zhang et al., 2015b). Tfh-like cells were also increased in the blood of SLE patients, and frequency was correlated with frequency of plasmablasts and levels of autoantibodies (Choi et al., 2015; Zhang et al., 2015a). In certain mouse models Tfh cells accumulate, causing autoimmunity. Sanroque mice are homozygous for the san allele of Roquin. Tfh cells accumulate in these mice, and this causes spontaneous GC formation and a SLE-like phenotype, suggesting that Tfh cell expansion and excessive positive selection of GC B cells could lead to autoimmunity (Linterman et al., 2009; Lee et al., 2012). It has been hypothesised that this may be because excessive Tfh cell numbers result in a reduced selection threshold within the GC, allowing lower affinity or self-reactive B cells to survive (Pratama and Vinuesa, 2014). Tfh cells also secrete IL-21, promoting plasma cell differentiation and antibody secretion (Ettinger et al., 2005). IL-21 also promotes $CD8^+$ T cell expansion (Li et al., 2005) and generation of pro-inflammatory Th17 cells (Korn et al., 2007).

Other B cell subsets are associated with autoimmunity. B-1 cells are enriched for self-reactive BCRs and may contribute to autoimmune disease by secreting low-affinity natural antibodies that bind to self-antigens (Duan and Morel, 2006). Additionally, there is a subset of B cells termed age-associated B cells. These are a heterogenous population of $CD21^-$ $CD23^-$ B cells that accumulate with age (Hao et al., 2011; Rubtsov et al., 2011; Rubtsova et al., 2015), forming up to 30% of mature B cells in 22-month-old mice (Hao et al., 2011). They do not divide in response to BCR-stimulation but are responsive to TLR7-stimulation (Hao et al., 2011; Rubtsov et al., 2011). They have been found to be expanded in mouse models of SLE and are enriched for self-reactive BCRs, and their depletion results in a reduction of autoantibodies (Rubtsov et al., 2011). Additionally, B cells with similar characteristics are expanded in human SLE patients (Wang et al., 2018; Jenks et al., 2018).

5.1.2 Chapter aims

The results from the previous chapters show that although the B cells in the IgMg1 model appear anergic, the mice are able to make GC responses to model TD antigens. Tfh cells are increased and undergo increased TCR signalling. This led to the hypothesis that IgMg1 mice may have a heightened immune response to self-antigens and could act as a useful model to study how anergic B cells can be reactivated leading to autoimmunity.

The aims of this chapter are as follows:

i) Testing whether induction of an autoantibody response by immunisation with a self- or highly conserved antigen in IgMg1 mice is more prone to development of autoantibodies.

ii) Testing whether non-immunised IgMg1 mice are more prone to autoimmunity when ageing.

iii) Testing whether induction of an autoantibody response in aged IgMg1 mice with a self- or highly conserved antigen is more prone to development of autoantibodies.

5.2 Results

5.2.1 Young adult IgMg1 mice do not make an increased response to conserved antigen chicken collagen type II

As shown in chapter 4, IgMg1 mice can make a T cell-dependent (TD) B cell response of a similar magnitude as WT mice. Additionally, they have increased Tfh cells with increased TCR signalling. Therefore, it was hypothesised that the IgMg1 mice may be more prone to developing autoimmunity.

To test this, an experiment was conducted where mice were immunised with a highly conserved or self-antigen. Chicken collagen type II was chosen for these experiments as it is used to induce collagen-induced arthritis in BL/6 mice. This disease model is characterised by anti-collagen antibodies, so it is an antigen that can be used to break tolerance (Inglis et al., 2007, 2008).

Young adult mice (aged 8-16 weeks old) were immunised with a priming injection of 10 µg chicken collagen type II precipitated in alum with heat inactivated *B. pertussis*. At three-week intervals, they received 1-3 boosts with 10 µg soluble chicken collagen type II (without adjuvants) (Figure 5.1A). Lymph nodes were analysed by flow cytometry 8 days after the final injection (Figure 5.1B). IgMg1 mice were able to make a GC B cell response and plasma cell response. However, there were no statistically significant differences compared with WT mice after either two or three boosts of soluble collagen type II, although there was a non-significant trend towards reduced GC B cells in IgMg1 mice (Figure 5.1C and D). Serum samples were taken at regular intervals for monitoring of anti-collagen antibody response. The collagen-specific IgM titres were not significantly different in IgMg1 mice at any time point (Figure 5.1E). Most of the mice had not made a detectable anti-collagen IgG response at 8 days after the

priming injection. More mice had responded by day 29 (8 days after the first boost with soluble collagen), and almost all the mice had made a response by day 50 (8 days after the second boost). However, there were no significant differences between WT and IgMg1 mice (Figure 5.1F).

As this immunisation protocol was sub-optimal for induction of an anti-collagen B cell response, it was decided to immunise mice with larger doses of collagen and with stronger adjuvant, using a well-established collagen-induced arthritis procedure (Inglis et al., 2007, 2008). Mice were immunised s.c. at the base of the tail with 100 µg chicken collagen type II emulsified in complete Freund's adjuvant. They then received a boost with 100 µg chicken collagen type II in incomplete Freund's adjuvant at day 21 (Figure 5.2A). Mice were monitored daily up until day 26 when they were culled by schedule 1 method, but no mice of either genotype developed any symptoms associated with arthritis. Serum samples were taken to measure anti-collagen antibodies by ELISA. At all timepoints analysed, there were no increased anti-collagen IgM in IgMg1 mice (Figure 5.2B). At day 21, there was a decreased anti-collagen IgG titre in IgMg1 mice (two-tailed T-test, p-value = 0.0247) (Figure 5.2C and D), although following the boost they appeared to reach equivalence with WT by day 26.

Overall, these data showed that the IgMg1 mice did not appear to be more susceptible to making a strong response against the conserved antigen collagen type II following immunisation, suggesting that, at a young age, they are not more prone to developing autoantibodies.

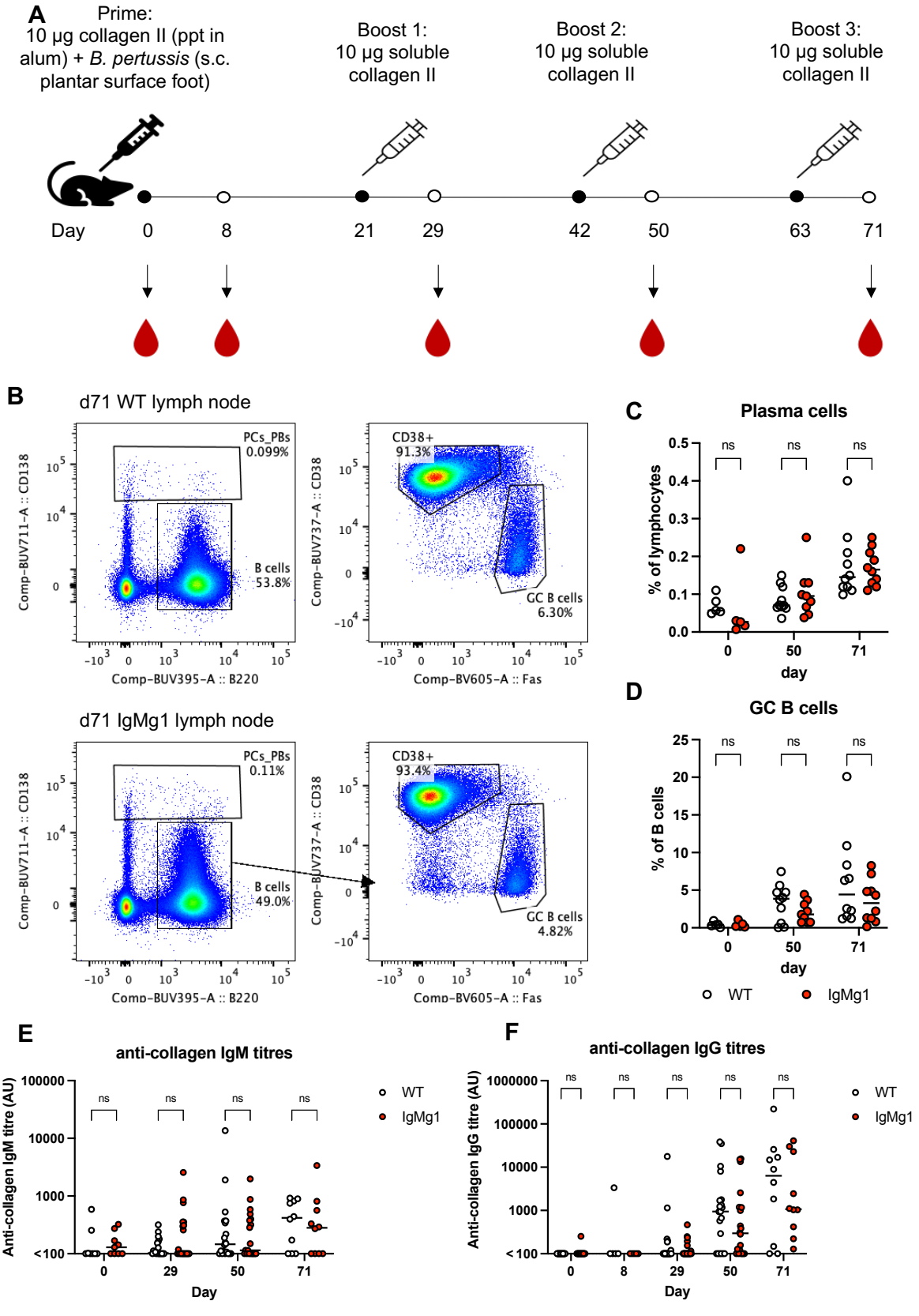
A
Prime:
10 µg collagen II (ppt in alum) + B. pertussis (s.c. plantar surface foot)
Boost 1:
10 µg soluble collagen II
Boost 2:
10 µg soluble collagen II
Boost 3:
10 µg soluble collagen II
Day 0 8 21 29 42 50 63 71
B
d71 WT lymph node
PCs_PBs 0.099%
B cells 53.8%
CD38+ 91.3%
GC B cells 6.30%
Comp-BUV711-A :: CD138
Comp-BUV395-A :: B220
Comp-BUV737-A :: CD38
Comp-BV605-A :: Fas
d71 IgMg1 lymph node
PCs_PBs 0.11%
B cells 49.0%
CD38+ 93.4%
GC B cells 4.82%
C
Plasma cells
% of lymphocytes
day
ns
D
GC B cells
% of B cells
WT
IgMg1
E
anti-collagen IgM titres
Anti-collagen IgM titre (AU)
Day
F
anti-collagen IgG titres
Anti-collagen IgG titre (AU)

Figure 5.1 IgMg1 mice do not make a stronger response than WT mice after immunisation with conserved antigen chicken collagen type II

(A) Schematic showing immunisation strategy. Mice were immunised s.c. with 10 µg chicken collagen type II (alum ppt) with heat inactivated *B. pertussis*. They then received 1-3 boosts with 10 µg soluble collagen type II at 3-week intervals. Mice were culled by schedule 1 method 8 days after their final boost. (B) Representative flow cytometry plots for WT and IgMg1 mice plasma cells (PCs) and GC B cells and at day 71 (8 days after third boost with soluble collagen type II). From the lymphocytes, PCs were gated as $CD138^+$ and B cells were gated as $B220^+$ $CD138^-$. From the B cells, GC B cells were gated as Fas^+ $CD38^-$. (C-D) Summary statistics for: (C) plasma cells as percentage of lymphocytes; (D) GC B cells as percentage of B cells. Flow cytometry data combined from 2 experiments per timepoint. Each symbol represents one mouse. (E-F) Sera was tested for anti-collagen antibody by ELISA. Summary statistics for: (E) anti-collagen IgM sera titres; (F) anti-collagen IgG sera titres. Each symbol represents one mouse. Statistical tests for C and D performed by 2way ANOVA with Tukey's multiple comparison test. Statistical tests for E and F performed by mixed-effects analysis with Šídák's multiple comparisons test (ns, not significant).

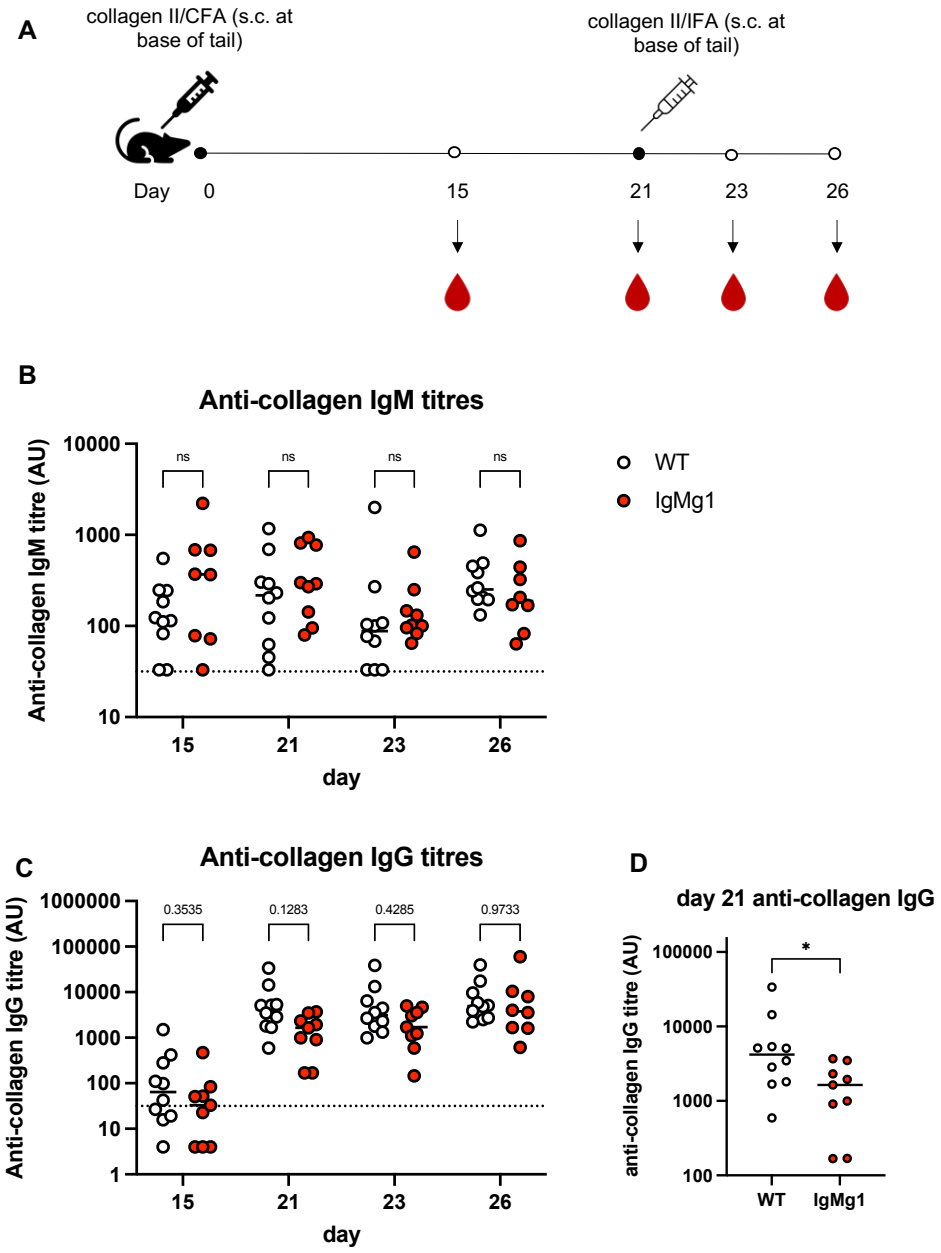

Figure 5.2 IgMg1 mice do not make a stronger anti-collagen antibody response in collagen-induced arthritis model

(A) Schematic showing immunisation schedule for collagen-induced arthritis model. Mice injected at base of tail with 100 µg chicken collagen type II emulsified in Freund's complete adjuvant (CFA) and boosted at day 21 at base of tail with 100 µg chicken collagen type II in incomplete Freund's adjuvant (IFA). Serum samples taken at day 15, 21, 23 and 26. Mice culled by schedule 1 method at day 26. (B) Summary statistics of anti-collagen IgM sera titres measured by ELISA at each time point. (C) Summary for anti-collagen IgM sera titres measured by ELISA. (D) Summary of anti-collagen IgG sera titres measured by ELISA at day 21. Data combined from two experiments. Each symbol represents one mouse. Statistical tests for B and C performed by mixed-effects analysis with Šídák's multiple comparisons test (ns, not significant). Statistical test for D performed by unpaired two-tailed T-test (*, $p < 0.05$).

5.2.2 Aged IgMg1 mice spontaneously develop autoantibodies

The risk of autoimmunity increases with age (Hasler and Zouali, 2005; Somers et al., 2007), and autoimmune disease and autoantibodies develop in multiple organs in aged WT C57BL/6 mice (Hayashi et al., 1989). To evaluate the development of autoimmunity in aged IgMg1 mice, rat liver, kidney and stomach slides were stained with sera from 12-18 month old mice (Figure 5.3A). These slides are clinically used to screen for human autoantibodies, and the pattern of staining detects anti-nuclear antibodies (ANA), anti-mitochondrial antibodies (AMA), anti-smooth muscle antibodies (ASMA) or anti-gastric parietal cell antibodies (AGPCA). The slides were analysed blind by a clinical immunologist to identify the types of autoantibodies present. Autoantibodies were detected in sera from aged WT (5 out of 13 samples) and aged IgMg1 mice (11 out of 13 samples), however incidence was significantly higher in IgMg1 sera (Fisher's exact test, p-value = 0.0167) (Figure 5.3B). Additionally, the types of autoantibodies present were more varied in the IgMg1 serum samples (Figure 5.3C). The mean pixel brightness across each section was measured using Fiji, and this trended higher for the tissues stained with IgMg1 sera (Figure 5.3D). The sections were also segregated into kidney, liver, smooth muscle and gut tissue by manually selecting regions of interest, and mean pixel brightness for each individual tissue was measured. These trended higher in IgMg1 mice for kidney, liver and gut but none of the differences were statistically significant (Figure 5.3E-I).

To further evaluate autoantibodies in sera of aged mice, ELISAs were performed to assess relative titres of collagen-specific IgG and IgM in serum samples from aged mice (aged 12-18 months old). There was around a 75% higher titre of collagen-

specific IgM ($p = 0.0022$) in aged IgMg1 mice (Figure 5.4A) and an approximately 40% increase in collagen-specific IgG (not-significant) in aged IgMg1 mice (Figure 5.4B). Additionally, rat pancreas sections were stained with sera from aged mice (aged 12-18 months old) to screen for anti-islet autoantibodies. Islets were identified in the pancreas tissue by co-staining with an insulin-specific antibody. Co-staining with mouse serum and the insulin-specific antibody was observed in 1 out of 11 aged IgMg1 samples and 1 out of 5 aged WT samples. However, the number of samples analysed was too low to conclusively test if anti-islet autoantibodies were more frequently found in aged IgMg1 mice (Figure 5.5).

Finally, levels of total IgG, IgM and IgA in aged (aged 12-18 months old) and young adult IgMg1 mice sera were assessed by ELISA. Although the relative amounts of all 3 classes of antibody were elevated in serum from aged mice compared with the young adult mice, no significant differences were observed between aged IgMg1 and aged WT samples. This indicated that the increased incidence of autoantibodies in aged IgMg1 mice was unlikely to be due to higher total concentrations of antibody in the blood (Figure 5.6).

Overall, these data indicated that although young adult IgMg1 mice have an anergic B cell phenotype and do not make a larger response to a conserved antigen, with ageing, IgMg1 mice develop autoantibodies more frequently than WT mice.

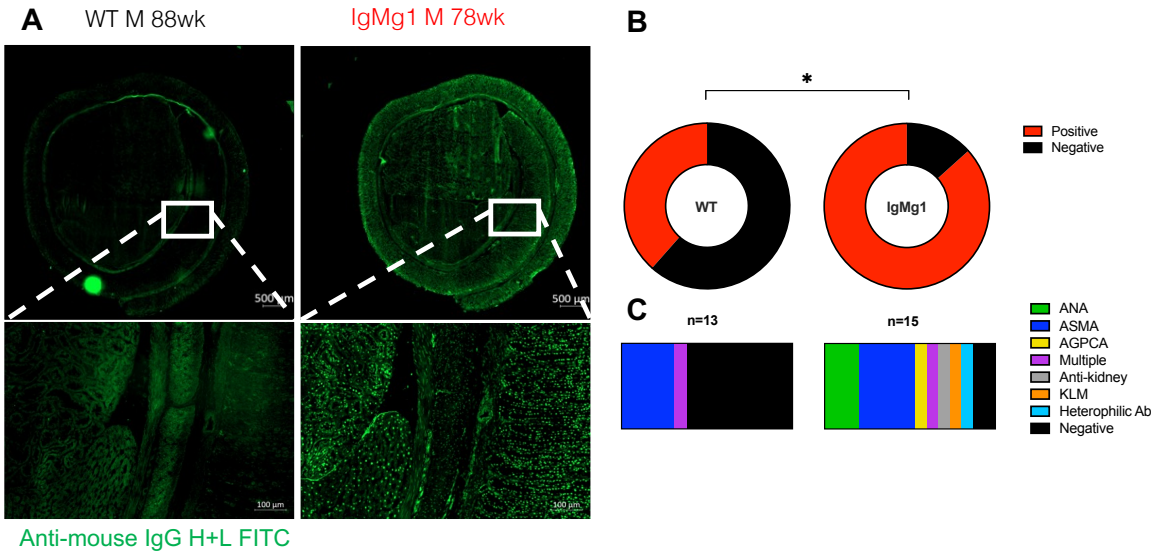
A
WT M 88wk
IgMg1 M 78wk
500 µm
100 µm
Anti-mouse IgG H+L FITC
B
*
WT
IgMg1
Positive
Negative
C
n=13
n=15
ANA
ASMA
AGPCA
Multiple
Anti-kidney
KLM
Heterophilic Ab
Negative

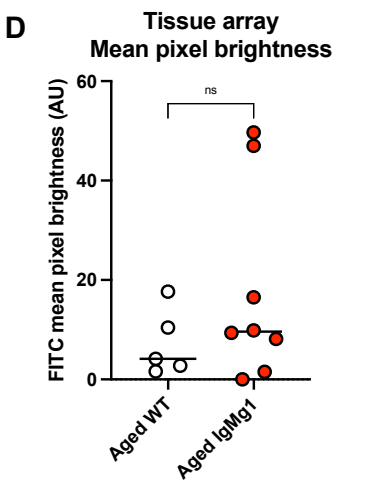
D
Tissue array
Mean pixel brightness
FITC mean pixel brightness (AU)
ns
Aged WT
Aged IgMg1

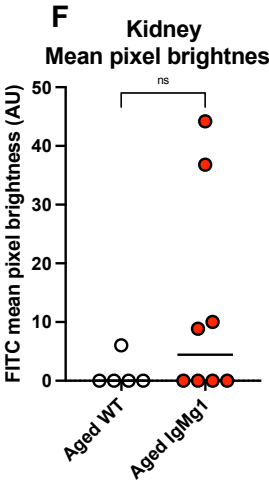
F
Kidney
Mean pixel brightness
FITC mean pixel brightness (AU)
ns
Aged WT
Aged IgMg1

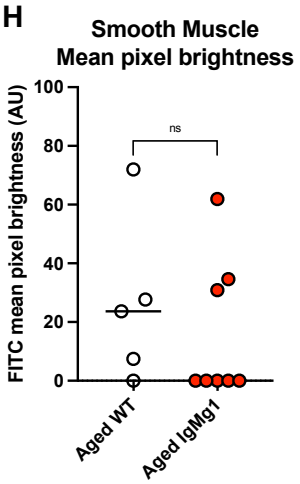
H
Smooth Muscle
Mean pixel brightness
FITC mean pixel brightness (AU)
ns
Aged WT
Aged IgMg1

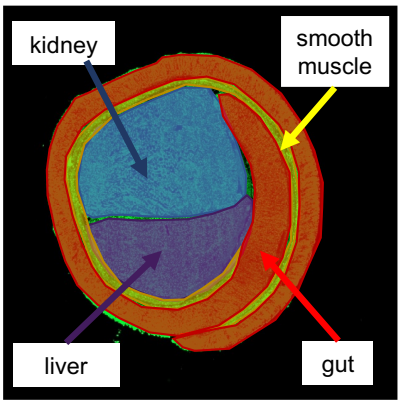
E
kidney
smooth muscle
liver
gut

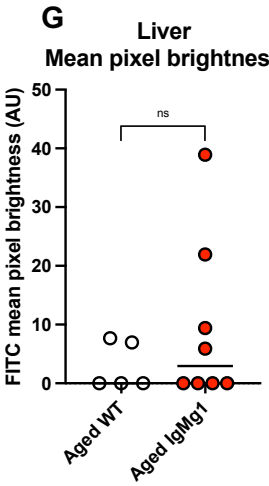
G
Liver
Mean pixel brightness
FITC mean pixel brightness (AU)
ns
Aged WT
Aged IgMg1

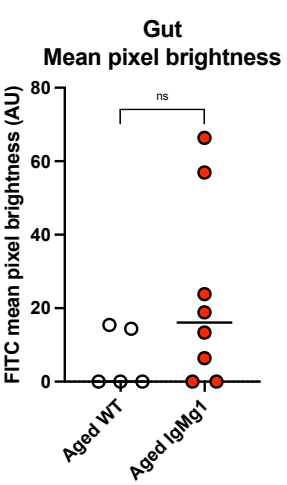
I
Gut
Mean pixel brightness
FITC mean pixel brightness (AU)
ns
Aged WT
Aged IgMg1

Figure 5.3 Tissue-specific autoantibodies increased in IgMg1 mice with ageing

Rat liver, kidney and stomach tissue slides were stained with sera from aged mice (aged 12-18 months old) and a FITC-conjugated anti-mouse IgG H+L secondary antibody to screen for presence of autoantibodies. (A) Example sections stained with aged WT serum (left) and aged IgMg1 serum (right). (B) Donut charts showing percentage of samples tested that were positive and negative for autoantibody. Statistical test performed by Fisher's exact test (*, $p < 0.05$). (C) Bar showing different types of autoantibodies identified in aged WT and IgMg1 sera (ANA – anti-nuclear antibody; ASMA – anti-smooth muscle antibody; AGPCA – anti-gastric parietal cell antibody; KLM - kidney-liver microsomal antibody). (D) Mean pixel brightness in the FITC channel across the tissue sections was measured using Fiji. Summary statistics shown. (E) Tissue section was segregated into kidney, liver, smooth muscle and gut by manually drawing regions of interest. Mean pixel brightness in the FITC channel in the individual tissues was then measured using Fiji. (F-I) Summary statistics shown for: (F) mean pixel brightness in kidney; (G) mean pixel brightness in liver; (H) mean pixel brightness in smooth muscle; (I) mean pixel brightness in gut. Each symbol represents one mouse. Statistical tests performed for D and F-I by unpaired two-tailed T-test (ns, not significant).

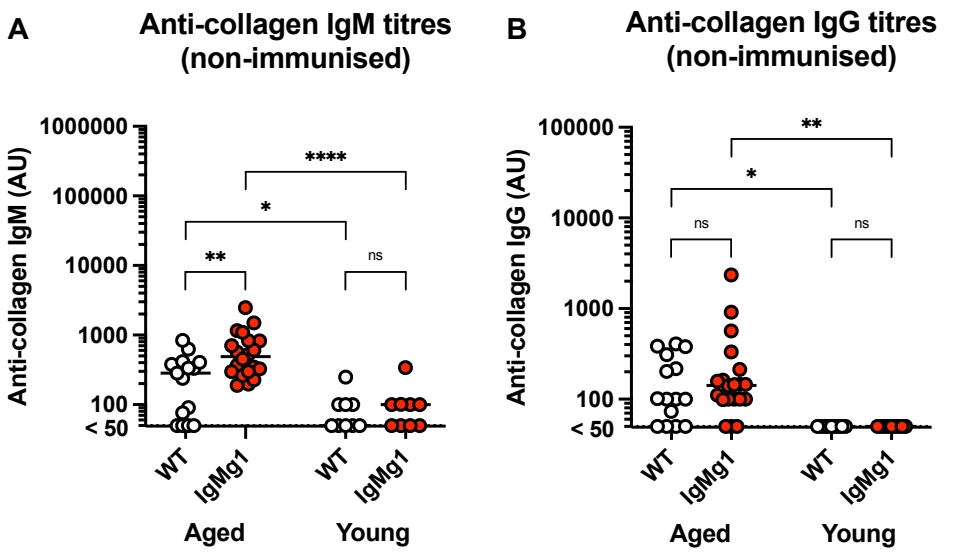

Figure 5.4 Anti-collagen antibody titres in non-immunised mice

Anti-collagen antibodies were measured in sera from non-immunised aged (aged 12-18 months old) and young adult (8-16 weeks old) mice by ELISA. Summary statistics for (A) anti-collagen IgG titres and (B) anti-collagen IgM titres. Each symbol represents one mouse. Statistical significance determined by 2-way ANOVA with Tukey's multiple comparison test (****, $p<0.0001$; **, $p<0.01$; *, $p<0.05$; ns, not significant).

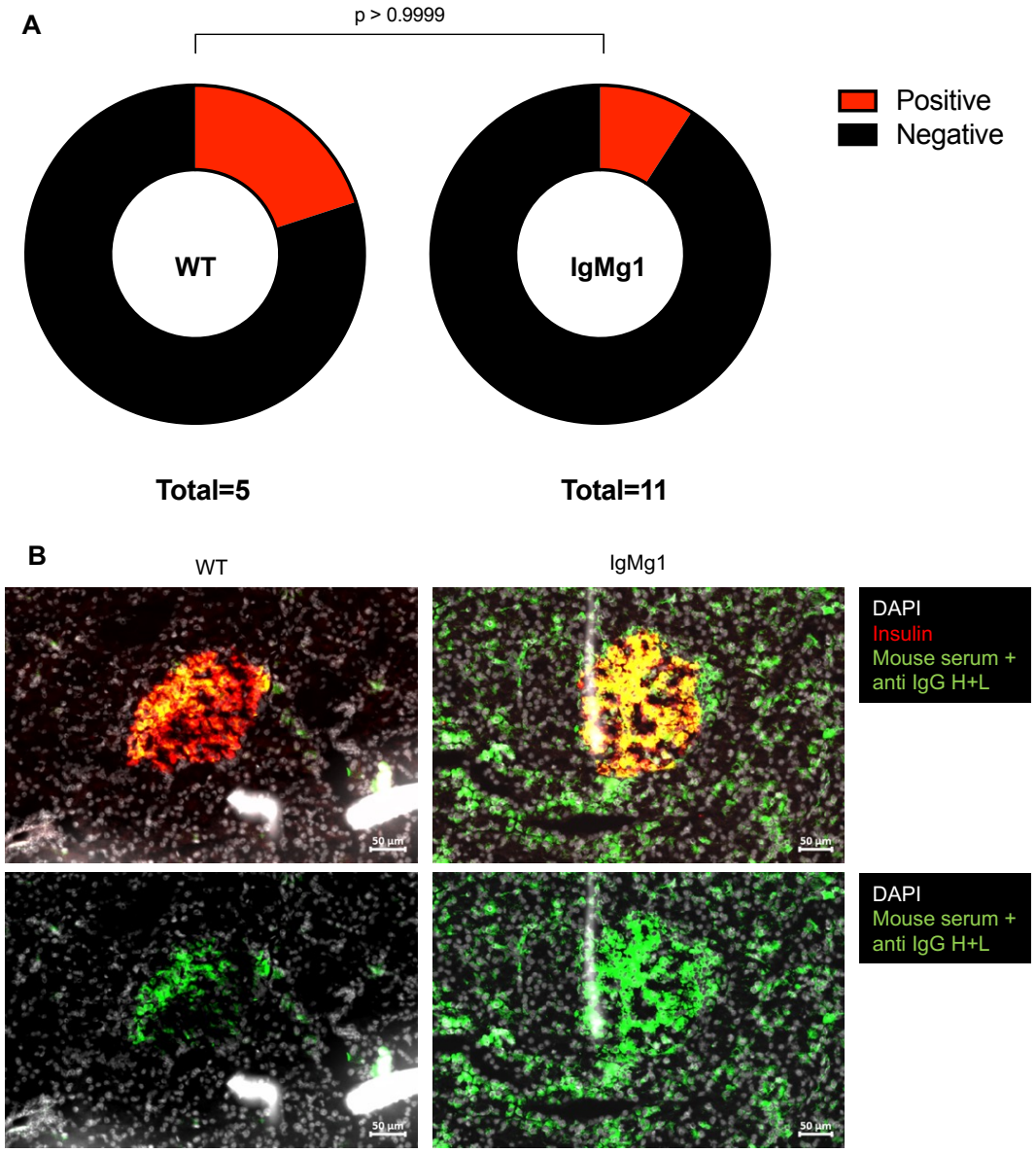

Figure 5.5 Identification of anti-islet antibodies in sera of aged mice

Rat pancreas sections were stained with anti-insulin antibody to identify islets and with sera from aged WT or IgMg1 mice (aged 12-18 months old). Slides were counterstained with DAPI. Anti-islet antibodies were identified by co-staining of mouse sera and anti-insulin antibody. (A) Summary showing samples positive and negative for anti-islet antibodies in sera from aged WT mice (n=5) and aged IgMg1 mice (n=11). Statistical test performed by Fisher's exact test ($p > 0.9999$). (B) Anti-islet antibody identified in WT sera (left) and IgMg1 sera (right). Top row shows staining with DAPI (white), anti-insulin antibody (red) and mouse serum (green), with co-staining of mouse serum and anti-insulin in yellow. Bottom row shows staining with DAPI and mouse serum only.

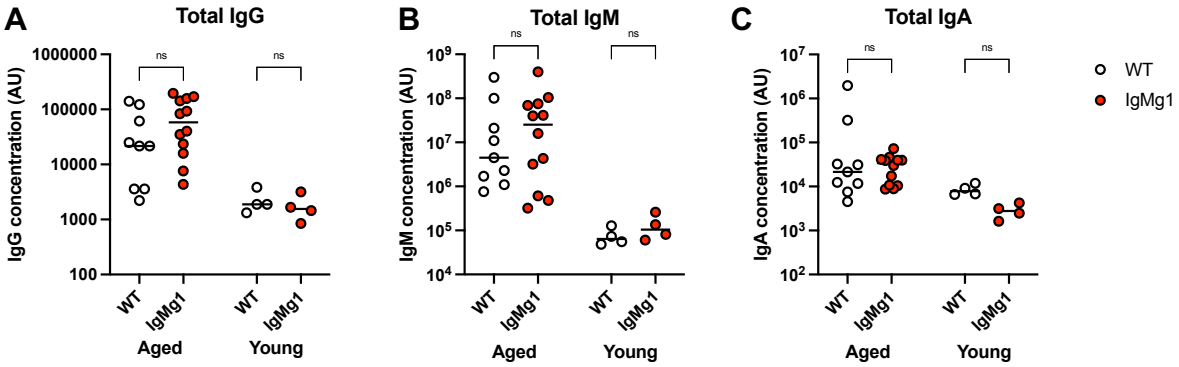

Figure 5.6 Total antibody in aged and young adult mouse sera

Total IgG, IgM and IgA were measured by ELISA in serum samples from aged (aged 12-18 months old) and young adult WT and IgMg1 mice. Summary statistics shown for (A) relative concentration of IgG; (B) relative concentration of IgM; (C) relative concentration of IgA. Each symbol represents one mouse. Statistical significance determined by 2way ANOVA with Tukey's multiple comparison test (ns, not significant).

5.2.3 GCs and plasma cells in spleens of aged mice

The increase in autoantibodies in aged IgMg1 mouse sera raised the question of whether spontaneous GCs and plasma cells would be increased in aged IgMg1 mice. Spontaneous GCs in the spleen have been found in autoimmune mouse strains, including non-obese diabetic (NOD) mice that spontaneously develop autoimmune diabetes, and several strains of mice that develop SLE-like disease (Luzina et al., 2001). Plasma cells are abundant in the spleen in several autoimmune mouse models, such as the NZ/B/W model of SLE (Hoyer et al., 2004) and the K/BxNSF model of autoantibody-dependent arthritis (Jang et al., 2011, 2016). To evaluate this, spleens from three cohorts of non-immunised aged mice (aged 12-18 months old) were analysed by flow cytometry (Figure 5.7A). The frequency of GC B cells and plasma cells had substantial variation between different cohorts of mice. However there appeared to be no significant increase in GC B cells or plasma cells in spleens from non-immunised aged IgMg1 mice compared with WT controls (Figure 5.7B and C).

To confirm the results of the flow cytometry, spleen sections were stained by fluorescent immunohistology for GCs (Fas^+ PNA^+) (Figure 5.8A) and plasma cells ($CD138^+$) (Figure 5.8B). GC and plasma cell areas were quantified using Fiji, showing that GCs and plasma cells were more abundant in spleens from aged mice (12-18 months old) than from young mice (8-16 weeks old), but that there were no significant differences in the frequency of GC B cells or plasma cells in the spleens of aged IgMg1 mice and WT mice (Figure 5.8C and D).

Overall, these data show that aged mice had more spontaneous GCs and plasma cells than young adult mice. However, despite the increased presence of autoantibodies in aged IgMg1 sera, IgMg1 mice did not have significantly more GCs or plasma cells than

aged WT mice. A caveat with these data is that the animal facility was specific pathogen free but not germ free. Therefore, the spontaneous GCs and plasma cells may be a result of a response to an infection rather than autoimmunity.

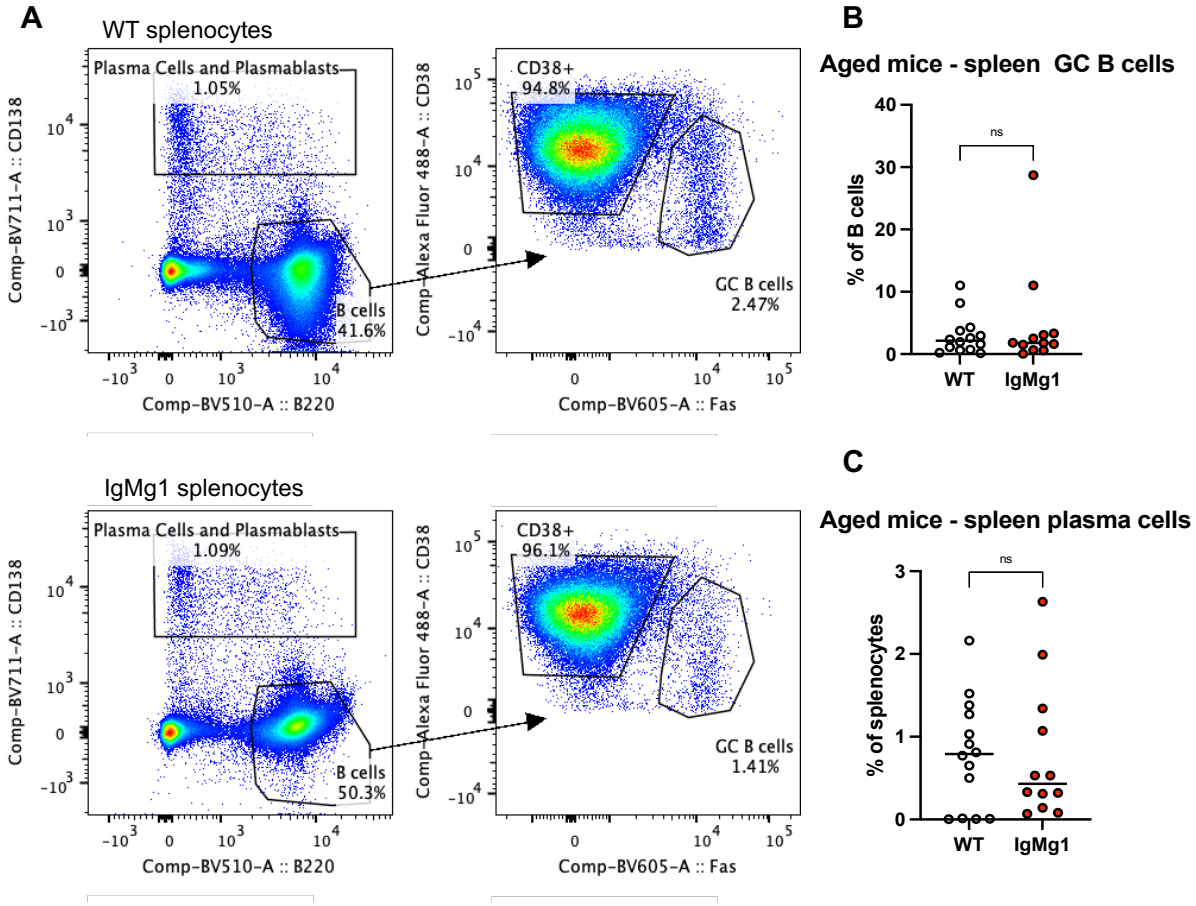

Figure 5.7 Flow cytometry analysis of splenic GC B cells and plasma cells in aged mouse spleens

Splenocytes from aged WT and IgMg1 mice were analysed for GC B cells and plasma cells by flow cytometry. (A) Representative flow cytometry plots showing GC B cells and plasma cells in aged WT and IgMg1 mice (aged 12-18 months old). From live splenocytes, plasma cells were gated as $CD138^{+}$ and B cells were gated as $B220^{+}$ $CD138^{-}$. From the B cells, GC B cells were gated as Fas^{+} $CD38^{-}$. (B-C) Summary statistics for (B) frequency of GC B cells as percentage of B cells; and (C) frequency of plasma cells as percentage of splenocytes. Results combined from three experiments. Each symbol represents one mouse. Statistical significance determined by unpaired two-tailed T-test (ns, not significant).

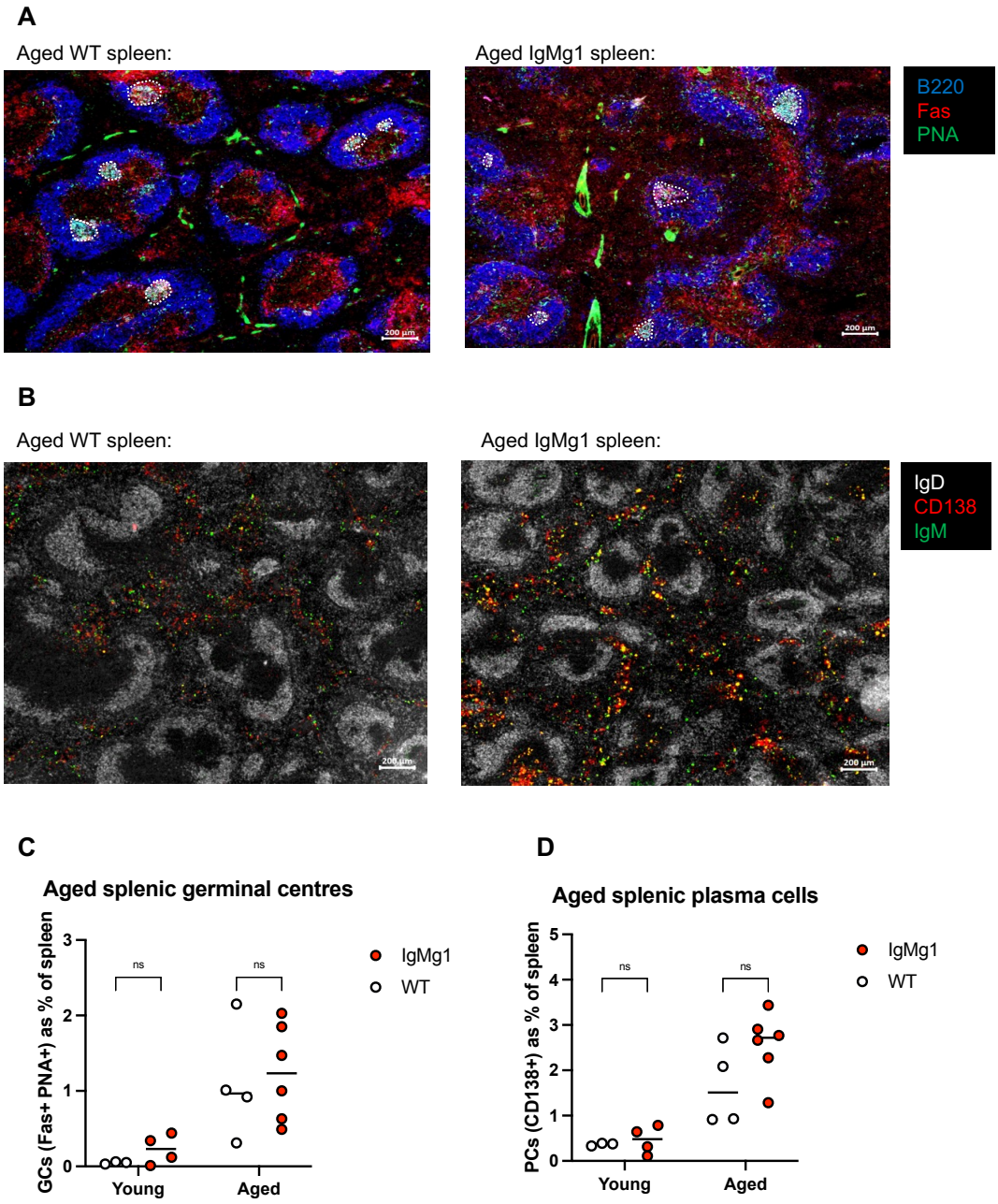

Figure 5.8 Fluorescent immunohistology analysis of GCs and plasma cells in aged mouse spleens

(A) Spleen sections from aged WT and IgMg1 mice (aged 12-18 months old) stained for B cells (B220) and GC B cells (Fas$^+$ PNA$^+$) with GCs outlined with dashed white lines. Representative images shown. Scale bar represents 200 µm. Images representative of 4-6 mice per group. (B) Spleen sections from aged WT and IgMg1 mice (aged 12-18 months old) stained for B cells (B220), plasma cells (CD138$^+$) and IgM. Representative images shown. Scale bar represents 200 µm. Images representative of 4-6 mice per group. (C-D) Areas of GC B cells and plasma cells quantified using Fiji. Summary statistics for: (C) GCs and (D) plasma cells as percentage of analysed area of spleen section for aged (12-18 months old) and young adult (8-16 weeks old) WT and IgMg1 mice. Each symbol represents one mouse. Statistical significance determined by 2way ANOVA with Tukey's multiple comparison test (ns, not significant).

5.2.4 Aged IgMg1 mice B cell development resembles B cell development in young adult IgMg1 mice

Aged IgMg1 mice had increased autoantibodies, and evidence of spontaneous GCs and PCs in the spleen, despite the anergic B cell phenotype. Therefore, B cell populations in aged mice were analysed by flow cytometry to determine if ageing had any impact on B cell development.

Bone marrow B cell development in aged IgMg1 and WT mice (aged 16-18 months old) was analysed using a similar gating strategy as used in chapter 3 with young adult mice. This allowed identification of pre-pro-B cells (fraction A), pro-B cells (fraction B and C), pre-B cells (fraction C' and D), immature B cells (fraction E), transitional B cells and mature B cells (fraction F) based on expression of surface markers (Hardy et al., 2000; Hardy, 2012) (Figure 5.9A). As shown in chapter 3, bone marrow B cell development in young adult IgMg1 mice appeared normal. As expected, bone marrow B cell development also appeared normal in aged IgMg1 nice. No significant differences were observed between aged IgMg1 and aged WT for any of the bone marrow B cell fractions, except a slight increase in transitional B cells in IgMg1 mice (Figure 5.9B-I). Of note, when bone marrow B cell development was investigated in young adult IgMg1 mice in section 3.2.1, there was an increased frequency of mature B cells (fraction F) compared with WT (Figure 3.2A). However, this was not evident in the aged mice (Figure 5.9I). A caveat with these data is that the experiment was underpowered as insufficient aged mice were available.

Splenic B cells from aged mice (aged 12-18 months old) were also analysed by flow cytometry (Figure 5.10A). As with the young adult IgMg1 mice, the frequency of marginal zone B cells was significantly decreased (Figure 5.10E), and the frequency

of follicular B cells in the aged IgMg1 mice was significantly increased compared to WT mice (Figure 5.10D). This showed that the mature B cell subsets remain altered as the IgMg1 mice aged. Additionally, as with young adult mice, aged IgMg1 mice appeared to have reduced splenic B-1 cells ($CD19^+$ $B220^-$ $CD43^+$ $CD23^-$) compared to aged WT mice (unpaired two-tailed T-test, $p = 0.0635$) (Figure 5.10B). Aged IgMg1 mice also had fewer age-associated $CD21^-$ $CD23^-$ B cells than aged WT mice (Figure 5.10F).

Surface IgM expression in splenic B cells was also examined (Figure 5.10G). IgM expression was found to be reduced in aged IgMg1 follicular and marginal zone B cells compared with aged WT B cells (Figure 5.10H and I). This indicates that the B cells in the IgMg1 mice likely still develop with an anergic phenotype as the mice aged. The percentage of lambda light chain expressing cells was also analysed in different B cell subsets (Figure 5.11A). There was no significant difference in lambda light chain expression frequency in the bone marrow immature B cells between the aged WT and aged IgMg1 mice (Figure 5.11B). However, in aged IgMg1 bone marrow transitional (Figure 5.11C) and mature B cells (Figure 5.11D) there was a significant increase in usage of lambda light chain, as well as in follicular B cells (Figure 5.11E) and marginal zone B cells (Figure 5.11F) in the spleen. Therefore, IgMg1 mice appear to continue to undergo increased negative selection during B cell development with ageing, and as with the young adult IgMg1 mice (Figure 3.7A-F) they have a higher lambda light chain usage from the bone marrow transitional B cell stage onwards.

These results indicate that the hyperactive BCR signalling in the IgMg1 mice caused similar B cell development in aged mice to what was observed in the young adult IgMg1

mice, with reduced marginal zone B cells and B-1 cells, reduced surface IgM expression, and increased lambda light chain gene usage.

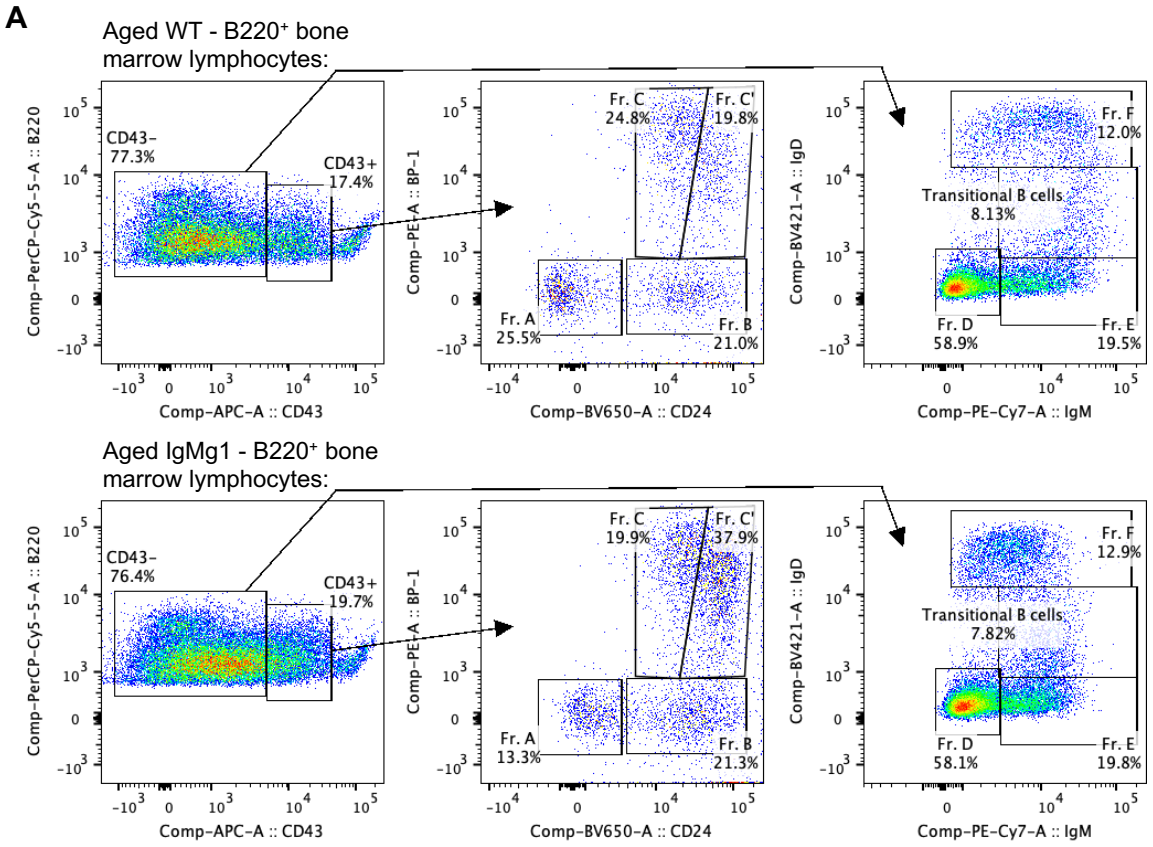
A
Aged WT - B220⁺ bone marrow lymphocytes:
CD43-
77.3%
CD43+
17.4%
Comp-PerCP-Cy5-5-A :: B220
Comp-APC-A :: CD43
Fr. C
24.8%
Fr. C'
19.8%
Fr. A
25.5%
Fr. B
21.0%
Comp-PE-A :: BP-1
Comp-BV650-A :: CD24
Fr. F
12.0%
Transitional B cells
8.13%
Fr. D
58.9%
Fr. E
19.5%
Comp-BV421-A :: IgD
Comp-PE-Cy7-A :: IgM
Aged IgMg1 - B220⁺ bone marrow lymphocytes:
CD43-
76.4%
CD43+
19.7%
Fr. C
19.9%
Fr. C'
37.9%
Fr. A
13.3%
Fr. B
21.3%
Fr. F
12.9%
Transitional B cells
7.82%
Fr. D
58.1%
Fr. E
19.8%

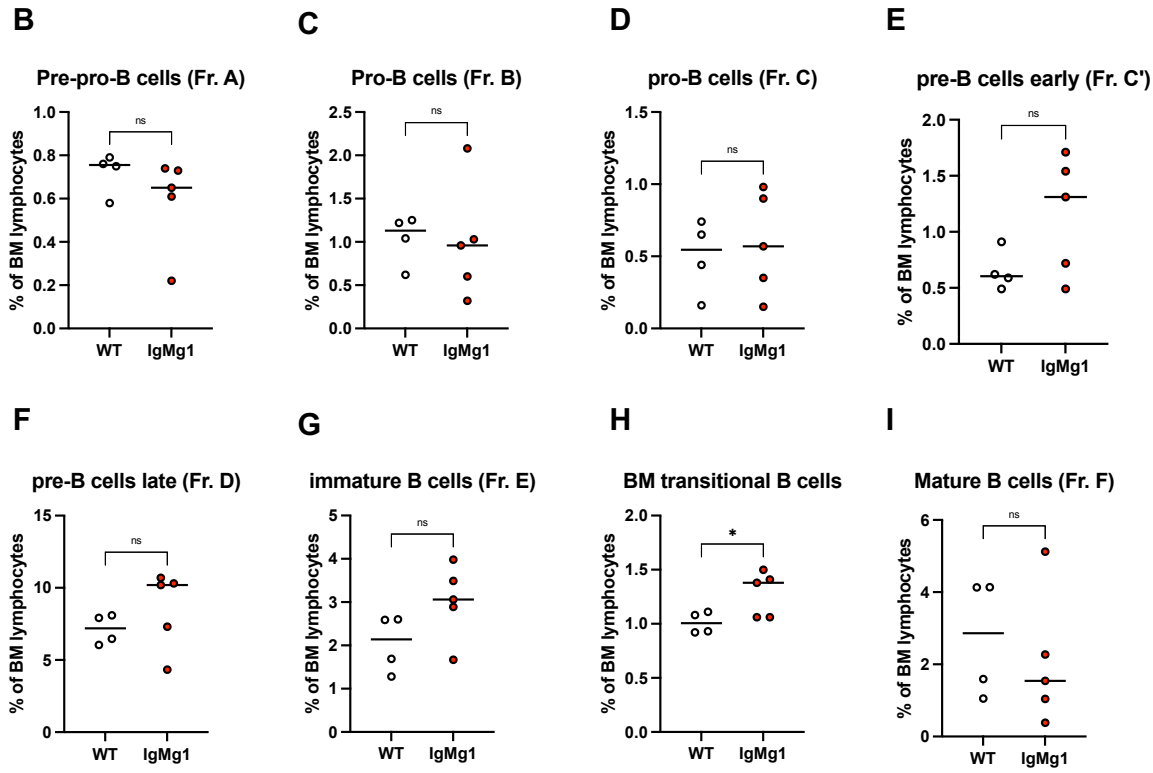
B
Pre-pro-B cells (Fr. A)
C
Pro-B cells (Fr. B)
D
pro-B cells (Fr. C)
E
pre-B cells early (Fr. C')
F
pre-B cells late (Fr. D)
G
immature B cells (Fr. E)
H
BM transitional B cells
I
Mature B cells (Fr. F)
% of BM lymphocytes
WT
IgMg1
ns
*

Figure 5.9 Bone marrow B cell development in aged WT and IgMg1 mice

Bone marrow from aged WT and IgMg1 mice was analysed by flow cytometry. (A) Gating strategy for identification of B cell populations in bone marrow for representative aged WT and IgMg1 mice. From From $B220^+$ $CD3^-$ $CD8^-$ $Gr1^-$ cells, fractions A to C' can be distinguished as $CD43^+$ and fractions D to F can be distinguished as $CD43^-$. $CD43^+$ cells can be split into fractions A to C' based on CD24 and BP-1 expression. Fractions D to F can be distinguished based on IgM and IgD expression. (B-I) Summary statistics showing: (B) frequency of pre-pro-B cells (fraction A) as percentage of bone marrow lymphocytes; (C) frequency of pro-B cells (fraction B) as percentage of bone marrow lymphocytes; (D) frequency of pro-B cells (fraction C) as percentage of bone marrow lymphocytes; (E) frequency of pre-B cells early (fraction C') as percentage of bone marrow lymphocytes; (F) frequency of pre-B cells late (fraction D) as percentage of bone marrow lymphocytes; (G) frequency of immature B cells (fraction E) as percentage of bone marrow lymphocytes; (H) frequency of transitional B cells as percentage of bone marrow lymphocytes; (I) frequency of mature B cells as percentage of bone marrow lymphocytes. Data from one experiment. Each symbol represents one mouse. Statistical tests were performed by two-tailed unpaired T-test for comparison of two groups (*, $p < 0.05$; ns, not significant).

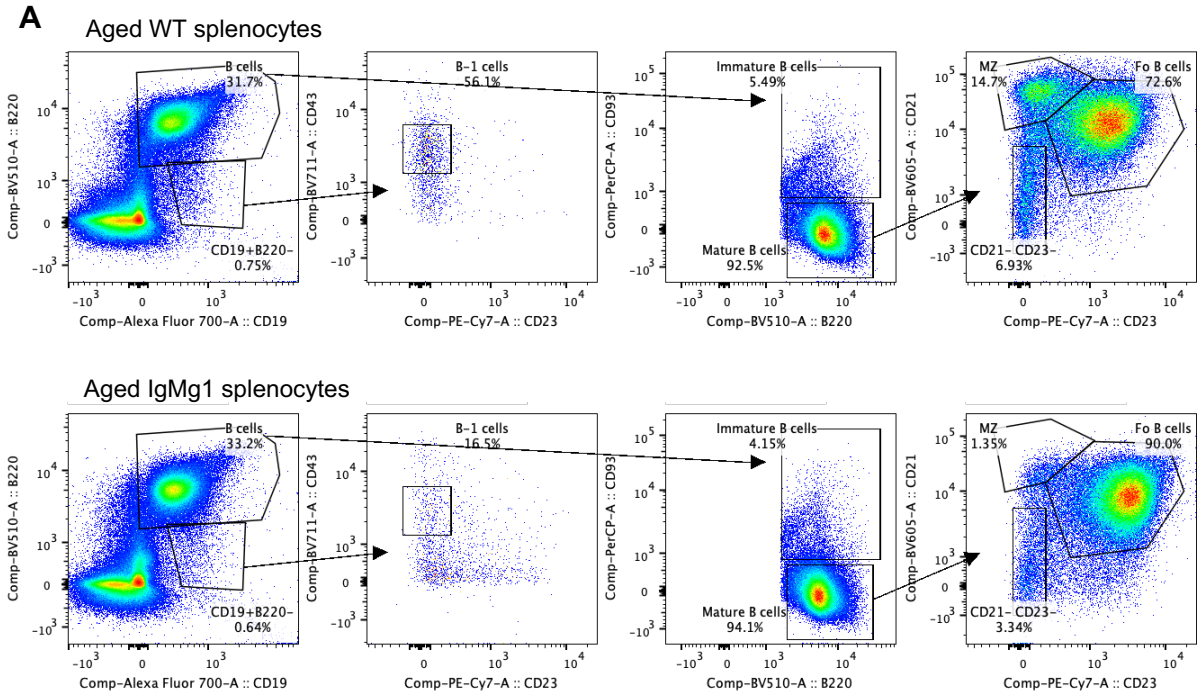
A
Aged WT splenocytes
B cells
31.7%
B-1 cells
56.1%
Immature B cells
5.49%
MZ
14.7%
Fo B cells
72.6%
CD19+B220-
0.75%
Mature B cells
92.5%
CD21- CD23-
6.93%
Comp-BV510-A :: B220
Comp-Alexa Fluor 700-A :: CD19
Comp-BV711-A :: CD43
Comp-PE-Cy7-A :: CD23
Comp-PerCP-A :: CD93
Comp-BV510-A :: B220
Comp-BV605-A :: CD21
Comp-PE-Cy7-A :: CD23
Aged IgMg1 splenocytes
B cells
33.2%
B-1 cells
16.5%
Immature B cells
4.15%
MZ
1.35%
Fo B cells
90.0%
CD19+B220-
0.64%
Mature B cells
94.1%
CD21- CD23-
3.34%

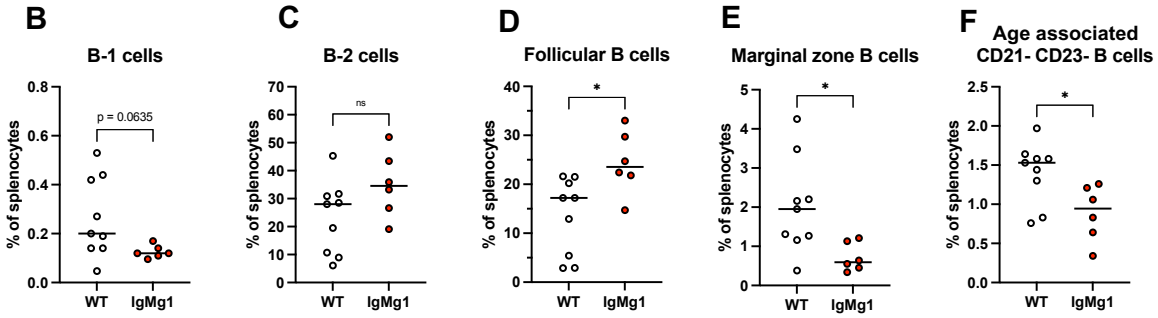
B
B-1 cells
p = 0.0635
% of splenocytes
WT
IgMg1
C
B-2 cells
ns
D
Follicular B cells
*
E
Marginal zone B cells
*
F
Age associated
CD21- CD23- B cells
*

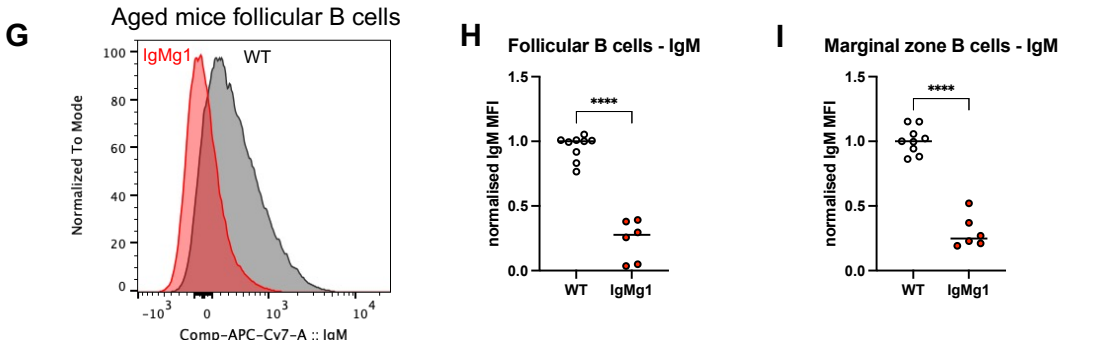
G
Aged mice follicular B cells
IgMg1
WT
Normalized To Mode
Comp-APC-Cy7-A :: IgM
H
Follicular B cells - IgM
****
normalised IgM MFI
I
Marginal zone B cells - IgM
****

Figure 5.10 Spleen B cell development in aged WT and IgMg1 mice

Splenocytes from aged WT and IgMg1 mice were analysed by flow cytometry. **(**A) Representative gating in WT, IgG1M and IgMg1 mice. From splenocytes, $CD19^+$ $B220^-$ cells and $B220^+$ $CD19^+$ (B-2 cells) were gated. From $CD19^+$ $B220^-$ cells, B-1 cells were gated as $CD43^+$ $CD23^-$. From B-2 cells, mature B cells were gated as $CD93^-$. From mature B cells, follicular B cells were gated as $CD23^+$ $CD21^+$, marginal zone B cells were gated as $CD21^{hi}$ $CD23^-$ and $CD21^-$ $CD23^-$ cells were gated as $CD21^-$ $CD23^-$ B cells. (B-F) Summary statstics showing frequencies of: (B) B-1 cells; (C) B-2 cells; (D) follicular B Cells; (E) marginal zone B cells; (F) $CD21^-$ $CD23^-$ B cells. All shown as percentage of splenocytes. (G-I) IgM expression in follicular and marginal zone B cells was assessed by flow cytometry. (G) Histograms showing IgM expression on follicular B cells for representative aged WT and IgMg1 mice. (H-I) Summary statistics showing IgM expression in: (H) follicular B cells and (I) marginal zone B cells. Data are normalised to the WT to correct for differences between experiments. Data combined from two experiments. Each symbol represents one mouse. Statistical tests were performed by two-tailed unpaired T-test for comparison of two groups (****, $p < 0.0001$; *, $p < 0.05$; ns, not significant).

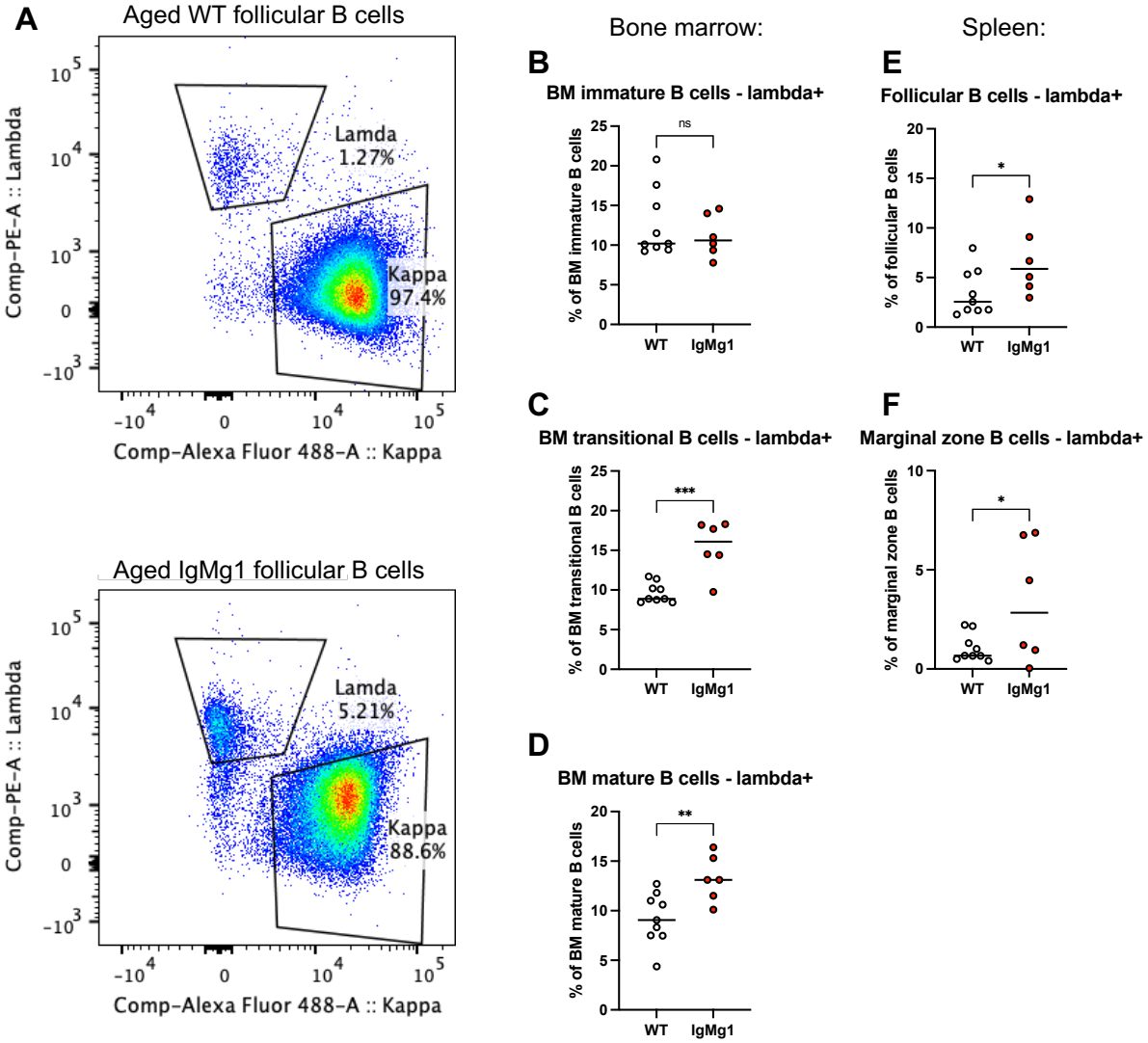

Figure 5.11 Lambda light chain usage in aged WT and IgMg1 mice

B cell subsets in aged WT and IgMg1 mice were stained with anti-kappa and lambda antibodies to assess lambda light chain usage. Bone marrow immature, transitional and mature B cells gated as shown in Figure 5.9. Spleen follicular B cells and marginal zone B cells gated as shown in Figure 5.10. (A) Representative plots showing lambda and kappa light chain expression in follicular B cells. (B-F) Summary statistics showing: (B) percentage of lambda$^+$ immature bone marrow B cells; (C) percentage of lambda$^+$ transitional bone marrow B cells; (D) percentage of lambda$^+$ mature bone marrow B cells; (E) percentage of lambda$^+$ splenic follicular B cells; (F) percentage of lambda$^+$ splenic marginal zone B cells. Data combined from two experiments. Each symbol represents one mouse. Statistical significance determined by unpaired two-tailed T-tests (***, p<0.001; **, p<0.01; *, p<0.05; ns, not significant).

5.2.5 No strong evidence of increased health problems in IgMg1 mice

Due to the increased risk of developing autoantibodies, it was hypothesised that IgMg1 mice may have more health problems with ageing. To test this, a cohort of IgMg1 and WT mice were aged and monitored for any health issues requiring them to be euthanised. Although at around 60-70 weeks of age the IgMg1 mice had slightly lower survival than WT mice, this was not statistically significant (Figure 5.12). At this timepoint, the mice were used for an immunisation, therefore no further events were recorded. If the experiment were run for longer the results may have been different. Therefore, it is not possible to conclude that IgMg1 mice have an increased risk of developing health problems related to the increased autoantibodies and further work is required to confirm.

Autoimmunity is an important cause of recurrent pregnancy loss (Gao et al., 2021). Therefore, breeding records for IgMg1 and WT mice were analysed to determine if the increased risk of developing autoantibodies was associated with reproductive or fertility problems. Eight pairs of WT breeders and thirteen pairs of IgMg1 breeders over a period of two years were included in the analysis. There were no significant differences in the number of litters per pair, total pups, average litter size or litter survival (Figure 5.13A-H). Data for the first litter from each pair were also analysed separately. Again, there were no significant differences in first litter size or survival (Figure 5.13I-L) and the time taken from pairing for the first litter to be born was slightly reduced for the IgMg1 pairs (unpaired two-tailed T-test, $p = 0.0662$) (Figure 5.13M). The average time between all litters was analysed to determine if IgMg1 breeding pairs took longer to produce litters, however there was no difference. Finally, the total time from pairing

until production of fourth or fifth litter was also not significantly different. Therefore, there was no evidence of breeding problems for IgMg1 mice.

Overall, these data indicate that the apparent increase in serum autoantibodies seen as IgMg1 mice age does not result in any increased illness as mice age. Further, there is no significant increase in reproductive fertility issues.

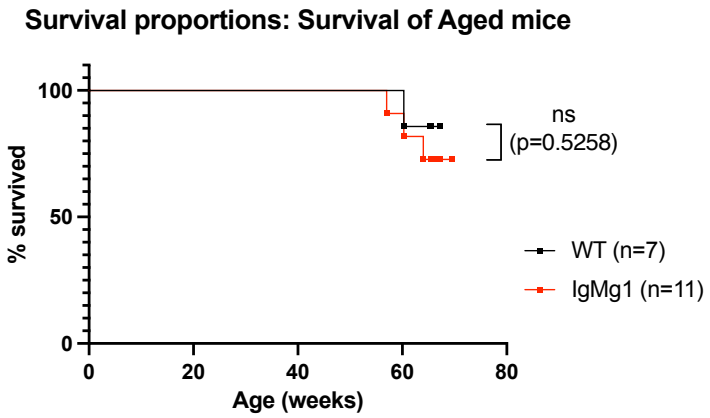

Figure 5.12 Survival of WT and IgMg1 mice

Survival curve showing survival of a cohort of WT and IgMg1 mice. Mice were monitored daily for signs of illness and euthanised by schedule 1 method if they became sick.

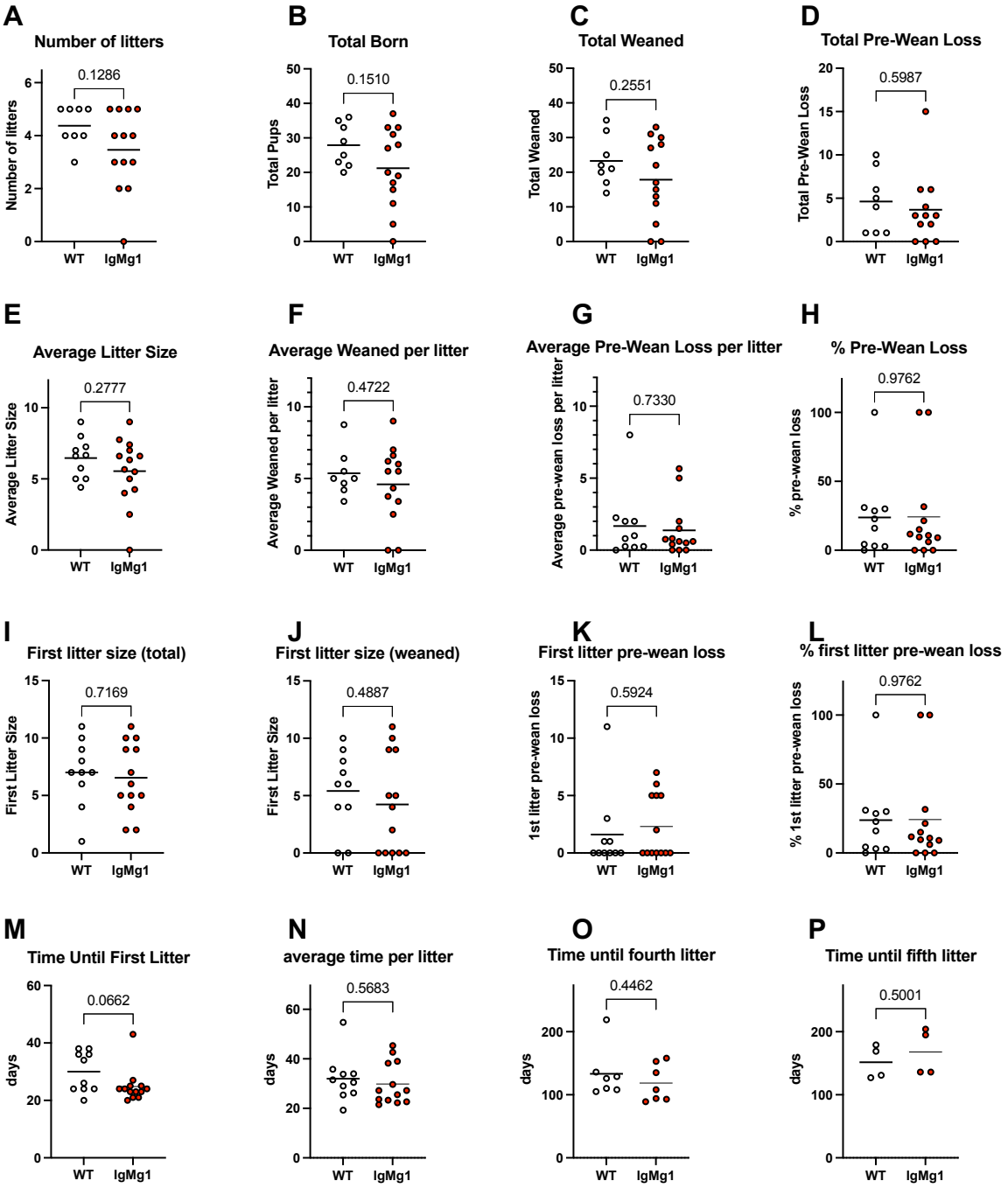

Figure 5.13 Breeding records for IgMg1 breeders

Litter sizes and survival from WT and IgMg1 breeding pairs over a two-year period were analysed. Summary statistics for: (A) number of litters; (B) total pups born; (C) total pups weaned; (D) total pre-weaned pups lost; (E) average litter size; (F) averaged pups weaned per litter; (G) average number of pups lost pre-weaned per litter; (H) percentage of pre-weaned pups lost; (I) first litter size; (J) pups weaned in first litter; (K) pre-weaned pups lost in first litter; (L) percentage of pups lost pre-weaned from first litter; (M) time taken from pairing for first litter to be born; (N) average time between litters; (O) time taken from pairing for fourth litter to be born; (P) average time taken from pairing for fifth litter to be born. Each symbol represents one breeding pair. Statistical tests performed by unpaired T-test with p-values indicated.

5.2.6 No evidence of autoimmune diabetes in aged IgMg1 mice

As autoantibodies were increased in aged IgMg1 mice, tissues from aged mice were examined for any signs of autoimmune disease by immunohistology. One tissue where autoimmunity may be observed is the pancreas, where type I diabetes mellitus can develop. Autoimmune diabetes is characterised by destruction of the islets of Langerhans that secrete insulin because of an autoimmune response against beta-cells (Graham et al., 2012), and this is also seen in the NOD mouse model of type I diabetes (Pechhold et al., 2009; Novikova et al., 2013). Therefore, pancreas sections from aged IgMg1, aged WT, and young adult mice were stained with anti-insulin antibody to visualise the islets. Insulin$^+$ islets were found in both aged WT and aged IgMg1 mice (Figure 5.14A and B), suggesting they were not being destroyed. Pancreas sections were also stained for lymphocyte infiltration of B cells (B220$^+$) and T cells (TCRβ^+), and plasma cells (CD138$^+$), as insulitis (infiltration of lymphocytes) is a pathological hallmark of type I diabetes (Pugliese, 2016) and the NOD model (Hancock et al., 1995). Staining of spleen sections as a positive control showed presence of B cells, T cells and plasma cells. However, there was no evidence of B cells, T cells or plasma cells in any of the stained pancreases (Figure 5.14A and B). Finally, as hyperglycaemia is a symptom of diabetes, and is used for diagnosis (Stumvoll et al., 2005), glucose concentration was measured in the serum of the mice. There was no difference in glucose concentration observed between aged IgMg1, aged WT mice, or the young adult controls (with the caveat that the mice had not been fasting prior to being culled) (Figure 5.15). Taken together these results indicate no evidence that IgMg1 mice are prone to autoimmune diabetes as they age.

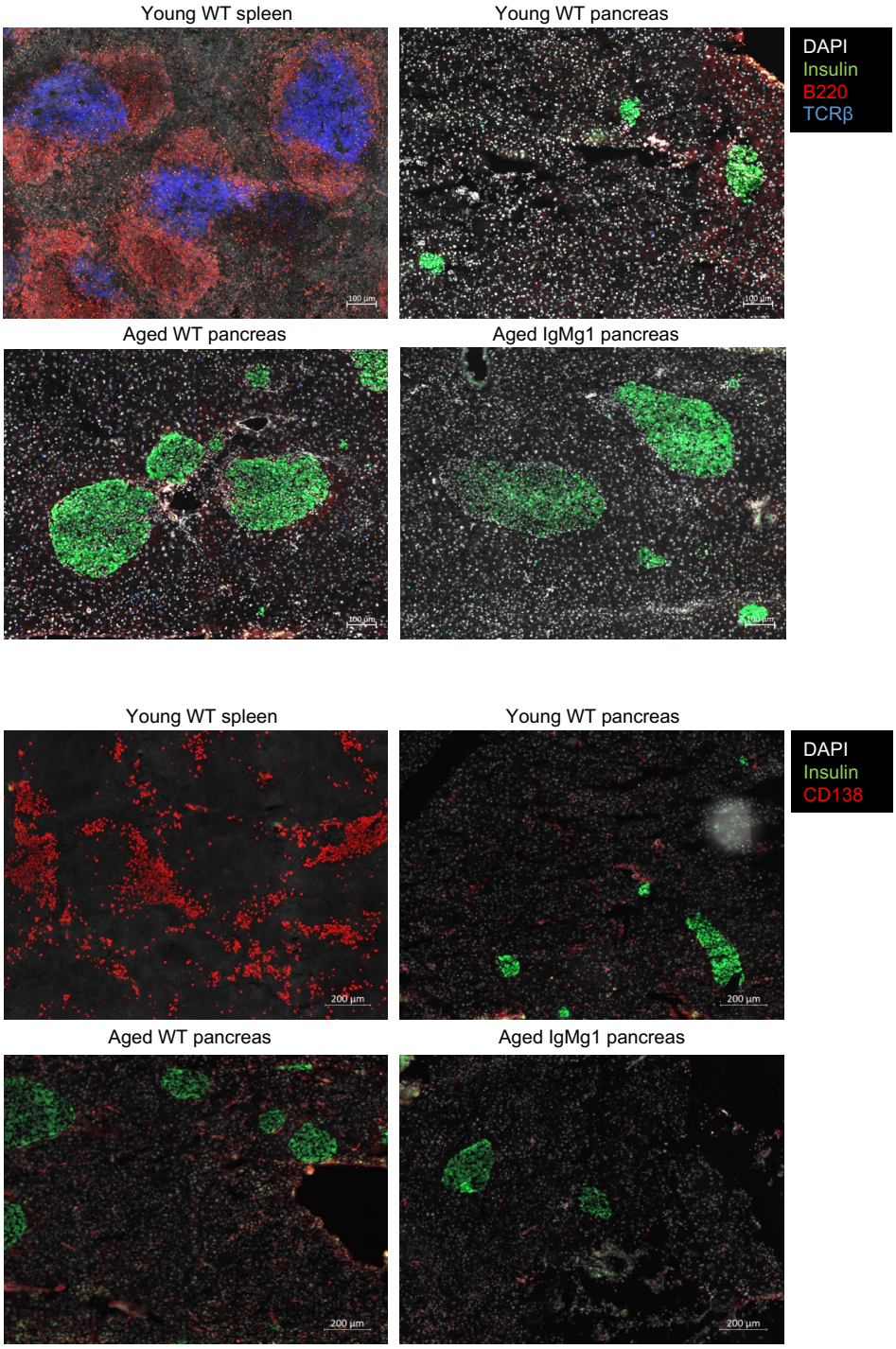

Figure 5.14 No evidence of lymphocyte infiltration in aged IgMg1 or WT pancreases

(A) Pancreas sections from young adult WT and aged WT and IgMg1 mice stained for B cells (B220), T cells (TCRβ) and islets (insulin). Spleen stained as positive control for B220 and TCRβ antibodies and negative control for insulin. Representative images shown. Scale bar represents 100 µm. Images representative of 4 mice per group. (B) Pancreas sections from young adult WT and aged WT and IgMg1 mice stained for plasma cells (CD138) and islets (insulin). Spleen stained as positive control for CD138 antibodies and negative control for insulin. Representative images shown. Scale bar represents 200 µm. Images representative of 4 mice per group.

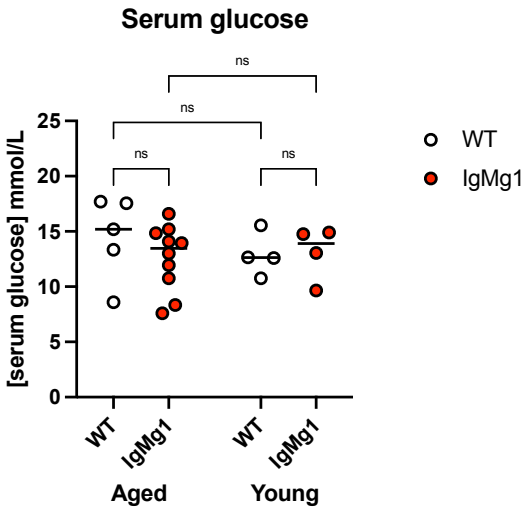

Figure 5.15 Serum glucose concentration not elevated in aged IgMg1 mice

Glucose concentration was measured in sera of aged and young adult WT and IgMg1 mice. Summary statistics showing glucose concentration. Each dot represents one mouse (mean of two measurements). Statistical significance determined by 2way ANOVA with Tukey's multiple comparison test (ns, not significant).

5.2.7 No evidence of lymphocyte infiltration in aged IgMg1 liver

Autoimmune hepatitis is associated with infiltration of lymphocytes and plasma cells (Vergani and Mieli-Vergani, 2008). Therefore, liver sections from aged mice (12-18 months old) were stained by fluorescence immunohistology for presence of B cells ($B220^+$), $CD4^+$ T cells, $CD8^+$ T cells and plasma cells ($CD138^+$). Staining of spleen sections as a positive control showed presence of B cells, $CD4^+$ and $CD8^+$ T cells, and plasma cells. Although the B220-FITC antibody had high background in the liver sections, this was non-specific binding and therefore no B cells were identified in either aged WT or aged IgMg1 liver (Figure 5.16A). Similarly, no T cells or plasma cells were found (Figure 5.16A and B). Therefore, no evidence of liver autoimmunity was found. However, the B cell staining was not optimal, making it difficult to confirm there were no B cell infiltrates. Ideally alternative B cell markers could have been used.

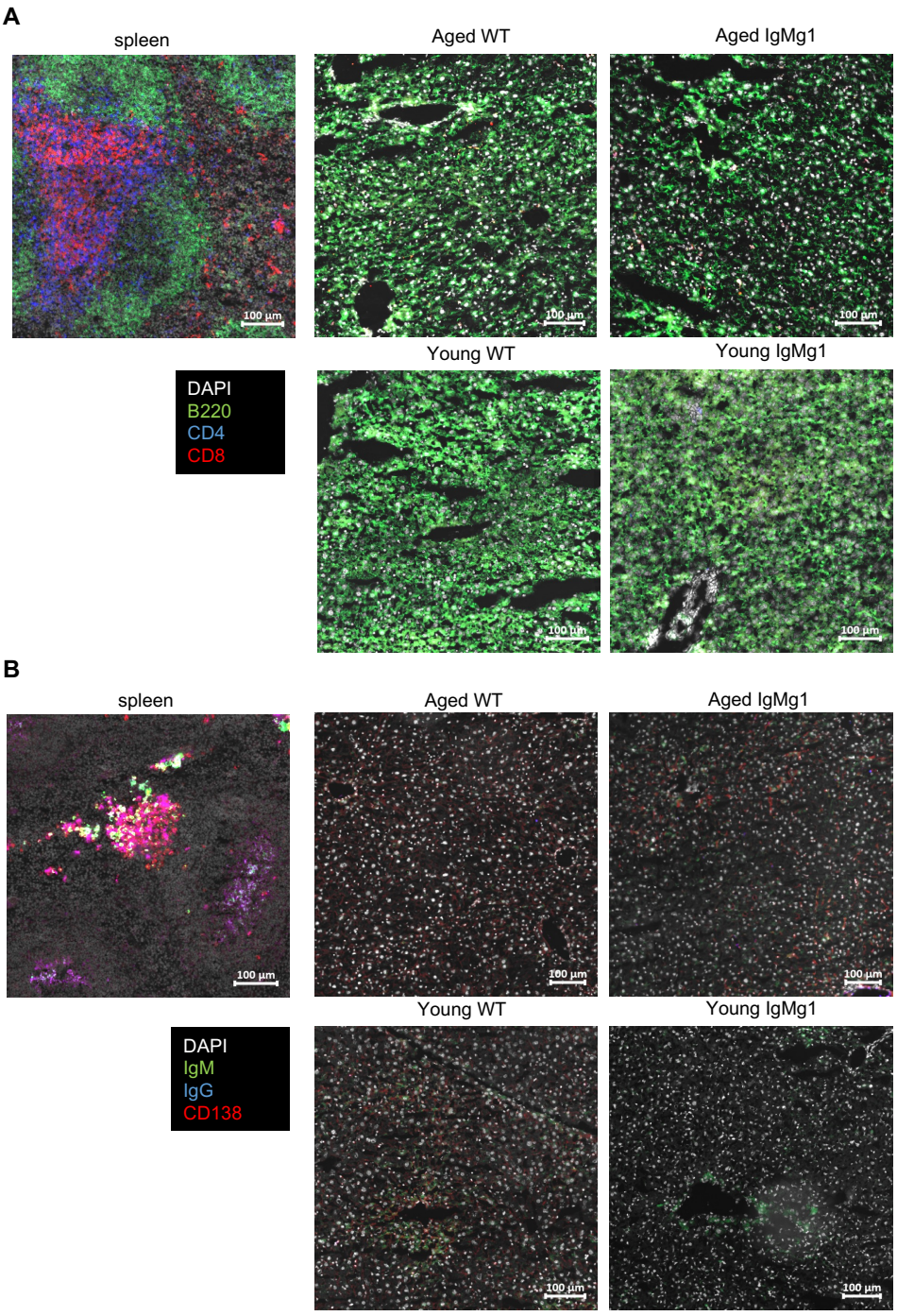

Figure 5.16 No evidence of lymphocyte infiltration into aged WT and IgMg1 liver

(A) Liver sections were stained for B cells (B220), CD4 T cells and CD8 T cells, and counterstained with DAPI. Sections from aged WT and IgMg1 and young adult WT and IgMg1 mice are shown. Spleen section shown as a positive control for antibody staining. Scale bar represents 100 µm. Images representative of 3-4 mice per group. (B) Spleen sections were stained for IgG^+ and IgM^+ plasma cells (CD138), and counterstained with DAPI. Areas of liver from aged WT and IgMg1 and young adult WT and IgMg1 mice are shown. Spleen section shown as a positive control for antibody staining. Scale bar represents 100 µm. Images representative of 3-4 mice per group.

5.2.8 Immune complexes in glomeruli of aged mice, but no significant difference between WT and IgMg1

Lupus nephritis is an autoimmune disease of the kidney and is characterised by T cell infiltration (Couzi et al., 2007; Hsieh et al., 2011; Alexopoulos et al., 1990; Tilstra et al., 2018), B cell infiltration and formation of spontaneous germinal centres (Shim et al., 2004). Given that, the kidneys of aged IgMg1 mice were analysed for any signs of autoimmunity. Kidney sections from aged IgMg1 and WT mice (12-18 months old), and young adult controls (8-16 weeks old), were stained for B220, CD4 and CD8 to look for B cell, $CD4^+$ T cell and $CD8^+$ T cell infiltration respectively. Staining of a spleen section as a positive control showed presence of B cells, $CD4^+$ and $CD8^+$ T cells. However, there was no evidence of any lymphocyte infiltration in the aged kidneys (Figure 5.17A). As infiltration of other immune cells is important in development of inflammatory kidney disease (Duffield, 2010; Rogers et al., 2014; Gorenjak, 2009; Xing et al., 2010), kidney sections from the aged IgMg1 mice were also stained for F4/80, Ly6G and CD11c to test for infiltrating macrophages, neutrophils and dendritic cells, respectively. Staining of a spleen section as a positive control showed presence of macrophages, neutrophils and dendritic cells. However, none were observed in either the aged IgMg1 or WT mouse kidneys (Figure 5.17B).

IgM deposits are frequently found in the glomeruli of patients with a wide range of kidney diseases and are often associated with complement components (Strassheim et al., 2013). Therefore, kidney sections were also stained for IgM and complement proteins C1q and C3. Glomeruli were identified by co-staining with podoplanin, a marker for glomerular podocytes (Breiteneder-Geleff et al., 1997). Both aged WT and IgMg1 kidneys were positive for C1q and C3, which co-localised with the IgM and the

podoplanin (Figure 5.18A). Fiji was used to analyse the intensity of the staining for IgM, C1q and C3 within the podoplanin^{+} glomeruli. However, there were no significant differences between IgMg1 and WT mice for staining of any of these (Figure 5.18B-D).

Overall, these data show that IgM and complement deposits are found in the glomeruli of aged mice, which may indicate kidney disease. However, there is no evidence that this is significantly more severe in aged IgMg1 mice compared with aged WT mice.

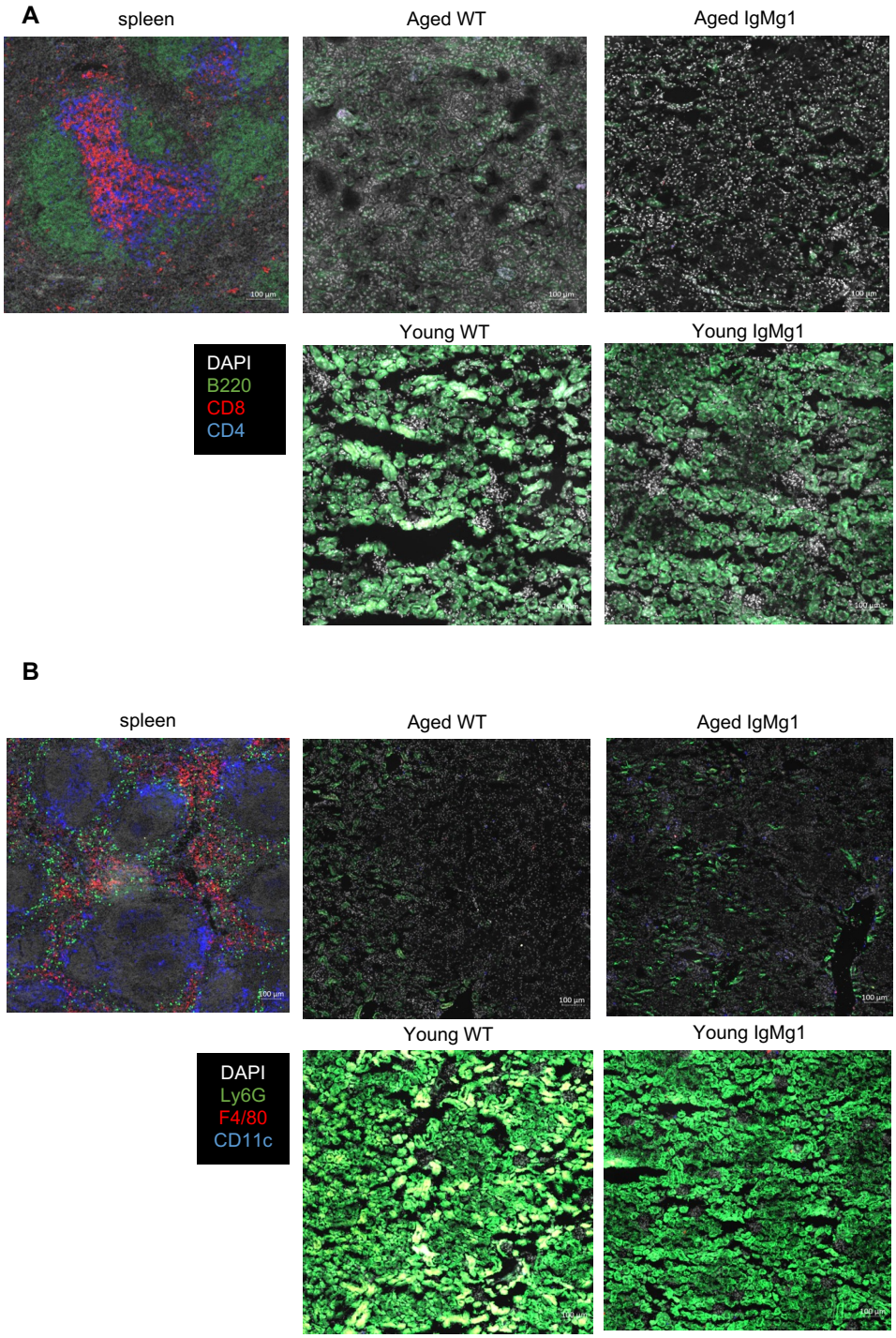

Figure 5.17 No evidence of immune cell infiltration into kidneys of aged IgMg1 mice

(A) Kidney sections were stained for B cells (B220), CD4 T cells and CD8 T cells, and counterstained with DAPI. Sections of kidney from aged WT and IgMg1 and young adult WT and IgMg1 mice are shown. Spleen section shown as a positive control for antibody staining. Scale bar represents 100 µm. Images representative of 4 mice per group. (B) Kidney sections were stained for neutrophils (Ly6G), dendritic cells (CD11c) and macrophages (F4/80), and counterstained with DAPI. Sections of kidney from aged WT and IgMg1 and young adult WT and IgMg1 mice are shown. Spleen section shown as a positive control for antibody staining. Scale bar represents 100 µm. Images representative of 4 mice per group.

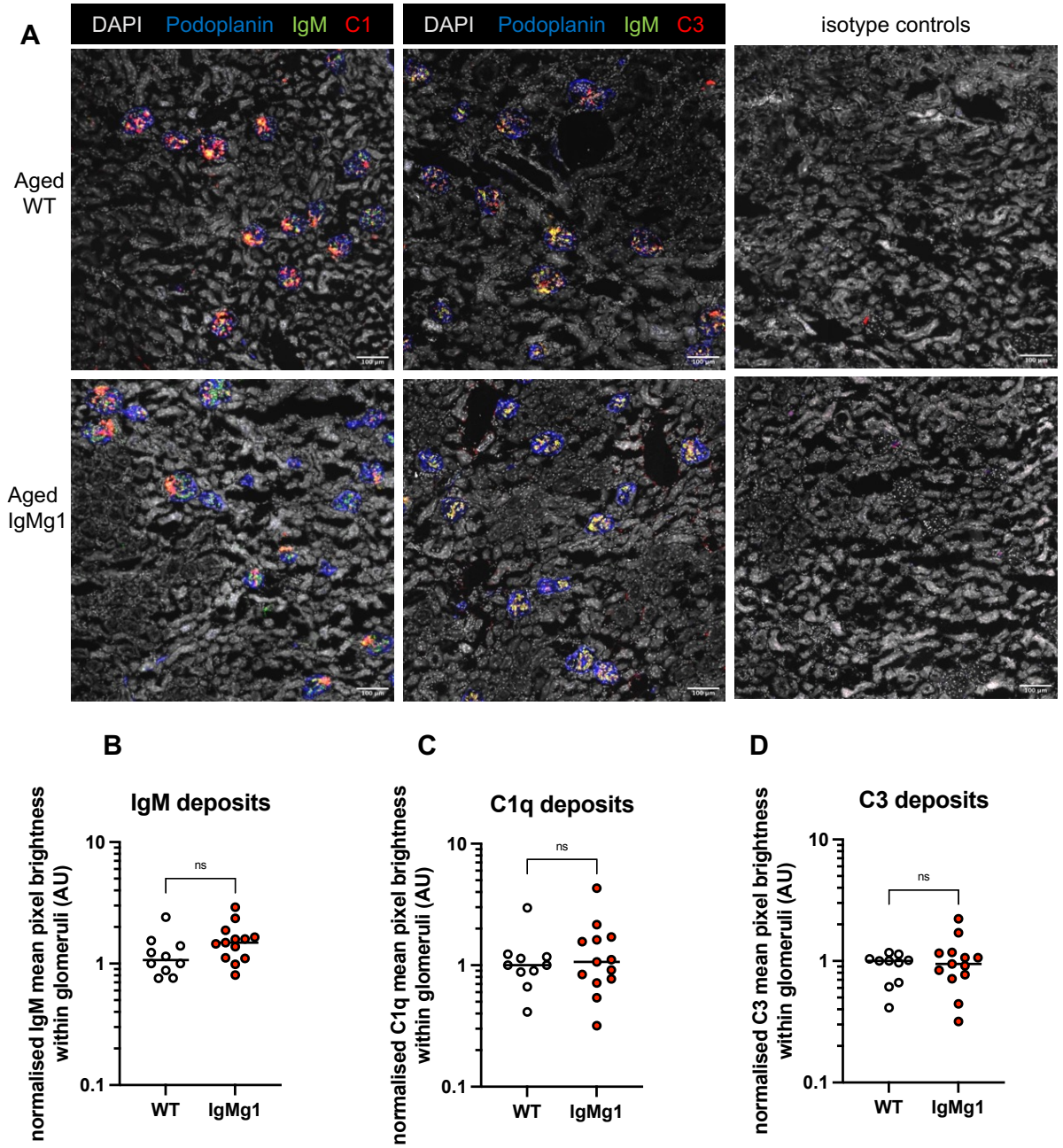

Figure 5.18 IgM and complement deposits in glomeruli of aged WT and IgMg1 mice

(A) Kidney sections from aged mice were stained for podoplanin, IgM and either C3 or C1q, and counterstained with DAPI. Areas of kidney from aged WT and IgMg1 mice are shown. Scale bar represents 100 µm. Images representative of 10-13 mice per group. (B-D) Glomeruli were identified in Fiji by podoplanin staining. The mean pixel brightness for IgM, C1q and C3 staining were measured within the glomeruli. Summary statistics shown for: (B) IgM median MFI per glomerulus; (C) C1q median MFI per glomerulus; (D) C3 median. Data are combined from two experiments and are presented as normalised to WT for each experiment. Each symbol represents one mouse. Statistical significance determined by unpaired two-tailed T-test (ns, not-significant).

5.2.9 Aged IgMg1 mice do not make an increased anti-collagen response following immunisation

Although young adult IgMg1 mice did not make an increased anti-collagen antibody response following immunisation (section 5.2.1), there was evidence of increased autoantibodies in aged IgMg1 mice (section 5.2.2). Therefore, it appeared that with ageing, the IgMg1 mice were more prone to a breach in B cell tolerance. To test if this was the case, a group of 14-16 month old mice were immunised with chicken collagen type II. Mice were primed with chicken collagen type II precipitated in alum and heat inactivated *B. pertussis*, and then boosted twice at three-week intervals with soluble chicken collagen type II (Figure 5.19A). This protocol was chosen as it was able to raise an anti-collagen response in young adult mice (as shown in Figure 5.1).

Draining lymph nodes at day 50 (8 days after the second boost) were analysed by flow cytometry for plasma cells and GC B cells (Figure 5.19B). Few plasma cells were present and there was no significant difference between WT and IgMg1 (Figure 5.19C). GC B cells were also present, but again there was no significant difference between WT and IgMg1 (Figure 5.19D). Serum samples were collected throughout the experiment to allow monitoring of the anti-collagen antibody response. At day 29 (8 days after the first boost) there was a small significant increase in anti-collagen IgG in WT and IgMg1 mice. However, this was not further increased by the second boost. Differences in anti-collagen IgG titre between IgMg1 and WT did not reach significance at any time point (Figure 5.19E). Anti-collagen IgM was significantly higher in aged IgMg1 sera at day 0, with more than a 5-fold increase over aged WT (Figure 5.20E), confirming the earlier result (Figure 5.4). It was also higher in IgMg1 mice at all

subsequent timepoints, although immunisation did not increase anti-collagen titres in either group (Figure 5.19F).

Overall, this data showed that although anti-collagen antibodies are elevated in aged non-immunised mice compared with young adult non-immunised mice, the aged mice did not make a strong anti-collagen antibody response after being immunised with collagen. Additionally, the experiment was underpowered due to insufficient availability of aged mice. This meant, we were unable to assess if aged IgMg1 mice make a stronger antibody response to self- or highly conserved antigen. This experiment should probably be repeated with the more aggressive collagen-induced arthritis immunisation protocol (section 5.2.1).

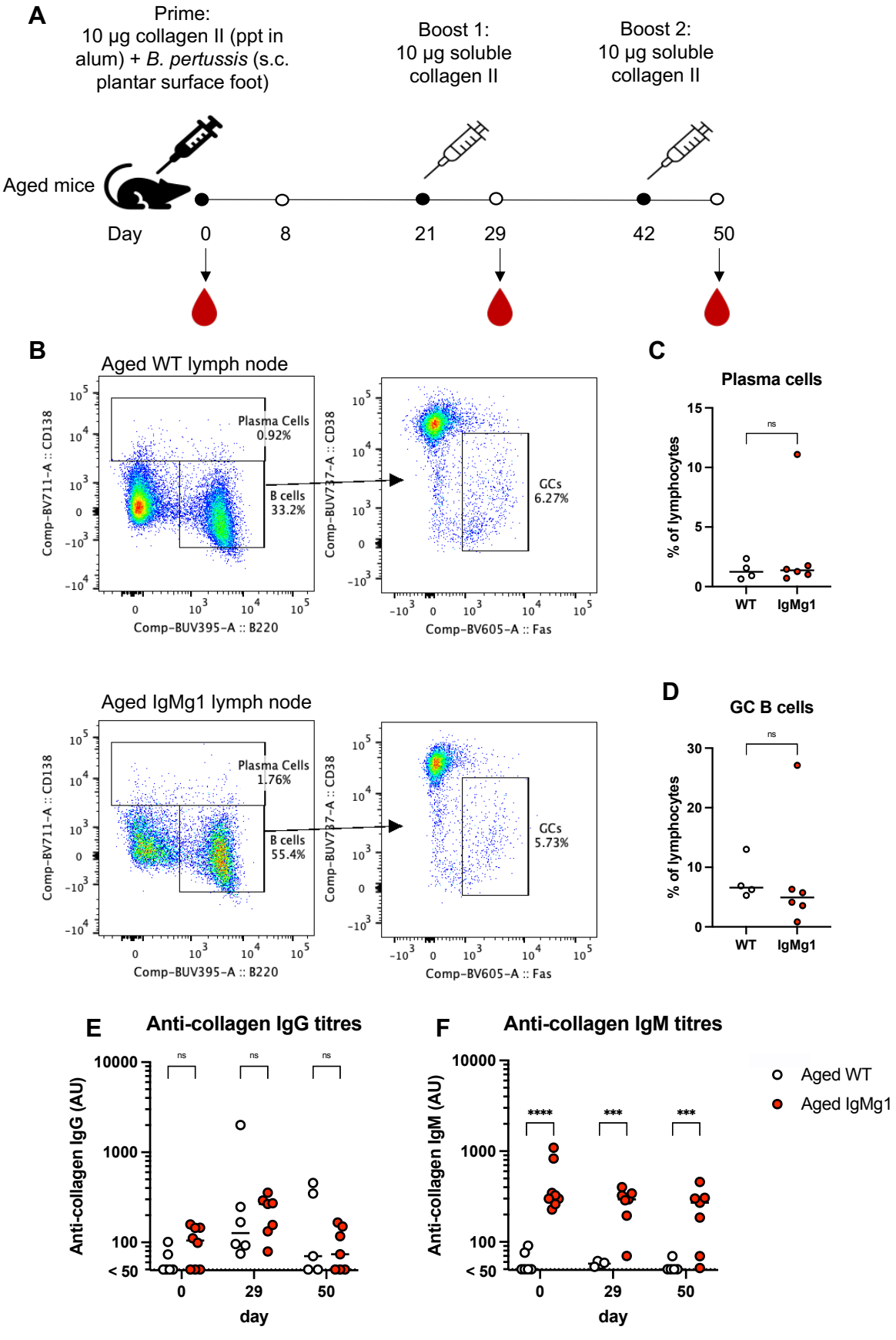
A
Prime:
10 µg collagen II (ppt in alum) + B. pertussis (s.c. plantar surface foot)
Boost 1:
10 µg soluble collagen II
Boost 2:
10 µg soluble collagen II
Aged mice
Day
0
8
21
29
42
50
B
Aged WT lymph node
Plasma Cells 0.92%
B cells 33.2%
GCs 6.27%
Comp-BV711-A :: CD138
Comp-BUV395-A :: B220
Comp-BUV737-A :: CD38
Comp-BV605-A :: Fas
Aged IgMg1 lymph node
Plasma Cells 1.76%
B cells 55.4%
GCs 5.73%
C
Plasma cells
% of lymphocytes
ns
WT
IgMg1
D
GC B cells
% of lymphocytes
ns
WT
IgMg1
E
Anti-collagen IgG titres
Anti-collagen IgG (AU)
ns
day
F
Anti-collagen IgM titres
Anti-collagen IgM (AU)
****
***
***
day
Aged WT
Aged IgMg1

Figure 5.19 Anti-collagen response in aged mice following immunisation

(A) Schematic showing immunisation strategy. Aged mice were immunised s.c. with 10 µg chicken collagen type II (alum ppt) with heat inactivated *B. pertussis*. They then received 2 boosts with 10 µg soluble collagen type II at 3-week intervals. Mice were culled by schedule 1 method 8 days after the second boost. (B) Representative flow cytometry plots for aged WT and IgMg1 mice plasma cells (PCs) and GC B cells and at day 50 (8 days after second boost with soluble collagen type II). From the lymphocytes, PCs were gated as $CD138^+$ and B cells were gated as $B220^+$ $CD138^-$. From the B cells, GC B cells were gated as Fas^+ CD38-. (C-D) Summary statistics for: (C) plasma cells as percentage of lymphocytes; (D) GC B cells as percentage of B cells. (E-F) Sera was tested for anti-collagen antibody by ELISA. Summary statistics for: (E) anti-collagen IgG sera titres; (F) anti-collagen IgM sera titres. Data are from one experiment. Each symbol represents one mouse. Statistical tests for C and D performed by unpaired two-tailed T-test. Statistical tests for E and F performed by mixed-effects analysis with Šídák's multiple comparisons test (****, $p<0.0001$; ***, $p< 0.001$; ns, not significant).

5.3 Discussion

5.3.1 Increased frequency of spontaneous autoantibodies in aged IgMg1 mice but no other evidence of autoimmunity

The results in this chapter show that aged IgMg1 mice have increased frequency of autoantibodies to a wide range of tissue antigens compared with WT mice. However, despite this, there was no evidence of increased autoimmune disease in tissues from aged IgMg1 mice: no immune cell infiltrates were found by immunohistology in liver, kidney or pancreas. Although IgM and complement-containing immune complex was identified in glomeruli in aged mouse kidneys there were no significant differences between aged IgMg1 and WT kidneys. Additionally, IgMg1 mice did not have any breeding problems because of autoimmunity and did not have significantly reduced survival compared with WT mice. A caveat with many of these analyses is that the experiments were underpowered due to the availability of sufficient numbers of aged mice. Additionally, the fluorescent immunohistology for immune cell infiltrates was not optimal and could be repeated to confirm these results.

Two subsets of B cells linked to autoimmunity are B-1 cells and $CD21^-$ $CD23^-$ age-associated B cells. Both subsets have been shown to be enriched for self-reactive BCRs (Duan and Morel, 2006; Rubtsov et al., 2011). However, interestingly, these subsets were reduced in IgMg1 mice, indicating that these cells are unlikely to be the source of the autoantibodies. As shown in chapter 3, altered BCR signalling in both IgMg1 and IgG1M mouse models affects the development of B-1 cells. It is possible that the altered BCR signalling also affects the development of $CD21^-$ $CD23^-$ age-associated B cells.

There are a few possible reasons why IgMg1 mice may be more prone to development of autoantibodies. Presence of the IgG1 cytoplasmic tail on the BCR during B cell development may affect BCR-mediated positive and negative selection, which could possibly result in an altered BCR repertoire with more self-reactivity. However, results from this chapter show that as in young adult IgMg1 mice, B cells from aged IgMg1 mice had increased usage of lambda light chain, suggesting they continue to undergo stronger negative selection with ageing. Results from the bulk and single cell RNA sequencing results in chapter 3 show, the IGHV gene usage in young adult IgMg1 mice appears to be similar to WT mice, which suggests that there were no major changes to the BCR repertoire in young adult IgMg1 mice due to altered BCR signalling. Stronger BCR signalling may result in increased activation of autoreactive cells, but the results in chapter 3 show that young adult IgMg1 B cells have reduced BCR signalling following BCR stimulation and have reduced surface BCR expression indicative of an anergic phenotype. Although B cells from aged mice were not assessed for calcium signalling, the data in this chapter show that they did still have reduced surface BCR expression, indicating that they are likely still anergic. The increase in Tfh cells in IgMg1 mice may be an important factor in the increased development of autoantibodies. Several models have been described where increased Tfh cells are implicated in development of autoantibodies and autoimmunity (Ma et al., 2012; Zhang et al., 2015b; Choi et al., 2015; Zhang et al., 2015a; Linterman et al., 2009; Lee et al., 2012). Additionally, Tfh cells in young adult gMg1 mice have increased Nr4a3 expression indicating increased TCR signalling. The increased TCR signalling in Tfh cells of IgMg1 mice may induce increased release of cytokines that could

promote plasma cell differentiation and antibody secretion in lower affinity B cells, including self-reactive cells.

The fact that the increased autoantibodies does not manifest in clear autoimmune disease in the aged IgMg1 mice, may be because although in many cases autoantibodies contribute directly to the development of autoimmune disease (Martin and Chan, 2004) and can be used as predictive markers of autoimmunity (Leslie et al., 2001), presence of autoantibodies does not always indicate presence of disease. While autoantibodies are frequently found in elderly people, actual autoimmune disease is much less frequent. Autoantibodies were found to be present in sera from all healthy adults using human tissue microarrays (Nagele et al., 2013), but prevalence of autoimmune disease is estimated to be only 3-5% of people (Wang et al., 2015). Additionally, there may be a lag between appearance of autoantibodies and pathogenesis, as autoantibodies can be detected years before disease onset (Burbelo et al., 2021).

5.3.2 Young adult IgMg1 mice did not make stronger antibody response to conserved antigen

Although aged IgMg1 mice developed autoantibodies more frequently than aged WT mice, immunisation of young adult IgMg1 mice with the conserved antigen chicken collagen type II did not result in an increased anti-collagen antibody response. Chicken collagen type II was chosen as an antigen with potential to trigger an autoantibody response in the IgMg1 mice, as it is used in the collagen-induced arthritis model to induce autoimmune arthritis in C57BL/6 mice. In that model, mice injected with a large dose of chicken collagen type II with Freund's complete adjuvant induces symptoms

of arthritis in 50-80% of the mice, and the model is characterised by an anti-collagen antibody response (Inglis et al., 2008). However, the incidence of collagen-induced arthritis is lower in C57BL/6 mice used here than in other strains of mice (such as DBA/1), and furthermore only chicken collagen type II is known to be capable of inducing arthritis in C57BL/6 mice, whereas other species of collagen can be used successfully in other strains (Inglis et al., 2007).

In the experiments presented here, although immunisation with chicken collagen type II did raise an anti-collagen antibody response, it took multiple boosts for a response in most of the mice. Additionally, when the collagen-induced arthritis protocol was used none of the mice developed any arthritis symptoms. It is possible that immunisation with a different antigen or tissue extract may have given a stronger response and a better opportunity to observe a difference between IgMg1 and WT mice at the young adult age. Additionally, there is an abundance of other inducible autoimmunity models that could be used. For example, streptozocin (STZ) has been used to chemically induce diabetes in mice (Like and Rossini, 1976). Anti-cardiolipin antibodies were associated with insulitis (Anzai et al., 1993) showing a role for B cells in this model. Another chemically induced autoimmunity model is pristane-induced lupus: a mouse model of SLE in which anti-Smith antigen, anti-double stranded DNA, and anti-ribosomal P autoantibodies are induced (Satoh et al., 2000; Reeves et al., 2009). Autoimmunity can also be induced by infection. For example, a salmonella-infection model may be useful, as infection with salmonella is associated with development of autoantibodies (Ktsoyan et al., 2019).

5.3.3 Aged mice did not make an antibody response following immunisation with conserved antigen

Aged mice were also immunised with chicken collagen type II to attempt to further investigate the development of autoimmunity with ageing. However, aged WT as well as aged IgMg1 mice failed to make strong antibody responses following the immunisations. It is well established that the immune response is weaker in elderly individuals leading to increased susceptibility to infections and impaired response to vaccination (Lee and Linterman, 2022). For example, SARS-CoV-2 infections are more severe in individuals over 65 years old due to impaired adaptive immunity (Rydyznski Moderbacher et al., 2020) and neutralising antibody titres are significantly lower in people over 80 years old after SARS-CoV-2 vaccination (Collier et al., 2021). This is also recapitulated in aged mice as shown by a reduced GC B cell response and antibody titres in mice over 22 months old following immunisation with the ChAdOx1 nCoV-19 (SARS-CoV-2) vaccine (Silva-Cayetano et al., 2021). The antibody response to influenza vaccination is also reduced in elderly individuals (Frasca and Blomberg, 2020), evidenced by significantly lower antibody titres in people aged over 65 years old compared to people aged 18-36 years old following season influenza vaccination (Stebegg et al., 2020; Hill et al., 2021). The reduced response is because of several changes that occur to the immune system with ageing, known as immune senescence. Several of these changes can impact B cell responses. B cell development is impaired in aged mice (Ma et al., 2019). However, B cells from aged individuals do not have impaired ability to differentiate into plasma cells *in vitro*, and aged B cells transferred to a young adult mouse host have an enhanced early plasma cell response (Lee et al., 2022), suggesting that other cells or the immune microenvironment may be responsible for the reduced antibody response in aged individuals. Thymic involution

results in a reduction in mature T cells with limited diversity (Pangrazzi and Weinberger, 2020), restricting the T cell help available. Additionally, aged mice have altered stromal cell populations including reduced follicular dendritic cell (FDC) networks, which play an important role in GC reactions (Turner and Mabbott, 2017), and altered follicular reticular cells (FRCs) which contribute to altered cytokine expression and impaired B and T cell recruitment (Minges Wols et al., 2010; Lefebvre et al., 2012; Masters et al., 2018). A mucosal adressin cell adhesion molecule-1 (MAdCAM-1)$^{+}$ stromal cell subset has also been identified that plays a role in initiation of GCs, but that are impaired in aged mice, contributing to the reduced response (Denton et al., 2022).

As the aged mice did not make an anti-collagen antibody response following immunisation with chicken collagen type II, further analysis of development of autoantibodies in aged IgMg1 mice was unsuccessful. It would be interesting to establish a robust way of inducing an autoantibody response in aged mice. This would allow questions of whether aged B cells or the aged microenvironment were responsible for the increased autoantibody response in aged IgMg1 mice to be answered. Adoptive cell transfer experiments where aged B cells are adoptively transferred to young adult animals, and vice versa, could help answer these questions. Heterochronic parabiosis experiments have also recently been used to investigate the relative importance of aged lymphocytes and aged microenvironment in the ageing weaker vaccine response (Denton et al., 2022).

5.3.4 Conclusions

The results presented in this chapter demonstrate that despite the anergic phenotype of the B cells in IgMg1 mice, there is a breach of anergy in aged mice and increased spontaneous production of tissue-specific autoantibodies. It remains to be investigated whether this is because aged autoreactive IgMg1 B cells have increased capacity to be activated due to the hyperactive IgG1 cytoplasmic tail on the BCRs, or if other changes to the immune microenvironment are responsible.

Chapter 6. Conclusions and future perspectives

6.1 Conclusions

B cell receptor (BCR) signalling is important at almost all stages of B cell development and differentiation. During development in the bone marrow, BCR signalling mediates both positive and negative selection of B cell precursors to ensure a diverse repertoire of mature B cells with minimal reactivity with self-antigens (Hardy, 2012). Within the periphery, transitional B cells complete their maturation as either follicular or marginal zone B cells, with this fate choice depending on BCR signalling strength (Pillai and Cariappa, 2009). BCR signals are also important for mature B cell survival (Lam et al., 1997). Mature B cells that encounter antigen through the BCR are activated to differentiate into extracellular plasma cells (MacLennan et al., 2003), or to participate in germinal centres (GCs) (MacLennan, 1994a; Victora and Nussenzweig, 2022). Within the dark zone (DZ) of the GC, B cells mutate their BCRs to generate variant BCRs with altered affinity. In the light zone (LZ) they test their mutated BCRs for affinity, with higher affinity variants being selected for further rounds of mutation and proliferation, or for differentiation into long-lived plasma cells or memory B cells (Victora and Nussenzweig, 2022; Zhang et al., 2016). Throughout all these processes there is a balance between excessive BCR signalling for self-antigen, and appropriate signalling of a functional receptor.

The work presented in this thesis has used mouse models in which all developing and naïve B cells express: (i) a chimeric IgMg1 BCR that has the IgM extracellular region but the IgG1 cytoplasmic tail; or (ii) the IgG1 BCR (extracellular and cytoplasmic

regions). The IgG1 cytoplasmic tail is thought to be important for conferring stronger BCR signalling in IgG1$^+$ class-switched B cells (Kaisho et al., 1997; Waisman et al., 2007; Horikawa et al., 2007; Engels et al., 2009), although there is evidence that the extracellular region may also play a role in stronger signalling (Sundling et al., 2021).

Mature class-switched IgG1$^+$ memory B cells are produced as part of immune responses to vaccines or infection (Toellner et al., 1996; Roco et al., 2019). However, the majority of the total mature B cell population consists largely of naïve B cells co-expressing IgM$^+$ IgD$^+$. Developing B cells naturally expressing IgG1$^+$ as their BCR have not been described, and a chimeric IgMg1 BCR never exists in nature, but these models can be used to investigate the effect of altered BCR signalling on B cell development, and the continuing ability of cells to take part in a B cell response.

Firstly, B cell development in the two mouse models was investigated (Table 6.1). B cell development in the bone marrow of IgMg1 mice appeared similar to WT mice, whereas pre-B cell differentiation was impaired in IgG1M mice. This showed that the IgM cytoplasmic tail is not essential for efficient B cell development, but the IgM extracellular region is required. Both models increase receptor editing during B cell development in the bone marrow, suggesting that the IgG1 cytoplasmic tail induces stronger signalling resulting in stronger negative selection. Both models have reduced surface BCR expression compared with WT B cells, consistent with studies reporting reports that presence of the IgG1 cytoplasmic tail results in downregulation of BCR (Kodama et al., 2020; Sundling et al., 2021). The IgMg1 B cells have impaired calcium flux in response to BCR stimulation. This, along with a previous observation that proteins downstream of BCR signalling had reduced phosphorylation following BCR

stimulation in IgMg1 B cells (Zhang, 2019), lead us to conclude that strong negative selection during B cell development results in B cells with an anergic phenotype. However, the IgG1M mice have enhanced calcium flux in response to BCR stimulation, showing that IgG1 cytoplasmic tail-mediated negative selection and downregulation of BCR are not sufficient for an anergic phenotype. The IgMg1 mice have reduced marginal zone B cells and the IgG1M mice have increased marginal zone B cells, possibly because of the divergent signalling strengths. This may reflect the importance of the BCR extracellular region and cytoplasmic tail for signalling in different contexts or could shed light on an inhibitory function for IgD, which is not expressed on B cells in IgG1M mice.

Gene expression in the anergic IgMg1 follicular B cells was analysed using bulk RNA sequencing. This identified 89 differentially expressed genes compared with WT follicular B cells, although statistical power was limited by high variability between samples. However, there was little overlap between the identified IgMg1 differentially expressed genes, and genes identified in similar studies of the classic B cell anergy model MD4 x ML5 (Sabouri et al., 2016; Schwickert et al., 2019). While distinct mechanisms for development of anergy in the separate models may explain these discrepancies, it could also be due to experimental differences. Therefore, the direct comparison of gene expression in IgMg1 B cells with other anergy models in the same experiment would be preferential. Additionally, the genes that were identified as differentially expressed in both IgMg1 B cells and MD4 x ML5 B cells need to be further investigated for their importance in maintaining B cell anergy. Further investigation could be conducted with gene knock-out or overexpression models.

B cell activation in response to immunisation with model antigens in IgMg1 and IgG1M mice was then investigated (Table 6.1). Despite being anergic, IgMg1 mice make only a slightly impaired T cell-independent (TI) type II (TI-II) response to model antigen NP-Ficoll. However, surprisingly there was a much more severe impairment in the TI-II response in IgG1M mice. Mirroring this, the IgMg1 mice made a normal T cell-dependent (TD) antibody response to NP-KLH, while the IgG1M mice again had a severely impaired antibody response. This is consistent with the importance of secreted IgM (either polyclonal or early low-affinity antibodies) in regulating the antibody response (Ehrenstein et al., 1998; Boes et al., 1998; Zhang et al., 2013; Baumgarth et al., 2000). Alternatively it could be explained by overactive signalling resulting in increased apoptosis of plasmablasts and GC B cells (Yam-Puc et al., 2021) Additionally, it was found that the overall number of GC B cells in IgMg1 mice appeared to be slightly reduced. Further analysis of the GC B cells in IgMg1 mice compared with WT mice suggested they are more dominated by class-switched B cells and have higher BCR affinity. However, IgMg1 GC B cells undergo increased apoptosis, and bulk RNA sequencing of GC B cells suggests they have reduced B cell selection and proliferation. Altogether, this indicates that B cells in the anergic IgMg1 model have less ability to participate in the GCs, with a higher affinity threshold for participation.

The ability of anergic B cells to take part in the GC response has been previously investigated with a monoclonal HEL-specific BCR model of anergy (Burnett et al., 2018). However, little work had been previously conducted to assess anergic B cell activation in a polyclonal B cell model. Here, we have been able to investigate anergic B cell participation in a GC response to a model antigen NP-KLH, in a mouse model that has a WT-like BCR repertoire. In physicological conditions, anergic B cells are a

pool of self-reactive B cells maintained in an inactive form to prevent autoimmunity. However, activation of anergic B cells may be useful in the case of infection against pathogens that use molecular mimicry to evade the immune response or for B cell vaccines against cancer antigens. Anti-tumour B cell immunity has been of recent interest, as increasing evidence suggests that presence of B cells in tumours is advantageous (Fridman et al., 2021; Conejo-Garcia et al., 2023). However, a B cell vaccine to a tumour antigen would require activation of self-reactive B cells (Zhuang et al., 2015). A further application could be in the discovery of therapeutic monoclonal antibodies. The therapeutic antibody market was worth $186 billion in 2021 and is projected to continue growing (Lyu et al., 2022), and has huge potential to generate therapies that can improve the lives of patients in several disease areas (Lu et al., 2020). Discovery of new therapeutics relies heavily on immunisation of animals and, as many human target antigens have high homology with the ones in the host animals, this can make the immunisations challenging (Dodd et al., 2018). The finding that anergic B cells may have a higher affinity threshold to overcome to participate in GCs could be taken into consideration for design of immunogens that aim to activate anergic B cells. It is possible that higher avidity antigen or highly cross-linked antigen may be a useful approach in these cases.

Furthermore, Tfh cells in IgMg1 mice are increased, and have increased expression of a reporter of T cell receptor signalling. This suggests that the IgMg1 B cells have increased ability to capture and present antigen to Tfh cells, resulting in their greater proliferation and activation. The fact that a change to the BCR in B cells has such an effect on cells that they interact with is an interesting finding. The role of the BCR in interactions between B cells and Tfh cells could be further investigated. Gene

expression in Tfh cells in the IgMg1 mice could be compared with WT mice by bulk or single cell RNA sequencing. Additionally, analysis at multiple time points could be beneficial, as the Tfh cell phenotype has been shown to be transient (Baumjohann et al., 2013) and the Tfh population undergoes dynamic phenotype changes throughout a GC reaction (Song and Craft, 2019). Another aspect that needs to be determined is if the increased activation of Tfh cells is a general feature of interaction with anergic B cells in GCs, or if it is specific to the IgMg1 model due to the chimeric BCR. It has not yet been established whether altered BCR signalling, or a BCR-signalling independent mechanism of antigen capture and presentation results in the increased activation of Tfh cells. Nr4a3-reporter mice have been used here to show TCR signalling in Tfh cells; however, Nr4a1 (Nur77)-reporter mice will allow assessment of BCR signalling as well as more sensitive analysis of TCR signalling (Moran et al., 2011; Zikherman et al., 2012; Elliot et al., 2022). Analysis of the impact of altered BCR signalling on interaction with other cells could also be interesting, for example follicular dendritic cells (FDCs) or other stromal cells that are important in the GC.

Finally, the development of autoimmunity in the IgMg1 mouse model was explored. When young adult IgMg1 mice were immunised with the conserved antigen collagen, they did not make an increased autoantibody response compared to WT mice. However, aged IgMg1 mice develop spontaneous autoantibodies to a range of different self-antigens (Table 6.1). No firm evidence of overt autoimmune disease was observed in tissues from aged mice, and immunisation of aged mice with a conserved antigen failed to induce a sufficiently strong response to further investigate the role of aged B cells, aged Tfh cells or an aged microenvironment. Further investigation of the breach of tolerance using aged mice was attempted but it was challenged by the length of

experiments and the high risk of illness in the mice. Alternative methods for experimental induction of autoimmunity need to be tested that may better recapitulate the increased spontaneous autoantibodies observed in aged mice. To assess if the aged microenvironment is important for the increased tendency of self-reactive IgMg1 B cells to secrete autoantibodies, B cells from young mice could be adoptively transferred to aged C57BL/6 mice (Yang et al., 1996), which are easier available. This work could provide a new model for research into the role of activation of anergic B cells in development of autoimmune disease.

Table 6.1 Summary of observations in IgMg1 and IgG1M altered BCR signalling models

	IgMg1 model	**IgG1M model**
Bone marrow B cell fractions	similar frequencies to WT	Impaired pre-B cell differentiation
Receptor editing during B cell development	Increased	Increased
BCR expression	Reduced	Reduced
Mature B cells	Increased follicular B cells and reduced marginal zone B cells	Reduced follicular B cells and increased marginal zone B cells
In vitro BCR-stimulated calcium flux	Impaired	Enhanced
B-1 cells	Reduced	Reduced
T cell-independent response	Slightly impaired	Strongly impaired
GC B cells	Reduction	Normal
GC B cell BCR affinity	Higher	Lower
T cell-dependent plasma cell response	Normal	Strongly impaired
Tfh cells	Increased	Normal
Tfh cell activation	Increased	unknown
Aged mice	Increased autoantibodies	unknown

6.2 Future perspectives

Future work following on from the results described in this thesis could focus on a few key areas:

(i) Genes identified as being differentially expressed in IgMg1 follicular B cells compared with WT follicular B cells that overlapped with the previously published MD4 x ML5 anergic gene signature could be assessed for their functional importance in maintaining B cell anergy. This could be done using RNAi-mediated knock-down of gene function in in vitro experiments, or with conditional B cell knock out mouse models.

(ii) Further work looking at the participation of anergic IgMg1 B cells in GCs in a polyclonal B cell environment could be conducted to determine how relevant the observations are for responses to other model antigens or for other anergy models and natural anergic B cells. In particular, the expansion and increased activation of Tfh cells observed in IgMg1 mice requires further investigation, due to the importance of Tfh cells in the reactivation of anergic B cells (Cooke et al., 1994; Seo et al., 2002; Burnett et al., 2018), and in the development of autoimmunity (Linterman et al., 2009; Lee et al., 2012; Pratama and Vinuesa, 2014).

(iii) The increase in autoantibodies in aged IgMg1 mice suggests that it may be a useful model for examining how anergic B cells can become reactivated and contribute to autoimmunity. However, it would be useful to establish an inducible autoimmunity model that results in increased autoantibodies in IgMg1 mice at a young age, such as an infection model or a chemically induced autoimmunity model. This would it less challenging to investigate

the development of autoimmunity as it would not require lengthy ageing experiments with increased risk of illness to the mice. Additionally, adoptive transfer of IgMg1 B cells in aged WT mice would be useful for investigation of the contribution of the aged immune microenvironment towards the increased autoantibodies observed in IgMg1 mice.

6.3 Summary

Overall, this work provides insight into how altered BCR signalling strength can impact B cell development and differentiation in different contexts. Analysis of gene expression in a polyclonal BCR anergic B cell model identified genes that could be important in regulating anergy. Anergic B cell participation in GCs within a WT-like BCR repertoire was also investigated and indicated there was an increased affinity threshold. Furthermore, we showed how the BCR can affect B cell interactions with Tfh cells. Finally, we demonstrated how alterations to BCR signalling may lead to development of autoantibodies in aged mice. These models should be useful for further investigation into how altered BCR signalling affects the GC and potentially lead to autoimmunity.

Chapter 7. References

Akashi, K., Kondo, M., Cheshier, S., Shizuru, J., Gandy, K., Domen, J., Mebius, R., Traver, D. and Weissman, I.L. (1999) "Lymphoid development from stem cells and the common lymphocyte progenitors." In *Cold Spring Harbor Symposia on Quantitative Biology*. 1 January 1999. Cold Spring Harbor Laboratory Press. pp. 1–12. doi:10.1101/sqb.1999.64.1.

Alexopoulos, E., Seron, D., Hartley, R.B. and Cameron, J.S. (1990) Lupus nephritis: Correlation of interstitial cells with glomerular function. *Kidney International*, 37 (1): 100–109. doi:10.1038/ki.1990.14.

Allen, C.D.C., Ansel, K.M., Low, C., Lesley, R., Tamamura, H., Fujii, N. and Cyster, J.G. (2004) Germinal center dark and light zone organization is mediated by CXCR4 and CXCR5. *Nature Immunology*, 5 (9): 943–952. doi:10.1038/ni1100.

Allen, C.D.C., Okada, T., Tang, H.L. and Cyster, J.G. (2007) Imaging of germinal center selection events during affinity maturation. *Science*, 315 (5811): 528–531. doi:10.1126/science.1136736.

Allman, D., Lindsley, R.C., DeMuth, W., Rudd, K., Shinton, S.A. and Hardy, R.R. (2001) Resolution of Three Nonproliferative Immature Splenic B Cell Subsets Reveals Multiple Selection Points During Peripheral B Cell Maturation. *The Journal of Immunology*, 167 (12): 6834–6840. doi:10.4049/jimmunol.167.12.6834.

Angelin-Duclos, C., Cattoretti, G., Lin, K.-I. and Calame, K. (2000) Commitment of B Lymphocytes to a Plasma Cell Fate Is Associated with Blimp-1 Expression In Vivo. *The Journal of Immunology*, 165 (10): 5462–5471. doi:10.4049/jimmunol.165.10.5462.

Ansel, K.M., Ngo, V.N., Hyman, P.L., Luther, S.A., Förster, R., Sedgwlck, J.D., Browning, J.L., Upp, M. and Cyster, J.G. (2000) A chemokine-driven positive feedback loop organizes lymphoid follicles. *Nature*, 406 (6793): 309–314. doi:10.1038/35018581.

Anzai, K., Nakamura, M., Nagafuchi, S., Iwakiri, R., Ichinose, I., Mitsugi, K., Kuroki, M., Nakano, S. and Niho, Y. (1993) Production of anti-cardiolipin antibody in AKR/J mice with streptozocin-induced insulitis and diabetes. *Diabetes Research and Clinical Practice*, 20 (1): 29–37. doi:10.1016/0168-8227(93)90019-2.

Arnon, T.I., Horton, R.M., Grigorova, I.L. and Cyster, J.G. (2013) Visualization of splenic marginal zone B-cell shuttling and follicular B-cell egress. *Nature*, 493 (7434): 684–688. doi:10.1038/nature11738.

Attanavanich, K. and Kearney, J.F. (2004) Marginal Zone, but Not Follicular B Cells, Are Potent Activators of Naive CD4 T Cells. *The Journal of Immunology*, 172 (2): 803–811. doi:10.4049/jimmunol.172.2.803.

Bai, L., Chen, Y., He, Y., Dai, X., Lin, X., Wen, R. and Wang, D. (2007) Phospholipase Cγ2 Contributes to Light-Chain Gene Activation and Receptor Editing. *Molecular and Cellular Biology*, 27 (17): 5957–5967. doi:10.1128/mcb.02273-06.

Barnett, L.G., Simkins, H.M.A., Barnett, B.E., Korn, L.L., Johnson, A.L., Wherry, E.J., Wu, G.F. and Laufer, T.M. (2014) B Cell Antigen Presentation in the Initiation of Follicular Helper T Cell and Germinal Center Differentiation. *The Journal of Immunology*, 192 (8): 3607–3617. doi:10.4049/jimmunol.1301284.

Basso, K. and Dalla-Favera, R. (2010) "BCL6. master regulator of the germinal center reaction and key oncogene in B Cell lymphomagenesis." In *Advances in Immunology*. Academic Press Inc. pp. 193–210. doi:10.1016/S0065-2776(10)05007-8.

Basso, K., Saito, M., Sumazin, P., Margolin, A.A., Wang, K., Lim, W.K., Kitagawa, Y., Schneider, C., Alvarez, M.J., Califano, A., et al. (2010) Integrated biochemical and computational approach identifies BCL6 direct target genes controlling multiple pathways in normal germinal center B cells. *Blood*, 115 (5): 975–984. doi:10.1182/blood-2009-06-227017.

Batista, F.D. and Harwood, N.E. (2009) The who, how and where of antigen presentation to B cells. *Nature Reviews Immunology*. 9 (1) pp. 15–27. doi:10.1038/nri2454.

Batista, F.D. and Neuberger, M.S. (2000) B cells extract and present immobilized antigen: implications for affinity discrimination. *The EMBO Journal*, 19 (4): 513–520. doi:10.1093/emboj/19.4.513.

Baumann, I., Kolowos, W., Voll, R.E., Manger, B., Gaipl, U., Neuhuber, W.L., Kirchner, T., Kalden, J.R. and Herrmann, M. (2002) Impaired uptake of apoptotic cells into tingible body macrophages in germinal centers of patients with systemic lupus erythematosus. *Arthritis and Rheumatism*, 46 (1): 191–201. doi:10.1002/1529-0131(200201)46:1<191::AID-ART10027>3.0.CO;2-K.

Baumgarth, N. (2011) The double life of a B-1 cell: Self-reactivity selects for protective effector functions. *Nature Reviews Immunology*, 11 (1): 34–46. doi:10.1038/nri2901.

Baumgarth, N., Herman, O.C., Jager, G.C., Brown, L.E., Herzenberg, L.A. and Chen, J. (2000) B-1 and B-2 Cell–Derived Immunoglobulin M Antibodies Are Nonredundant Components of the Protective Response to Influenza Virus Infection. *Journal of Experimental Medicine*, 192 (2): 271–280. doi:10.1084/jem.192.2.271.

Baumjohann, D., Preite, S., Reboldi, A., Ronchi, F., Ansel, K.M., Lanzavecchia, A. and Sallusto, F. (2013) Persistent Antigen and Germinal Center B Cells Sustain T Follicular Helper Cell Responses and Phenotype. *Immunity*, 38 (3): 596–605. doi:10.1016/j.immuni.2012.11.020.

Begovich, A.B., Carlton, V.E.H., Honigberg, L.A., Schrodi, S.J., Chokkalingam, A.P., Alexander, H.C., Ardlie, K.G., Huang, Q., Smith, A.M., Spoerke, J.M., et al. (2004) A missense single-nucleotide polymorphism in a gene encoding a protein tyrosine phosphatase (PTPN22) is associated with rheumatoid arthritis. *American Journal of Human Genetics*, 75 (2): 330–337. doi:10.1086/422827.

Bending, D., Martín, P.P., Paduraru, A., Ducker, C., Marzaganov, E., Laviron, M., Kitano, S., Miyachi, H., Crompton, T. and Ono, M. (2018) A timer for analyzing temporally dynamic changes in transcription during differentiation in vivo. *Journal of Cell Biology*, 217 (8): 2931–2950. doi:10.1083/jcb.201711048.

Benschop, R.J., Aviszus, K., Zhang, X., Manser, T., Cambier, J.C. and Wysocki, L.J. (2001) Activation and anergy in bone marrow B cells of a novel immunoglobulin transgenic mouse that is both hapten specific and autoreactive. *Immunity*, 14 (1): 33–43. doi:10.1016/S1074-7613(01)00087-5.

Bergtold, A., Desai, D.D., Gavhane, A. and Clynes, R. (2005) Cell surface recycling of internalized antigen permits dendritic cell priming of B cells. *Immunity*, 23 (5): 503–514. doi:10.1016/j.immuni.2005.09.013.

Berland, R. and Wortis, H.H. (2002) Origins and functions of B-1 cells with notes on the role of CD5. *Annual Review of Immunology*. 20 pp. 253–300. doi:10.1146/annurev.immunol.20.100301.064833.

Biram, A., Davidzohn, N. and Shulman, Z. (2019) T cell interactions with B cells during germinal center formation, a three-step model. *Immunological Reviews*, 288 (1): 37–48. doi:10.1111/imr.12737.

Boes, M., Esau, C., Fischer, M.B., Schmidt, T., Carroll, M. and Chen, J. (1998) Enhanced B-1 cell development, but impaired IgG antibody responses in mice deficient in secreted IgM. *Journal of immunology (Baltimore, Md.: 1950)*, 160 (10): 4776–87. Available at: http://www.ncbi.nlm.nih.gov/pubmed/9590224 (Accessed: 10 November 2022).

Bonacina, F., Coe, D., Wang, G., Longhi, M.P., Baragetti, A., Moregola, A., Garlaschelli, K., Uboldi, P., Pellegatta, F., Grigore, L., et al. (2018) Myeloid apolipoprotein E controls dendritic cell antigen presentation and T cell activation. *Nature Communications*, 9 (1): 1–15. doi:10.1038/s41467-018-05322-1.

Borrero, M. and Clarke, S.H. (2002) Low-Affinity Anti-Smith Antigen B Cells Are Regulated by Anergy as Opposed to Developmental Arrest or Differentiation to B-1. *The Journal of Immunology*, 168 (1): 13–21. doi:10.4049/jimmunol.168.1.13.

Bottini, N., Musumeci, L., Alonso, A., Rahmouni, S., Nika, K., Rostamkhani, M., MacMurray, J., Meloni, G.F., Lucarelli, P., Pellecchia, M., et al. (2004) A functional variant of lymphoid tyrosine phosphatase is associated with type I diabetes. *Nature Genetics*, 36 (4): 337–338. doi:10.1038/ng1323.

Boyer, A.E., Quinn, C.P., Beesley, C.A., Gallegos-Candela, M., Marston, C.K., Cronin, L.X., Lins, R.C., Stoddard, R.A., Li, H., Schiffer, J., et al. (2011) Lethal factor toxemia and anti-protective antigen antibody activity in naturally acquired cutaneous anthrax. *Journal of Infectious Diseases*, 204 (9): 1321–1327. doi:10.1093/infdis/jir543.

Breiteneder-Geleff, S., Matsui, K., Soleiman, A., Meraner, P., Poczewski, H., Kalt, R., Schaffner, G. and Kerjaschki, D. (1997) Podoplanin, novel 43-kd membrane protein of glomerular epithelial cells, is down-

regulated in puromycin nephrosis. *The American journal of pathology*, 151 (4): 1141–52. Available at: http://www.ncbi.nlm.nih.gov/pubmed/9327748 (Accessed: 12 December 2022).

Breitfeld, D., Ohl, L., Kremmer, E., Ellwart, J., Sallusto, F., Lipp, M. and Förster, R. (2000) Follicular B helper T cells express CXC chemokine receptor 5, localize to B cell follicles, and support immunoglobulin production. *Journal of Experimental Medicine*, 192 (11): 1545–1551. doi:10.1084/jem.192.11.1545.

Brenneman, K.E., Doganay, M., Akmal, A., Goldman, S., Galloway, D.R., Mateczun, A.J., Cross, A.S. and Baillie, L.W. (2011) The early humoral immune response to Bacillus anthracistoxins in patients infected with cutaneous anthrax. *FEMS Immunology and Medical Microbiology*, 62 (2): 164–172. doi:10.1111/j.1574-695X.2011.00800.x.

Brink, R. (2014) The imperfect control of self-reactive germinal center B cells. *Current Opinion in Immunology*, 28 (1): 97–101. doi:10.1016/j.coi.2014.03.001.

Burbelo, P.D., Iadarola, M.J., Keller, J.M. and Warner, B.M. (2021) Autoantibodies Targeting Intracellular and Extracellular Proteins in Autoimmunity. *Frontiers in Immunology*, 12. doi:10.3389/fimmu.2021.548469.

Burnett, D.L., Langley, D.B., Schofield, P., Hermes, J.R., Chan, T.D., Jackson, J., Bourne, K., Reed, J.H., Patterson, K., Porebski, B.T., et al. (2018) Germinal center antibody mutation trajectories are determined by rapid self/foreign discrimination. *Science*, 360 (6385): 223–226. doi:10.1126/science.aao3859.

Burnett, D.L., Reed, J.H., Christ, D. and Goodnow, C.C. (2019) Clonal redemption and clonal anergy as mechanisms to balance B cell tolerance and immunity. *Immunological Reviews*, 292 (1): 61–75. doi:10.1111/imr.12808.

Calado, D.P., Sasaki, Y., Godinho, S.A., Pellerin, A., Köchert, K., Sleckman, B.P., De Alborán, I.M., Janz, M., Rodig, S. and Rajewsky, K. (2012) The cell-cycle regulator c-Myc is essential for the formation and maintenance of germinal centers. *Nature Immunology*, 13 (11): 1092–1100. doi:10.1038/ni.2418.

Cambier, J.C., Gauld, S.B., Merrell, K.T. and Vilen, B.J. (2007) B-cell anergy: From transgenic models to naturally occurring anergic B cells? *Nature Reviews Immunology*. 7 (8) pp. 633–643. doi:10.1038/nri2133.

Cappione, A., Anolik, J.H., Pugh-Bernard, A., Barnard, J., Dutcher, P., Silverman, G. and Sanz, I. (2005) Germinal center exclusion of autoreactive B cells is defective in human systemic lupus erythematosus. *Journal of Clinical Investigation*, 115 (11): 3205–3216. doi:10.1172/jci24179.

Cariappa, A., Takematsu, H., Liu, H., Diaz, S., Haider, K., Boboila, C., Kalloo, G., Connole, M., Shi, H.N., Varki, N., et al. (2009) B cell antigen receptor signal strength and peripheral B cell development are regulated by a 9-O-acetyl sialic acid esterase. *Journal of Experimental Medicine*, 206 (1): 125–138. doi:10.1084/jem.20081399.

Cariappa, A., Tang, M., Parng, C., Nebelitskiy, E., Carroll, M., Georgopoulos, K. and Pillai, S. (2001) The follicular versus marginal zone B lymphocyte cell fate decision is regulated by Aiolos, Btk, and CD21. *Immunity*, 14 (5): 603–615. doi:10.1016/S1074-7613(01)00135-2.

Carrasco, Y.R. and Batista, F.D. (2007) B Cells Acquire Particulate Antigen in a Macrophage-Rich Area at the Boundary between the Follicle and the Subcapsular Sinus of the Lymph Node. *Immunity*, 27 (1): 160–171. doi:10.1016/j.immuni.2007.06.007.

Carsetti, R. (2000) The development of B cells in the bone marrow is controlled by the balance between cell-autonomous mechanisms and signals from the microenvironment. *Journal of Experimental Medicine*, 191 (1): 5–8. doi:10.1084/jem.191.1.5.

Casamayor-Palleja, M., Feuillard, J., Ball, J., Drew, M. and MacLennan, I.C.M. (1996) Centrocytes rapidly adopt a memory B cell phenotype on co-culture with autologous germinal centre T cell-enriched preparations. *International Immunology*, 8 (5): 737–744. doi:10.1093/intimm/8.5.737.

Casola, S., Otipoby, K.L., Alimzhanov, M., Humme, S., Uyttersprot, N., Kutok, J.L., Carroll, M.C. and Rajewsky, K. (2004) B cell receptor signal strength determines B cell fate. *Nature Immunology*, 5 (3): 317–327. doi:10.1038/ni1036.

Chan, T.D., Wood, K., Hermes, J.R., Butt, D., Jolly, C.J., Basten, A. and Brink, R. (2012) Elimination of Germinal-Center-Derived Self-Reactive B Cells Is Governed by the Location and Concentration of Self-Antigen. *Immunity*, 37 (5): 893–904. doi:10.1016/j.immuni.2012.07.017.

Chaplin, D.D. (2010) Overview of the immune response. *Journal of Allergy and Clinical Immunology*, 125 (2 SUPPL. 2): S3–S23. doi:10.1016/j.jaci.2009.12.980.

Chaudhuri, J., Tian, M., Khuong, C., Chua, K., Pinaud, E. and Alt, F.W. (2003) Transcription-targeted DNA deamination by the AID antibody diversification enzyme. *Nature*, 422 (6933): 726–730. doi:10.1038/nature01574.

Chen, X., Li, G., Wan, Z., Liu, C., Zeng, Y. and Liu, W. (2015) How B cells remember? A sophisticated cytoplasmic tail of mIgG is pivotal for the enhanced transmembrane signaling of IgG-switched memory B cells. *Progress in Biophysics and Molecular Biology*, 118 (3): 89–94. doi:10.1016/j.pbiomolbio.2015.04.010.

Chen, Z., Krinsky, A., Woolaver, R.A., Wang, X., Chen, S.M.Y., Popolizio, V., Xie, P. and Wang, J.H. (2020) TRAF3 Acts as a Checkpoint of B Cell Receptor Signaling to Control Antibody Class Switch Recombination and Anergy. *The Journal of Immunology*, 205 (3): 830–841. doi:10.4049/jimmunol.2000322.

Choi, J.Y., Ho, J.H.E., Pasoto, S.G., Bunin, V., Kim, S.T., Carrasco, S., Borba, E.F., Gonçalves, C.R., Costa, P.R., Kallas, E.G., et al. (2015) Circulating follicular helper-like T cells in systemic lupus erythematosus: association with disease activity. *Arthritis & rheumatology (Hoboken, N.J.)*, 67 (4): 988–999. doi:10.1002/ART.39020.

Choi, Y.S. and Baumgarth, N. (2008) Dual role for B-1a cells in immunity to influenza virus infection. *Journal of Experimental Medicine*, 205 (13): 3053–3064. doi:10.1084/jem.20080979.

Chtanova, T., Tangye, S.G., Newton, R., Frank, N., Hodge, M.R., Rolph, M.S. and Mackay, C.R. (2004) T Follicular Helper Cells Express a Distinctive Transcriptional Profile, Reflecting Their Role as Non-Th1/Th2 Effector Cells That Provide Help for B Cells. *The Journal of Immunology*, 173 (1): 68–78. doi:10.4049/jimmunol.173.1.68.

Chumley, M.J., Dal Porto, J.M. and Cambier, J.C. (2002) The Unique Antigen Receptor Signaling Phenotype of B-1 Cells Is Influenced by Locale but Induced by Antigen. *The Journal of Immunology*, 169 (4): 1735–1743. doi:10.4049/jimmunol.169.4.1735.

Cinamon, G., Zachariah, M.A., Lam, O.M., Foss, F.W. and Cyster, J.G. (2008) Follicular shuttling of marginal zone B cells facilitates antigen transport. *Nature Immunology*, 9 (1): 54–62. doi:10.1038/ni1542.

Colino, J., Shen, Y. and Snapper, C.M. (2002) Dendritic cells pulsed with intact Streptococcus pneumoniae elicit both protein- and polysaccharide-specific immunoglobulin isotype responses in vivo through distinct mechanisms. *Journal of Experimental Medicine*, 195 (1): 1–13. doi:10.1084/jem.20011432.

Collier, D.A., Ferreira, I.A.T.M., Kotagiri, P., Datir, R.P., Lim, E.Y., Touizer, E., Meng, B., Abdullahi, A., Baker, S., Dougan, G., et al. (2021) Age-related immune response heterogeneity to SARS-CoV-2 vaccine BNT162b2. *Nature*, 596 (7872): 417–422. doi:10.1038/s41586-021-03739-1.

Collins, A.M. (2016) IgG subclass co-expression brings harmony to the quartet model of murine IgG function. *Immunology and Cell Biology*, 94 (10): 949–954. doi:10.1038/icb.2016.65.

Conejo-Garcia, J.R., Biswas, S., Chaurio, R. and Rodriguez, P.C. (2023) Neglected no more: B cell-mediated anti-tumor immunity. *Seminars in Immunology*, 65: 101707. doi:10.1016/J.SMIM.2022.101707.

Cooke, M.P., Heath, A.W., Shokat, K.M., Zeng, Y., Finkelman, F.D., Linsley, P.S., Howard, M. and Goodnow, C.C. (1994) Immunoglobulin signal transduction guides the specificity of B cell-T cell interactions and is blocked in tolerant self-reactive B cells. *Journal of Experimental Medicine*, 179 (2): 425–438. doi:10.1084/jem.179.2.425.

Couzi, L., Merville, P., Deminière, C., Moreau, J.F., Combe, C., Pellegrin, J.L., Viallard, J.F. and Blanco, P. (2007) Predominance of CD8+ T lymphocytes among periglomerular infiltrating cells and link to the

prognosis of class III and class IV lupus nephritis. *Arthritis and Rheumatism*, 56 (7): 2362–2370. doi:10.1002/art.22654.

Covens, K., Verbinnen, B., Geukens, N., Meyts, I., Schuit, F., Van Lommel, L., Jacquemin, M. and Bossuyt, X. (2013) Characterization of proposed human B-1 cells reveals pre-plasmablast phenotype. *Blood*, 121 (6): 5176–5183. doi:10.1182/blood-2012-12-471953.

Crotty, S. (2011) Follicular Helper CD4 T Cells (T FH) . *Annual Review of Immunology*, 29 (1): 621–663. doi:10.1146/annurev-immunol-031210-101400.

Cuitiño, M.C., Pécot, T., Sun, D., Kladney, R., Okano-Uchida, T., Shinde, N., Saeed, R., Perez-Castro, A.J., Webb, A., Liu, T., et al. (2019) Two Distinct E2F Transcriptional Modules Drive Cell Cycles and Differentiation. *Cell Reports*, 27 (12): 3547-3560.e5. doi:10.1016/j.celrep.2019.05.004.

Cunningham, A.F., Flores-Langarica, A., Bobat, S., Medina, C.C.D., Cook, C.N.L., Ross, E.A., Lopez-Macias, C. and Henderson, I.R. (2014) B1b cells recognize protective antigens after natural infection and vaccination. *Frontiers in Immunology*, 5 (OCT). doi:10.3389/fimmu.2014.00535.

Dai, X., James, R.G., Habib, T., Singh, S., Jackson, S., Khim, S., Moon, R.T., Liggitt, D., Wolf-Yadlin, A., Buckner, J.H., et al. (2013) A disease-associated PTPN22 variant promotes systemic autoimmunity in murine models. *Journal of Clinical Investigation*, 123 (5): 2024–2036. doi:10.1172/JCI66963.

Dale, G.A., Wilkins, D.J., Bohannon, C.D., Dilernia, D., Hunter, E., Bedford, T., Antia, R., Sanz, I. and Jacob, J. (2019) Clustered Mutations at the Murine and Human IgH Locus Exhibit Significant Linkage Consistent with Templated Mutagenesis. *The Journal of Immunology*, 203 (5): 1252–1264. doi:10.4049/jimmunol.1801615.

Daley, S.R., Teh, C., Hu, D.Y., Strasser, A. and Gray, D.H.D. (2017) Cell death and thymic tolerance. *Immunological Reviews*, 277 (1): 9–20. doi:10.1111/imr.12532.

Denton, A.E., Dooley, J., Cinti, I., Silva-Cayetano, A., Fra-Bido, S., Innocentin, S., Hill, D.L., Carr, E.J., McKenzie, A.N.J., Liston, A., et al. (2022) Targeting TLR4 during vaccination boosts MAdCAM-1+ lymphoid stromal cell activation and promotes the aged germinal center response. *Science Immunology*, 7 (71): eabk0018. doi:10.1126/sciimmunol.abk0018.

Dickerson, S.K., Market, E., Besmer, E. and Papavasiliou, F.N. (2003) AID mediates hypermutation by deaminating single stranded DNA. *Journal of Experimental Medicine*, 197 (10): 1291–1296. doi:10.1084/jem.20030481.

Ding, B.B., Bi, E., Chen, H., Yu, J.J. and Ye, B.H. (2013) IL-21 and CD40L Synergistically Promote Plasma Cell Differentiation through Upregulation of Blimp-1 in Human B Cells. *The Journal of Immunology*, 190 (4): 1827–1836. doi:10.4049/jimmunol.1201678.

Dispinseri, S., Secchi, M., Pirillo, M.F., Tolazzi, M., Borghi, M., Brigatti, C., De Angelis, M.L., Baratella, M., Bazzigaluppi, E., Venturi, G., et al. (2021) Neutralizing antibody responses to SARS-CoV-2 in symptomatic COVID-19 is persistent and critical for survival. *Nature Communications*, 12 (1): 1–12. doi:10.1038/s41467-021-22958-8.

Dodd, R.B., Wilkinson, T. and Schofield, D.J. (2018) Therapeutic Monoclonal Antibodies to Complex Membrane Protein Targets: Antigen Generation and Antibody Discovery Strategies. *BioDrugs*, 32 (4): 339–355. doi:10.1007/s40259-018-0289-y.

Dominguez-Sola, D., Victora, G.D., Ying, C.Y., Phan, R.T., Saito, M., Nussenzweig, M.C. and Dalla-Favera, R. (2012) The proto-oncogene MYC is required for selection in the germinal center and cyclic reentry. *Nature Immunology*, 13 (11): 1083–1091. doi:10.1038/ni.2428.

Duan, B. and Morel, L. (2006) Role of B-1a cells in autoimmunity. *Autoimmunity Reviews*. 5 (6) pp. 403–408. doi:10.1016/j.autrev.2005.10.007.

Duchez, S., Rodrigues, M., Bertrand, F. and Valitutti, S. (2011) Reciprocal Polarization of T and B Cells at the Immunological Synapse. *The Journal of Immunology*, 187 (9): 4571–4580. doi:10.4049/jimmunol.1100600.

Duffield, J.S. (2010) Macrophages and immunologic inflammation of the kidney. *Seminars in Nephrology*, 30 (3): 234–254. doi:10.1016/j.semnephrol.2010.03.003.

Dumas, E.K., Demiraslan, H., Ingram, R.J., Sparks, R.M., Muns, E., Zamora, A., Larabee, J., Garman, L., Ballard, J.D., Boons, G.J., et al. (2020) Toxin-neutralizing antibodies elicited by naturally acquired cutaneous anthrax are elevated following severe disease and appear to target conformational epitopes Turner, W.C. (ed.). *PLoS ONE*, 15 (4): e0230782. doi:10.1371/journal.pone.0230782.

Ehrenstein, M.R., O'Keefe, T.L., Davies, S.L. and Neuberger, M.S. (1998) Targeted gene disruption reveals a role for natural secretory IgM in the maturation of the primary immune response. *Proceedings of the National Academy of Sciences*, 95 (17): 10089–10093. doi:10.1073/pnas.95.17.10089.

Elliot, T.A.E., Jennings, E.K., Lecky, D.A.J., Rouvray, S., Mackie, G.M., Scarfe, L., Sheriff, L., Ono, M., Maslowski, K.M. and Bending, D. (2022) Nur77-Tempo mice reveal T cell steady state antigen recognition. *Discovery Immunology*. doi:10.1093/DISCIM/KYAC009.

Engels, N., König, L.M., Heemann, C., Lutz, J., Tsubata, T., Griep, S., Schrader, V. and Wienands, J. (2009) Recruitment of the cytoplasmic adaptor Grb2 to surface IgG and IgE provides antigen receptor-intrinsic costimulation to class-switched B cells. *Nature Immunology*, 10 (9): 1018–1025. doi:10.1038/ni.1764.

Erikson, J., Radic, M.Z., Camper, S.A., Hardy, R.R., Carmack, C. and Weigert, M. (1991) Expression of anti-DNA immunoglobulin transgenes in non-autoimmune mice. *Nature*, 349 (6307): 331–334. doi:10.1038/349331a0.

Ettinger, R., Sims, G.P., Fairhurst, A.-M., Robbins, R., da Silva, Y.S., Spolski, R., Leonard, W.J. and Lipsky, P.E. (2005) IL-21 Induces Differentiation of Human Naive and Memory B Cells into Antibody-Secreting Plasma Cells. *The Journal of Immunology*, 175 (12): 7867–7879. doi:10.4049/jimmunol.175.12.7867.

Fairfax, K.A., Kallies, A., Nutt, S.L. and Tarlinton, D.M. (2008) Plasma cell development: From B-cell subsets to long-term survival niches. *Seminars in Immunology*. 20 (1) pp. 49–58. doi:10.1016/j.smim.2007.12.002.

Frasca, D. and Blomberg, B.B. (2020) Aging induces B cell defects and decreased antibody responses to influenza infection and vaccination. *Immunity & Ageing 2020 17:1*, 17 (1): 1–10. doi:10.1186/S12979-020-00210-Z.

Fridman, W.H., Petitprez, F., Meylan, M., Chen, T.W.-W., Sun, C.-M., Roumenina, L.T. and Sautès-Fridman, C. (2021) B cells and cancer: To B or not to B? *Journal of Experimental Medicine*, 218 (1). doi:10.1084/jem.20200851.

Gao, R., Zeng, X. and Qin, L. (2021) Systemic autoimmune diseases and recurrent pregnancy loss: research progress in diagnosis and treatment. *Chinese Medical Journal*, 134 (17): 2140–2142. doi:10.1097/CM9.0000000000001691.

Garside, P., Ingulli, E., Merica, R.R., Johnson, J.G., Noelle, R.J. and Jenkins, M.K. (1998) Visualization of Specific B and T Lymphocyte Interactions in the Lymph Node. *Science*, 281 (5373): 96–99. doi:10.1126/science.281.5373.96.

Gauld, S.B., Benschop, R.J., Merrell, K.T. and Cambier, J.C. (2005) Maintenance of B cell anergy requires constant antigen receptor occupancy and signaling. *Nature Immunology*, 6 (11): 1160–1167. doi:10.1038/ni1256.

Gay, D., Saunders, T., Camper, S. and Weigert, M. (1993) Receptor editing: An approach by autoreactive B cells to escape tolerance. *Journal of Experimental Medicine*, 177 (4): 999–1008. doi:10.1084/jem.177.4.999.

Geier, C.B., Sauerwein, K.M.T., Leiss-Piller, A., Zmek, I., Fischer, M.B., Eibl, M.M. and Wolf, H.M. (2018) Hypomorphic Mutations in the BCR Signalosome Lead to Selective Immunoglobulin M Deficiency and Impaired B-cell Homeostasis. *Frontiers in Immunology*, 9: 2984. doi:10.3389/fimmu.2018.02984.

Genestier, L., Taillardet, M., Mondiere, P., Gheit, H., Bella, C. and Defrance, T. (2007) TLR Agonists Selectively Promote Terminal Plasma Cell Differentiation of B Cell Subsets Specialized in Thymus-Independent Responses. *The Journal of Immunology*, 178 (12): 7779–7786. doi:10.4049/jimmunol.178.12.7779.

Gitlin, A.D., Mayer, C.T., Oliveira, T.Y., Shulman, Z., Jones, M.J.K., Koren, A. and Nussenzweig, M.C.

(2015) T cell help controls the speed of the cell cycle in germinal center B cells. *Science*, 349 (6248): 643–646. doi:10.1126/science.aac4919.

Gitlin, A.D., Shulman, Z. and Nussenzweig, M.C. (2014) Clonal selection in the germinal centre by regulated proliferation and hypermutation. *Nature*, 509 (7502): 637–640. doi:10.1038/nature13300.

Glauzy, S., Sng, J., Bannock, J.M., Gottenberg, J.E., Korganow, A.S., Cacoub, P., Saadoun, D. and Meffre, E. (2017) Defective Early B Cell Tolerance Checkpoints in Sjögren's Syndrome Patients. *Arthritis & rheumatology (Hoboken, N.J.)*, 69 (11): 2203–2208. doi:10.1002/ART.40215.

Glynne, R., Akkaraju, S., Healy, J.I., Rayner, J., Goodnow, C.C. and Mack, D.H. (2000) How self-tolerance and the immunosuppressive drug FK506 prevent B-cell mitogenesis. *Nature*, 403 (6770): 672–676. doi:10.1038/35001102.

Goenka, R., Barnett, L.G., Silver, J.S., O'Neill, P.J., Hunter, C.A., Cancro, M.P. and Laufer, T.M. (2011) Cutting Edge: Dendritic Cell-Restricted Antigen Presentation Initiates the Follicular Helper T Cell Program but Cannot Complete Ultimate Effector Differentiation. *The Journal of Immunology*, 187 (3): 1091–1095. doi:10.4049/jimmunol.1100853.

Gong, S. and Ruprecht, R.M. (2020) Immunoglobulin M: An Ancient Antiviral Weapon – Rediscovered. *Frontiers in Immunology*, 11: 1943. doi:10.3389/fimmu.2020.01943.

Goodnow, C.C., Brink, R. and Adams, E. (1991) Breakdown of self-tolerance in anergic B lymphocytes. *Nature*, 352 (6335): 532–536. doi:10.1038/352532a0.

Goodnow, C.C., Crosbie, J., Adelstein, S., Lavoie, T.B., Smith-Gill, S.J., Brink, R.A., Pritchard-Briscoe, H., Wotherspoon, J.S., Loblay, R.H., Raphael, K., et al. (1988) Altered immunoglobulin expression and functional silencing of self-reactive B lymphocytes in transgenic mice. *Nature*, 334 (6184): 676–682. doi:10.1038/334676a0.

Goodnow, C.C., Crosbie, J., Jorgensen, H., Brink, R.A. and Basten, A. (1989) Induction of self-tolerance in mature peripheral B lymphocytes. *Nature*, 342 (6248): 385–391. doi:10.1038/342385a0.

Gorenjak, M. (2009) 4. Kidneys and Autoimmune Disease. *eJIFCC*, 20 (1): 28–32. Available at: http://www.ncbi.nlm.nih.gov/pubmed/27683324 (Accessed: 1 December 2022).

Graham, K.L., Sutherland, R.M., Mannering, S.I., Zhao, Y., Chee, J., Krishnamurthy, B., Thomas, H.E., Lew, A.M. and Kay, T.W.H. (2012) Pathogenic mechanisms in type 1 diabetes: The islet is both target and driver of disease. *Review of Diabetic Studies*. 9 (4) pp. 148–168. doi:10.1900/RDS.2012.9.148.

Griffin, D.O., Holodick, N.E. and Rothstein, T.L. (2011) Human B1 cells in umbilical cord and adult peripheral blood express the novel phenotype CD20+CD27+CD43+CD70-. *Journal of Experimental Medicine*, 208 (1): 67–80. doi:10.1084/jem.20101499.

Griffin, D.O. and Rothstein, T.L. (2012) Human B1 cell frequency: Isolation and analysis of human B1 cells. *Frontiers in Immunology*, 3 (MAY): 122. doi:10.3389/fimmu.2012.00122.

Guinamard, R., Okigaki, M., Schlessinger, J. and Ravetch, J. V. (2000) Absence of marginal zone B cells in Pyk-2-deficient mice defines their role in the humoral response. *Nature Immunology*, 1 (1): 31–36. doi:10.1038/76882.

Gutzeit, C., Chen, K. and Cerutti, A. (2018) The enigmatic function of IgD: some answers at last. *European Journal of Immunology*. 48 (7) pp. 1101–1113. doi:10.1002/eji.201646547.

Halverson, R., Torres, R.M. and Pelanda, R. (2004) Receptor editing is the main mechanism of B cell tolerance toward membrane antigens. *Nature Immunology*, 5 (6): 645–650. doi:10.1038/ni1076.

Han, J.-I. (2006) RGS1 and RGS13 mRNA silencing in a human B lymphoma line enhances responsiveness to chemoattractants and impairs desensitization. *Journal of Leukocyte Biology*, 79 (6): 1357–1368. doi:10.1189/jlb.1105693.

Han, S., Hathcock, K., Zheng, B., Kepler, T.B., Hodes, R. and Kelsoe, G. (1995a) Cellular interaction in germinal centers. Roles of CD40 ligand and B7-2 in established germinal centers. *The Journal of Immunology*, 155 (2): 556 LP – 567. Available at: http://www.jimmunol.org/content/155/2/556.abstract.

Han, S., Zheng, B., Dal Porto, J. and Kelsoe, G. (1995b) In situ studies of the primary immune response to (4-hydroxy-3-nitrophenyl)acetyl. IV. Affinity-dependent, antigen-driven B cell apoptosis in germinal

centers as a mechanism for maintaining self-tolerance. *Journal of Experimental Medicine*, 182 (6): 1635–1644. doi:10.1084/jem.182.6.1635.

Hancock, W.W., Polanski, M., Zhang, J., Blogg, N. and Weiner, H.L. (1995) Suppression of insulitis in non-obese diabetic (NOD) mice by oral insulin administration is associated with selective expression of interleukin-4 and - 10, transforming growth factor-β, and prostaglandin-E. *American Journal of Pathology*, 147 (5): 1193–1199. Available at: http://www.ncbi.nlm.nih.gov/pubmed/7485382 (Accessed: 15 May 2020).

Hao, Y., O'Neill, P., Naradikian, M.S., Scholz, J.L. and Cancro, M.P. (2011) A B-cell subset uniquely responsive to innate stimuli accumulates in aged mice. *Blood*, 118 (5): 1294–1304. doi:10.1182/blood-2011-01-330530.

Hardy, R.R. (2006) B-1 B Cell Development. *The Journal of Immunology*, 177 (5): 2749–2754. doi:10.4049/jimmunol.177.5.2749.

Hardy, R.R. (2012) "B-lymphocyte Development and Biology." In Paul, W.E. (ed.) *Fundamental Immunology*. 7th ed. Philadelphia, UNITED STATES: Wolters Kluwer. pp. 215–245. Available at: http://ebookcentral.proquest.com/lib/bham/detail.action?docID=3417830.

Hardy, R.R., Carmack, C.E., Shinton, S.A., Kemp, J.D. and Hayakawa, K. (1991) Resolution and characterization of pro-B and pre-pro-B cell stages in normal mouse bone marrow. *Journal of Experimental Medicine*, 173 (5): 1213–1225. doi:10.1084/jem.173.5.1213.

Hardy, R.R., Li, Y.-S., Allman, D., Asano, M., Gui, M. and Hayakawa, K. (2000) B-cell commitment, development and selection. *Immunological Reviews*, 175 (1): 23–32. doi:10.1111/j.1600-065x.2000.imr017517.x.

Hargreaves, C.E., Grasso, M., Hampe, C.S., Stenkova, A., Atkinson, S., Joshua, G.W.P., Wren, B.W., Buckle, A.M., Dunn-Walters, D. and Banga, J.P. (2013) Yersinia enterocolitica Provides the Link between Thyroid-Stimulating Antibodies and Their Germline Counterparts in Graves' Disease . *The Journal of Immunology*, 190 (11): 5373–5381. doi:10.4049/jimmunol.1203412.

Hartley, S.B., Cooke, M.P., Fulcher, D.A., Harris, A.W., Cory, S., Basten, A. and Goodnow, C.C. (1993) Elimination of self-reactive B lymphocytes proceeds in two stages: Arrested development and cell death. *Cell*, 72 (3): 325–335. doi:10.1016/0092-8674(93)90111-3.

Hartley, S.B., Crosbie, J., Brink, R., Kantor, A.B., Basten, A. and Goodnow, C.C. (1991) Elimination from peripheral lymphoid tissues of self-reactive B lymphocytes recognizing membrane-bound antigens. *Nature*, 353 (6346): 765–769. doi:10.1038/353765a0.

Härzschel, A., Li, L., Krenn, P.W., Szenes-Nagy, E., Andrieux, G., Bayer, E., Pfeifer, D., Polcik, L., Denk, U., Höpner, J.P., et al. (2021) Kindlin-3 maintains marginal zone B cells but confines follicular B cell activation and differentiation. *Journal of Leukocyte Biology*. doi:10.1002/jlb.1hi0621-313r.

Hasler, P. and Zouali, M. (2005) Immune receptor signaling, aging, and autoimmunity. *Cellular Immunology*, 233 (2): 102–108. doi:10.1016/j.cellimm.2005.04.012.

Hayakawa, K., Asano, M., Shinton, S.A., Gui, M., Allman, D., Stewart, C.L., Silver, J. and Hardy, R.R. (1999) Positive selection of natural autoreactive B cells. *Science*, 285 (5424): 113–116. doi:10.1126/science.285.5424.113.

Hayashi, Y., Utsuyama, M., Kurashima, C. and Hirokawa, K. (1989) Spontaneous development of organ-specific autoimmune lesions in aged C57BL/6 mice. *Clinical and experimental immunology*, 78 (1): 120–6. Available at: http://www.ncbi.nlm.nih.gov/pubmed/2805415 (Accessed: 12 December 2022).

Haynes, B.F., Fleming, J., St. Clair, E.W., Katinger, H., Stiegler, G., Kunert, R., Robinson, J., Scearce, R.M., Plonk, K., Staats, H.F., et al. (2005) Immunology: Cardiolipin polyspecific autoreactivity in two broadly neutralizing HIV-1 antibodies. *Science*, 308 (5730): 1906–1908. doi:10.1126/science.1111781.

Heath, W.R., Kato, Y., Steiner, T.M. and Caminschi, I. (2019) Antigen presentation by dendritic cells for B cell activation. *Current Opinion in Immunology*, 58: 44–52. doi:10.1016/j.coi.2019.04.003.

Henderson, R.B., Grys, K., Vehlow, A., De Bettignies, C., Zachacz, A., Henley, T., Turner, M., Batista, F. and Tybulewicz, V.L.J. (2010) A novel Rac-dependent checkpoint in B cell development controls entry into the splenic white pulp and cell survival. *Journal of Experimental Medicine*, 207 (4): 837–853.

doi:10.1084/jem.20091489.

Hertz, M. and Nemazee, D. (1997) BCR ligation induces receptor editing in IgM+IgD- bone marrow B cells in vitro. *Immunity*, 6 (4): 429–436. doi:10.1016/S1074-7613(00)80286-1.

Hess, J., Werner, A., Wirth, T., Melchers, F., Jäck, H.M. and Winkler, T.H. (2001) Induction of pre-B cell proliferation after de novo synthesis of the pre-B cell receptor. *Proceedings of the National Academy of Sciences of the United States of America*, 98 (4): 1745–1750. doi:10.1073/pnas.98.4.1745.

Hill, D.L., Whyte, C.E., Innocentin, S., Le Lee, J., Dooley, J., Wang, J., James, E.A., Lee, J.C., Kwok, W.W., Zand, M.S., et al. (2021) Impaired HA-specific T follicular helper cell and antibody responses to influenza vaccination are linked to inflammation in humans. *eLife*, 10. doi:10.7554/ELIFE.70554.

Horikawa, K., Martin, S.W., Pogue, S.L., Silver, K., Peng, K., Takatsu, K. and Goodnow, C.C. (2007) Enhancement and suppression of signaling by the conserved tail of IgG memory-type B cell antigen receptors. *Journal of Experimental Medicine*, 204 (4): 759–769. doi:10.1084/jem.20061923.

Hoyer, B.F., Moser, K., Hauser, A.E., Peddinghaus, A., Voigt, C., Eilat, D., Radbruch, A., Hiepe, F. and Manz, R.A. (2004) Short-lived plasmablasts and long-lived plasma cells contribute to chronic humoral autoimmunity in NZB/W mice. *Journal of Experimental Medicine*, 199 (11): 1577–1584. doi:10.1084/jem.20040168.

Hsieh, C., Chang, A., Brandt, D., Guttikonda, R., Utset, T.O. and Clark, M.R. (2011) Predicting outcomes of lupus nephritis with tubulointerstitial inflammation and scarring. *Arthritis Care and Research*, 63 (6): 865–874. doi:10.1002/acr.20441.

Hsu, M.C., Toellner, K.M., Vinuesa, C.G. and MacLennan, I.C.M. (2006) B cell clones that sustain long-term plasmablast growth in T-independent extrafollicular antibody responses. *Proceedings of the National Academy of Sciences of the United States of America*, 103 (15): 5905–5910. doi:10.1073/pnas.0601502103.

Hwang, I.Y., Hwang, K.S., Park, C., Harrison, K.A. and Kehrl, J.H. (2013) Rgs13 Constrains Early B Cell Responses and Limits Germinal Center Sizes. *PLoS ONE*, 8 (3): 60139. doi:10.1371/journal.pone.0060139.

Inglis, J.J., Criado, G., Medghalchi, M., Andrews, M., Sandison, A., Feldmann, M. and Williams, R.O. (2007) Collagen-induced arthritis in C57BL/6 mice is associated with a robust and sustained T-cell response to type II collagen. *Arthritis Research and Therapy*, 9 (5): 1–8. doi:10.1186/ar2319.

Inglis, J.J., Šimelyte, E., McCann, F.E., Criado, G. and Williams, R.O. (2008) Protocol for the induction of arthritis in C57BL/6 mice. *Nature Protocols*, 3 (4): 612–618. doi:10.1038/nprot.2008.19.

Inoue, T., Moran, I., Shinnakasu, R., Phan, T.G. and Kurosaki, T. (2018) Generation of memory B cells and their reactivation. *Immunological Reviews*, 283 (1): 138–149. doi:10.1111/imr.12640.

Jackson, S.W., Kolhatkar, N.S. and Rawlings, D.J. (2015) B cells take the front seat: Dysregulated B cell signals orchestrate loss of tolerance and autoantibody production. *Current Opinion in Immunology*, 33: 70–77. doi:10.1016/j.coi.2015.01.018.

Jacob, J., Kassir, R. and Kelsoe, G. (1991a) In situ studies of the primary immune response to (4-hydroxy-3-nitrophenyl)acetyl. I. The architecture and dynamics of responding cell populations. *Journal of Experimental Medicine*, 173 (5): 1165–1175. doi:10.1084/jem.173.5.1165.

Jacob, J. and Kelsoe, G. (1992) In situ studies of the primary immune response to (4-hydroxy-3-nitrophenyl)acetyl. II. A common clonal origin for periarteriolar lymphoid sheath-associated foci and germinal centers. *Journal of Experimental Medicine*, 176 (3): 679–687. doi:10.1084/jem.176.3.679.

Jacob, J., Kelsoe, G., Rajewsky, K. and Weiss, U. (1991b) Intraclonal generation of antibody mutants in germinal centres. *Nature*, 354 (6352): 389–392. doi:10.1038/354389a0.

Jacob, J., Przylepa, J., Miller, C. and Kelsoe, G. (1993) In situ studies of the primary immune response to (4-hydroxy-3-nitrophenyl)acetyl. III. The kinetics of V region mutation and selection in germinal center B cells. *Journal of Experimental Medicine*, 178 (4): 1293–1307. doi:10.1084/jem.178.4.1293.

Jang, E., Cho, W.S., Cho, M.-L., Park, H.-J., Oh, H.-J., Kang, S.M., Paik, D.-J. and Youn, J. (2011) Foxp3 + Regulatory T Cells Control Humoral Autoimmunity by Suppressing the Development of Long-

Lived Plasma Cells . *The Journal of Immunology*, 186 (3): 1546–1553. doi:10.4049/jimmunol.1002942.

Jang, E., Cho, W.S., Oh, Y.-K., Cho, M.-L., Kim, J.M., Paik, D.-J. and Youn, J. (2016) Splenic Long-Lived Plasma Cells Promote the Development of Follicular Helper T Cells during Autoimmune Responses. *The Journal of Immunology*, 196 (3): 1026–1035. doi:10.4049/jimmunol.1401059.

Jenks, S.A., Cashman, K.S., Zumaquero, E., Marigorta, U.M., Patel, A. V., Wang, X., Tomar, D., Woodruff, M.C., Simon, Z., Bugrovsky, R., et al. (2018) Distinct Effector B Cells Induced by Unregulated Toll-like Receptor 7 Contribute to Pathogenic Responses in Systemic Lupus Erythematosus. *Immunity*, 49 (4): 725-739.e6. doi:10.1016/j.immuni.2018.08.015.

Junt, T., Moseman, E.A., Iannacone, M., Massberg, S., Lang, P.A., Boes, M., Fink, K., Henrickson, S.E., Shayakhmetov, D.M., Di Paolo, N.C., et al. (2007) Subcapsular sinus macrophages in lymph nodes clear lymph-borne viruses and present them to antiviral B cells. *Nature*, 450 (7166): 110–114. doi:10.1038/nature06287.

Kaisho, T., Schwenk, F. and Rajewsky, K. (1997) The roles of γ1 heavy chain membrane expression and cytoplasmic tail in IgG1 responses. *Science*, 276 (5311): 412–415. doi:10.1126/science.276.5311.412.

Kanayama, N., Cascalho, M. and Ohmori, H. (2005) Analysis of Marginal Zone B Cell Development in the Mouse with Limited B Cell Diversity: Role of the Antigen Receptor Signals in the Recruitment of B Cells to the Marginal Zone. *The Journal of Immunology*, 174 (3): 1438–1445. doi:10.4049/jimmunol.174.3.1438.

Karasuyama, H., Kudo, A. and Melchers, F. (1990) The proteins encoded by the VpreB and λ5 Pre-B cell-specific genes can associate with each other and with μ heavy chain. *Journal of Experimental Medicine*, 172 (3): 969–972. doi:10.1084/jem.172.3.969.

Karnell, F.G., Brezski, R.J., King, L.B., Silverman, M.A. and Monroe, J.G. (2005) Membrane cholesterol content accounts for developmental differences in surface B cell receptor compartmentalization and signaling. *Journal of Biological Chemistry*, 280 (27): 25621–25628. doi:10.1074/jbc.M503162200.

Kawabe, T., Naka, T., Yoshida, K., Tanaka, T., Fujiwara, H., Suematsu, S., Yoshida, N., Kishimoto, T. and Kikutani, H. (1994) The immune responses in CD40-deficient mice: Impaired immunoglobulin class switching and germinal center formation. *Immunity*, 1 (3): 167–178. doi:10.1016/1074-7613(94)90095-7.

Kawahara, T., Ohdan, H., Zhao, G., Yang, Y.-G. and Sykes, M. (2003) *Peritoneal Cavity B Cells Are Precursors of Splenic IgM Natural Antibody-Producing Cells*. doi:10.4049/jimmunol.171.10.5406.

Kerfoot, S.M., Yaari, G., Patel, J.R., Johnson, K.L., Gonzalez, D.G., Kleinstein, S.H. and Haberman, A.M. (2011) Germinal Center B Cell and T Follicular Helper Cell Development Initiates in the Interfollicular Zone. *Immunity*, 34 (6): 947–960. doi:10.1016/j.immuni.2011.03.024.

Khalil, A.M., Cambier, J.C. and Shlomchik, M.J. (2012) B cell receptor signal transduction in the GC is short-circuited by high phosphatase activity. *Science*, 336 (6085): 1178–1181. doi:10.1126/science.1213368.

Khan, W.N., Alt, F.W., Gerstein, R.M., Malynn, B.A., Larsson, I., Rathbun, G., Davidson, L., Müller, S., Kantor, A.B., Herzenberg, L.A., et al. (1995) Defective B cell development and function in Btk-deficient mice. *Immunity*, 3 (3): 283–299. doi:10.1016/1074-7613(95)90114-0.

Khoury, D.S., Cromer, D., Reynaldi, A., Schlub, T.E., Wheatley, A.K., Juno, J.A., Subbarao, K., Kent, S.J., Triccas, J.A. and Davenport, M.P. (2021) Neutralizing antibody levels are highly predictive of immune protection from symptomatic SARS-CoV-2 infection. *Nature Medicine*, 27 (7): 1205–1211. doi:10.1038/s41591-021-01377-8.

Kitamura, D., Roes, J., Kühn, R. and Rajewsky, K. (1991) A B cell-deficient mouse by targeted disruption of the membrane exon of the immunoglobulin μ chain gene. *Nature*, 350 (6317): 423–426. doi:10.1038/350423a0.

Kitano, M., Moriyama, S., Ando, Y., Hikida, M., Mori, Y., Kurosaki, T. and Okada, T. (2011) Bcl6 Protein Expression Shapes Pre-Germinal Center B Cell Dynamics and Follicular Helper T Cell Heterogeneity. *Immunity*, 34 (6): 961–972. doi:10.1016/j.immuni.2011.03.025.

Kodama, T., Hasegawa, M., Sakamoto, Y., Haniuda, K. and Kitamura, D. (2020) Ubiquitination of IgG1 cytoplasmic tail modulates B-cell signalling and activation. *International Immunology*, 32 (6): 385–395. doi:10.1093/intimm/dxaa009.

Kolhatkar, N.S., Brahmandam, A., Thouvene, C.D., Becker-Herman, S., Jacobs, H.M., Schwartz, M.A., Allenspach, E.J., Khim, S., Panigrahi, A.K., Prak, E.T.L., et al. (2015) Altered BCR and TLR signals promote enhanced positive selection of autoreactive transitional B cells in Wiskott-Aldrich syndrome. *Journal of Experimental Medicine*, 212 (10): 1663–1667. doi:10.1084/jem.20150585.

Korn, T., Bettelli, E., Gao, W., Awasthi, A., Jäger, A., Strom, T.B., Oukka, M. and Kuchroo, V.K. (2007) IL-21 initiates an alternative pathway to induce proinflammatory T H17 cells. *Nature*, 448 (7152): 484–487. doi:10.1038/nature05970.

Kraus, M., Pao, L.I., Reichlin, A., Hu, Y., Canono, B., Cambier, J.C., Nussenzweig, M.C. and Rajewsky, K. (2001) Interference with immunoglobulin (Ig)α immunoreceptor tyrosine-based activation motif (ITAM) phosphorylation modulates or blocks B cell development, depending on the availability of an Igβ cytoplasmic tail. *Journal of Experimental Medicine*, 194 (4): 455–469. doi:10.1084/jem.194.4.455.

Kreslavsky, T., Vilagos, B., Tagoh, H., Poliakova, D.K., Schwickert, T.A., Wöhner, M., Jaritz, M., Weiss, S., Taneja, R., Rossner, M.J., et al. (2017) Essential role for the transcription factor Bhlhe41 in regulating the development, self-renewal and BCR repertoire of B-1a cells. *Nature Immunology*, 18 (4): 442–455. doi:10.1038/ni.3694.

Kreslavsky, T., Wong, J.B., Fischer, M., Skok, J.A. and Busslinger, M. (2018) Control of B-1a cell development by instructive BCR signaling. *Current opinion in immunology*, 51: 24. doi:10.1016/J.COI.2018.01.001.

Kreuk, L.S.M., Koch, M.A., Slayden, L.C., Lind, N.A., Chu, S., Savage, H.P., Kantor, A.B., Baumgarth, N. and Barton, G.M. (2019) B cell receptor and toll-like receptor signaling coordinate to control distinct B-1 responses to both self and the microbiota. *eLife*, 8. doi:10.7554/eLife.47015.

Ktsoyan, Z., Budaghyan, L., Agababova, M., Mnatsakanyan, A., Arakelova, K., Gevorgyan, Z., Sedrakyan, A., Hovhannisyan, A., Mkrtchyan, M., Zakharyan, M., et al. (2019) Potential involvement of salmonella infection in autoimmunity. *Pathogens*, 8 (3): 96. doi:10.3390/pathogens8030096.

Kuo, T.C. and Schlissel, M.S. (2009) Mechanisms controlling expression of the RAG locus during lymphocyte development. *Current Opinion in Immunology*. 21 (2) pp. 173–178. doi:10.1016/j.coi.2009.03.008.

Kuraoka, M., Schmidt, A.G., Nojima, T., Feng, F., Watanabe, A., Kitamura, D., Harrison, S.C., Kepler, T.B. and Kelsoe, G. (2016) Complex Antigens Drive Permissive Clonal Selection in Germinal Centers. *Immunity*, 44 (3): 542–552. doi:10.1016/j.immuni.2016.02.010.

Kurosaki, T., Kometani, K. and Ise, W. (2015) Memory B cells. *Nature Reviews Immunology*, 15 (3): 149–159. doi:10.1038/nri3802.

Kyogoku, C., Langefeld, C.D., Ortmann, W.A., Lee, A., Selby, S., Carlton, V.E.H., Chang, M., Ramos, P., Baechler, E.C., Batliwalla, F.M., et al. (2004) Genetic association of the R620W polymorphism of protein tyrosine phosphatase PTPN22 with human SLE. *American Journal of Human Genetics*, 75 (3): 504–507. doi:10.1086/423790.

Lam, K.P., Kühn, R. and Rajewsky, K. (1997) In vivo ablation of surface immunoglobulin on mature B cells by inducible gene targeting results in rapid cell death. *Cell*, 90 (6): 1073–1083. doi:10.1016/S0092-8674(00)80373-6.

Lankar, D., Vincent-Schneider, H., Briken, V., Yokozeki, T., Raposo, G. and Bonnerot, C. (2002) Dynamics of major histocompatibility complex class II compartments during B cell receptor-mediated cell activation. *Journal of Experimental Medicine*, 195 (4): 461–472. doi:10.1084/jem.20011543.

Lee, J. Le, Fra-Bido, S.C., Burton, A.R., Innocentin, S., Hill, D.L. and Linterman, M.A. (2022) B cell-intrinsic changes with age do not impact antibody-secreting cell formation but delay B cell participation in the germinal centre reaction. *Aging cell*, p. e13692. doi:10.1111/acel.13692.

Lee, J. Le and Linterman, M.A. (2022) Mechanisms underpinning poor antibody responses to vaccines in ageing. *Immunology Letters*, 241: 1–14. doi:10.1016/j.imlet.2021.11.001.

Lee, S.K., Silva, D.G., Martin, J.L., Pratama, A., Hu, X., Chang, P.P., Walters, G. and Vinuesa, C.G. (2012) Interferon-γ Excess Leads to Pathogenic Accumulation of Follicular Helper T Cells and Germinal Centers. *Immunity*, 37 (5): 880–892. doi:10.1016/j.immuni.2012.10.010.

Lefebvre, J.S., Maue, A.C., Eaton, S.M., Lanthier, P.A., Tighe, M. and Haynes, L. (2012) The aged microenvironment contributes to the age-related functional defects of CD4 T cells in mice. *Aging Cell*, 11 (5): 732–740. doi:10.1111/j.1474-9726.2012.00836.x.

Lentz, V.M. and Manser, T. (2001) Cutting Edge: Germinal Centers Can Be Induced in the Absence of T Cells. *The Journal of Immunology*, 167 (1): 15–20. doi:10.4049/jimmunol.167.1.15.

Leslie, D., Lipsky, P. and Louis Notkins, A. (2001) Autoantibodies as predictors of disease. *Journal of Clinical Investigation*, 108 (10): 1417–1422. doi:10.1172/JCI14452.

Lewis, S.M., Williams, A. and Eisenbarth, S.C. (2019) Structure and function of the immune system in the spleen. *Science Immunology*. 4 (33). doi:10.1126/sciimmunol.aau6085.

Li, Y., Bleakley, M. and Yee, C. (2005) IL-21 Influences the Frequency, Phenotype, and Affinity of the Antigen-Specific CD8 T Cell Response. *The Journal of Immunology*, 175 (4): 2261–2269. doi:10.4049/jimmunol.175.4.2261.

Liberzon, A., Birger, C., Thorvaldsdóttir, H., Ghandi, M., Mesirov, J.P. and Tamayo, P. (2015) The Molecular Signatures Database Hallmark Gene Set Collection. *Cell Systems*, 1 (6): 417–425. doi:10.1016/j.cels.2015.12.004.

Liberzon, A., Subramanian, A., Pinchback, R., Thorvaldsdóttir, H., Tamayo, P. and Mesirov, J.P. (2011) Molecular signatures database (MSigDB) 3.0. *Bioinformatics*, 27 (12): 1739–1740. doi:10.1093/bioinformatics/btr260.

Like, A.A. and Rossini, A.A. (1976) Streptozotocin-induced pancreatic insulitis: New model of diabetes mellitus. *Science*, 193 (4251): 415–417. doi:10.1126/science.180605.

Linterman, M.A., Beaton, L., Yu, D., Ramiscal, R.R., Srivastava, M., Hogan, J.J., Verma, N.K., Smyth, M.J., Rigby, R.J. and Vinuesa, C.G. (2010) IL-21 acts directly on B cells to regulate Bcl-6 expression and germinal center responses. *Journal of Experimental Medicine*, 207 (2): 353–363. doi:10.1084/jem.20091738.

Linterman, M.A., Rigby, R.J., Wong, R.K., Yu, D., Brink, R., Cannons, J.L., Schwartzberg, P.L., Cook, M.C., Walters, G.D. and Vinuesa, C.G. (2009) Follicular helper T cells are required for systemic autoimmunity. *Journal of Experimental Medicine*, 206 (3): 561–576. doi:10.1084/jem.20081886.

Liu, D., Xu, H., Shih, C., Wan, Z., Ma, X., Ma, W., Luo, D. and Qi, H. (2015) T-B-cell entanglement and ICOSL-driven feed-forward regulation of germinal centre reaction. *Nature*, 517 (7533): 214–218. doi:10.1038/nature13803.

Liu, D., Yan, J., Sun, J., Liu, B., Ma, W., Li, Y., Shao, X. and Qi, H. (2021) BCL6 controls contact-dependent help delivery during follicular T-B cell interactions. *Immunity*, 54 (10): 2245-2255.e4. doi:10.1016/j.immuni.2021.08.003.

Liu, W., Chen, E., Zhao, X.W., Wan, Z.P., Gao, Y.R., Davey, A., Huang, E., Zhang, L., Crocetti, J., Sandoval, G., et al. (2012) The scaffolding protein synapse-associated protein 97 is required for enhanced signaling through isotype-switched IgG memory B cell receptors. *Science Signaling*, 5 (235): ra54–ra54. doi:10.1126/scisignal.2002820.

Liu, W., Meckel, T., Tolar, P., Won Sohn, H. and Pierce, S.K. (2010) Intrinsic properties of immunoglobulin IgG1 isotype-switched B cell receptors promote microclustering and the initiation of signaling. *Immunity*, 32 (6): 778–789. doi:10.1016/j.immuni.2010.06.006.

Liu, X., Zhao, Y. and Qi, H. (2022) T-independent antigen induces humoral memory through germinal centers. *Journal of Experimental Medicine*, 219 (3). doi:10.1084/jem.20210527.

Liu, Y. -J, Mason, D.Y., Johnson, G.D., Abbot, S., Gregory, C.D., Hardie, D.L., Gordon, J. and MacLennan, I.C.M. (1991) Germinal center cells express bcl-2 protein after activation by signals which prevent their entry into apoptosis. *European Journal of Immunology*, 21 (8): 1905–1910. doi:10.1002/eji.1830210819.

Liu, Y.J., Joshua, D.E., Williams, G.T., Smith, C.A., Gordon, J. and MacLennan, I.C.M. (1989) Mechanism of antigen-driven selection in germinal centres. *Nature*, 342 (6252): 929–931. doi:10.1038/342929a0.

Loder, F., Mutschler, B., Ray, R.J., Paige, C.J., Sideras, P., Torres, R., Lamers, M.C. and Carsetti, R. (1999) B cell development in the spleen takes place in discrete steps and is determined by the quality of B cell receptor-derived signals. *Journal of Experimental Medicine*, 190 (1): 75–89. doi:10.1084/jem.190.1.75.

Loh, D.Y., Bothwell, A.L.M., White-Scharf, M.E., Imanishi-Kari, T. and Baltimore, D. (1983) Molecular basis of a mouse strain-specific anti-hapten response. *Cell*, 33 (1): 85–93. doi:10.1016/0092-8674(83)90337-9.

Lopez, A.F., Strath, M. and Sanderson, C.J. (1983) Mouse immunoglobulin isotypes mediating cytotoxicity of target cells by eosinophils and neutrophils. *Immunology*, 48 (3): 503–509. Available at: /pmc/articles/PMC1454033/?report=abstract (Accessed: 19 December 2021).

Love, M.I., Huber, W. and Anders, S. (2014) Moderated estimation of fold change and dispersion for RNA-seq data with DESeq2. *Genome Biology*, 15 (12): 550. doi:10.1186/s13059-014-0550-8.

Lu, L. and Osmond, D.G. (2000) Apoptosis and its modulation during B lymphopoiesis in mouse bone marrow. *Immunological Reviews*, 175 (1): 158–174. doi:10.1111/j.1600-065x.2000.imr017506.x.

Lu, R.M., Hwang, Y.C., Liu, I.J., Lee, C.C., Tsai, H.Z., Li, H.J. and Wu, H.C. (2020) Development of therapeutic antibodies for the treatment of diseases. *Journal of Biomedical Science*, 27 (1): 1–30. doi:10.1186/s12929-019-0592-z.

Luo, W., Weisel, F. and Shlomchik, M.J. (2018) B Cell Receptor and CD40 Signaling Are Rewired for Synergistic Induction of the c-Myc Transcription Factor in Germinal Center B Cells. *Immunity*, 48 (2): 313-326.e5. doi:10.1016/j.immuni.2018.01.008.

Luzina, I.G., Atamas, S.P., Storrer, C.E., daSilva, L.C., Kelsoe, G., Papadimitriou, J.C. and Handwerger, B.S. (2001) Spontaneous formation of germinal centers in autoimmune mice. *Journal of leukocyte biology*, 70 (4): 578–84. doi:10.1189/jlb.70.4.578.

Lyu, X., Zhao, Q., Hui, J., Wang, T., Lin, M., Wang, K., Zhang, J., Shentu, J., Dalby, P.A., Zhang, H., et al. (2022) The global landscape of approved antibody therapies. *Antibody Therapeutics*, 5 (4): 233. doi:10.1093/ABT/TBAC021.

Ma, J., Zhu, C., Ma, B., Tian, J., Baidoo, S.E., Mao, C., Wu, W., Chen, J., Tong, J., Yang, M., et al. (2012) Increased frequency of circulating follicular helper T cells in patients with rheumatoid arthritis. *Clinical & developmental immunology*, 2012. doi:10.1155/2012/827480.

Ma, S., Wang, C., Mao, X. and Hao, Y. (2019) R Cells dysfunction associated with aging and autoimmune disease. *Frontiers in Immunology*, 10 (FEB): 318. doi:10.3389/fimmu.2019.00318.

Ma, X., Zhu, Y., Dong, D., Chen, Y., Wang, S., Yang, D., Ma, Z., Zhang, A., Zhang, F., Guo, C., et al. (2022) Cryo-EM structures of two human B cell receptor isotypes. *Science*, 377 (6608): 880–885. doi:10.1126/science.abo3828.

Van Der Maaten, L. and Hinton, G. (2008) Visualizing data using t-SNE. *Journal of Machine Learning Research*, 9: 2579–2625.

MacLennan, I.C.M. (1994a) Germinal Centers. *Annual Review of Immunology*, 12 (1): 117–139. doi:10.1146/annurev.iy.12.040194.001001.

MacLennan, I.C.M. (1994b) Somatic Mutation: From the dark zone to the light. *Current Biology*, 4 (1): 70–72. doi:10.1016/S0960-9822(00)00017-8.

MacLennan, I.C.M., Toellner, K.M., Cunningham, A.F., Serre, K., Sze, D.M.Y., Zúñiga, E., Cook, M.C. and Vinuesa, C.G. (2003) Extrafollicular antibody responses. *Immunological Reviews*, 194 (1): 8–18. doi:10.1034/j.1600-065X.2003.00058.x.

Maki, R., Roeder, W., Traunecker, A., Sidman, C., Wabl, M., Raschke, W. and Tonegawa, S. (1981) The role of DNA rearrangement and alternative RNA processing in the expression of immunoglobulin delta genes. *Cell*, 24 (2): 353–365. doi:10.1016/0092-8674(81)90325-1.

Marshall, J.L., Flores-Langarica, A., Kingsley, R.A., Hitchcock, J.R., Ross, E.A., López-Macías, C., Lakey, J., Martin, L.B., Toellner, K.-M., MacLennan, C.A., et al. (2012) The Capsular Polysaccharide Vi from Salmonella Typhi Is a B1b Antigen . *The Journal of Immunology*, 189 (12): 5527–5532. doi:10.4049/jimmunol.1103166.

Marshall, J.L., Zhang, Y., Pallan, L., Hsu, M.C., Khan, M., Cunningham, A.F., Maclennan, I.C.M. and Toellner, K.M. (2011) Early B blasts acquire a capacity for Ig class switch recombination that is lost as they become plasmablasts. *European Journal of Immunology*, 41 (12): 3506–3512. doi:10.1002/eji.201141762.

Martin, F. and Chan, A.C. (2004) Pathogenic roles of B cells in human autoimmunity: Insights from the clinic. *Immunity*. 20 (5) pp. 517–527. doi:10.1016/S1074-7613(04)00112-8.

Martin, F., Oliver, A.M. and Kearney, J.F. (2001) Marginal zone and B1 B cells unite in the early response against T-independent blood-borne particulate antigens. *Immunity*, 14 (5): 617–629. doi:10.1016/S1074-7613(01)00129-7.

Martin, S.W. and Goodnow, C.C. (2002) Burst-enhancing role of the IgG membrane tail as a molecular determinant of memory. *Nature Immunology*, 3 (2): 182–188. doi:10.1038/ni752.

Mason, D.Y., Jones, M. and Good Now, C.C. (1992) Development and follicular localization of tolerant b lymphocytes in lysozyme/anti-lysozyme igm/lgd transgenic mice. *International Immunology*, 4 (2): 163–175. doi:10.1093/intimm/4.2.163.

Masters, A.R., Jellison, E.R., Puddington, L., Khanna, K.M. and Haynes, L. (2018) Attrition of T Cell Zone Fibroblastic Reticular Cell Number and Function in Aged Spleens. *ImmunoHorizons*, 2 (5): 155–163. doi:10.4049/immunohorizons.1700062.

Mayer, C.T., Gazumyan, A., Kara, E.E., Gitlin, A.D., Golijanin, J., Viant, C., Pai, J., Oliveira, T.Y., Wang, Q., Escolano, A., et al. (2017) The microanatomic segregation of selection by apoptosis in the germinal center. *Science*, 358 (6360): eaao2602. doi:10.1126/science.aao2602.

Mayer, C.T., Nieke, J.P., Gazumyan, A., Cipolla, M., Wang, Q., Oliveira, T.Y., Ramos, V., Monette, S., Li, Q.Z., Gershwin, M.E., et al. (2020) An apoptosis-dependent checkpoint for autoimmunity in memory B and plasma cells. *Proceedings of the National Academy of Sciences of the United States of America*, 117 (40): 24957–24963. doi:10.1073/pnas.2015372117.

Medzhitov, R. and Janeway, C.A. (1997) Innate immunity: The virtues of a nonclonal system of recognition. *Cell*. 91 (3) pp. 295–298. doi:10.1016/S0092-8674(00)80412-2.

Merkenschlager, J., Finkin, S., Ramos, V., Kraft, J., Cipolla, M., Nowosad, C.R., Hartweger, H., Zhang, W., Olinares, P.D.B., Gazumyan, A., et al. (2021) Dynamic regulation of TFH selection during the germinal centre reaction. *Nature*, 591 (7850): 458–463. doi:10.1038/s41586-021-03187-x.

Merle, N.S., Church, S.E., Fremeaux-Bacchi, V. and Roumenina, L.T. (2015a) Complement system part I - molecular mechanisms of activation and regulation. *Frontiers in Immunology*. 6 (JUN). doi:10.3389/fimmu.2015.00262.

Merle, N.S., Noe, R., Halbwachs-Mecarelli, L., Fremeaux-Bacchi, V. and Roumenina, L.T. (2015b) Complement system part II: Role in immunity. *Frontiers in Immunology*. 6 (MAY). doi:10.3389/fimmu.2015.00257.

Merrell, K.T., Benschop, R.J., Gauld, S.B., Aviszus, K., Decote-Ricardo, D., Wysocki, L.J. and Cambier, J.C. (2006) Identification of Anergic B Cells within a Wild-Type Repertoire. *Immunity*, 25 (6): 953–962. doi:10.1016/j.immuni.2006.10.017.

Mesin, L., Ersching, J. and Victora, G.D. (2016) Germinal Center B Cell Dynamics. *Immunity*. 45 (3) pp. 471–482. doi:10.1016/j.immuni.2016.09.001.

Michaelsen, T.E., Kolberg, J., Aase, A., Herstad, T.K. and Høiby, E.A. (2004) The four mouse IgG isotypes differ extensively in bactericidal and opsonophagocytic activity when reacting with the P1.16 epitope on the outer membrane PorA protein of Neisseria meningitidis. *Scandinavian Journal of Immunology*, 59 (1): 34–39. doi:10.1111/j.0300-9475.2004.01362.x.

Minges Wols, H.A., Johnson, K.M., Ippolito, J.A., Birjandi, S.Z., Su, Y., Le, P.T. and Witte, P.L. (2010) Migration of immature and mature B cells in the aged microenvironment. *Immunology*, 129 (2): 278–

290. doi:10.1111/j.1365-2567.2009.03182.x.

Minnich, M., Tagoh, H., Bönelt, P., Axelsson, E., Fischer, M., Cebolla, B., Tarakhovsky, A., Nutt, S.L., Jaritz, M. and Busslinger, M. (2016) Multifunctional role of the transcription factor Blimp-1 in coordinating plasma cell differentiation. *Nature Immunology*, 17 (3): 331–343. doi:10.1038/ni.3349.

Moran, A.E., Holzapfel, K.L., Xing, Y., Cunningham, N.R., Maltzman, J.S., Punt, J. and Hogquist, K.A. (2011) T cell receptor signal strength in Treg and iNKT cell development demonstrated by a novel fluorescent reporter mouse. *Journal of Experimental Medicine*, 208 (6): 1279–1289. doi:10.1084/jem.20110308.

Morris, D.L. and Rothstein, T.L. (1993) Abnormal transcription factor induction through the surface immunoglobulin M receptor of B-1 lymphocytes. *Journal of Experimental Medicine*, 177 (3): 857–861. doi:10.1084/jem.177.3.857.

Mueller, J., Matloubian, M. and Zikherman, J. (2015) Cutting Edge: An In Vivo Reporter Reveals Active B Cell Receptor Signaling in the Germinal Center. *The Journal of Immunology*, 194 (7): 2993–2997. doi:10.4049/jimmunol.1403086.

Muramatsu, M., Kinoshita, K., Fagarasan, S., Yamada, S., Shinkai, Y. and Honjo, T. (2000) Class switch recombination and hypermutation require activation-induced cytidine deaminase (AID), a potential RNA editing enzyme. *Cell*, 102 (5): 553–563. doi:10.1016/S0092-8674(00)00078-7.

Murphy, K., Travers, P. and Walport, M. (2008) *Janeway's Immunobiology*. 7th Ed. New York: Garland Science.

Nagasawa, T. (2006) Microenvironmental niches in the bone marrow required for B-cell development. *Nature Reviews Immunology*. 6 (2) pp. 107–116. doi:10.1038/nri1780.

Nagele, E.P., Han, M., Acharya, N.K., Demarshall, C., Kosciuk, M.C. and Nagele, R.G. (2013) Natural IgG Autoantibodies Are Abundant and Ubiquitous in Human Sera, and Their Number Is Influenced By Age, Gender, and Disease. *PLoS ONE*, 8 (4): e60726. doi:10.1371/journal.pone.0060726.

Nakagawa, R. and Calado, D.P. (2021) Positive Selection in the Light Zone of Germinal Centers. *Frontiers in Immunology*, 12: 1053. doi:10.3389/fimmu.2021.661678.

Nakagawa, R., Toboso-Navasaa, A., Schipsb, M., Young, G., Bhaw-Rosun, L., Llorian-Sopena, M., Chakravarty, P., Sesay, A.K., Kassiotis, G., Meyer-Hermann, M., et al. (2021) Permissive selection followed by affinity-based proliferation of GC light zone B cells dictates cell fate and ensures clonal breadth. *Proceedings of the National Academy of Sciences of the United States of America*, 118 (2). doi:10.1073/PNAS.2016425118.

Nemazee, D. (2006) Receptor editing in lymphocyte development and central tolerance. *Nature Reviews Immunology*. 6 (10) pp. 728–740. doi:10.1038/nri1939.

Nemazee, D. (2017) Mechanisms of central tolerance for B cells. *Nature Reviews Immunology*, 17 (5): 281–294. doi:10.1038/nri.2017.19.

Nemazee, D.A. and Bürki, K. (1989) Clonal deletion of B lymphocytes in a transgenic mouse bearing anti-MHC class I antibody genes. *Nature*, 337 (6207): 562–566. doi:10.1038/337562a0.

Neuberger, M.S. and Rajewsky, K. (1981) Activation of mouse complement by monoclonal mouse antibodies. *European Journal of Immunology*, 11 (12): 1012–1016. doi:10.1002/eji.1830111212.

Nguyen, T.T.T., Elsner, R.A. and Baumgarth, N. (2015) Natural IgM Prevents Autoimmunity by Enforcing B Cell Central Tolerance Induction. *The Journal of Immunology*, 194 (4): 1489–1502. doi:10.4049/jimmunol.1401880.

Nimmerjahn, F., Bruhns, P., Horiuchi, K. and Ravetch, J. V. (2005) FcγRIV: A novel FcR with distinct IgG subclass specificity. *Immunity*, 23 (1): 41–51. doi:10.1016/j.immuni.2005.05.010.

Nimmerjahn, F. and Ravetch, J. V. (2005) Immunology: Divergent immunoglobulin G subclass activity through selective Fc receptor binding. *Science*, 310 (5753): 1510–1512. doi:10.1126/science.1118948.

Di Noia, J.M. and Neuberger, M.S. (2007) Molecular Mechanisms of Antibody Somatic Hypermutation. *Annual Review of Biochemistry*, 76 (1): 1–22. doi:10.1146/annurev.biochem.76.061705.090740.

Nojima, T., Reynolds, A.E., Kitamura, D., Kelsoe, G. and Kuraoka, M. (2020) Tracing Self-Reactive B Cells in Normal Mice. *The Journal of Immunology*, 205 (1): 90–101. doi:10.4049/jimmunol.1901015.

Novikova, L., Smirnova, I. V, Rawal, S., Dotson, A.L., Benedict, S.H. and Stehno-Bittel, L. (2013) Variations in Rodent Models of Type 1 Diabetes: Islet Morphology. *Journal of Diabetes Research*, 2013: 1–13. doi:10.1155/2013/965832.

Noviski, M., Mueller, J.L., Satterthwaite, A., Garrett-Sinha, L.A., Brombacher, F. and Zikherman, J. (2018) IgM and igD b cell receptors differentially respond to endogenous antigens and control B cell fate. *eLife*, 7. doi:10.7554/eLife.35074.

Nowosad, C.R., Spillane, K.M. and Tolar, P. (2016) Germinal center B cells recognize antigen through a specialized immune synapse architecture. *Nature Immunology*, 17 (7): 870–877. doi:10.1038/ni.3458.

Nutt, S.L., Hodgkin, P.D., Tarlinton, D.M. and Corcoran, L.M. (2015) The generation of antibody-secreting plasma cells. *Nature Reviews Immunology*, 15 (3): 160–171. doi:10.1038/nri3795.

O'Connor, B.P., Vogel, L.A., Zhang, W., Loo, W., Shnider, D., Lind, E.F., Ratliff, M., Noelle, R.J. and Erickson, L.D. (2006) Imprinting the Fate of Antigen-Reactive B Cells through the Affinity of the B Cell Receptor. *The Journal of Immunology*, 177 (11): 7723–7732. doi:10.4049/jimmunol.177.11.7723.

Odagiu, L., May, J., Boulet, S., Baldwin, T.A. and Labrecque, N. (2021) Role of the Orphan Nuclear Receptor NR4A Family in T-Cell Biology. *Frontiers in Endocrinology*, 11. doi:10.3389/fendo.2020.624122.

Okada, T., Miller, M.J., Parker, I., Krummel, M.F., Neighbors, M., Hartley, S.B., O'Garra, A., Cahalan, M.D. and Cyster, J.G. (2005) Antigen-engaged B cells undergo chemotaxis toward the T zone and form motile conjugates with helper T cells Jenkins, M. (ed.). *PLoS Biology*, 3 (6): 1047–1061. doi:10.1371/journal.pbio.0030150.

Oliver, A.M., Martin, F., Gartland, G.L., Carter, R.H. and Kearney, J.F. (1997) Marginal zone B cells exhibit unique activation, proliferative and immunoglobulin secretory responses. *European Journal of Immunology*, 27 (9): 2366–2374. doi:10.1002/eji.1830270935.

Ota, T., Ota, M., Duong, B.H., Gavin, A.L. and Nemazee, D. (2011) Liver-expressed Igκ superantigen induces tolerance of polyclonal B cells by clonal deletion not κ to λ receptor editing. *Journal of Experimental Medicine*, 208 (3): 617–629. doi:10.1084/jem.20102265.

Otipoby, K.L., Waisman, A., Derudder, E., Srinivasan, L., Franklin, A. and Rajewsky, K. (2015) The B-cell antigen receptor integrates adaptive and innate immune signals. *Proceedings of the National Academy of Sciences of the United States of America*, 112 (39): 12145–12150. doi:10.1073/pnas.1516428112.

Ottens, K. and Satterthwaite, A.B. (2021) IRF4 Has a Unique Role in Early B Cell Development and Acts Prior to CD21 Expression to Control Marginal Zone B Cell Numbers. *Frontiers in Immunology*, 12: 779085. doi:10.3389/fimmu.2021.779085.

Ozaki, K., Spolski, R., Ettinger, R., Kim, H.-P., Wang, G., Qi, C.-F., Hwu, P., Shaffer, D.J., Akilesh, S., Roopenian, D.C., et al. (2004) Regulation of B Cell Differentiation and Plasma Cell Generation by IL-21, a Novel Inducer of Blimp-1 and Bcl-6. *The Journal of Immunology*, 173 (9): 5361–5371. doi:10.4049/jimmunol.173.9.5361.

Palm, A.K.E. and Henry, C. (2019) Remembrance of Things Past: Long-Term B Cell Memory After Infection and Vaccination. *Frontiers in immunology*. 10 p. 1787. doi:10.3389/fimmu.2019.01787.

Pang, N.Y.L., Pang, A.S.R., Chow, V.T. and Wang, D.Y. (2021) Understanding neutralising antibodies against SARS-CoV-2 and their implications in clinical practice. *Military Medical Research*, 8 (1): 1–17. doi:10.1186/s40779-021-00342-3.

Pangrazzi, L. and Weinberger, B. (2020) T cells, aging and senescence. *Experimental Gerontology*, 134: 110887. doi:10.1016/j.exger.2020.110887.

Pape, K.A., Catron, D.M., Itano, A.A. and Jenkins, M.K. (2007) The Humoral Immune Response Is Initiated in Lymph Nodes by B Cells that Acquire Soluble Antigen Directly in the Follicles. *Immunity*, 26 (4): 491–502. doi:10.1016/j.immuni.2007.02.011.

Pape, K.A., Maul, R.W., Dileepan, T., Paustian, A.S., Gearhart, P.J. and Jenkins, M.K. (2018) Naive B Cells with High-Avidity Germline-Encoded Antigen Receptors Produce Persistent IgM+ and Transient IgG+ Memory B Cells. *Immunity*, 48 (6): 1135-1143.e4. doi:10.1016/j.immuni.2018.04.019.

Pape, K.A., Taylor, J.J., Maul, R.W., Gearhart, P.J. and Jenkins, M.K. (2011) Different B cell populations mediate early and late memory during an endogenous immune response. *Science*, 331 (6021): 1203–1207. doi:10.1126/science.1201730.

Paus, D., Tri, G.P., Chan, T.D., Gardam, S., Basten, A. and Brink, R. (2006) Antigen recognition strength regulates the choice between extrafollicular plasma cell and germinal center B cell differentiation. *Journal of Experimental Medicine*, 203 (4): 1081–1091. doi:10.1084/jem.20060087.

Pechhold, K., Zhu, X., Harrison, V.S., Lee, J., Chakrabarty, S., Koczwara, K., Gavrilova, O. and Harlan, D.M. (2009) Dynamic changes in pancreatic endocrine cell abundance, distribution, and function in antigen-induced and spontaneous autoimmune diabetes. *Diabetes*, 58 (5): 1175–1184. doi:10.2337/db08-0616.

Pelanda, R., Braun, U., Hobeika, E., Nussenzweig, M.C. and Reth, M. (2002) B Cell Progenitors Are Arrested in Maturation but Have Intact VDJ Recombination in the Absence of Ig-α and Ig-β. *The Journal of Immunology*, 169 (2): 865–872. doi:10.4049/jimmunol.169.2.865.

Petro, J.B., Gerstein, R.M., Lowe, J., Carter, R.S., Shinners, N. and Khan, W.N. (2002) Transitional type 1 and 2 B lymphocyte subsets are differentially responsive to antigen receptor signaling. *Journal of Biological Chemistry*, 277 (50): 48009–48019. doi:10.1074/jbc.M200305200.

Phan, R.T. and Dalla-Favera, R. (2004) The BCL6 proto-oncogene suppresses p53 expression in germinal-centre B cells. *Nature*, 432 (7017): 635–639. doi:10.1038/nature03147.

Phan, R.T., Saito, M., Basso, K., Niu, H. and Dalla-Favera, R. (2005) BCL6 interacts with the transcription factor Miz-1 to suppress the cyclin-dependent kinase inhibitor p21 and cell cycle arrest in germinal center B cells. *Nature Immunology*, 6 (10): 1054–1060. doi:10.1038/ni1245.

Phan, T.G., Amesbury, M., Gardam, S., Crosbie, J., Hasbold, J., Hodgkin, P.D., Basten, A. and Brink, R. (2003) B cell receptor-independent stimuli trigger immunoglobulin (Ig) class switch recombination and production of IgG autoantibodies by anergic self-reactive B cells. *Journal of Experimental Medicine*, 197 (7): 845–860. doi:10.1084/jem.20022144.

Phan, T.G., Grigorova, I., Okada, T. and Cyster, J.G. (2007) Subcapsular encounter and complement-dependent transport of immune complexes by lymph node B cells. *Nature Immunology*, 8 (9): 992–1000. doi:10.1038/ni1494.

Phan, T.G., Paus, D., Chan, T.D., Turner, M.L., Nutt, S.L., Basten, A. and Brink, R. (2006) High affinity germinal center B cells are actively selected into the plasma cell compartment. *Journal of Experimental Medicine*, 203 (11): 2419–2424. doi:10.1084/jem.20061254.

Pierce, S.K. (2002) Lipid rafts and B-cell activation. *Nature Reviews Immunology*, 2 (2): 96–105. doi:10.1038/nri726.

Pillai, S. and Cariappa, A. (2009) The follicular versus marginal zone B lymphocyte cell fate decision. *Nature Reviews Immunology*. 9 (11) pp. 767–777. doi:10.1038/nri2656.

Pone, E.J., Zhang, J., Mai, T., White, C.A., Li, G., Sakakura, J.K., Patel, P.J., Al-Qahtani, A., Zan, H., Xu, Z., et al. (2012) BCR-signalling synergizes with TLR-signalling for induction of AID and immunoglobulin class-switching through the non-canonical NF-κB pathway. *Nature Communications*, 3 (1): 1–12. doi:10.1038/ncomms1769.

Pratama, A. and Vinuesa, C.G. (2014) Control of TFH cell numbers: Why and how? *Immunology and Cell Biology*, 92 (1): 40–48. doi:10.1038/icb.2013.69.

Pugliese, A. (2016) Insulitis in the pathogenesis of type 1 diabetes. *Pediatric Diabetes*. 17 (Suppl Suppl 22) pp. 31–36. doi:10.1111/pedi.12388.

Pulendran, B., Kannourakis, G., Nouri, S., Smith, K.G.C. and Nossal, G.J.V. (1995) Soluble antigen can cause enhanced apoptosis of germinal-centre B cells. *Nature*, 375 (6529): 331–334. doi:10.1038/375331a0.

Qi, H., Egen, J.G., Huang, A.Y.C. and Germain, R.N. (2006) Extrafollicular activation of lymph node B cells by antigen-bearing dendritic cells. *Science*, 312 (5780): 1672–1676. doi:10.1126/science.1125703.

Quách, T.D., Manjarrez-Orduño, N., Adlowitz, D.G., Silver, L., Yang, H., Wei, C., Milner, E.C.B. and Sanz, I. (2011) Anergic Responses Characterize a Large Fraction of Human Autoreactive Naive B Cells Expressing Low Levels of Surface IgM. *The Journal of Immunology*, 186 (8): 4640–4648. doi:10.4049/jimmunol.1001946.

Rahman, Z.S.M., Shao, W.-H., Khan, T.N., Zhen, Y. and Cohen, P.L. (2010) Impaired Apoptotic Cell Clearance in the Germinal Center by Mer-Deficient Tingible Body Macrophages Leads to Enhanced Antibody-Forming Cell and Germinal Center Responses. *The Journal of Immunology*, 185 (10): 5859–5868. doi:10.4049/jimmunol.1001187.

Rakhmanov, M., Keller, B., Gutenberger, S., Foerster, C., Hoenig, M., Driessen, G., Van Der Burg, M., Van Dongen, J.J., Wiech, E., Visentini, M., et al. (2009) Circulating CD21low B cells in common variable immunodeficiency resemble tissue homing, innate-like B cells. *Proceedings of the National Academy of Sciences of the United States of America*, 106 (32): 13451–13456. doi:10.1073/pnas.0901984106.

Ramiro, A.R., Stavropoulos, P., Jankovic, M. and Nussenzweig, M.C. (2003) Transcription enhances AID-mediated cytidine deamination by exposing single-stranded DNA on the nontemplate strand. *Nature Immunology*, 4 (5): 452–456. doi:10.1038/ni920.

Ranuncolo, S.M., Polo, J.M., Dierov, J., Singer, M., Kuo, T., Greally, J., Green, R., Carroll, M. and Melnick, A. (2007) Bcl-6 mediates the germinal center B cell phenotype and lymphomagenesis through transcriptional repression of the DNA-damage sensor ATR. *Nature Immunology*, 8 (7): 705–714. doi:10.1038/ni1478.

Raudvere, U., Kolberg, L., Kuzmin, I., Arak, T., Adler, P., Peterson, H. and Vilo, J. (2019) G:Profiler: A web server for functional enrichment analysis and conversions of gene lists (2019 update). *Nucleic Acids Research*, 47 (W1): W191–W198. doi:10.1093/nar/gkz369.

Rauschmeier, R., Reinhardt, A., Gustafsson, C., Glaros, V., Artemov, A. V., Dunst, J., Taneja, R., Adameyko, I., Månsson, R., Busslinger, M., et al. (2021) Bhlhe40 function in activated B and TFH cells restrains the GC reaction and prevents lymphomagenesis. *Journal of Experimental Medicine*, 219 (2). doi:10.1084/jem.20211406.

Rawlings, D.J., Metzler, G., Wray-Dutra, M. and Jackson, S.W. (2017) Altered B cell signalling in autoimmunity. *Nature Reviews Immunology*, 17 (7): 421–436. doi:10.1038/nri.2017.24.

Reed, J.H., Jackson, J., Christ, D. and Goodnow, C.C. (2016) Clonal redemption of autoantibodies by somatic hypermutation away from self-reactivity during human immunization. *Journal of Experimental Medicine*, 213 (7): 1255–1265. doi:10.1084/jem.20151978.

Reeves, W.H., Lee, P.Y., Weinstein, J.S., Satoh, M. and Lu, L. (2009) Induction of autoimmunity by pristane and other naturally occurring hydrocarbons. *Trends in Immunology*, 30 (9): 455–464. doi:10.1016/j.it.2009.06.003.

Reimand, J., Isserlin, R., Voisin, V., Kucera, M., Tannus-Lopes, C., Rostamianfar, A., Wadi, L., Meyer, M., Wong, J., Xu, C., et al. (2019) Pathway enrichment analysis and visualization of omics data using g:Profiler, GSEA, Cytoscape and EnrichmentMap. *Nature Protocols*, 14 (2): 482–517. doi:10.1038/s41596-018-0103-9.

Roco, J.A., Mesin, L., Binder, S.C., Nefzger, C., Gonzalez-Figueroa, P., Canete, P.F., Ellyard, J., Shen, Q., Robert, P.A., Cappello, J., et al. (2019) Class-Switch Recombination Occurs Infrequently in Germinal Centers. *Immunity*, 51 (2): 337-350.e7. doi:10.1016/j.immuni.2019.07.001.

Rogers, N.M., Ferenbach, D.A., Isenberg, J.S., Thomson, A.W. and Hughes, J. (2014) Dendritic cells and macrophages i. The kidney: A spectrum of good and evil. *Nature Reviews Nephrology*. 10 (11) pp. 625–643. doi:10.1038/nrneph.2014.170.

Rojas, M., Hulbert, C. and Thomas, J.W. (2001) Anergy and not Clonal Ignorance Determines the Fate of B Cells that Recognize a Physiological Autoantigen. *The Journal of Immunology*, 166 (5): 3194–3200. doi:10.4049/jimmunol.166.5.3194.

Rubtsov, A. V., Rubtsova, K., Fischer, A., Meehan, R.T., Gillis, J.Z., Kappler, J.W. and Marrack, P.

(2011) Toll-like receptor 7 (TLR7)-driven accumulation of a novel CD11c+ B-cell population is important for the development of autoimmunity. *Blood*, 118 (5): 1305–1315. doi:10.1182/blood-2011-01-331462.

Rubtsova, K., Rubtsov, A. V., Cancro, M.P. and Marrack, P. (2015) Age-Associated B Cells: A T-bet–Dependent Effector with Roles in Protective and Pathogenic Immunity. *The Journal of Immunology*, 195 (5): 1933–1937. doi:10.4049/jimmunol.1501209.

Russell, D.M., Dembić, Z., Morahan, G., Miller, J.F.A.P., BÜrki, K. and Nemazee, D. (1991) Peripheral deletion of self-reactive B cells. *Nature*, 354 (6351): 308–311. doi:10.1038/354308a0.

Rydyznski Moderbacher, C., Ramirez, S.I., Dan, J.M., Grifoni, A., Hastie, K.M., Weiskopf, D., Belanger, S., Abbott, R.K., Kim, C., Choi, J., et al. (2020) Antigen-Specific Adaptive Immunity to SARS-CoV-2 in Acute COVID-19 and Associations with Age and Disease Severity. *Cell*, 183 (4): 996-1012.e19. doi:10.1016/j.cell.2020.09.038.

Sabouri, Z., Perotti, S., Spierings, E., Humburg, P., Yabas, M., Bergmann, H., Horikawa, K., Roots, C., Lambe, S., Young, C., et al. (2016) IgD attenuates the IgM-induced anergy response in transitional and mature B cells. *Nature Communications*, 7 (1): 1–11. doi:10.1038/ncomms13381.

Sabouri, Z., Schofield, P., Horikawa, K., Spierings, E., Kipling, D., Randall, K.L., Langley, D., Roome, B., Vazquez-Lombardi, R., Rouet, R., et al. (2014) Redemption of autoantibodies on anergic B cells by variable-region glycosylation and mutation away from self-reactivity. *Proceedings of the National Academy of Sciences of the United States of America*, 111 (25): E2567–E2575. doi:10.1073/pnas.1406974111.

Sacquin, A., Gador, M. and Fazilleau, N. (2017) The strength of BCR signaling shapes terminal development of follicular helper T cells in mice. *European Journal of Immunology*, 47 (8): 1295–1304. doi:10.1002/eji.201746952.

Saito, M., Gao, J., Basso, K., Kitagawa, Y., Smith, P.M., Bhagat, G., Pernis, A., Pasqualucci, L. and Dalla-Favera, R. (2007) A Signaling Pathway Mediating Downregulation of BCL6 in Germinal Center B Cells Is Blocked by BCL6 Gene Alterations in B Cell Lymphoma. *Cancer Cell*, 12 (3): 280–292. doi:10.1016/j.ccr.2007.08.011.

Saito, M., Novak, U., Piovan, E., Basso, K., Sumazin, P., Schneider, C., Crespo, M., Shen, Q., Bhagat, G., Califano, A., et al. (2009) BCL6 suppression of BCL2 via Miz1 and its disruption in diffuse large B cell lymphoma. *Proceedings of the National Academy of Sciences of the United States of America*, 106 (27): 11294–11299. doi:10.1073/pnas.0903854106.

Samardzic, T., Marinkovic, D., Danzer, C.P., Gerlach, J., Nitschke, L. and Wirth, T. (2002) Reduction of marginal zone B cells in CD22-deficient mice. *European Journal of Immunology*, 32 (2): 561–567. doi:10.1002/1521-4141(200202)32:2<561::AID-IMMU561>3.0.CO;2-H.

Samuels, J., Ng, Y.S., Coupillaud, C., Paget, D. and Meffre, E. (2005) Impaired early B cell tolerance in patients with rheumatoid arthritis. *The Journal of experimental medicine*, 201 (10): 1659–1667. doi:10.1084/JEM.20042321.

Satoh, M., Richards, H.B., Shaheen, V.M., Yoshida, H., Shaw, M., Naim, J.O., Wooley, P.H. and Reeves, W.H. (2000) Widespread susceptibility among inbred mouse strains to the induction of lupus autoantibodies by pristane. *Clinical and Experimental Immunology*, 121 (2): 399–405. doi:10.1046/j.1365-2249.2000.01276.x.

Schaerli, P., Willimann, K., Lang, A.B., Lipp, M., Loetscher, P. and Moser, B. (2000) CXC chemokine receptor 5 expression defines follicular homing T cells with B cell helper function. *Journal of Experimental Medicine*, 192 (11): 1553–1562. doi:10.1084/jem.192.11.1553.

Schindelin, J., Arganda-Carreras, I., Frise, E., Kaynig, V., Longair, M., Pietzsch, T., Preibisch, S., Rueden, C., Saalfeld, S., Schmid, B., et al. (2012) Fiji: An open-source platform for biological-image analysis. *Nature Methods*, 9 (7): 676–682. doi:10.1038/nmeth.2019.

Schriek, P., Ching, A.C., Moily, N.S., Moffat, J., Beattie, L., Steiner, T.M., Hosking, L.M., Thurman, J.M., Holers, V.M., Ishido, S., et al. (2022) Marginal zone B cells acquire dendritic cell functions by trogocytosis. *Science*, 375 (6581). doi:10.1126/science.abf7470.

Schroeder, H.W. and Cavacini, L. (2010) Structure and function of immunoglobulins. *Journal of Allergy*

and Clinical Immunology, 125 (2 SUPPL. 2): S41. doi:10.1016/j.jaci.2009.09.046.

Schwickert, T.A., Lindquist, R.L., Shakhar, G., Livshits, G., Skokos, D., Kosco-Vilbois, M.H., Dustin, M.L. and Nussenzweig, M.C. (2007) In vivo imaging of germinal centres reveals a dynamic open structure. *Nature*, 446 (7131): 83–87. doi:10.1038/nature05573.

Schwickert, T.A., Tagoh, H., Schindler, K., Fischer, M., Jaritz, M. and Busslinger, M. (2019) Ikaros prevents autoimmunity by controlling anergy and Toll-like receptor signaling in B cells. *Nature Immunology*, 20 (11): 1517–1529. doi:10.1038/s41590-019-0490-2.

Schwickert, T.A., Victora, G.D., Fooksman, D.R., Kamphorst, A.O., Mugnier, M.R., Gitlin, A.D. and Nussenzweig, M.L.D. (2011) A dynamic T cell-limited checkpoint regulates affinity-dependent B cell entry into the germinal center. *Journal of Experimental Medicine*, 208 (6): 1243–1252. doi:10.1084/jem.20102477.

Sebbag, M., Clavel, C., Nogueira, L., Arnaud, J. and Serre, G. (2009) “Autoimmune Response to Post-Translationally Modified (Citrullinated) Proteins: Prime Suspect in the Pathophysiology of Rheumatoid Arthritis.” In *The Epigenetics of Autoimmune Diseases*. Chichester, UK: John Wiley and Sons. pp. 279–308. doi:10.1002/9780470743553.ch16.

Seo, S.-J., Fields, M.L., Buckler, J.L., Reed, A.J., Mandik-Nayak, L., Nish, S.A., Noelle, R.J., Turka, L.A., Finkelman, F.D., Caton, A.J., et al. (2002) The Impact of T Helper and T Regulatory Cells on the Regulation of Anti-Double-Stranded DNA B Cells. *Immunity*, 16 (4): 535–546. doi:10.1016/s1074-7613(02)00298-4.

Setz, C.S., Hug, E., Khadour, A., Abdelrasoul, H., Bilal, M., Hobeika, E. and Jumaa, H. (2018) PI3K-Mediated Blimp-1 Activation Controls B Cell Selection and Homeostasis. *Cell Reports*, 24 (2): 391–405. doi:10.1016/j.celrep.2018.06.035.

Shaffer, A.L., Lin, K.I., Kuo, T.C., Yu, X., Hurt, E.M., Rosenwald, A., Giltnane, J.M., Yang, L., Zhao, H., Calame, K., et al. (2002) Blimp-1 orchestrates plasma cell differentiation by extinguishing the mature B cell gene expression program. *Immunity*, 17 (1): 51–62. doi:10.1016/S1074-7613(02)00335-7.

Shaffer, A.L., Yu, X., He, Y., Boldrick, J., Chan, E.P. and Staudt, L.M. (2000) BCL-6 represses genes that function in lymphocyte differentiation, inflammation, and cell cycle control. *Immunity*, 13 (2): 199–212. doi:10.1016/S1074-7613(00)00020-0.

Shannon, P., Markiel, A., Ozier, O., Baliga, N.S., Wang, J.T., Ramage, D., Amin, N., Schwikowski, B. and Ideker, T. (2003) Cytoscape: A software Environment for integrated models of biomolecular interaction networks. *Genome Research*, 13 (11): 2498–2504. doi:10.1101/gr.1239303.

Shi, G.-X., Harrison, K., Wilson, G.L., Moratz, C. and Kehrl, J.H. (2002) RGS13 Regulates Germinal Center B Lymphocytes Responsiveness to CXC Chemokine Ligand (CXCL)12 and CXCL13. *The Journal of Immunology*, 169 (5): 2507–2515. doi:10.4049/jimmunol.169.5.2507.

Shim, G.J., Kis, L.L., Warner, M. and Gustafsson, J.Å. (2004) Autoimmune glomerulonephritis with spontaneous formation of splenic germinal centers in mice lacking the estrogen receptor alpha gene. *Proceedings of the National Academy of Sciences of the United States of America*, 101 (6): 1720–1724. doi:10.1073/pnas.0307915100.

Shimizu, T., Mundt, C., Licence, S., Melchers, F. and Mårtensson, I.-L. (2002) VpreB1/VpreB2/λ5 Triple-Deficient Mice Show Impaired B Cell Development but Functional Allelic Exclusion of the IgH Locus . *The Journal of Immunology*, 168 (12): 6286–6293. doi:10.4049/jimmunol.168.12.6286.

Shinnakasu, R., Inoue, T., Kometani, K., Moriyama, S., Adachi, Y., Nakayama, M., Takahashi, Y., Fukuyama, H., Okada, T. and Kurosaki, T. (2016) Regulated selection of germinal-center cells into the memory B cell compartment. *Nature Immunology*, 17 (7): 861–869. doi:10.1038/ni.3460.

Shokat, K.M. and Goodnow, C.C. (1995) Antigen-induced B-cell death and elimination during germinal-centre immune responses. *Nature*, 375 (6529): 334–338. doi:10.1038/375334a0.

Shukla, A., Chen, C., Jellusova, J., Leung, C.R., Kao, E., Bhat, N., Lin, W.W., Apgar, J.R. and Rickert, R.C. (2019) Self-reactive B cells in the GALT are actively curtailed to prevent gut inflammation. *JCI Insight*, 4 (16). doi:10.1172/jci.insight.130621.

Shulman, Z., Gitlin, A.D., Weinstein, J.S., Lainez, B., Esplugues, E., Flavell, R.A., Craft, J.E. and

Nussenzweig, M.C. (2014) Germinal centers: Dynamic signaling by T follicular helper cells during germinal center B cell selection. *Science*, 345 (6200): 1058–1062. doi:10.1126/science.1257861.

Silva-Cayetano, A., Foster, W.S., Innocentin, S., Belij-Rammerstorfer, S., Spencer, A.J., Burton, O.T., Fra-Bidó, S., Le Lee, J., Thakur, N., Conceicao, C., et al. (2021) A booster dose enhances immunogenicity of the COVID-19 vaccine candidate ChAdOx1 nCoV-19 in aged mice. *Med*, 2 (3): 243-262.e8. doi:10.1016/j.medj.2020.12.006.

De Silva, N.S. and Klein, U. (2015) Dynamics of B cells in germinal centres. *Nature Reviews Immunology*, 15 (3): 137–148. doi:10.1038/nri3804.

Slot, L.M., Vergroesen, R.D., Kerkman, P.F., Staudinger, E., Reijm, S., van Dooren, H.J., van der Voort, E.I.H., Huizinga, T.W.J., Toes, R.E.M. and Scherer, H.U. (2021) Light chain skewing in autoantibodies and B-cell receptors of the citrullinated antigen-binding B-cell response in rheumatoid arthritis. *PLoS ONE*, 16 (3 March). doi:10.1371/journal.pone.0247847.

Smith, K.G.C., Light, A., Nossal, G.J.V. and Tarlinton, D.M. (1997) The extent of affinity maturation differs between the memory and antibody-forming cell compartments in the primary immune response. *EMBO Journal*, 16 (11): 2996–3006. doi:10.1093/emboj/16.11.2996.

Smith, K.G.C., Light, A., O'Reilly, L.A., Ang, S.M., Strasser, A. and Tarlinton, D. (2000) bcl-2 Transgene expression inhibits apoptosis in the germinal center and reveals differences in the selection of memory B cells and bone marrow antibody-forming cells. *Journal of Experimental Medicine*, 191 (3): 475–484. doi:10.1084/jem.191.3.475.

Snapper, C.M. and Mond, J.J. (1993) Towards a comprehensive view of immunoglobulin class switching. *Immunology Today*, 14 (1): 15–17. doi:10.1016/0167-5699(93)90318-F.

Somers, E.C., Thomas, S.L., Smeeth, L., Schoonen, W.M. and Hall, A.J. (2007) Incidence of systemic lupus erythematosus in the United Kingdom, 1990-1999. *Arthritis Care and Research*, 57 (4): 612–618. doi:10.1002/art.22683.

Song, W. and Craft, J. (2019) T follicular helper cell heterogeneity: Time, space, and function. *Immunological Reviews*, 288 (1): 85–96. doi:10.1111/imr.12740.

Stebegg, M., Bignon, A., Hill, D.L., Silva-Cayetano, A., Krueger, C., Vanderleyden, I., Innocentin, S., Boon, L., Wang, J., Zand, M.S., et al. (2020) Rejuvenating conventional dendritic cells and T follicular helper cell formation after vaccination. *eLife*, 9. doi:10.7554/eLife.52473.

Stewart, I., Radtke, D., Phillips, B., McGowan, S.J. and Bannard, O. (2018) Germinal Center B Cells Replace Their Antigen Receptors in Dark Zones and Fail Light Zone Entry when Immunoglobulin Gene Mutations are Damaging. *Immunity*, 49 (3): 477-489.e7. doi:10.1016/j.immuni.2018.08.025.

Strassheim, D., Renner, B., Panzer, S., Fuquay, R., Kulik, L., Ljubanović, D., Holers, V.M. and Thurman, J.M. (2013) IgM contributes to glomerular injury in FSGS. *Journal of the American Society of Nephrology*, 24 (3): 393–406. doi:10.1681/ASN.2012020187.

Stumvoll, M., Goldstein, B.J. and van Haeften, T.W. (2005) Type 2 diabetes: principles of pathogenesis and therapy. *The Lancet*, 365 (9467): 1333–1346. doi:10.1016/S0140-6736(05)61032-X.

Suan, D., Kräutler, N.J., Maag, J.L.V., Butt, D., Bourne, K., Hermes, J.R., Avery, D.T., Young, C., Statham, A., Elliott, M., et al. (2017) CCR6 Defines Memory B Cell Precursors in Mouse and Human Germinal Centers, Revealing Light-Zone Location and Predominant Low Antigen Affinity. *Immunity*, 47 (6): 1142-1153.e4. doi:10.1016/j.immuni.2017.11.022.

Subramanian, A., Tamayo, P., Mootha, V.K., Mukherjee, S., Ebert, B.L., Gillette, M.A., Paulovich, A., Pomeroy, S.L., Golub, T.R., Lander, E.S., et al. (2005) Gene set enrichment analysis: A knowledge-based approach for interpreting genome-wide expression profiles. *Proceedings of the National Academy of Sciences of the United States of America*, 102 (43): 15545–15550. doi:10.1073/pnas.0506580102.

Sundling, C., Lau, A.W.Y., Bourne, K., Young, C., Laurianto, C., Hermes, J.R., Menzies, R.J., Butt, D., Kräutler, N.J., Zahra, D., et al. (2021) Positive selection of IgG+ over IgM+ B cells in the germinal center reaction. *Immunity*, 54. doi:10.1016/j.immuni.2021.03.013.

Sutton, B., Davies, A., Bax, H. and Karagiannis, S. (2019) IgE Antibodies: From Structure to Function and Clinical Translation. *Antibodies*, 8 (1): 19. doi:10.3390/antib8010019.

Suzuki, K., Grigorova, I., Phan, T.G., Kelly, L.M. and Cyster, J.G. (2009) Visualizing B cell capture of cognate antigen from follicular dendritic cells. *Journal of Experimental Medicine*, 206 (7): 1485–1493. doi:10.1084/jem.20090209.

Takahashi, Y., Dutta, P.R., Cerasoli, D.M. and Kelsoe, G. (1998) In Situ Studies of the Primary Immune Response to (4-Hydroxy-3-Nitrophenyl)Acetyl. V. Affinity Maturation Develops in Two Stages of Clonal Selection. *Journal of Experimental Medicine*, 187 (6): 885–895. doi:10.1084/jem.187.6.885.

Tan, C., Hiwa, R., Mueller, J.L., Vykunta, V., Hibiya, K., Noviski, M., Huizar, J., Brooks, J.F., Garcia, J., Heyn, C., et al. (2020) NR4A nuclear receptors restrain B cell responses to antigen when second signals are absent or limiting. *Nature Immunology*, 21 (10): 1267–1279. doi:10.1038/s41590-020-0765-7.

Tangye, S.G. (2013) To B1 or not to B1: That really is still the question! *Blood*, 121 (26): 5109–5110. doi:10.1182/blood-2013-05-500074.

Tas, J.M.J., Mesin, L., Pasqual, G., Targ, S., Jacobsen, J.T., Mano, Y.M., Chen, C.S., Weill, J.C., Reynaud, C.A., Browne, E.P., et al. (2016) Visualizing antibody affinity maturation in germinal centers. *Science*, 351 (6277): 1048–1054. doi:10.1126/science.aad3439.

Taylor, J.J., Pape, K.A. and Jenkins, M.K. (2012) A germinal center-independent pathway generates unswitched memory B cells early in the primary response. *Journal of Experimental Medicine*, 209 (3): 597–606. doi:10.1084/jem.20111696.

Tea, F., Stella, A.O., Aggarwal, A., Darley, D.R., Pilli, D., Vitale, D., Merheb, V., Lee, F.X.Z., Cunningham, P., Walker, G.J., et al. (2021) SARS-CoV-2 neutralizing antibodies: Longevity, breadth, and evasion by emerging viral variants. *PLoS Medicine*, 18 (7): e1003656. doi:10.1371/journal.pmed.1003656.

Teague, B.N., Pan, Y., Mudd, P.A., Nakken, B., Zhang, Q., Szodoray, P., Kim-Howard, X., Wilson, P.C. and Farris, A.D. (2007) Cutting Edge: Transitional T3 B Cells Do Not Give Rise to Mature B Cells, Have Undergone Selection, and Are Reduced in Murine Lupus. *The Journal of Immunology*, 178 (12): 7511–7515. doi:10.4049/jimmunol.178.12.7511.

Tellier, J., Shi, W., Minnich, M., Liao, Y., Crawford, S., Smyth, G.K., Kallies, A., Busslinger, M. and Nutt, S.L. (2016) Blimp-1 controls plasma cell function through the regulation of immunoglobulin secretion and the unfolded protein response. *Nature Immunology*, 17 (3): 323–330. doi:10.1038/ni.3348.

Tew, J.G., Wu, J., Qin, D., Helm, S., Burton, G.F. and Szakal, A.K. (1997) Follicular dendritic cells and presentation of antigen and costimulatory signals to B cells. *Immunological Reviews*, 156: 39–52. doi:10.1111/j.1600-065X.1997.tb00957.x.

Tiegs, S.L., Russell, D.M. and Nemazee, D. (1993) Receptor editing in self-reactive bone marrow B cells. *Journal of Experimental Medicine*, 177 (4): 1009–1020. doi:10.1084/jem.177.4.1009.

Tilstra, J.S., Avery, L., Menk, A. V., Gordon, R.A., Smita, S., Kane, L.P., Chikina, M., Delgoffe, G.M. and Shlomchik, M.J. (2018) Kidney-infiltrating T cells in murine lupus nephritis are metabolically and functionally exhausted. *Journal of Clinical Investigation*, 128 (11): 4884–4897. doi:10.1172/JCI120859.

Toboso-Navasa, A., Gunawan, A., Morlino, G., Nakagawa, R., Taddei, A., Damry, D., Patel, Y., Chakravarty, P., Janz, M., Kassiotis, G., et al. (2020) Restriction of memory B cell differentiation at the germinal center B cell positive selection stage. *Journal of Experimental Medicine*, 217 (7). doi:10.1084/jem.20191933.

Toellner, K., Sze, D.M. and Zhang, Y. (2018) What are the primary limitations in B-cell affinity maturation, and how much affinity maturation can we drive with vaccination?: Is affinity maturation a self-defeating process for eliciting broad protection? *Cold Spring Harbor Perspectives in Biology*, 10 (5): a028795. doi:10.1101/cshperspect.a028803.

Toellner, K.M., Gulbranson-Judge, A., Taylor, D.R., Sze, D.M.Y. and MacLennan, I.C.M. (1996) Immunoglobulin switch transcript production in vivo related to the site and time of antigen-specific B cell activation. *Journal of Experimental Medicine*, 183 (5): 2303–2312. doi:10.1084/jem.183.5.2303.

Toellner, K.M., Luther, S.A., Sze, D.M.Y., Choy, R.K.W., Taylor, D.R., MacLennan, I.C.M. and Acha-Orbea, H. (1998) T helper 1 (Th1) and Th2 characteristics start to develop during T cell priming and are associated with an immediate ability to induce immunoglobulin class switching. *Journal of Experimental*

Medicine, 187 (8): 1193–1204. doi:10.1084/jem.187.8.1193.

Tomayko, M.M., Karaaslan, S., Lainez, B., Conter, L.J., Song, E., Venkatesan, S., Mishina, Y. and Shlomchik, M.J. (2021) Roles of Bone Morphogenetic Protein Receptor 1A in Germinal Centers and Long-Lived Humoral Immunity. *ImmunoHorizons*, 5 (5): 284–297. doi:10.4049/immunohorizons.2100019.

Tonegawa, S. (1983) Somatic generation of antibody diversity. *Nature*, 302 (5909): 575–581. doi:10.1038/302575a0.

Torres, R.M., Flaswinkel, H., Reth, M. and Rajewsky, K. (1996) Aberrant B cell development and immune response in mice with a compromised BCR complex. *Science*, 272 (5269): 1804–1808. doi:10.1126/science.272.5269.1804.

Tsalavos, S., Segklia, K., Passa, O., Petryk, A., O'Connor, M.B. and Graf, D. (2011) Involvement of Twisted Gastrulation in T Cell-Independent Plasma Cell Production. *The Journal of Immunology*, 186 (12): 6860–6870. doi:10.4049/jimmunol.1001833.

Tsiantoulas, D., Kiss, M., Bartolini-Gritti, B., Bergthaler, A., Mallat, Z., Jumaa, H. and Binder, C.J. (2017) Secreted IgM deficiency leads to increased BCR signaling that results in abnormal splenic B cell development. *Scientific Reports*, 7 (1): 1–9. doi:10.1038/s41598-017-03688-8.

Tsitsikov, E.N., Laouini, D., Dunn, I.F., Sannikova, T.Y., Davidson, L., Alt, F.W. and Geha, R.S. (2001) TRAF1 is a negative regulator of TNF signaling: Enhanced TNF signaling in TRAF1-deficient mice. *Immunity*, 15 (4): 647–657. doi:10.1016/S1074-7613(01)00207-2.

Tsubata, T. and Reth, M. (1990) The products of pre-B cell-specific genes (λ5 and VpreB) and the immunoglobulin μ chain form a complex that is transported onto the cell surface. *Journal of Experimental Medicine*, 172 (3): 973–976. doi:10.1084/jem.172.3.973.

Tumang, J.R., Hastings, W.D., Bai, C. and Rothstein, T.L. (2004) Peritoneal and splenic B-1 cells are separable by phenotypic, functional, and transcriptomic characteristics. *European Journal of Immunology*, 34 (8): 2158–2167. doi:10.1002/eji.200424819.

Tung, J.W., Parks, D.R., Moore, W.A., Herzenberg, L.A. and Herzenberg, L.A. (2004) Identification of B-Cell Subsets. *B Cell Protocols*, pp. 37–58. doi:10.1385/1-59259-796-3:037.

Turner, V.M. and Mabbott, N.A. (2017) Structural and functional changes to lymph nodes in ageing mice. *Immunology*, 151 (2): 239–247. doi:10.1111/imm.12727.

Unanue, E.R., Engers, H.D. and Karnovsky, M.J. (1973) Antigen receptors on lymphocytes. *Federation Proceedings*. 32 (1) pp. 44–47. doi:10.1146/annurev.iy.10.040192.000525.

Vale, A.M., Kearney, J.F., Nobrega, A. and Schroeder, H.W. (2015) "Development and Function of B Cell Subsets." In Alt, F.W., Honjo, T., Radbruch, A. and Reth, M. (eds.) *Molecular Biology of B Cells: Second Edition*. Academic Press. pp. 99–119. doi:10.1016/B978-0-12-397933-9.00007-2.

Vallé, A., Zuber, C.E., Defrance, T., Djossou, O., Riem, M. De and Banchereau, J. (1989) Activation of human B lymphocytes through CD40 and interleukin 4. *European Journal of Immunology*, 19 (8): 1463–1467. doi:10.1002/eji.1830190818.

Vergani, D. and Mieli-Vergani, G. (2008) Aetiopathogenesis of autoimmune hepatitis. *World Journal of Gastroenterology*, 14 (21): 3306–3312. doi:10.3748/wjg.14.3306.

Viant, C., Weymar, G.H.J., Escolano, A., Chen, S., Hartweger, H., Cipolla, M., Gazumyan, A. and Nussenzweig, M.C. (2020) Antibody Affinity Shapes the Choice between Memory and Germinal Center B Cell Fates. *Cell*, 183 (5): 1298-1311.e11. doi:10.1016/j.cell.2020.09.063.

Victora, G.D., Dominguez-Sola, D., Holmes, A.B., Deroubaix, S., Dalla-Favera, R. and Nussenzweig, M.C. (2012) Identification of human germinal center light and dark zone cells and their relationship to human B-cell lymphomas. *Blood*, 120 (11): 2240–2248. doi:10.1182/blood-2012-03-415380.

Victora, G.D. and Nussenzweig, M.C. (2022) Germinal Centers. *Annual Review of Immunology*, 40 (1): 413–442. doi:10.1146/annurev-immunol-120419-022408.

Victora, G.D., Schwickert, T.A., Fooksman, D.R., Kamphorst, A.O., Meyer-Hermann, M., Dustin, M.L. and Nussenzweig, M.C. (2010) Germinal center dynamics revealed by multiphoton microscopy with a

photoactivatable fluorescent reporter. *Cell*, 143 (4): 592–605. doi:10.1016/j.cell.2010.10.032.

Vidarsson, G., Dekkers, G. and Rispens, T. (2014) IgG subclasses and allotypes: From structure to effector functions. *Frontiers in Immunology*, 5 (OCT): 520. doi:10.3389/fimmu.2014.00520.

Vinuesa, C.G. de, Cook, M.C., Ball, J., Drew, M., Sunners, Y., Cascalho, M., Wabl, M., Klaus, G.G.B. and MacLennan, I.C.M. (2000) Germinal centers without T cells. *Journal of Experimental Medicine*, 191 (3): 485–493. doi:10.1084/jem.191.3.485.

Vinuesa, C.G. de, O'Leary, P., Sze, D.M.-Y., Toellner, K.-M. and MacLennan, I.C.M. (1999) T-independent type 2 antigens induce B cell proliferation in multiple splenic sites, but exponential growth is confined to extrafollicular foci. *European Journal of Immunology*, 29 (4): 1314–1323. doi:10.1002/(sici)1521-4141(199904)29:04<1314::aid-immu1314>3.0.co;2-4.

Waisman, A., Kraus, M., Seagal, J., Ghosh, S., Melamed, D., Song, J., Sasaki, Y., Classen, S., Lutz, C., Brombacher, F., et al. (2007) IgG1 B cell receptor signaling is inhibited by CD22 and promotes the development of B cells whose survival is less dependent on Igα/β. *Journal of Experimental Medicine*, 204 (4): 747–758. doi:10.1084/jem.20062024.

Wang, L., Wang, F.-S.S., Gershwin, & M.E., Wang, A., Wang, L., Me, G. and Gershwin, M.E. (2015) Human autoimmune diseases: A comprehensive update. *Journal of Internal Medicine*, 278 (4): 369–395. doi:10.1111/joim.12395.

Wang, S., Wang, J., Kumar, V., Karnell, J.L., Naiman, B., Gross, P.S., Rahman, S., Zerrouki, K., Hanna, R., Morehouse, C., et al. (2018) IL-21 drives expansion and plasma cell differentiation of autoreactive CD11chiT-bet+ B cells in SLE. *Nature Communications*, 9 (1). doi:10.1038/s41467-018-03750-7.

Wang, Y., Thomson, C.A., Allan, L.L., Jackson, L.M., Olson, M., Hercus, T.R., Nero, T.L., Turner, A., Parker, M.W., Lopez, A.L., et al. (2013) Characterization of pathogenic human monoclonal autoantibodies against GM-CSF. *Proceedings of the National Academy of Sciences of the United States of America*, 110 (19): 7832–7837. doi:10.1073/pnas.1216011110.

Wardemann, H., Yurasov, S., Schaefer, A., Young, J.W., Meffre, E. and Nussenzweig, M.C. (2003) Predominant autoantibody production by early human B cell precursors. *Science*, 301 (5638): 1374–1377. doi:10.1126/science.1086907.

Watanabe, A., Su, K.Y., Kuraoka, M., Yang, G., Reynolds, A.E., Schmidt, A.G., Harrison, S.C., Haynes, B.F., St. Clair, E.W. and Kelsoe, G. (2019) Self-tolerance curtails the B cell repertoire to microbial epitopes. *JCI Insight*, 4 (10). doi:10.1172/jci.insight.122551.

Waters, L.R., Ahsan, F.M., Wolf, D.M., Shirihai, O. and Teitell, M.A. (2018) Initial B Cell Activation Induces Metabolic Reprogramming and Mitochondrial Remodeling. *iScience*, 5: 99–109. doi:10.1016/j.isci.2018.07.005.

Watson, L., Wilson, B.J. and Waugh, N. (2002) Pneumococcal polysaccharide vaccine: A systematic review of clinical effectiveness in adults. *Vaccine*, 20 (17–18): 2166–2173. doi:10.1016/S0264-410X(02)00112-3.

Wellmann, U., Letz, M., Herrmann, M., Angermüller, S., Kalden, J.R. and Winkler, T.H. (2005) The evolution of human anti-double-stranded DNA autoantibodies. *Proceedings of the National Academy of Sciences of the United States of America*, 102 (26): 9258–9263. doi:10.1073/pnas.0500132102.

Wen, L., Brill-Dashoff, J., Shinton, S.A., Asano, M., Hardy, R.R. and Hayakawa, K. (2005) Evidence of marginal-zone B cell- positive selection in spleen. *Immunity*, 23 (3): 297–308. doi:10.1016/j.immuni.2005.08.007.

William, J., Euler, C., Christensen, S. and Shlomchik, M.J. (2002) *Evolution of autoantibody responses via somatic hypermutation outside of germinal centers*., 297 (5589): 2066–2070. Available at: https://www.science.org/doi/10.1126/science.1073924 (Accessed: 25 November 2022).

Wong, J.B., Hewitt, S.L., Heltemes-Harris, L.M., Mandal, M., Johnson, K., Rajewsky, K., Koralov, S.B., Clark, M.R., Farrar, M.A. and Skok, J.A. (2019) B-1a cells acquire their unique characteristics by bypassing the pre-BCR selection stage. *Nature Communications*, 10 (1): 1–15. doi:10.1038/s41467-019-12824-z.

Woof, J.M. and Ken, M.A. (2006) The function of immunoglobulin A in immunity. *Journal of Pathology*,

208 (2): 270–282. doi:10.1002/path.1877.

Wykes, M., Pombo, A., Jenkins, C. and MacPherson, G.G. (1998) Dendritic cells interact directly with naive B lymphocytes to transfer antigen and initiate class switching in a primary T-dependent response. *Journal of immunology (Baltimore, Md.: 1950)*, 161 (3): 1313–9. Available at: http://www.ncbi.nlm.nih.gov/pubmed/9686593 (Accessed: 29 April 2020).

Xie, P., Hostager, B.S., Munroe, M.E., Moore, C.R. and Bishop, G.A. (2006) Cooperation between TNF Receptor-Associated Factors 1 and 2 in CD40 Signaling. *The Journal of Immunology*, 176 (9): 5388–5400. doi:10.4049/jimmunol.176.9.5388.

Xing, G.Q., Chen, M., Liu, G., Wang, S.X. and Zhao, M.H. (2010) Renal neutrophils infiltration in antineutrophil cytoplasmic antibodies-negative pauci-immune crescentic glomerulonephritis. *American Journal of the Medical Sciences*, 340 (6): 474–480. doi:10.1097/MAJ.0b013e3181f0768e.

Xu, S., Tan, J.E.L., Wong, E.P.Y., Manickam, A., Ponniah, S. and Lam, K.P. (2000) B cell development and activation defects resulting in xid-like immunodeficiency in BLNK/SLP-65-deficient mice. *International Immunology*, 12 (3): 397–404. doi:10.1093/intimm/12.3.397.

Xu, Y., Xu, L., Zhao, M., Xu, C., Fan, Y., Pierce, S.K. and Liu, W. (2014) No receptor stands alone: IgG B-cell receptor intrinsic and extrinsic mechanisms contribute to antibody memory. *Cell Research*, 24 (6): 651–664. doi:10.1038/cr.2014.65.

Yam-Puc, J.C., Zhang, L., Maqueda-Alfaro, R.A., Garcia-Ibanez, L., Zhang, Y., Davies, J., Senis, Y.A., Snaith, M. and Toellner, K.-M. (2021) Enhanced BCR signaling inflicts early plasmablast and germinal center B cell death. *iScience*, 24 (2): 102038. doi:10.1016/j.isci.2021.102038.

Yam-Puc, J.C., Zhang, L., Zhang, Y. and Toellner, K.M. (2018) Role of B-cell receptors for B-cell development and antigen-induced differentiation. *F1000 Research*, 7: 429. doi:10.12688/f1000research.13567.1.

Yang, X., Stedra, J. and Cerny, J. (1996) Relative contribution of T and B cells to hypermutation and selection of the antibody repertoire in germinal centers of aged mice. *The Journal of experimental medicine*, 183 (3): 959–970. doi:10.1084/JEM.183.3.959.

Yang, Y., Li, X., Ma, Z., Wang, C., Yang, Q., Byrne-Steele, M., Hong, R., Min, Q., Zhou, G., Cheng, Y., et al. (2021) CTLA-4 expression by B-1a B cells is essential for immune tolerance. *Nature Communications*, 12 (1): 1–17. doi:10.1038/s41467-020-20874-x.

Yarkoni, Y., Getahun, A. and Cambier, J.C. (2010) Molecular underpinning of B-cell anergy. *Immunological Reviews*, 237 (1): 249–263. doi:10.1111/j.1600-065X.2010.00936.x.

Yasuda, S., Sun, J., Zhou, Y., Wang, Y., Lu, Q., Yamamura, M. and Wang, J.Y. (2018) Opposing roles of IgM and IgD in BCR-induced B-cell survival. *Genes to Cells*, 23 (10): 868–879. doi:10.1111/gtc.12635.

Ye, B.H., Cattoretti, G., Shen, Q., Zhang, J., Hawe, N., De Waard, R., Leung, C., Nouri-Shirazi, M., Orazi, A., Chaganti, R.S.K., et al. (1997) The BCL-6 proto-oncogene controls germinal-centre formation and Th2- type inflammation. *Nature Genetics*, 16 (2): 161–170. doi:10.1038/ng0697-161.

Yurasov, S., Wardemann, H., Hammersen, J., Tsuiji, M., Meffre, E., Pascual, V. and Nussenzweig, M.C. (2005) *Defective B cell tolerance checkpoints in systemic lupus erythematosus*., 201 (5). doi:10.1084/JEM.20042251.

Yuseff, M.I., Pierobon, P., Reversat, A. and Lennon-Duménil, A.M. (2013) How B cells capture, process and present antigens: A crucial role for cell polarity. *Nature Reviews Immunology*. 13 (7) pp. 475–486. doi:10.1038/nri3469.

Zehentmeier, S. and Pereira, J.P. (2019) Cell circuits and niches controlling B cell development. *Immunological Reviews*, 289 (1): 142–157. doi:10.1111/imr.12749.

Zhang, L. (2019) *Characterisation of anergic B cells in a new mouse model with altered B cell receptor signalling*. University of Birmingham. Available at: https://etheses.bham.ac.uk/id/eprint/9523/.

Zhang, X., Lindwall, E., Gauthier, C., Lyman, J., Spencer, N., Alarakhia, A., Fraser, A., Ing, S., Chen, M., Webb-Detiege, T., et al. (2015a) Circulating CXCR5+CD4+helper T cells in systemic lupus

erythematosus patients share phenotypic properties with germinal center follicular helper T cells and promote antibody production. *Lupus*, 24 (9): 909–917. doi:10.1177/0961203314567750.

Zhang, Y., Garcia-Ibanez, L. and Toellner, K.M. (2016) Regulation of germinal center B-cell differentiation. *Immunological Reviews*. 270 (1) pp. 8–19. doi:10.1111/imr.12396.

Zhang, Y., Li, Y., Lv, T.T., Yin, Z.J. and Wang, X.B. (2015b) Elevated circulating Th17 and follicular helper CD4+ T cells in patients with rheumatoid arthritis. *APMIS*, 123 (8): 659–666. doi:10.1111/APM.12399.

Zhang, Y., Meyer-Hermann, M., George, L.A., Figge, M.T., Khan, M., Goodall, M., Young, S.P., Reynolds, A., Falciani, F., Waisman, A., et al. (2013) Germinal center B cells govern their own fate via antibody feedback. *Journal of Experimental Medicine*, 210 (3): 457–464. doi:10.1084/jem.20120150.

Zhang, Y., Tech, L., George, L.A., Acs, A., Durrett, R.E., Hess, H., Walker, L.S.K., Tarlinton, D.M., Fletcher, A.L., Hauser, A.E., et al. (2018) Plasma cell output from germinal centers is regulated by signals from Tfh and stromal cells. *Journal of Experimental Medicine*, 215 (4): 1227–1243. doi:10.1084/jem.20160832.

Zhang, Y. and Toellner, K.M. (2022) Germinal center derived B cell memory without T cells. *Journal of Experimental Medicine*, 219 (3). doi:10.1084/jem.20220012.

Zheng, G.X.Y., Terry, J.M., Belgrader, P., Ryvkin, P., Bent, Z.W., Wilson, R., Ziraldo, S.B., Wheeler, T.D., McDermott, G.P., Zhu, J., et al. (2017) Massively parallel digital transcriptional profiling of single cells. *Nature Communications*, 8 (1): 1–12. doi:10.1038/ncomms14049.

Zhuang, X., Ahmed, F., Zhang, Y., Ferguson, H.J., Steele, J.C., Steven, N.M., Nagy, Z., Heath, V.L., Toellner, K.M. and Bicknell, R. (2015) Robo4 vaccines induce antibodies that retard tumor growth. *Angiogenesis*, 18 (1): 83–95. doi:10.1007/s10456-014-9448-z.

Zikherman, J., Parameswaran, R. and Weiss, A. (2012) Endogenous antigen tunes the responsiveness of naive B cells but not T cells. *Nature*, 489 (7414): 160–164. doi:10.1038/nature11311.

Zotos, D., Coquet, J.M., Zhang, Y., Light, A., D'Costa, K., Kallies, A., Corcoran, L.M., Godfrey, D.I., Toellner, K.M., Smyth, M.J., et al. (2010) IL-21 regulates germinal center B cell differentiation and proliferation through a B cell-intrinsic mechanism. *Journal of Experimental Medicine*, 207 (2): 365–378. doi:10.1084/jem.20091777.